ROMA TRE
UNIVERSITÀ DEGLI STUDI

Dottorato in Scienze della Terra

Curriculum Risorse e Territorio

Structural-Thermal evolution of the Apenninic-Maghrebian fold-and-thrust belt in NW Sicily: insight from 1D to 3D modelling

Ciclo XXXI

Martina Balestra

Supervisore

Prof.ssa Sveva Corrado

Co-supervisori

Dott. Luca Aldega

Dott. Maurizio Gasparo Morticelli

Dott. Jean-Luc Rudkiewicz

Dott. William Sassi

Coordinatore Scuola Dottorale

Prof. Claudio Faccenna

Revisori

Prof. Robert W.H. Butler
School of Geosciences
University of Aberdeen
United Kingdom

Prof. Dominique Frizon de Lamotte
Université de Cergy Pontoise, France

A.A. 2017/2018

TABLE OF CONTENTS

Abstract.....7

Riassunto.....10

Chapter I - Introduction and thesis scheme.....13

Chapter II: Thermal and structural modelling of the Scillato wedge-top basin source to sink system: Insights into the Sicilian fold-and-thrust belt building (Italy).....20

2.1. Abstract 20

2.2. Introduction 21

2.3. Geological Setting 22

2.3.1. Deformed pre-orogenic substratum of the Scillato wedge-top basin 26

2.3.2. Scillato wedge-top basin.....28

2.4. Methods and Materials 29

2.4.1. Organic matter optical analysis 29

2.4.2. X-ray diffraction (XRD) analysis 30

2.4.3. 3D Geological modelling.....31

2.5. Results.....33

2.5.1. Organic matter optical analysis 35

2.5.1.1. Deformed pre-orogenic substratum.....35

2.5.1.2. Scillato wedge-top basin 35

2.5.2. *X-ray diffraction analysis on fine grained sediments*.....36

2.5.2.1. Deformed pre-orogenic substratum of the Scillato wedge-top basin 36

2.5.2.2. Scillato wedge-top basin 37

2.5.3. 3D Geological modelling.....38

2.6. Discussion 40

2.6.1. Thermal maturity of the Scillato wedge-top basin and its pre-orogenic substratum...40

2.6.2. Evolutionary scenarios for the Lercara unit 45

2.6.3. Source to sink system: insights into kinematic evolution of the belt 49

2.7. Conclusions.....52

Chapter III - 3D structural modeling and restoration in fold-and-thrust belts: examples from the Kumeta and Busambra Mts., NW Sicily (Italy) 54

3.1 Abstract 54

3.2 Introduction 54

3.3 Geological setting.....57

3.3.1 The Trapanese unit and the development of the Kumeta and Busambra ridges 61

3.3.2 Previous interpretations for the Kumeta and Busambra Mts.....62

3.4 Methods and Materials.....65

3.4.1 Seismic Interpretation.....65

3.4.2 3D Geological model reconstruction.....67

3.4.3 3D depth conversion.....68

3.4.4 3D Restoration.....69

3.5 Results and discussion.....70

3.5.1 Seismic facies interpretation.....70

3.5.2 Previous structural model.....74

3.5.3 New model.....79

3.5.4 Impact of inherited structures.....84

3.5.5 Implication for hydrocarbon exploration.....88

3.6 Conclusions.....89

Chapter IV - Paleothermal data as a tool for kinematic reconstruction of the Sicilian fold-and-thrust belt: implication for the tectonics evolution and petroleum system of the Kumeta and Busambra Mts. area (Apennine-Maghrebian FTB).....91

4.1 Abstract 91

4.2 Introduction 92

4.3 Geological Setting 95

4.4 Methods and Materials 101

4.4.1 Sampled structures 101

4.4.2 Organic matter optical analysis 103

4.4.3 X-ray diffraction (XRD) analysis 103

4.4.4 Pyrolysis 104

4.4.5 Thermal modelling 104

4.5 Results 107

4.5.1 Organic matter optical analysis 108

4.5.1.1 Imerese unit and Numidian Flysch 108

4.5.1.2 Trapanese unit 110

4.5.2 X-ray diffraction (XRD) analysis 112

4.5.2.1 Imerese unit and Numidian Flysch 112

4.5.2.2 Trapanese unit 113

4.5.3 Pyrolysis 114

4.5.4 1D Thermal modelling 117

4.5.4.1 Imerese unit 117

4.5.4.2 Trapanese unit 118

4.5.5 3D Thermal modelling 121

4.6 Discussion 124

4.6.1 Paleothermal data as a tool for kinematic reconstruction of the Sicilian fold-and-thrust belt 124

4.6.2 Implications for hydrocarbon exploration 131

4.7 Conclusions 135

Chapter V - Thesis Discussion 137

5.1 Geometric and kinematic implications at a regional scale 137

5.1.1 The Sicilian Fold-and-thrust belt: comparison between Western, Central and Eastern Sicily paleothermal, structural and paleomagnetic data 137

5.1.2 The SFTB in the Western Mediterranean.....148

5.1.3 Kinematic evolution of Western SFTB 153

5.2 3D modelling strengths and limitations 155

Chapter - VI: Concluding remarks and Future perspectives.....162

6.1 Concluding remarks 162

6.2 Future perspectives.....164

References cited.....166

APPENDIX 192

Acknowledgements

First of all I would like to thank Prof. Sveva Corrado for giving me the possibility to develop this project. From a pure geological point of view, what I really appreciated, and probably (I hope so) I learned, is her incredible capability in linking all the geological information, finding always a consistent solution, especially in complex areas such as fold-and-thrust belt. On the other hand, the most important quality that I found in her was the ability to control my work but at the same time, leaving me the necessary space to develop my ideas and to make mistakes, exactly like an excellent professor. Secondly, I must thank Dr. Luca Aldega. He taught me not only the lab technique but also how to write a scientific paper and how to be a researcher (with enormous patient). Effectively, he was the first person who believed in me, and advised me to do a PhD and he was the first to get me into the "paleothermal indicator" topic.

Dr. Maurizio Gasparo Morticelli is acknowledged for the indispensable help in the field and, together with the Prof. Attilio Sulli for all the discussions regarding the study area, the seismic lines, the structural data and all the different interpretations. I am grateful to all the "Palermo group" for the help, the amazing outcrops they show me and the hospitality.

Dr. William Sassi is kindly acknowledged for all his lessons regarding faults geometry and mechanics, for all the advices, the papers and the support. He is still motivating me, and I really appreciate this. I am indebted to Dr. Jean-Luc Rudkiewicz for the help with the Skua-Gocad software and for the interesting discussions on my paleothermal data and seismic interpretation. I admired his capability to have deep knowledge both in the analytical part (software development) and in the pure geological part. I am still waiting to go in the field with him to continue our discussions. I am grateful to both for the nice time spent together and I am grateful to IFPen for the five months stage opportunity.

Prof. Dominique Frizon de Lamotte and Prof. Rob Butler are acknowledged for the interesting suggestions and discussions about this thesis, I really appreciated the time they spent reading and reviewing my manuscript. It was really important for me.

I need to thank Jean Letouzey and Giuseppe Cadel, as teachers and external advisors. As masters in seismic interpretation, they advised me a lot. In particular, their contribution in Chapter III was significant. I would like to thank Massimiliano Barchi for interesting discussion about Sicilian peculiarity such us the Lercara unit and Fabio Speranza for the discussions about paleomagnetic data. I also want to thank Massimo Santantonio and Nino Mariotti for the books and papers they provided me and the interesting lessons on the Mesozoic sedimentology and tectonic in Sicily and Sergio Lo Mastro for the time spent on XRD samples scanning.

Emerson (ex-Paradigm) and Midland valley are also acknowledged for the Skua-Gocad and Move licenses.

The people I am grateful more are my family members. I do not need to spend lot of words because they already know how much love and how much grateful I am. They are all my world and they are always proud of me even thought my mistakes, they know we can solve everything.

Beside my family, I am grateful to Jacopo, my other half, who always supported me and helped me with all his energy during these last three years (thanks for the informatics support!). He makes me happy, especially in the difficult moments, he is proud of me and he never stopped to believe in me and in my work. Furthermore, I want to thank his family who followed the progress of my PhD since the beginning, supporting me. Last but not least, I am really grateful to: my best friends (and geologists) Martina e Gaia for the support, the interest on my work and the interesting geological discussion about my study area; my ex colleague and still friend Luca, for the precious advises and help; Simone and Andrea to be the best flatmates ever, and Andrea to be also the best officemate, together with Riccardo, they know how to have a break and relax; Stefania, Gabriii and the “coffeemaker” Amhad for funny moments in these last years; the amazing Kenya group for the best fieldtrip ever! I enjoyed these three years, I had the possibility to travel a lot and to meet amazing people, so I am grateful for this.

Abstract

Two geologically complex areas located in the northern Sicilian fold-and-thrust belt, the Termini-Imerese and the Kumeta and Busambra Mts. areas, are investigated using 3D modelling techniques for structural interpretation of existing 2D seismic profiles, surface geology and by means of a new acquisition and modelling of paleothermal indicators.

The investigation of the organic and inorganic fraction of sediments, for the two study areas, by means of a multi-method approach of optical, geochemical and X-ray diffraction analysis provided new paleothermal data in the diagenetic realm, for the Mesozoic-Cenozoic Imerese and Trapanese units and the Cenozoic Numidian Flysch and wedge-top basin (Scillato basin) successions.

As a result, in both study areas, the Imerese unit, experienced the highest stage of thermal maturity followed by the Numidian Flysch succession. Lower maturity levels are recorded by the Trapanese unit sampled in the Kumeta-Busambra Mts. area and by the Scillato wedge-top basin succession sampled in the Termini-Imerese area.

For the Imerese unit, R_o% values of 0.58-0.94% and R0 to R1 structures with an illite content of 60-84% in mixed layer Illite-Smectite (I-S) have been measured. The Numidian Flysch succession samples give R_o% values of 0.40-0.60% and R0 to R1 structures with an illite content of 40-76% in mixed layer I-S. The Trapanese unit, cropping out only in the Kumeta and Busambra Mts. area, shows R_o% value of 0.34-0.47% and R0 to R1 structures with an illite content of 33-60% in mixed layer I-S. The wedge-top basin (Scillato basin) succession samples show R_o% values of 0.33-0.47% and R0 structures with an illite content of 40-50% in mixed layer I-S, experiencing the lowest maturity levels.

1D and 3D burial and thermal histories have been constrained by means of these measured paleothermal values. Resulting amount of overburden (nowadays removed by erosion) fall in the range of ~1.6-2.0 km of sedimentary/tectonic load reconstructed for the Imerese unit, ~1.2-1.3

km of tectonic load reconstructed for Trapanese unit and about 0.8km of sedimentary load reconstructed for the Scillato wedge-top basin.

Geological modelling in 3D of the two study areas allowed me to represent and describe the structural complexity characterized by fault sets with different orientations.

Twenty-eight new geological cross-sections have been drawn in order to build the 3D geological model in the Termini-Imerese area. Two fault sets were individuated and represented in the 3D reconstruction by NW-SE striking thrust and NE-SW high angle transpressive faults.

Thirteen seismic lines were interpreted in order to build the 3D geological model in the Kumeta and Busambra Mts. area. In this study area the focus was on the structural interpretation of the Trapanese unit (carbonate platform facies). Along-strike variability of structural style has been highlighted: WNW-ESE backthrusts with a transport towards the NNE linked by hard linkage (NNE-SSW to NE-SW tear faults) characterize the Mt. Kumeta structure; an imbricate backthrust system (sense of transport towards the NNE) converts westward into thrusts (sense of transport towards the SSW) along the Mt. Busambra structure. The WNW-ESE to E-W high angle transpressive to reverse faults, which join thrusts at depth, characterize both the Kumeta and Busambra Mts. Using the 3D geomechanical restoration performed on the 3D geological model reconstructed in the Kumeta and Busambra Mts. area, I can delineate and validate a new structural interpretation of the area. Low shortening amount (<15%) affects the Trapanese unit investigated in this area.

Inherited paleogeographic setting and Mesozoic normal faults play a key role in the chain building determining high structural complexity and along strike variability. In particular, when Cenozoic vertical axis rotation is removed, two main fault sets are recognised: ~NNE-SSW to ~NE-SW and ~NW-SE striking faults. These two sets of faults are consistent with major Mesozoic structures described in Tunisia and, more in general, along North Africa belts.

In the Kumeta and Busambra Mts. area, 3D thermal simulations have been performed on a simplified 3D model and scenario of burial history. As a result, maturity distribution of different

stratigraphic intervals within the Trapanese unit has been computed in three dimensions. Maturity levels consistent with the oil generation stage are reached in the structural low between the Kumeta and Busambra Mts. by the upper Triassic-Eocene Trapanese succession.

In conclusion, the integrated approach proposed in this thesis allowed me to improve kinematic reconstructions of the study areas and can be further explored and improved to be applied in many other structurally complex areas. It highlights the importance to gather, assemble and integrate paleothermal data in the 2D to 3D structural interpretations. In detail, combining constrained burial histories and thermal maturity modelling computations with 3D geological models allow to validate the structural interpretations and to better understand the structural complexity of areas such as the northern Sicilian fold-and-thrust-belt.

Riassunto

In questo lavoro sono state analizzate due aree geologicamente complesse (chiamate Termini-Imerese e Kumeta-Busambra Mt.) localizzate lungo la catena a pieghe e sovrascorrimenti Siciliana. Le metodologie utilizzate sono l'acquisizione e modellazione di nuovi indicatori paleotermici, l'interpretazione sismica e tecniche di modellazione 3D.

Le frazioni organiche e inorganiche dei sedimenti sono state investigate mediante un approccio multi-metodologico che consiste in analisi ottiche, geochimiche e diffrazione a raggi X. Nuovi dati paleotermici sono stati ottenuti per le successioni Meso-Cenozoiche Imerese e Trapanese e per le successioni Cenozoiche del Flysch Numidico e del bacino di wedge-top di Scillato.

Nelle due aree investigate, l'unità Imerese ha sperimentato i valori più alti di maturità termica (strutture R0 to R1 e contenuto in illite tra 60-84% negli strati misti I-S e R_o% tra 0.58-0.94%), seguita dal Flysch Numidico (strutture R0 to R1 e contenuto in illite tra 40-76% negli strati misti I-S e R_o% tra 0.40-0.60%). L'unità Trapanese, affiorante solo nell'area Mt. Kumeta-Busambra ha sperimentato valori più bassi di maturità termica (strutture R0 to R1 e contenuto in illite tra 33-60% negli strati misti I-S e R_o% tra 0.34-0.47%), seguita dalla successione di wedge-top (bacino di Scillato) campionata nell'area di Termini-Imerese (strutture R0 e contenuto in illite tra 40-50% negli strati misti I-S e R_o% tra 0.33-0.47%).

I valori così ottenuti sono stati utilizzati per vincolare le storie termiche e di seppellimento 1D e 3D. I valori di carico sedimentario/tettonico misurato e adesso eroso, sono: 1,6-2,0 km di carico tettonico/sedimentario nell'unità Imerese; 1,2-1,3 di carico tettonico nell'unità Trapanese; 0,8 km di carico sedimentario nel bacino di Scillato (wedge-top).

La modellazione geologica 3D ha permesso di rappresentare e descrivere la complessità strutturale delle due aree di studio che sono caratterizzate da famiglie di faglie con diverse orientazioni.

Ventotto sezioni geologiche sono state realizzate per ricostruire il modello 3D nella zona di Termini-Imerese. Sono quindi stati individuati e rappresentati nel modello 3D due trend di faglie

principali: sovrascorrimenti orientati NW-SE e faglie transpressive ad alto angolo orientate NE-SW.

Tredici linee sismiche sono state interpretate per ricostruire il modello geologico 3D nell'area di Mt. Kumeta-Busambra. In questo lavoro mi sono focalizzata sull'interpretazione strutturale dell'unità Trapanese (piattaforma carbonatica) dove è stata riconosciuta una forte variabilità laterale delle strutture coinvolte. In dettaglio: la struttura di Mt. Kumeta è caratterizzata da retroscorrimenti orientati WNW-ESE (senso di trasporto verso NNE), connessi tra loro da faglie di strappo orientate NNE-SSW a NE-SW; la struttura di Mt. Busambra è caratterizzata da un sistema a retroscorrimenti con senso di trasporto NNE che verso ovest passa a sovrascorrimenti con senso di trasporto SSW. Faglie transpressive ad alto angolo che si ricongiungono ai sovrascorrimenti (e retroscorrimenti) in profondità (orientate da WNW-ESE a E-W), sono state individuate lungo entrambe le strutture.

L'interpretazione strutturale proposta per il modello 3D ricostruito nell'area di Mt. Kumeta-Busambra è stata validata mediante la tecnica di retrodeformazione geomeccanica 3D. I valori di raccorciamento così misurati non superano il 15%.

Inoltre, in questo lavoro, è stato evidenziato il ruolo chiave giocato delle strutture ereditate nella strutturazione della catena che hanno portato alla forte complessità strutturale e variabilità strutturale. In particolare, una volta rimosse le rotazioni Cenozoiche, si riconoscono due famiglie di faglie principali, orientate da ~NNE-SSW a ~NE-SW e ~NW-SE. Tali orientazioni sono consistenti con quelle delle diverse strutture Mesozoiche riconosciute e descritte in Tunisia e più in generale lungo le catene Nord Africane.

Nell'area di Mt. Kumeta-Busambra, è stato possibile realizzare delle simulazioni termiche 3D usando come base geometrica il modello geologico 3D semplificato

Come risultato della simulazione, sono state ottenute le mappe di distribuzione della maturità termica per le diverse formazioni che costituiscono l'unità Trapanese. Le mappe così ricostruite

hanno evidenziato che le formazioni Triassiche-Eoceniche sono entrate in finestra a olio nell'area compresa tra i Monti Kumeta e Busambra.

In conclusione, il nuovo approccio proposto in questa tesi mi ha permesso di migliorare le ricostruzioni geologiche e cinematiche per le due aree investigate. Da sottolineare è l'importanza di integrare dati paleotermici nelle interpretazioni strutturali 2D e 3D e in particolare, di combinare le storie di seppellimento e le modellazioni di maturità termica con i modelli geologici 3D per validare le interpretazioni strutturali e per capire meglio la complessità strutturale di aree come la catena a pieghe e sovrascorrimenti Siciliana. Questo approccio, che può essere ulteriormente investigato e migliorato, può essere utilizzato in altre aree di studio geologicamente complesse.

Over the years, many techniques have been adopted in order to understand the deformation history and evolution of fold-and-thrust belts (FTBs).

Albeit surface mapping is becoming more and more diffuse, subsurface knowledge in FTBs is often incomplete due to difficulties in the seismic acquisition, processing and interpretation and in some cases, to limited amount of well data. Thus, several interpretations can be proposed, satisfying the available data but implying completely different tectonic styles and kinematic evolution (e.g. Tozer et al., 2002; Shiner et al., 2004; Butler et al., 2005, 2018). Therefore, in order to discriminate the most viable model and to predict the structural behaviour in such poorly constrained areas (FTBs) balancing and restoration as well as analogue sandbox modelling are widely adopted techniques.

Balancing and restoration, have been widely employed in order to verify the correctness of an interpretation and to make prediction in poorly constrained areas (among the others, Butler, 1992a, 2013; Schönborn, 1999; Tozer et al., 2002, 2006; Butler et al., 2005; Watkins et al., 2014, 2017; Berthelon and Sassi, 2016; Tavani et al., 2018). Since the first works of Chamberlin (1910) and Dahlstrom (1969), several steps forward have been made, especially involving more and more computer codes (see Groshong et al., 2012, for a review) making these techniques faster and more accurate.

Analogue modelling, as well, has provided significant insights into the evolution of fold-and-thrust belts describing the three-dimensional variation of the structures and related displacement (Colletta et al., 1991; Liu and Dixon, 1991; McClay and Bonora, 2001; Costa and Speranza, 2003; Dotare et al., 2016; Boutelier et al., 2018) and how different mechanical proprieties (Corrado et al., 1998a; Ellis et al., 2004; Sadeghi et al., 2016; Bonanno et al., 2017) of the investigated succession as well as inherited structures (McClay, 1995; Mattioni et al., 2007; Di Domenica et al., 2014; Ferrer et al., 2016; D'Adda et al., 2017; Granado et al., 2017) can affect the folds and thrusts propagation and structural style.

On the other hand, thermal-burial histories and exhumation rates of sedimentary rocks can provide, when linked with the structural record, critical time-temperature constraints necessary for a more complete understanding of thrust belt kinematics and dynamics (among the others, Andreucci et al., 2015; Aldega et al., 2007, 2018; Caricchi et al., 2014, 2015; Corrado et al., 2005, 2009; Di Paolo et al., 2012, 2014; Mazzoli et al., 2006, 2008; Zattin et al., 2011).

For this purpose, some authors (Toro et al., 2004; Schneider, 2005; Deville and Sassi, 2006; Roure et al., 2010; Neumaier et al., 2014; Roure, 2014; Jirman et al., 2018) have proposed the integration of conventional structural and restoration techniques along 2D cross-sections with thermal and geochemical data by means of thermo-kinematic modelling.

Nevertheless, in complex areas such as fold-and-thrust belt which lack in cylindricity along strike, 2D sections do not allow to fully describe the shortening amount and rates and structural style variations of the involved structures along strike and to represent out-of-plane movements.

In these cases, working with an array of cross-section kinematically compatible is envisaged to depict the along strike variation of the investigated structures (e.g. Alvarez-Marron, 1995; Qayyum et al., 2015; Castelluccio et al., 2016; Watkins et al., 2017; Molli et al., 2018) whereas fully 3D models are requested to take into account out-of-plane movements (Egbue and Kellog, 2012; Bigi et al., 2013; Li et al., 2013, 2016; Shuwei et al., 2013; Guo et al., 2017; Turrini et al., 2017).

The Sicilian fold and thrust belt (SFTB) is part of the Apennine-Maghrebide arcuate orogenic system (Fig. 1.1 A) and it presents an extremely complex configuration, probably influenced by the former paleogeographic setting and evolution, as well as inherited Mesozoic (and Paleozoic?) structures. Such a complex configuration is also linked to two different thin-skinned tectonic events (shallow seated and deep seated thrusting events in Bello et al., 2000; Catalano et al., 2000; Avellone and Barchi, 2003; Avellone et al., 2010) accompanied by large vertical-axis clockwise rotations (Fig. 1.1 B; Channel et al., 1990; Grasso et al., 1987; Oldow et al., 1990; Speranza et al., 1999, 2003, 2018) decreasing from the internal units (e.g., Imerese and

Panormide units ~130°) toward the foreland (e.g. no rotation in the Sciacca area). Resulting structures are not-coaxial showing thus, different tectonic directions.

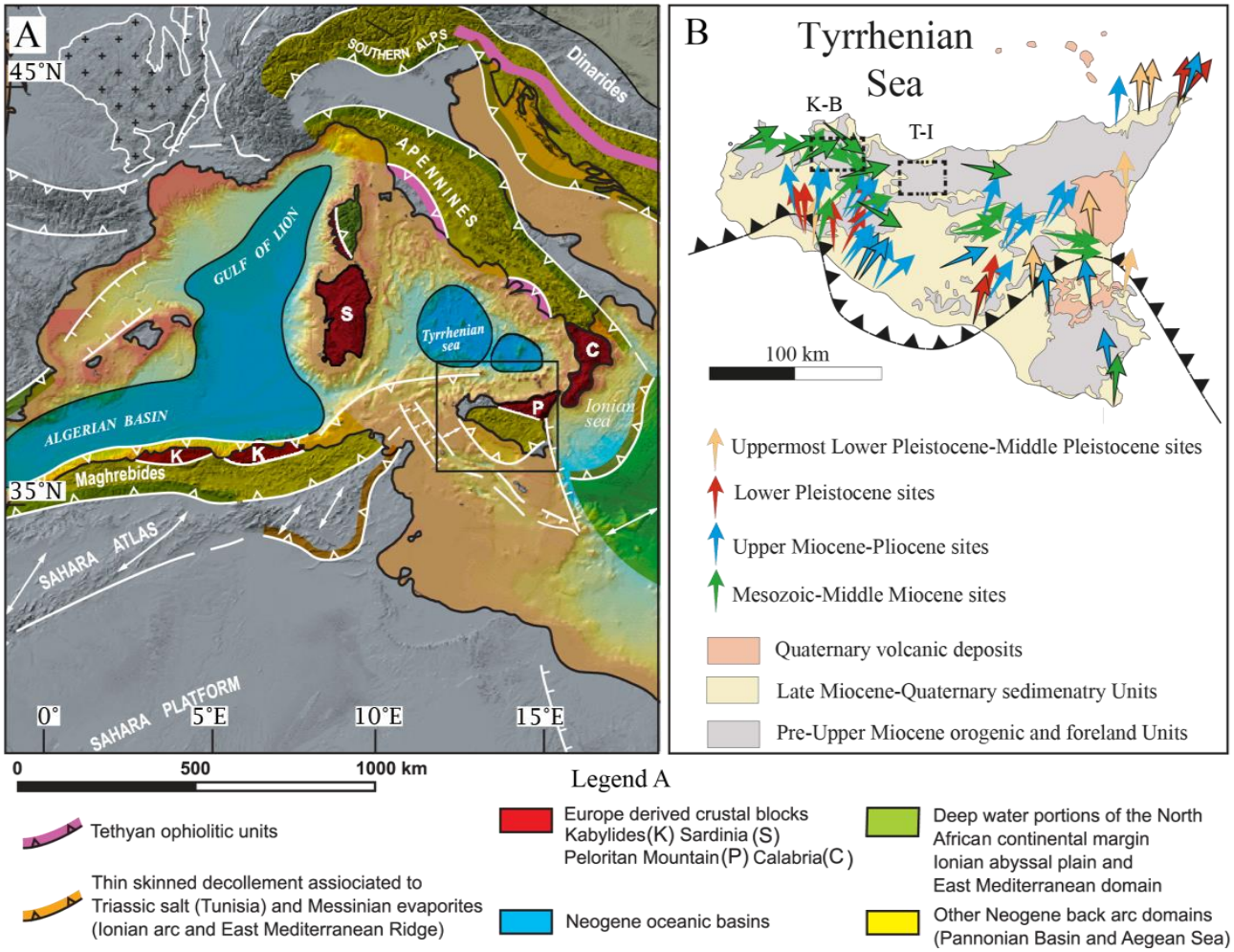

Figure 1.1 (A) Generalized map of the Western Mediterranean showing main domain and structures modified after Roure et al., (2012). Sicily is enclosed in the black rectangle. (B) Detail of estimated paleomagnetic rotations characterizing the Sicilian fold-and-thrust belt indicated by different arrows (modified after Cifelli et al., 2007). Each arrow represents results from one site (thin arrow) or group of sites (thick arrow). Dotted squares indicate the two study areas (K-B, Kumeta and Busambra Mts. area; T-I Termini-Imerese area)

The kinematic evolution of the Eastern SFTB was largely investigated by means of classical structural and stratigraphic methods, coupled with thermal and thermochronological indicators able to constrain amounts and rates of burial and subsequent exhumation of this sector of the chain (Corrado et al., 2009; Aldega et al., 2007, 2011; Di Paolo et al., 2012, 2014). On the other hand, up to now Western Sicily has been investigated using only classical structural and stratigraphic methods to constrain the timing and modes of the different tectonic events lacking independent constrains, such as paleothermal data and their modelling.

For these reasons and for the high structural complexity displayed by this sector of the SFTB we need to use as many tools as we can in order to reduce the interpretation uncertainty. Thus, paleothermal data, coupled with 3D geometrical reconstruction, form an important contribution to the toolbox.

This PhD project tested the combined approach of collecting new paleothermal data and reconstructing new 3D geological and thermal models in order to:

i) define the complex structural setting of the study area and to validate the existing and new structural models through seismic interpretation, 3D geological modelling and restoration;

ii) unravel the kinematic evolution of the SFTB in the study area (Central-Western Sicily) though coupling geological reconstruction with thermal data;

iii) reconstruct a simplified 3D thermal model in order to improve the petroleum system knowledge in the study area that includes the Kumeta and Busambra Mts.;

iv) create an iconic workflow to study FTBs integrating geometric, kinematic and thermal models in three-dimensions.

In this work we investigated two different key sectors, namely Termini-Imerese and Kumeta and Busambra Mts. areas (Fig. 1.1 B), of the SFTB described in the following three chapters of the thesis (Chapter II, Chapter III and Chapter IV).

The overall scheme of the thesis comprises five chapters beyond this introduction and is organised as follow:

In the **Chapter II**, I present the Termini-Imerese key area (Fig. 1 B). This area has been chosen because it had been already deeply investigated before this thesis. In detail, until now, the timing and modes of deformation of the SFTB in the study area were unravelled combining sedimentological and stratigraphic data of the Scillato wedge-top basins succession with structural analysis of its deformed substratum (Gugliotta, 2012; Gugliotta and Gasparo

Morticelli, 2012; Gugliotta et al., 2013, 2014). Thus, in this case, paleothermal data were able to provide independent constrains.

3D geological model building allowed to describe the structural complexity of the study area defining the along-strike variation of the investigated structures. It was reconstructed based on geological cross-sections and constrained using a deep seismic reflection profile. In this work, paleothermal data coupled with 3D geological model allowed me: i) to define maximum burial the deformed substratum (Imerese unit, Mesozoic-Cenozoic) and the Scillato wedge-top basin (Serravallian-Tortonian) successions underwent; ii) to confirm and detail the tectonic history reconstructed for the Scillato wedge-top basin and its deformed substratum.

This work is currently under review on *GSA bulletin*.

Author's contribution to the article

M. Balestra – field work, organic matter optical analysis, X-ray diffraction of clay minerals, cross-section construction, 3D geological modelling, thermal modelling, data interpretation, paper writing;
S. Corrado – field work, organic matter optical analysis, thermal modeling, data interpretation;
L. Aldega – Field work, X-ray diffraction of clay minerals, thermal modeling, data interpretation;
M. Gasparo Morticelli - field work, data interpretation;
A. Sulli - field work, data interpretation;
W. Sassi – 3D geological modelling, data interpretation;
J.L. Rudkiewicz - 3D geological modelling, data interpretation;
All the co-authors contributed in the review of the paper.

Chapters III and IV concern the Kumeta and Busambra Mts. sector (Fig. 1 B). This study area has been chosen because it was widely investigated by means of structural and stratigraphic methods before this thesis (Catalano et al., 2000, Avellone and Barchi, 2003; Basilone, 2009; Avellone et al., 2010; Barreca and Maesano, 2012; Gugliotta et al., 2014; Gasparo Morticelli et al., 2017) lacking in independent constrains (Paleothermal data and modelling) as well as the Termini-Imerese area. In addition, several seismic reflection profiles (12 lines) were available in the area providing subsurface constrains for the 3D geological model reconstruction. In detail:

Chapter III focuses on the seismic interpretation of the available seismic lines and the 3D geological model reconstruction and restoration of the Trapanese unit (Mesozoic-Cenozoic) which widely crops out along the Kumeta and Busambra Mts. Seismic reflection profiles were interpreted in order to build the 3D geological model. The full methodology, starting from building an initial 3D structural model setup and then followed by testing elastic block model restorations is described to propose the best interpretation of the outcropping Kumeta and Busambra Mountains. 3D geological model reconstruction, in particular, allowed me to define along strike variation of the structural style affecting the Trapanese unit, where pre-existing discontinuities (e.g. inherited normal faults) play an important role.

This work will be published on *Tectonophysics, special volume: "Style of deformation and tectono-sedimentary evolution of fold-and-thrust belts and foreland basins: from nature to models" (Lacombe O. Ed.)*;

Author's contribution to the article

M. Balestra – field work, seismic interpretation, 3D geological modelling, 3D restoration, data interpretation, paper writing;
S. Corrado – field work, data interpretation, review of the paper;
L. Aldega – field work, data interpretation, review of the paper;
M. Gasparo Morticelli - Field work, data interpretation;
A. Sulli - Field work, seismic interpretation, data interpretation;
W. Sassi – 3D geological modelling, data interpretation, review of the paper;
J.L. Rudkiewicz - 3D geological modelling, 3D restoration, data interpretation, review of the paper.

Chapter IV focuses on the paleothermal and geochemical data collected in the area (on both the Trapanese unit and the tectonically overlying Imerese unit) and 1D-3D thermal modelling. In detail, a simplified 3D thermal model of the Trapanese unit has been reconstructed based on the geometrical model proposed in Chapter III and constrained by paleothemal data. Paleothermal and geochemical data coupled with 1D-3D thermal modelling allowed me: i) to define maximum burial the two investigated successions (Imerese and Trapanese unit) underwent; ii) to reconstruct a new kinematic evolution scenario taking into account the inheritance of the pre-

compressional structural configuration; iii) to describe the petroleum system of the area identifying potential source rocks and kitchen areas.

This work will be published on *Marine and Petroleum geology*.

Author's contribution to the article

M. Balestra – field work, organic matter optical analysis, X-ray diffraction of clay minerals, pyrolysis, thermal modelling, data interpretation, paper writing;
S. Corrado – field work, organic matter optical analysis, thermal modeling, data interpretation, review of the paper;
L. Aldega – Field work, X-ray diffraction of clay minerals, thermal modeling, data interpretation, review of the paper;
M. Gasparo Morticelli - field work;
A. Sulli - field work;
W. Sassi – thermal modelling, data interpretation, review of the paper;
J.L. Rudkiewicz - thermal modelling, data interpretation;

Chapter V concerns the results related to the two key areas. In the first part, Chapters II, III and IV were integrated in a wider regional framework that takes into account the orogenic evolution of the Tyrrhenian-Apennines system since lower Miocene times with special attention to rotation patterns about vertical axes in the restoration process. The second part, focussed on the methodological implication of this work, describes the strengths and limitation of the 3D modelling technique

Chapter VI provides a brief synthesis of the main results and future perspectives.

Chapter II: Thermal and structural modelling of the Scillato wedge-top basin source to sink system: Insights into the Sicilian fold-and-thrust belt building (Italy)

2.1. Abstract

Temperature-dependent clay mineral assemblages, vitrinite reflectance and 1D thermal and 3D geological modelling of a Neogene wedge-top basin in the Sicilian fold-and-thrust belt and its pre-orogenic substratum allowed us to: (i) define the burial history of the sedimentary succession filling the wedge-top basin and its substratum, (ii) reconstruct the wedge-top basin geometry, depocenter migration and sediments provenance through time in the framework of a source to sink system and (iii) shed new light into the kinematic evolution of the Apennine-Maghrebian fold-and-thrust belt.

The pre-orogenic substratum of the Scillato basin shows an increase of levels of thermal maturity as function of stratigraphic age that is consistent with a maximum burial of 3.5 km in deep diagenetic conditions. In detail, R_o% values range from 0.40 to 0.94% and random ordered illite-smectite (I-S) firstly convert to short-range ordered structures and then evolve to long-range ordered structures at the base of the Imerese unit.

The wedge-top basin fill experienced shallow burial (~2 km) and levels of thermal maturity in the immature stage of hydrocarbon generation and early diagenesis.

Both vitrinite reflectance and mixed layers show two populations of authigenic and inherited phases. The indigenous population corresponds to macerals with R_o% values of 0.38-0.45% and I-S with no preferred sequence in stacking of layers whereas the reworked group corresponds to macerals with R_o% values of 0.42-0.47% and short-range ordered I-S with no correlation as function of depth. Authigenic and reworked components of the Scillato basin fill allowed us to unravel sediments provenance during the Neogene, identifying two main source areas feeding the wedge-top basin (crystalline units of the European domain and sedimentary units of the

African domain) and to detect an early phase of exhumation driven by low-angle extensional faults that predates Neogene compression.

2.2. Introduction

Source to sink systems consist of areas which contribute to erosion (e.g., hillslopes), transportation (e.g., rivers) and deposition (e.g., river flood plains, deltas, deep marine basins) of sediments within a denudation-accumulation system (Allen, 2008; Sømme et al., 2009; Allen and Allen, 2013; Michael et al., 2014). Fold-and-thrust belts and their foreland basin systems (DeCelles and Giles, 1996) represent source to sink systems closely linked in space and through time (Barnes and Heins, 2008). Their burial evolution, uplift and exhumation is recorded by the sedimentary successions and architecture of associated basins. In particular, wedge-top basins, lying on top of orogenic belts, are affected by paleo-topographic and structural variations related to syn-orogenic deformation (Butler and Grasso, 1993; Pinter et al., 2017). Thus, the study of wedge-top basins provides essential pieces of information on vertical movements and tectonic evolution of the source areas for sediments (e.g., orogenic belt).

However, amounts and timing of vertical motions in frontal parts of fold-and-thrust belt are not easily quantifiable as burial is generally limited to few kilometers and very few techniques may be applied to sedimentary rocks to detect tectonic thickening and exhumation (e.g., fission track and U-Th/He on apatite, organic matter optical analysis, X-ray diffraction of clay minerals; Garver et al., 1999; Jolivet et al., 2007; Corrado et al., 1998, 2009, 2010; Zattin et al., 2011; Whitchurch et al., 2011; Izquierdo-Llavall et al., 2013; Di Paolo et al., 2014; Caricchi et al., 2015; Aldega et al., 2017, 2018; Schito et al., 2018).

Recently, the timing and modes of deformation of the Sicilian Fold-and-Thrust belt (SFTB) in the study area were unravelled combining sedimentological and stratigraphic data of the wedge-top basins succession with structural analysis of its deformed substratum (Gugliotta, 2012; Gugliotta and Gasparo Morticelli, 2012; Gugliotta et al., 2013, 2014). Nevertheless, this

approach provides only hints on the kinematic evolution of the SFTB without quantifying and validating tectonic thickening, sedimentary loads and amounts of exhumation.

Thus, we combined paleothermal indicators (e.g., vitrinite reflectance and illite content in mixed layers illite-smectite) and organic petrographic studies of the fine fraction of sediments of the Scillato wedge-top basin and its deformed substratum with 1D thermal and 3D geometrical modelling to: (i) define the burial and thermal history of the sedimentary succession filling the Scillato wedge-top basin and its substratum, (ii) reconstruct the wedge-top basin geometry, depocenter migration and sediments provenance through time and (iii) shed new light into the kinematic evolution of the Apennine-Maghrebian fold-and-thrust belt suggesting an early phase of exhumation, driven by low-angle extensional faults, which predates Neogene compression.

In the end, we propose that the integration of the aforementioned approach with reconstruction of vertical motions of wedge-top basin margins can be a useful tool for unravelling source to sink systems in fold-and-thrust belts.

2.3. Geological Setting

Sicily is located in the Central Mediterranean area as a segment of the Apennine-Maghrebian chain (Fig. 2.1) which is originated from the tectonic inversion of the Africa continental passive margin (Catalano and D'Argenio, 1982a; Roure et al., 1990; Catalano et al., 1996; Catalano et al., 2007). The SFTB has been developing since the early Miocene as a SSE-verging chain, resulting from the post-collisional convergence between Africa and Europe (Dercourt et al., 1986; Dewey et al., 1989; Catalano et al., 1996, 2000; Faccenna et al., 2004) and the rollback of the subduction hinge of the Ionian lithosphere (Fig., 2.2; Caputo et al., 1970; Doglioni et al., 1999; Faccenna et al., 2001). These processes are responsible for deformation and tectonic transport of different paleogeographic domains, now stacked to form the tectonic wedge (Finetti et al., 2005; Catalano et al., 2013a; Di Paolo et al., 2012, 2014; Gasparo Morticelli et al., 2015).

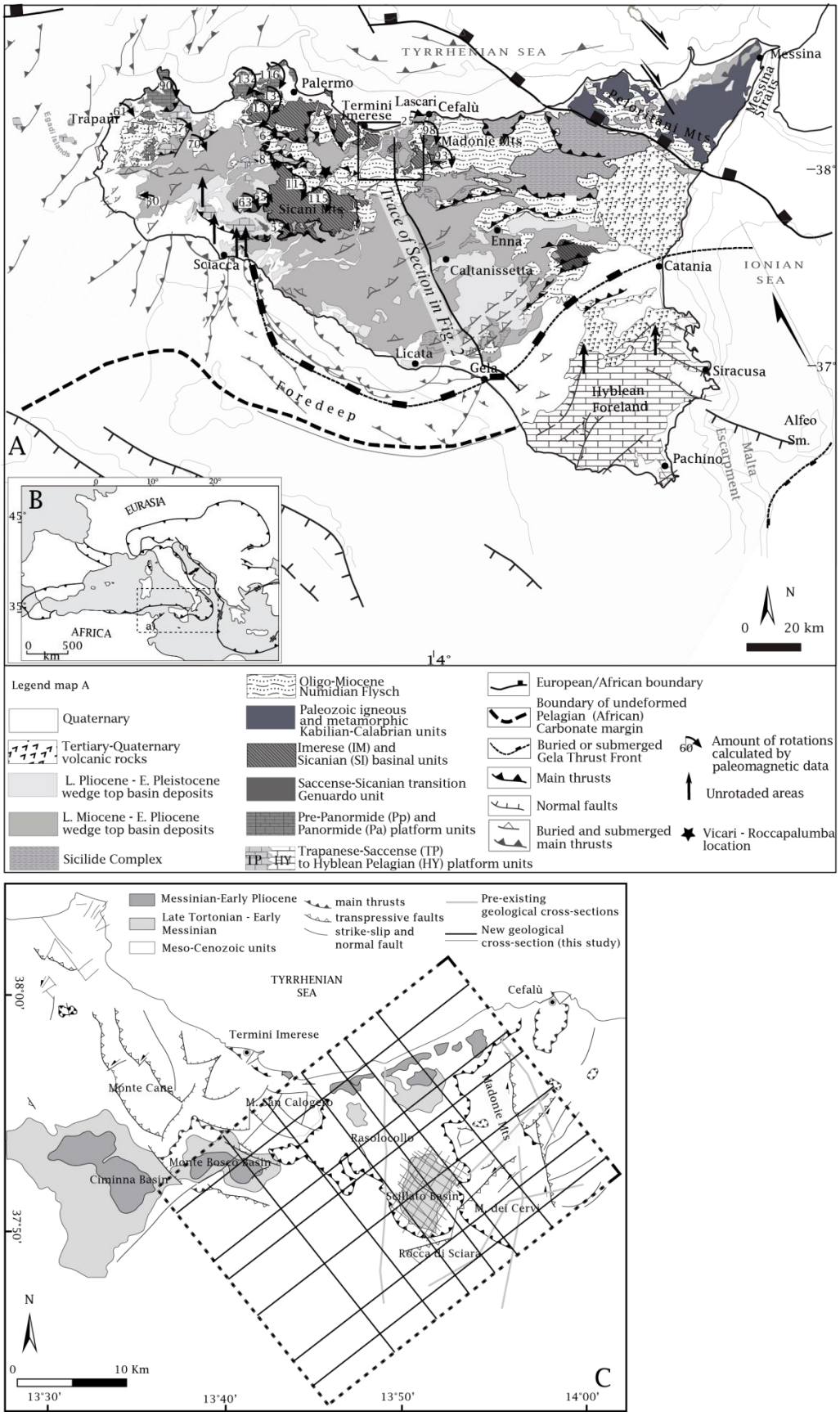

Figure 2.1 - (A) Geological map of Sicily (modified and redrawn after Gasparo Morticelli et al., 2015). The black rectangle indicates the study area. Palaeomagnetic data are from Channel et al. (1990), Grasso et al. (1987), Speranza et al. (2003). (B) tectonic map of central Mediterranean area (modified and redrawn after Gasparo Morticelli et al., 2015). (C) Simplified structural map of the central-northern Sicily showing major Miocene-

Pliocene basins and large-scale tectonic structures (modified after Gugliotta and Gasparo Morticelli, 2012). Dashed rectangle indicates the areal extension of the 3D geological model. Traces of pre-existing (grey lines) and new geological section (thick and thin black lines) built using Move software, are also indicated. Pre-existing cross-sections are from Catalano et al. (2011).

From the innermost to the outermost domain, they are: i) the European domain exposed in the NE part of Sicily (e.g., Peloritani Mts.) which is mainly constituted by crystalline and metamorphic units (Vignaroli, et al., 2008; Aldega et al., 2011); ii) the Tethyan domain (Sicilide Complex) which corresponds to Cretaceous-early Miocene pelagic successions detached from their substratum (Ogniben, 1960; Bianchi et al., 1989; Catalano et al., 1996; Corrado et al., 2009); iii) the African domain composed of different tectono-stratigraphic units subdivided into deep water (Imerese and Sicanian units), shallow water (Panormide unit) and carbonate-pelagic platforms (Trapanese and Saccense units; Catalano and D'Argenio, 1982a; Catalano et al., 2000; Nigro and Renda, 1999; Zarcone et al., 2010).

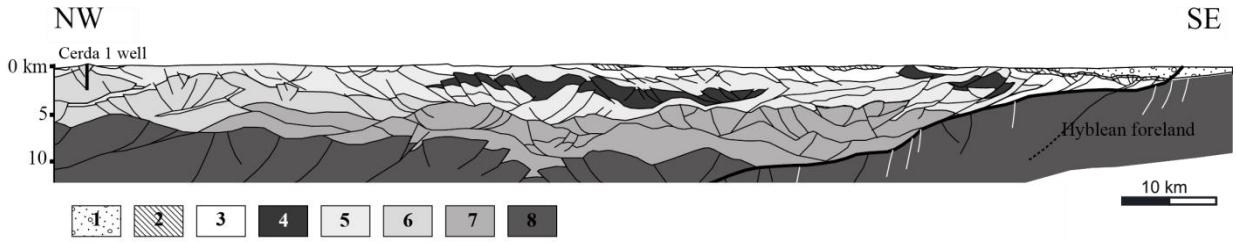

Figure 2.2 Regional cross-section (see Fig. 1 for location) showing the overall architecture of the Sicilian wedge (modified and redrawn after Catalano et al., 2013). Interpretation at depth is from the SI.RI.PRO. seismic profile. 1-Pleistocene foreland succession; 2-Pliocene- Pleistocene wedge-top successions; 3-upper Miocene-Pliocene successions; 4-detached Sicilide Complex (Cretaceous-early Miocene); 5-Numidian Flysch (late Oligocene-early Miocene); 6-Imerese unit (Triassic-Oligocene); 7-Sicanian unit (Triassic-Miocene); 8-Carbonate platform units (Triassic-Miocene). Black lines indicate reverse faults; thick black line indicates the sole thrust; white lines indicate normal faults.

From the latest Oligocene to the early Miocene a foreland basin developed filled by the Numidian Flysch (Catalano et al., 1989; Nigro and Renda 2000; Grasso 2001). The foreland basin system progressively migrated toward the Hyblean foreland which is exposed in south-eastern Sicily and extends offshore along the Sicily Channel in the Mediterranean Sea (Catalano et al., 1989; Butler and Grasso, 1993; Nigro and Renda, 2000; Grasso, 2001; Gasparo Morticelli et al., 2015).

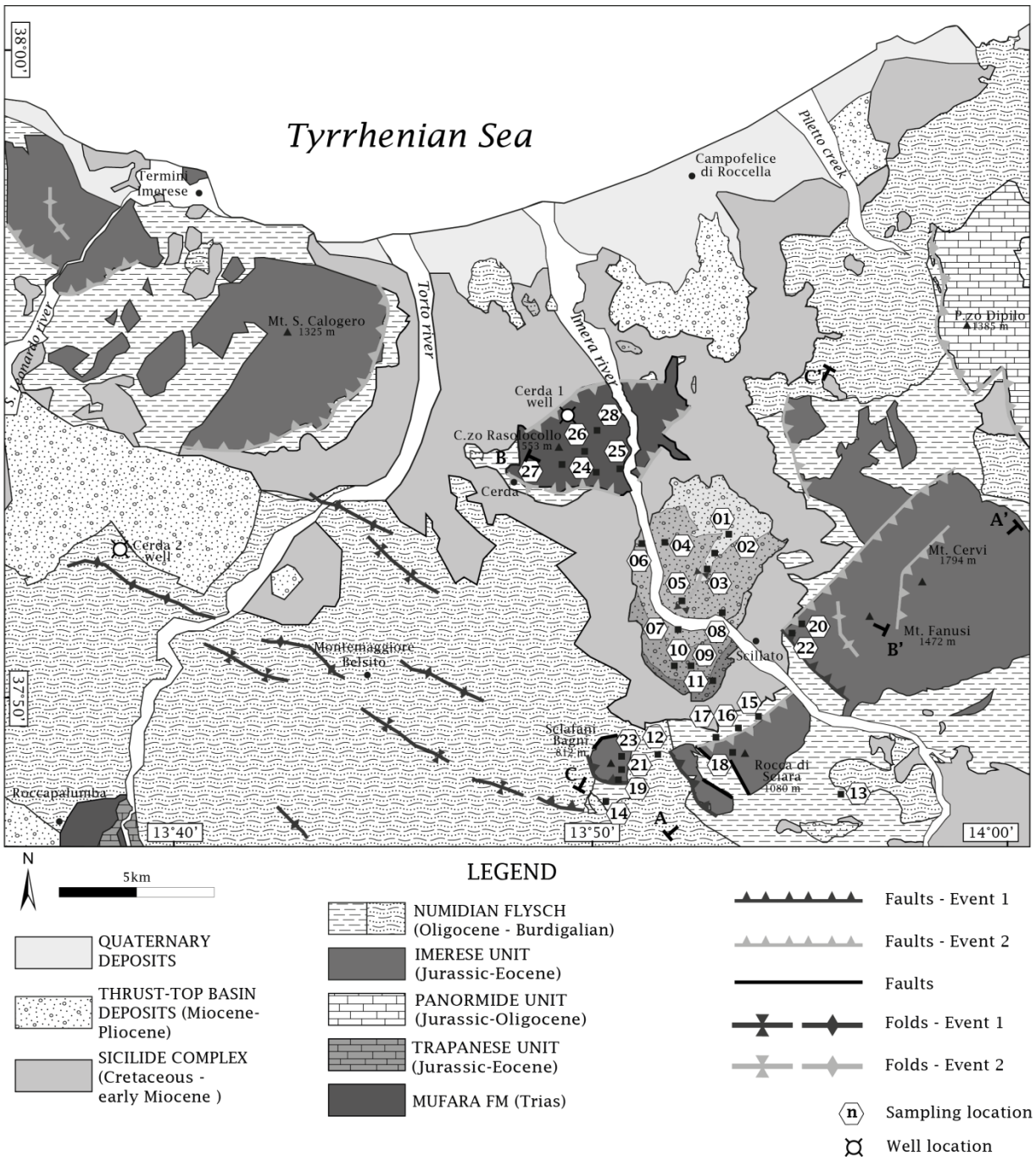

Figure 2.3 - Tectonic sketch map of the study area with sampling sites (modified after Catalano et al., 2011). Location of cross-sections of Figs. 2.7 and 2.8 is shown.

Since the middle Miocene the study area recorded a polyphase deformation. During the Serravallian, the emplacement of the allochtonous units (Numidian Flysch, Sicilide Complex, Imerese-Sicanian units) onto the Trapanese-Hyblean foreland through low-angle regional thrusts produced shallow seated structures (Event I in Fig. 2.3) with a present-day SW-ward tectonic transport (Catalano et al., 2000; Avellone et al., 2010; Gasparo Morticelli et. al., 2015). During

the latest Tortonian-early Pleistocene, the ongoing compressional deformation gave rise to the nucleation of deep-seated thrusts which re-folded and breached the previously stacked thin-skinned tectonic units, along high angle transpressive faults (Event II in Fig. 2.3; Bello et al., 2000; Catalano et al., 2000; Gasparo Morticelli et al., 2015).

Structures generated as a consequence of the two tectonic events are strongly non-coaxial and their present-day setting can be explained by the occurrence of large vertical-axis clockwise rotations (Fig. 2.1; Channel et al., 1980, 1990; Grasso et al., 1987; Oldow et al., 1990; Speranza et al., 1999, 2003, 2018; Avellone and Barchi 2003; Guarnieri, 2004; Monaco and De Guidi, 2006; Avellone et al., 2010; Cifelli and Mattei 2010; Barreca and Monaco, 2013); which decrease from the internal units (e.g., Imerese and Panormide units ~130°) toward the foreland (e.g. no rotation in the Sciacca area). Part of this rotation (~ 25°) is post- Early Pliocene in age (Grasso et al., 1987). Wedge-top basins, as well as the Scillato Basin, record with their shape, internal architecture and sedimentary fill, these two tectonic events (Gugliotta et al., 2014).

2.3.1. Deformed pre-orogenic substratum of the Scillato wedge-top basin

The substratum of the Scillato wedge-top basin is made up of thrust sheets mainly deforming the Imerese unit (Upper Triassic–Eocene), the Numidian Flysch (Upper Oligocene-Lower Miocene), the Sicilide Complex (Cretaceous-early Miocene) and the Lercara unit exposed in the north-western part of the study area (Fig. 2.3; Mt. Rasolocollo-Cerda area; Di Stefano and Gullo 1997; Giunta et al., 2000a).

The Imerese marly-cherty-calcareous succession in pelagic basin facies is exposed along the Mt. Cervi, Rocca di Sciara and Sclafani Bagni (CRSSB) structural alignment and the Mt. S. Calogero structure (Fig. 2.3). From the bottom, the Imerese succession (Fig. 2.4B) is subdivided into: the Carnian Mufara Fm. (~300m thick); the Carnian-Rethian cherty limestones (Scillato Fm. about 650 m thick); the lower Jurassic dolostones of the Fanusi Fm. up to 200 m thick; the lower Jurassic-upper Cretaceous shales, limestones and radiolarites of the Crisanti Fm. with a thickness

of 350 m and the uppermost Paleocene-lowermost Oligocene marls and limestones of the Caltavuturo Fm. about 150 m thick. Late Oligocene-Langhian Numidian Flysch (from 300 m up to 2,000 m thick) covers the Caltavuturo Fm. and it is mainly composed of claystones/siltstones with subordinates quarzarenites evolving to quarzarenites alternating with thin-bedded claystones and siltstones toward the top.

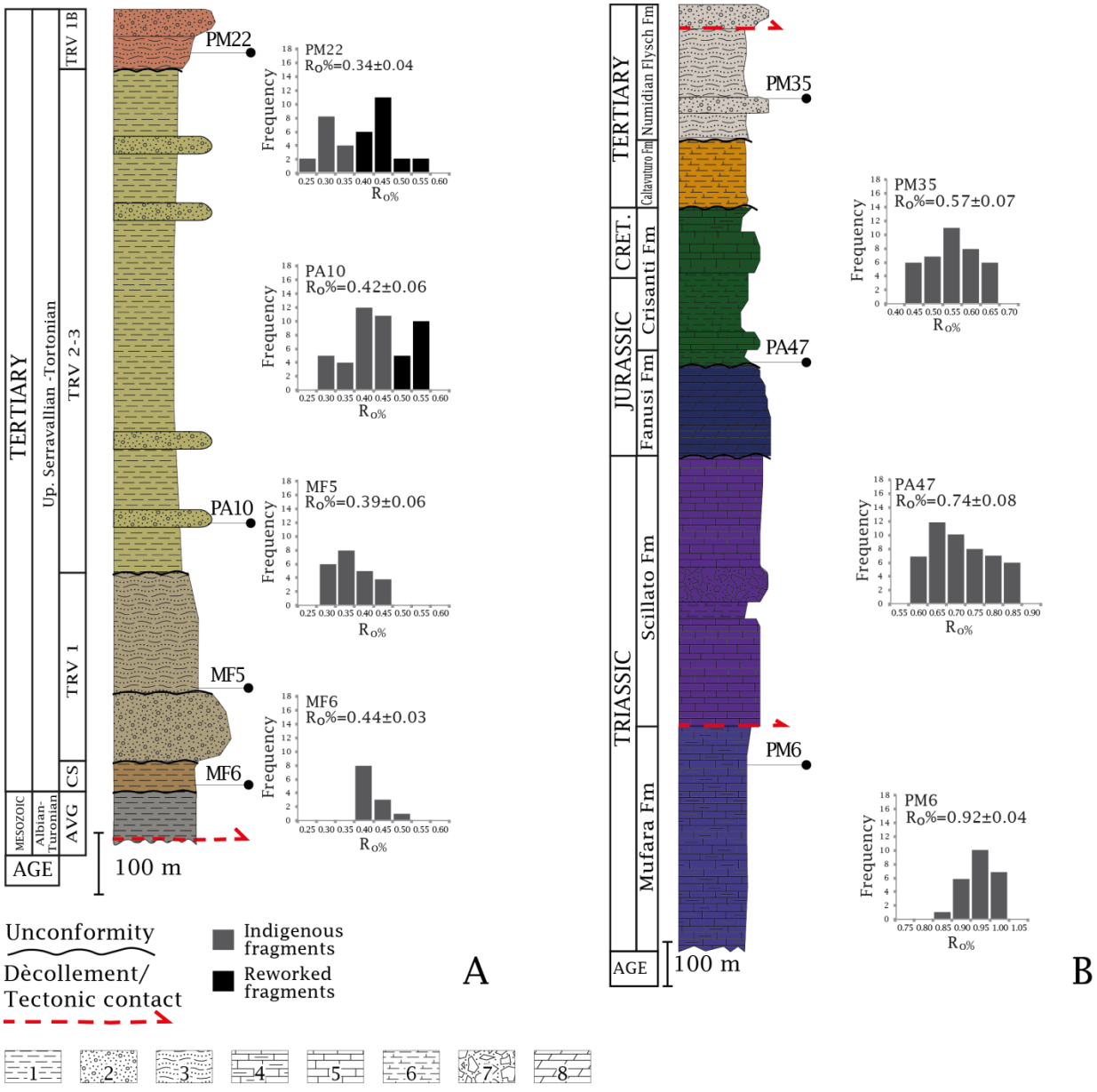

Figure 2.4 Simplified stratigraphic columns of the Scillato wedge-top basin (A) and Imerese unit (B) successions, with representative histograms of vitrinite reflectance data. Main unconformities and detachment levels are indicated. Cal—Caltavuturo Fm; AVG— Sicilide Complex.; CS—Castellana Sicula Fm; TRV1—Terravecchia 1 member; TRV2-3, TRV1B—Terravecchia 2-3 and 1b members. 1—claystones/shales; 2—gravelly sandstones/conglomerates; 3—sandstones; 4—alternating limestones/shales/sandstones; 5—limestones; 6—marls; 7—breccias; 8—dolostones.

The Sicilide Complex is made up of Cretaceous-early Miocene highly deformed claystones, marls and limestones up to 300 m thick. The Imerese and Sicilide successions (Fig. 2.4) show strong vertical and lateral variations also of mechanical proprieties (Avellone et al., 2010) which affect the geometry of the SFTB, generating detachment levels and disharmonic and/or polyharmonic folds. Major detachment levels occur in the Mufara Fm., the basal portion of the Numidian Flysch and in the Sicilide Complex.

The Lercara unit has been drilled in several wells in the SFTB (e.g., Cerda 1, Cerda 2, Vicari 1, Roccapalumba 1; Miuccio et al., 2000; Basilone et al., 2016a) and consists of a Permian-Triassic siliciclastic and carbonate succession. Various authors (Catalano et al., 1991; Flügel et al., 1991; Kozur et al., 1996; Di Stefano and Gullo, 1997; Di Stefano et al., 2012; Basilone et al., 2016a) described the Lercara unit as made up of turbidites passing upward to deep water limestones and siliciclastic deposits with a minimum thickness of about 2.1 km.

The subsurface extension of the Triassic deposits in the Cerda 1 well (Fig. 2.2, 2.3 for location) is ~3 km (probably due to tectonic thickening since maximum thickness evaluated for the Mufara Fm. is ~300m; Basilone et al., 2016a) where they are mainly composed of claystones locally rich in organic matter, limestones, calcareous breccias, and quartz-rich sandstones. The Lercara unit in western Sicily shows the juxtaposition of the Numidian Flysch onto the Mufara Fm. (Fig. 2.3). This boundary has been interpreted either as an extensional detachment (Giunta et al., 2000a) or a younger-on-older thrust (Di Stefano and Gullo, 1997). In the study area, the boundary between the Mufara Fm. and the Numidian Flysch is not well exposed and understood and the Mufara Fm. is bordered to the East and the West by NNE-SSW high angle faults (Fig. 2.3).

2.3.2. Scillato wedge-top basin

The Scillato wedge-top basin is located in the central-northern sector of the SFTB, along the western edge of the Madonie Mts. (Figs. 2.1 and 2.3). It consists of a local NNE-SSW oriented structural trough ~3.5 km-wide and ~6 km-long. The basin is bounded by the CRSSB structural

highs to the SE and the Mt. S. Calogero structure to the NW. The upper Serravallian-upper Tortonian basin fill is composed of about 1,250 m thick open marine and delta-river siliciclastic sediments (Gugliotta and Morticelli, 2012; Gugliotta et al., 2014). The sedimentary succession is subdivided into the Castellana Sicula and Terravecchia Fms. (Fig. 2.4A).

The Castellana Sicula Fm. is constituted by 50 m thick hemipelagic clays, siltstones, gravity flow sandstones and conglomerates of late Serravallian-early Tortonian age deposited in an outer shelf-to-slope setting.

The Terravecchia Fm. (Upper Tortonian) is up to 1,200 m thick and it is constituted by a coarsening-to-fining upward to a fining-to-coarsening upward sedimentary succession made up of different lithotypes: (i) conglomerates and sandstones (alluvial and paralic facies), (ii) sandstones, (iii) marls and clays (transitional to shallow-marine facies). In detail, it is subdivided into three members bounded by unconformities, namely from bottom (Figs. 2.3 and 2.4): Terravecchia 1, Terravecchia 2-3 and Terravecchia 1b (TS1, TS2 and RS, respectively, in Gugliotta et al., 2012). The Terravecchia 1 member, about 300 m thick, is mainly composed of red conglomerates with metamorphic pebbles and sandstones passing upward to claystones/siltstones indicating a gravelly braided fluvial system. The Terravecchia 2-3 member, up to 800 m thick, is mainly composed of interbedded siltstones, cross-bedded sandstones to siltites and clayey siltites. The Terravecchia 1b, 100 m thick, is mainly composed of silts and clays interbedded with conglomeratic bodies passing to cross-bedded sandstones and conglomerates.

2.4. Methods and Materials

2.4.1. Organic matter optical analysis

Organic matter optical analysis was performed on dispersed organic matter from twenty-three samples. Eleven samples were collected from claystones/siltstones of the Castellana Sicula Fm and the sandy portions of the Terravecchia Fm. Twelve samples were collected from the

deformed substratum of the Scillato wedge-top basin (Fig. 2.3) and they pertain to claystones/siltstones of the Mufara Fm. located in the Mt. Rasolocollo - Cerda area, to the Crisanti organic-rich shales and to the Numidian Flysch sandstones/claystones, exposed along the CRSSB structural alignment. Samples were collected at distance > 1 m from major faults in order to avoid potential temperature increase due to frictional heating (Balsamo et al., 2014).

Whole-rock samples were crushed in an agate mortar, mounted in epoxy resin and polished according to standard procedures (Bustin et al., 1990). Vitrinite reflectance (R_o%) measurements were performed on randomly oriented grains using a Zeiss Axioplan microscope, under oil immersion (n=1.518) in reflected monochromatic non-polarized light, equipped with a J&M reflectance system. Various reflectance standards (R_o% = 0.426%; 0.595% and 0.905) were used for calibration. The number of measurements ranges from 10 in samples with small amounts of organic matter to 50 for organic matter-rich specimen. On each sample, measurements were carried out on unaltered, non-oxidized, and unfractured fragments of humite-vitrinite macerals and coal seams. Mean reflectance values were calculated using the arithmetic mean of these measurements.

2.4.2. X-ray diffraction (XRD) analysis

A suite of twenty-seven samples (Fig. 2.3) was collected from the wedge-top succession (eleven samples) and its substratum (sixteen samples). In the Scillato wedge-top basin, samples are from claystones/siltstones of the Castellana Sicula and Terravecchia Fms. In the substratum, samples are from the Mufara Fm., the shales of the Crisanti Fm., the reddish marls of Caltavuturo Fm., and from the Numidian Flysch cropping out along the CRSSB structural alignment.

Qualitative and semi-quantitative analyses of the <2 μm grain-size fraction (equivalent spherical diameter) were performed using a Scintag X1 X-ray system (CuKα radiation). After centrifugation, the suspension containing the <2 μm grain-size fraction was decanted, pipetted, and dried at room temperature on glass slides to produce a thin highly oriented aggregate. Oriented air-dried samples were scanned from 1° to 48° 2θ with a step size of 0.05° 2θ and a

count time of 4 s per step at 40 kV and 45 mA. The presence of expandable clays was determined for samples treated with ethylene glycol at 25 °C for 24 h. Ethylene glycol–solvated samples were scanned at the same conditions as air-dried aggregates, with a scanning interval of 1°–30° 2θ. Expandability measurements were determined according to Moore and Reynolds (1997) by using the Δ2θ method after decomposing the composite peaks between 9°–10° and 16°–17° 2θ with Pearson VII functions.

2.4.3. 3D Geological modelling

Twenty-eight original geological cross-sections (Fig. 2.1 C for location) were used to build the 3D basin geometry of the Scillato wedge-top basin and its pre-orogenic substratum. Geological cross-sections were first reconstructed using Move software (Midland valley). From older to younger, the represented horizons are: top Mufara, top Scillato, top Crisanti, top Caltavuturo and top Numidian Flysch which describe the Imerese substratum and top Castellana Sicula, top Terravecchia 1 and top Terravecchia 2-3 which refer to the wedge-top basin units.

The Imerese succession has been modelled assuming layer cake geometry, as lateral heterogeneities of the pelagic facies in the study area can be neglected. Stratigraphic horizons and faults after a first check of consistency (e.g., no overlaps and intersections) have been exported as pointsets (.dat file) and imported in Skua-Gocad software to construct a more refined water-tight 3D geological model. A 3D model is said to be water-tight when every stratigraphic horizon is continuously defined over the area of interest and has clean intersections with either lateral boundaries, faults, unconformities or erosion surfaces (Caumont et al., 2004).

Only major faults with vertical displacements >500 m and longer than 3km have been exported. Smaller faults geometrically close and belonging to the same set were merged (e.g., faults bounding the CRSSB alignment), in order to reduce the complexity of the model and its simulation time.

Stratigraphic horizons and faults have been interpreted individually by Move software (e.g., Tanner et al., 2003) and simultaneously by the Skua software (Jayr et al., 2008). Skua

technology is based upon the definition of stratigraphic horizons, as values of a parametric function on a tetrahedral support (e.g., Frank et al., 2007). A chronostratigraphic scale has been built using the selected horizons to guarantee that no horizons crossing occurs. The software offers the possibility to choose different types of geological boundary: conformable, unconformable, baselap and erosive. Stratigraphic horizon tops for the Imerese unit have been selected as conformable, whereas boundaries between the wedge-top horizon tops are unconformable. A volume of interest (V.O.I. = 26 x 38 x 8 km) which indicates the amount of three-dimensional space occupied by faults and horizons, has been defined to include the interpreted structures. The first step in the 3D model construction results in a fault network that interpolate the fault points and defines the branching relations of the various sets of faults. Once the V.O.I. is split into fault blocks bounded by the interpreted faults, the horizons are constructed, for each stratigraphic sequence. Horizons are defined as isovalues of a spatial varying function representing the stratigraphic time in the faulted blocks. As a consequence, horizon-fault definitions are consistent and geometrical cuts on faults are clean. Building a water-tight model is also a good test on the quality of the data. Whenever some data points are incorrectly interpreted, for example, being assigned to the wrong side of a fault, the resulting time function becomes geologically incorrect. Thus, the possibility of consistently interpreting and building a water-tight model is a first step in the quality control of the resulting model.

2.5. Results

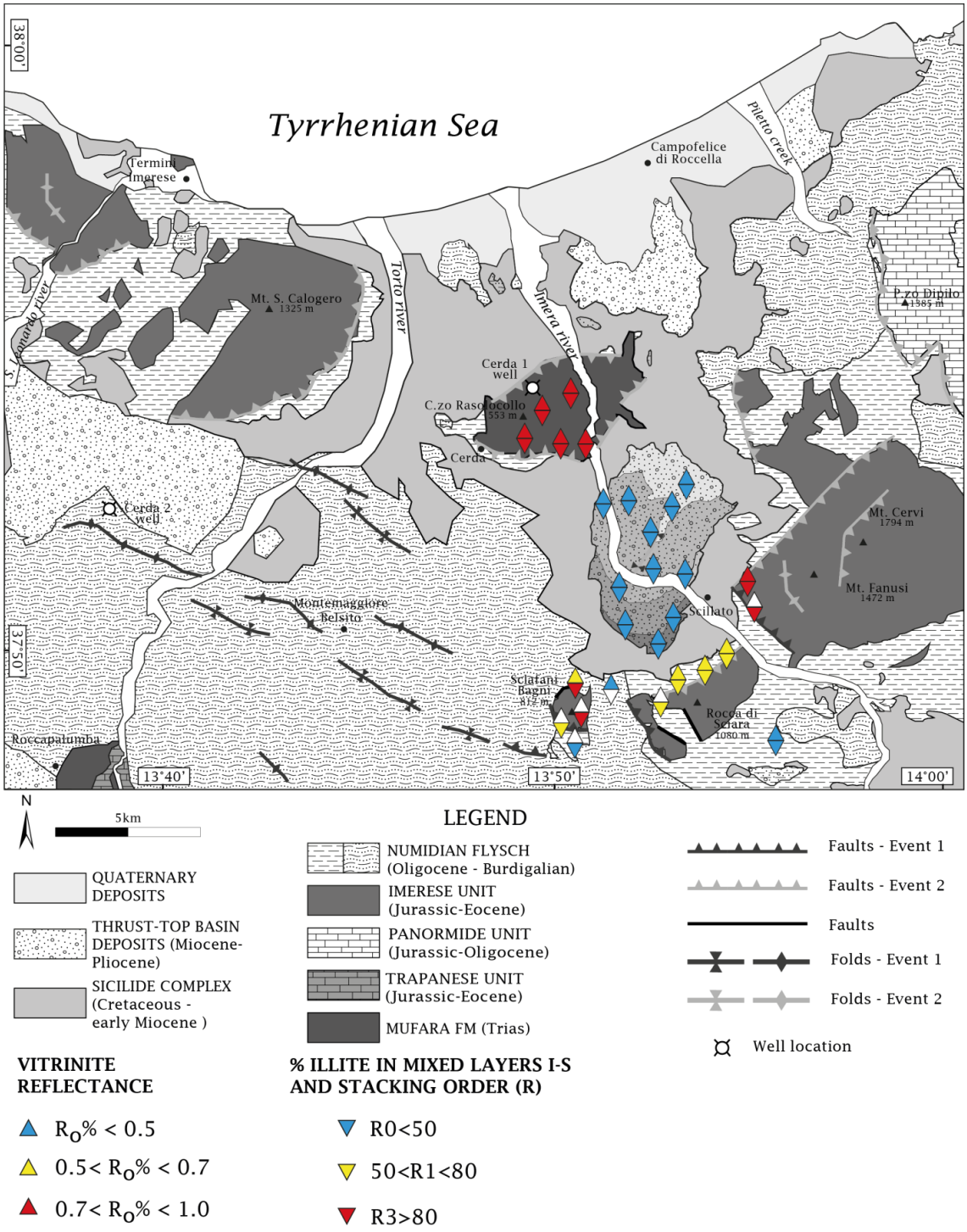

Figure 2.4 - Map distribution of R_o% and illite content in mixed layers illite-smectite (%I in I-S) and stacking order data.

Site	Sample	Coordinates	Formation	Age	R_o% (± s.d.)	X-ray analysis (<2μm)	%I in I-S and stacking order	%C in C-S
01	PM22	37°53'12.78"N 13°53'34.20"E	Terravecchia 1b	up. Tortonian-low. Messinian	0.33±0.04	I_{26} I-S_{24} K_{40} Chl_{10} *	R0 40 + R1 78	
02	PM23	37°52'56.28"N 13°53'16.55"E	Terravecchia 1b	up. Tortonian-low. Messinian	0.42±0.04	I_{31} I-S_{18} K_{40} Chl_{11} *	R0 42 + R1 78	
03	PM28	37°52'37.18"N 13°52'58.36"E	Terravecchia 1b	up. Tortonian-low. Messinian	0.47±0.06	I_{24} I-S_{21} $K_{43}Chl_{12}$ *	R0 42 + R1 78	
04	PM29	37°53'4.24"N 13°52'11.28"E	Terravecchia 2-3	up. Tortonian-low. Messinian	0.46±0.03	I_{28} I-S_{21} K_{36} Chl_{15} *	R0 42 + R1 78	
05	PM25	37°51'58.04"N 13°52'33.68"E	Terravecchia 2-3	up. Tortonian-low. Messinian	0.44±0.02	I_{29} I-S_{22} K_{35} Chl_{14} *	R0 42 + R1 78	
06	PM14	37°53'13.90"N 13°51'43.15"E	Terravecchia 2-3	up. Tortonian-low. Messinian	0.47±0.03	I_{30} I-S_{19} K_{33} Chl_{18} *	R0 40 + R1 78	
07	PA10	37°51'35.30"N 13°52'23.52"E	Terravecchia 2-3	up. Tortonian-low. Messinian	0.42±0.06	I_{25} I-S_{24} K_{37} Chl_{14} *	R0 50 + R1 80	
08	PM18-19	37°51'44.71"N 13°53'25.29"E	Terravecchia 2-3	up. Tortonian-low. Messinian	0.42±0.03	I_{26} I-S_{22} K_{36} Chl_{16}	R0 45 + R1 70	
09	PA08	37°50'56.37"N 13°52'42.47"E	Terravecchia 1	up. Tortonian-low. Messinian	0.38±0.05	I_{28} I-$S_{24}K_{34}Chl_{14}$	R0 50 + R1 80	
10	MF5	37°50'58.33"N 13°52'34.42"E	Terravecchia 1	up. Tortonian-low. Messinian	0.39±0.06	I_{34} I-$S_{22}K_{38}Chl_6$	R0 50 + R1 80	
11	MF6	37°50'44.98"N 13°53'14.10"E	Castellana Sicula	up. Serravallian-low. Tortonian	0.45±0.03	I_{24} I-S_{35} K_{39} Chl_2	R0 50	
12	PA44	37°49'50.00"N 13°51'49.20"E	Numidian Flysch	up. Oligocene-low. Miocene	0.46±0.05			
13	PA60	37°48'53.8'' 13°55'36.8''	Numidian Flysch	up. Oligocene-low. Miocene	0.40±0.07	I_9 I-S_{14} K_{73} Chl_4	R0 50 + R1 78	
14	PA43	37°48'44.40"N 13°51'10.80"E	Numidian Flysch	up. Oligocene-low. Miocene		I_7 I-S_{10} K_{83}	R1 55	
15	PM35	37°50'22.40"N 13°54'34.50"E	Numidian Flysch	up. Oligocene-low. Miocene	0.57±0.07	I_{24} I-S_{23} K_{52} Chl_1 *	R1 70	
16	PM34	37°50'3.51"N 13°53'50.35"E	Numidian Flysch	up. Oligocene-low. Miocene	0.54±0.04	I_{37} I-S_{22} K_{13} Chl_{28} *	R1 76	
17	MF4	37°49'52.81"N 13°53'36.23"E	Numidian Flysch	up. Oligocene-low. Miocene	0.57±0.04	I_{16} I-S_6 K_{70} Chl_8	R1 72	
18	PA45	37°49'37.70"N 13°53'32.20"E	Caltavuturo	up. Paleocene -low. Oligocene		I_{47} I-S_{13} C-S_{21} Chl_{19}	R1 78	80
19	PA41	37°49'4.40"N 13°51'19.70"E	Caltavuturo	up. Paleocene -low. Oligocene		I_{20} I-S_{19} C-S_{32} Chl_{29}	R1 78	80
20	PA46	37°51'36.70"N 13°54'50.60"E	Crisanti	up. Toarcian - Albian		I_{72} I-S_{12} Chl_{16}	R3 83	
21	PA40	37°49'13.80"N 13°51'23.90"E	Crisanti	up. Toarcian - Albian		I_{69} I-S_{23} Chl_8	R3 83	
22	PA47	37°51'38.20"N 13°54'52.20"E	Crisanti	up. Toarcian - Albian	0.74±0.08	I_{65} I-S_{33} Chl_2	R3 85	
23	PA39	37°49'22.90"N 13°51'23.30"E	Crisanti	up. Toarcian - Albian	0.68±0.08	I_{76} I-S_{16} K_7 Chl_1	R3 86	
24	PM1	37°54'19.59"N 13°50'39.61"E	Mufara	middle-upper Carnian	0.83±0.05	I_{38} I-S_{26} Chl_{36}	R3 86	
25	PM2	37°54'23.67"N 13°51'10.38"E	Mufara	middle-upper Carnian	0.82±0.05	I_{40} I-S_{28} Chl_{32} *	R3 84	
26	PM6	37°54'37.82"N 13°50'19.79"E	Mufara	middle-upper Carnian	0.92±0.04	I_{44} I-S_{37} C-S_{13} K_3 Chl_3	R3 84	60
27	PM7	37°54'34.72"N 13°49'59.63"E	Mufara	middle-upper Carnian	0.83±0.05	I_{30} I-S_{16} C-S_{19} $K_{11}Chl_{24}$	R3 83	80
28	PM5	37°54'43.68"N 13°50'30.19"E	Mufara	middle-upper Carnian	0.94±0.05	I_{25} I-S_{16} C-S_{36} K_{10} Chl_{13} *	R3 84	80

Note: **R_o%—vitrinite reflectance; s.d.—standard deviation; I—illite; I-S—mixed-layer illite-smectite; C-S—mixed-layer chlorite-smectite; K—kaolinite; Chl—chlorite; R parameter—mixed layer illite-smectite stacking order; %I in I-S—illite content in mixed layers illite-smectite; %C in C-S—chlorite content in mixed layers chlorite-smectite. Subscript numbers correspond to mineral weight percentage. *Rectorite**

Table 2.1 - Organic matter maturity and clay mineralogy data for the Scillato wedge-top basin and its deformed substratum

2.5.1. Organic matter optical analysis

2.5.1.1. Deformed pre-orogenic substratum

Samples from the Mufara, Crisanti and Numidian Flysch Fms provided suitable results for the organic matter optical analysis (Fig. 2.5). No significant variation of levels of thermal maturity and trend has been recognised in the CRSSB structural alignment. The Mufara Fm. contains small maceral fragments (10 - 20 μm) which belong to the huminite-vitrinite and inertinite groups. R_o% values ranging between 0.82% and 0.94% (sites 28-24, Tab. 2.1) indicate middle-late mature stages of hydrocarbon generation. Organic matter in the Crisanti Fm. is abundant and mainly made up of maceral fragments belonging to the huminite-vitrinite and inertinite groups. R_o% values of 0.68% and 0.74% (sites 22 and 23, Tab. 2.1) indicate early-middle mature stages of hydrocarbon generation. Organic matter in the Numidian Flysch is mainly made up of macerals which belong to the huminite-vitrinite and subordinately the inertinite groups. Vitrinite fragments, 30 - 60 μm in size, are typically fractured. Pyrite, either finely dispersed or in small globular aggregates, is locally present. R_o% values ranging between 0.40% and 0.57% indicate immature to early mature stages for hydrocarbon generation. In conclusion, the succession shows an increase of levels of thermal maturity as a function of stratigraphic age (Fig. 2.4).

2.5.1.2. Scillato wedge-top basin

Organic matter dispersed in the Castellana Sicula and Terravecchia Fms is heterogeneous and mainly composed of macerals belonging to the huminite-vitrinite and subordinately to the inertinite groups. Pyrite, either finely dispersed or in small globular aggregates, is locally present, associated with both groups of macerals. The Castellana Sicula Fm. (site 11, Tab. 2.1) has a R_o% value of 0.45%. The Terravecchia 1 member shows R_o% values of 0.38%-0.39% (sites 09-10, Tab. 2.1) and the Terravecchia 2-3 member displays R_o% values ranging between 0.42% and 0.47% (sites 04-08, Tab. 2.1). The Terravecchia 1b member has macerals with R_o% values between 0.33% and 0.47% (sites 01-03, Tab. 2.1). In particular, two samples (PA10 and

PM22 in Fig. 2.4) show two separate clusters of R_o% values indicating both indigenous (0.33-0.42%) and reworked (0.49-0.55%) populations of vitrinite fragments.

The Castellana Sicula Fm. and the Terravecchia 1 member are characterized by a thermal maturity increase as a function of stratigraphic age. On the contrary, the Terravecchia 2-3 and Terravecchia 1b are characterized by a reverse trend, showing an increase of R_o% values moving upward in the succession (Fig. 2.4), interpreted as due to reworked organic fragments. Generally, the entire succession experienced the immature stage of hydrocarbon generation (Fig. 2.5).

2.5.2. X-ray diffraction analysis on fine grained sediments

2.5.2.1. Deformed pre-orogenic substratum of the Scillato wedge-top basin

X-ray diffraction analysis for the Numidian Flysch and the Imerese succession is listed in Tab. 2.1. Clay minerals assemblage for the Mufara Fm. (sites 24-28, Tab. 2.1) is mainly constituted by illite ranging from 25% to 44%, mixed-layers I-S (16-37%), and chlorite (up to 36%). In the basal portion of the Mufara Fm. (sites 26-28, Tab. 2.1), mixed layers chlorite-smectite (13-36%) and kaolinite (3-11%) occur. The Crisanti Fm. is characterized by illite (65-76%), mixed-layers I-S (12-33%), and subordinate amounts of chlorite. Kaolinite occasionally occurs in sample PA39 (site 23, Tab. 2.1). The Caltavuturo Fm. (sites 18-19, Tab. 2.1) contains illite (20-47%), mixed-layers I-S (13-19%) and chlorite-smectite (21-32%) and chlorite (19-29%). The Numidian Flysch (sites 13-17, Tab. 2.1) is mainly constituted by a kaolinite-rich assemblage with contents between 13% and 83% and subordinate amounts of illite (from 7% to 37%), mixed-layers I-S (6-23%) and chlorite (up to 28%). X-ray diffraction patterns of the Numidian Flysch and the Mufara Fm. display the occurrence of first order superstructure reflection of rectorite (sites 15, 16, 25 and 28).

Random-ordered I-S (R0) with high expandability (50% of illitic layers), that characterize the upper portion of the Numidian Flysch, convert into short range ordered structures (R1) with an illite content of 55–78% in the lower portion of the Numidian Flysch and Caltavuturo Fms (sites

12-19, Tab. 2.1) and evolve to long-range ordered structures (R3) in the Crisanti and Mufara Fms. (sites 20-28, Tab. 2.1) with an illite content of 83-86%. The Numidian Flysch and the Caltavuturo Fm. experienced levels of thermal maturity consistent with early diagenetic conditions whereas the Crisanti and Mufara Fms underwent deeper burial in late diagenesis (Merriman and Frey, 1999; Aldega et al., 2007).

2.5.2.2. Scillato wedge-top basin

XRD analyses of the <2 μm grain-size fraction for the Terravecchia and Castellana Sicula Fms are shown in Tab. 2.1. Castellana Sicula Fm. (site 11, Tab. 2.1) is mainly constituted by mixed-layers illite-smectite (35%) and kaolinite (39%) and subordinate amounts of illite (24%). Chlorite does not exceed 2%. Mixed layers I-S are randomly ordered structures with an illite content of 50% (Fig. 2.4).

Terravecchia 1 member (sites 09-10, Tab. 2.1) is composed of kaolinite (36% mean value), illite (31%), mixed-layers illite-smectite (23%), and chlorite (10%). Similar mineralogical assemblages and contents were observed in the Terravecchia 2-3 member (sites 04-08, Tab. 2.1) that is constituted by kaolinite (33-37%), illite (25-30%), mixed-layers illite-smectite (19-24%) and chlorite (14-18%). In the Terravecchia 1b member (sites 01-03, Tab. 2.1) kaolinite is the most abundant clay mineral with contents of 43%, followed by illite (24-31%), mixed-layers illite-smectite (18-24%) and chlorite (10-12%).

Two population of mixed-layers I-S with different composition and stacking order have been recorded in the Terravecchia Fm. and have been interpreted as a mixture of diagenetic and inherited phases. I-S with no preferred sequence in stacking of layers (R0) show a slight increase of illite content as a function of stratigraphic age from 40% to 50% indicating burial diagenesis (Fig. 2.4), whereas short-range ordered I-S (R1) with illite contents of 70%-80% show no correlation with depth and have been interpreted as inherited phases. Both in the Terravecchia 2-3 and in the Terravecchia 1b members, XRD patterns show the first order superstructure

reflection (d-spacing: ~2.7 nm) which correspond to mixed-layer clay minerals with alternating layer types of illite and smectite (rectorite).

2.5.3. 3D Geological modelling

Reconstructed geological cross-sections (Fig. 2.1 C) are both NE-SW oriented (perpendicular to main thrusts direction) and NW-SE oriented (perpendicular to the high angle transpressive faults direction) in order to build the 3D model extrapolating thrusts and high angle faults both laterally and at depth. The main constraint for depths is from the SIRIPRO seismic reflection profile (Fig. 2.2). According to the seismic profile interpretation (Catalano et al., 2013a), the Imerese unit reaches depths of 5-6 km. Thrust geometry and their lateral connections were reconstructed by using field data and geological maps (Brocquet, 1969; Mascle, 1979; Catalano et al., 2011; Gugliotta and Gasparo Morticelli, 2012; Barreca and Monaco, 2013). NE-dipping thrust sheets characterizing Mt. Cervi, Mt. San Calogero and Rocca di Sciara, Sclafani Bagni structures are exhumed and emergent due to the high angle transpressive faults activity.

Between these structures and toward the SW, folds showing the same orientation of emerging thrust (NW-SE), affecting the Numidian Flysch are observed. Blind thrusts have then been interpreted and reconstructed at the base of these folds. Conversely, the thrust fault affecting the Lercara unit shows a different orientation (WNW-ESE).

Based on reconstructed cross-sections, the geological model for the study area was firstly built by using Move software, which allows to obtain a $2\frac{1}{2}$ D model (Fig. 2.6A) and then, by SKUA-GOCAD software, which allows to reconstruct the 3D geometry (Fig. 2.6B, C). The Move model allows to detect two main fault sets with clear intersection relationships: i) NW-SE striking thrusts with SW-ward tectonic transport (blue faults in Fig. 2.6A); ii) NE-SW high angle transpressive faults (red faults in Fig. 2.6A). The 3D representation creates a geometrically consistent model, where seven major high angle faults displace four main thrusts (Fig. 2. 6B).

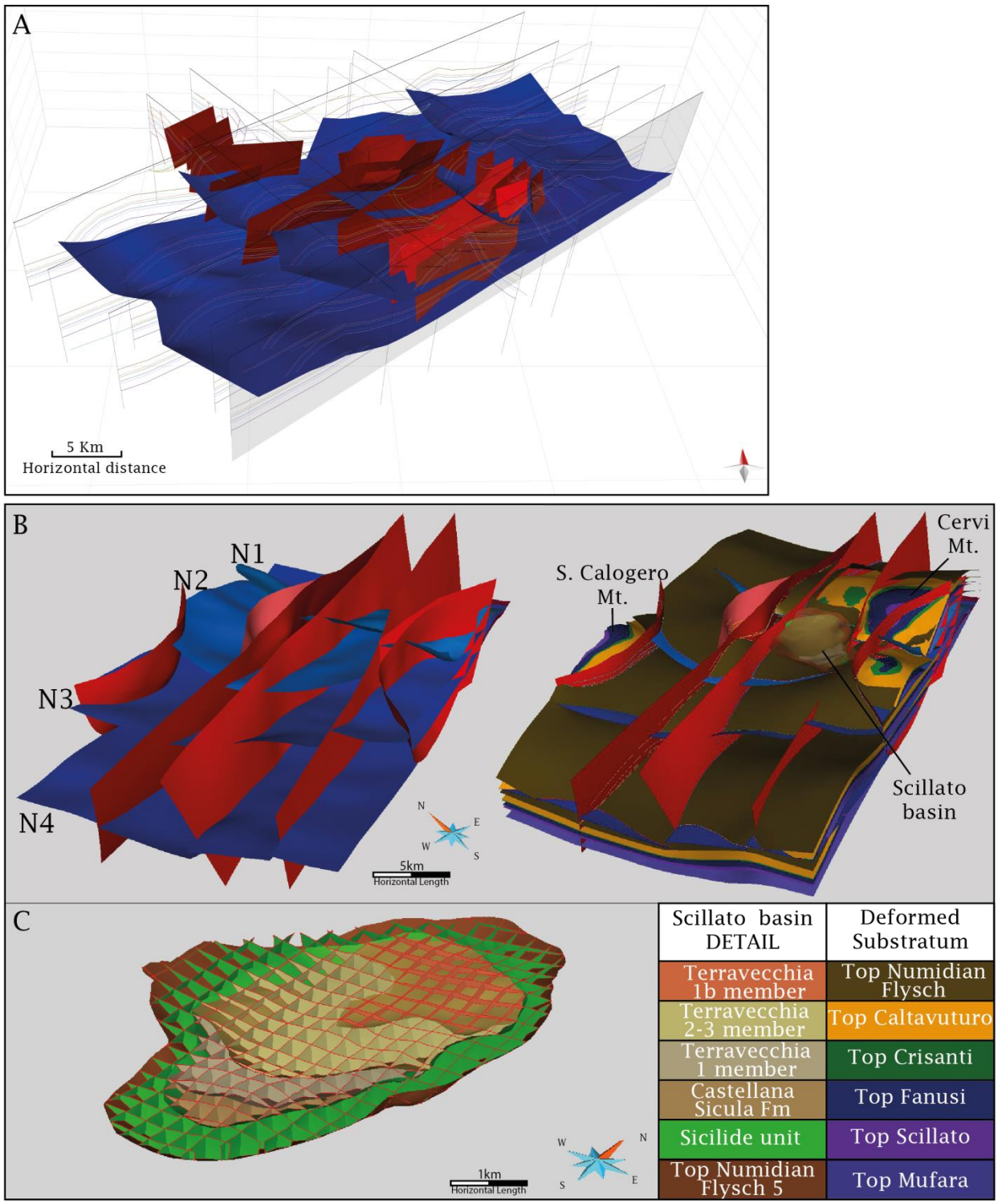

Figure 2.6 - A) Geological model reconstructed using Move software and constrained by original geological cross-sections (see Fig. 1C for location). Blue surfaces indicate thrusts related to the first tectonic event; red surfaces indicate high angle transpressive faults related to the second tectonic event. Horizons representing tops of different formations are shown along the cross-sections. (B) 3D geological model extracted by Skua Gocad software. The model to the left shows faults surfaces: blue surfaces indicate thrusts namely N1, N2, N3 and N4; red surfaces indicate high angle transpressive faults. In the model to the right, horizons representing tops formation and location of Scillato wedge-top basin, S. Calogero and Cervi Mts., preserved from erosion, are shown. (C) Detailed 3D geological model for the Scillato wedge-top basin. Surfaces for the Castellana Sicula Fm. and Terravecchia members are reconstructed above the deformed substratum made up of the Sicilide Complex and Numidian Flysch.

In general, NE-dipping thrusts (labelled N1, N3 and N4 in Fig. 2.6B) deform the Imerese succession and the Numidian Flysch creating hangingwall ramp open anticlines. The NNE-dipping thrust (N2 in Fig. 2.6B) branches against N1 thrust and involves the Lercara unit. Thrust dip angles vary from almost horizontal along the basal detachment level (Mufara Fm.) up to ~40° close to N1 thrust emergence (SW edge of Mt. Cervi). These faults describe an imbricate thrust system (Boyer and Elliott, 1982; McClay, 1992). Reconstructed thrust displacement and dip angles increase toward the NE. In the south-western sector, deformation is accommodated by major folds and the Scillato wedge-top basin depocenter is located within the synform generated between N1 and N3 thrusts (Fig. 2.6B).

High angle faults (red faults in Fig. 2.6B) striking NE-SW, are almost vertical and cut the pile of thin-skinned thrusts, involving deeper crustal levels. Faults displacement increases toward NE along the CRSSB alignment and across the Mt. S. Calogero structure, as shown in the official geological map of the area (Catalano et al., 2011). In the north-eastern portion of the study area, the interaction between thrusts and high angle faults generates a non-coaxial fold system (axes show two preferential distributions NW-SE and NE-SW) recognised in the gentle dome of the Mt. Cervi structure (Barreca and Monaco, 2013). The second fault set generates a main depocenter located between the CRSSB alignment and Mt. S. Calogero. The 3D model of Figure 2.6 C shows the geometry of Scillato wedge-top basin characterised by: i) depocenter migration toward the N through time, recorded by the decreasing dip angles of the evolving Terravecchia Fm., from ~40° (Terravecchia 1 member) to ~10° (Terravecchia 1b member); ii) NNE-SSW elongated synform.

2.6. Discussion

2.6.1. Thermal maturity of the Scillato wedge-top basin and its pre-orogenic substratum

Burial and thermal models of the Scillato wedge-top basin and its deformed substratum were carried out using BASIN MOD 2D software and have been calibrated against the indigenous

population of vitrinite reflectance data and authigenic mixed layers I-S. For this reason, we considered: a R_o% value of 0.45% and I% in mixed-layer I-S value of 50% (site 11, Tab. 2.1) for the Castellana Sicula Fm.; R_o% values ranging between 0.38 and 0.42 (sites 07-10, Tab.2.1) and I% ranging between 40% and 50% (sites 04-10, Tab 2.1) for the Terravecchia 1 and 2-3 members; a R_o% value of 0.33% (site 01, Tab 2.1) and I% in I-S ranging between 40% and 42% (sites 01-03 Tab 2.1) for the Terravecchia 1b member.

The main assumptions for modelling are: (1) rock decompaction factors apply only to clastic deposits, according to Sclater and Christie's method (1980); (2) sea-level changes are neglected, as thermal evolution is mainly affected by sediment thickness than by water depth (Butler, 1992); (3) thermal modelling is performed using LLNL Easy %Ro method based on Burnham and Sweeney (1989) and Sweeney and Burnham (1990); (4) thrusting is considered instantaneous when compared with the duration of sedimentation, as generally suggested by theoretical models (Endignoux and Wolf, 1990); (5) present-day heat flow of 60-70 mWm^{-2} is extracted from borehole datasets and available maps (GeoThopica, http://geothopica.igg.cnr.it/; Granath and Casero, 2004), whereas paleo-heat flow values were evaluated using the correlation of vitrinite reflectance and mixed layers I-S data based on the kinetic model of vitrinite maturation of Burnham and Sweeney (1989) and the kinetics of the I-S reaction determined by Hillier et al. (1995); and (6) thickness, lithology and age of sediments are from geological maps (Brocquet, 1968; Catalano et al., 2011).

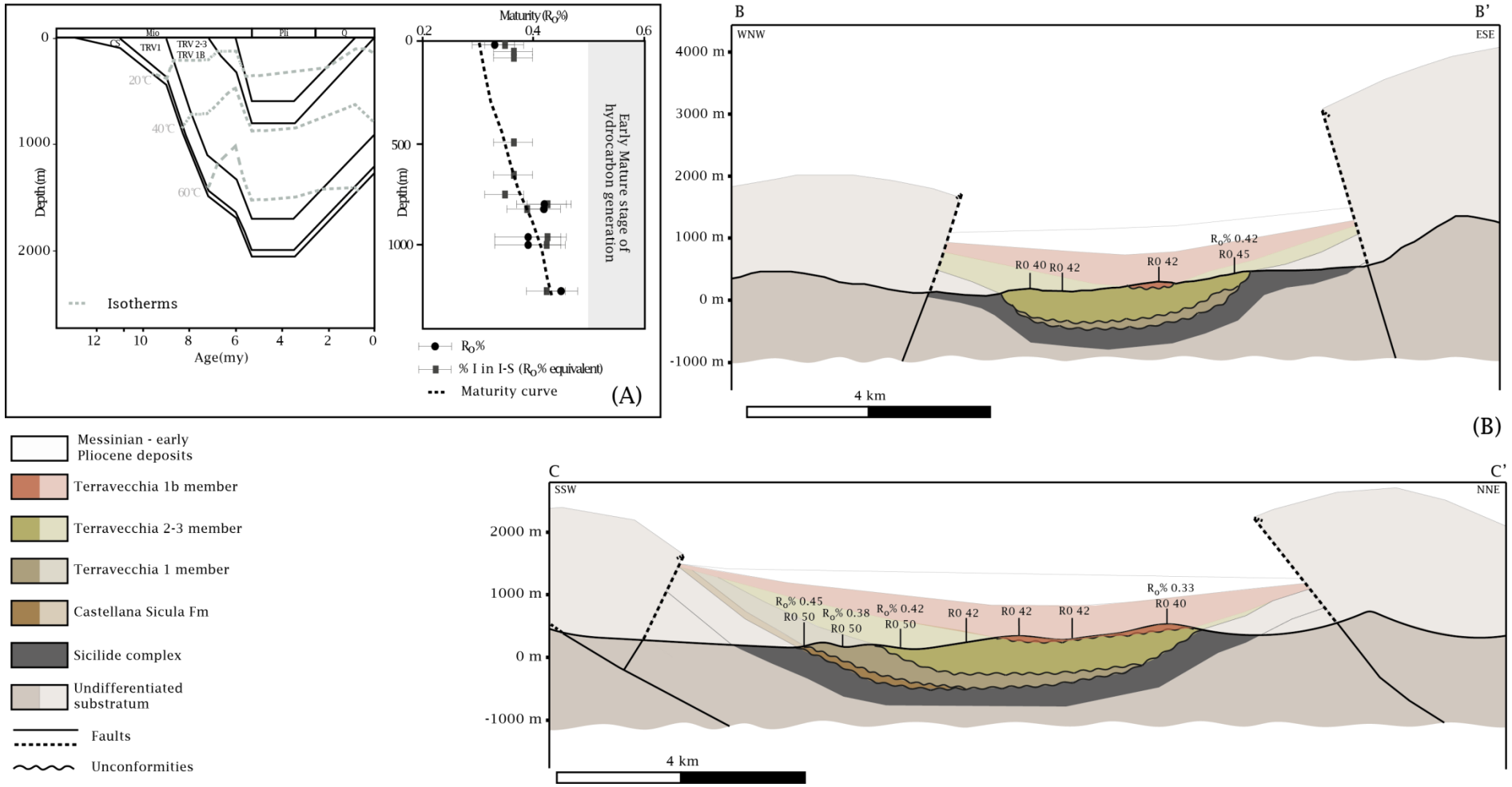

Figure 2.7 - (A) Representative one-dimensional burial and thermal model of the Scillato wedge-top basin. (B) Original cross sections B-B 'and C-C' (see Fig. 2 for location) with projected paleothermal data showing the thickness of the eroded strata calculated from thermal models. Shaded colours indicate the eroded Fms. %I in I-S—illite content in mixed layers illite-smectite; R_o%—vitrinite reflectance data; CS—Castellana Sicula Fm; TRV1—Terravecchia 1 member; TRV2-3, TRV1B—Terravecchia 2-3 and 1b members; Mio—Miocene; Pli—Pliocene; Q—Quaternary.

Burial history reconstructed for the Scillato wedge-top basin (Fig. 2.7A) began during the late Serravallian with the deposition of the Castellana Sicula marls (50 m), followed by a 1,200 m thick sequence of conglomerates, sandstones and claystones of the Terravecchia Fm. during the Tortonian. A regional unconformity between the Castellana Sicula and Terravecchia Fms (Fig. 2.7 B,C) marks a first episode of subaerial exposure. From the Messinian until the early Pliocene, the deposition of gypsum-arenites, calcarenites and marls pertaining to the Gessoso-Solfifero group and Trubi Fm. occurred with a minimum thickness of 800 m (Fig. 2.7). A comparable amount of Messinian-early Pliocene deposits (~550 m) is exposed in the Ciminna wedge-top basin, located at about 20 km west of the Scillato wedge-top basin (see Fig. 2.1 C; Gugliotta et al., 2014).

Thermal model shows a maximum sedimentary burial of ~2km for the base of the Castellana SiculaFm. During the Messinian-early Pliocene time and related maximum temperature of 78°C (Fig. 2.7 A). Exhumation started during the late Pliocene after the end of the Trubi Fm. deposition and erosion removed about 0.8 km of sediments.

The reconstructed evolution of the Imerese unit began during the middle Triassic with the deposition of claystones, sandstones and limestones of the Mufara Fm. and continued until the lowermost Oligocene with the deposition of limestones, dolostones, calcilutites and marls of the Scillato, Fanusi, Crisanti and Caltavuturo Fms (Fig. 2.8A). During the Oligocene, a depositional hiatus, associated with the end of carbonate sedimentation and the onset of the Numidian Flysch deposition occurred. Modelled sedimentary thickness for the Numidian Flysch is about 1.3 km. During the Serravallian, the Imerese unit and Numidian Flysch were incorporated into the advancing orogenic wedge (Gugliotta et al., 2014) and stacked up into thrust sheets buried by about 0.8 km of more internal units (made up of part of the Numidian Flysch and Sicilide units).

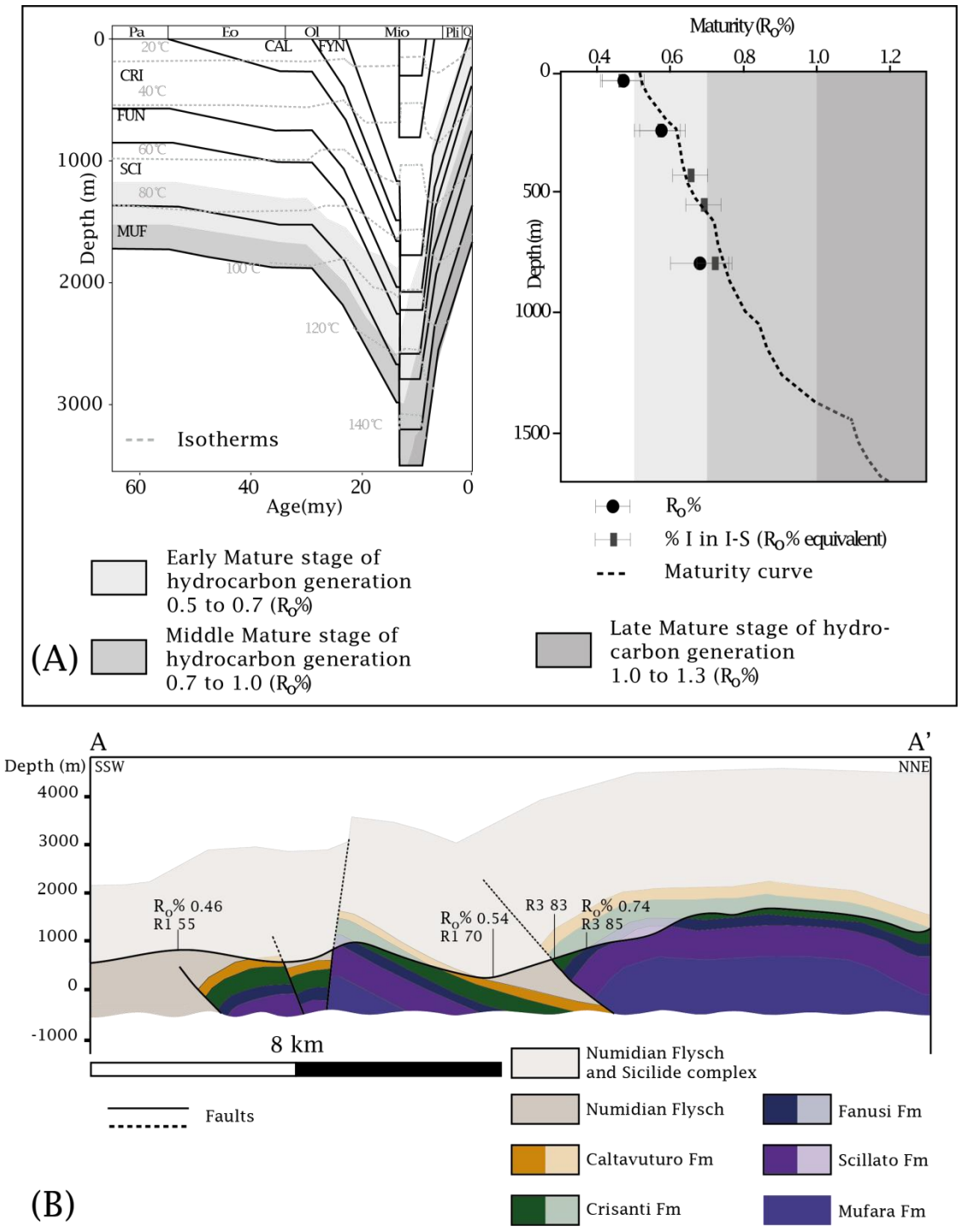

Figure 2.8 - (A) Representative one-dimensional burial and thermal model of the Imerese unit in the last 60 Ma. (B) Original cross section A-A' (see Fig. 2.2 for location) with projected paleothermal data showing the thickness of the eroded strata. Shaded colours indicate the eroded formations. %I in I-S—illite content in mixed layers illite-smectite; R_o%—vitrinite reflectance data; MUF—Mufara Fm.; SCI— Scillato Fm.; FUN—Fanusi Fm.; CRI—Crisanti Fm.; CAL—Caltavuturo Fm.; FYN—Numidian Flysch; Pa—Paleocene; Eo—Eocene; Ol—Oligocene; Mio—Miocene; Pli—Pliocene; Q—Quaternary.

At that time, the base of the Imerese unit along the CRSSB alignment experienced maximum burial at depth of about 3.5 km with maximum temperatures of about 150°C (Fig. 2.8). Since the

latest Tortonian, the exhumation of the Imerese unit occurred, driven by high angle faults activity (Event II). U-Th/He dating on apatite crystals were tentatively performed on the Mufara and Numidian Flysch Fms. in order to obtain quantitative constrains for the exhumation age of the Imerese unit. Unfortunately, very few (three crystals for the Numidian Flysch and one for the Mufara Fm.) and highly broken apatite crystals (<60 μm of diameters) were separated. Only two apatite grains from the Numidian Flysch (site 15 Fig. 2.3) provided reliable results indicating different ages for their closure temperature: 113.94 ± 2.7 Ma and 5.13 ± 0.22 Ma (Zattin M., personal communication). The older age clearly refers to an inherited apatite grain as it is older than the Numidian Flysch stratigraphic age whereas the Pliocene age could refer to the exhumation phase of the Imerese unit, and this indication is taken into account in the performed models. Nevertheless, the small number of crystals and the wide age interval do not allow to have statistically checked results (Reiners and Ehlers, 2005).

2.6.2. Evolutionary scenarios for the Lercara unit

A different tectonic evolutionary scenario is proposed for the Lercara unit as its origin and emplacement mechanism are still matter of debate. In the Mt. Rasolocollo-Cerda area, the Mufara Fm. is surrounded by the Numidian Flysch and the Sicilide Complex with a contact of uncertain nature. For the Mufara Fm., R_o% values ranging from 0.82% to 0.94% and R3 I-S with an illite content of 83- 86% indicate levels of thermal maturity consistent with the late mature stage of hydrocarbon generation. The Numidian Flysch in surrounding areas shows random-ordered (R0) and/or short range ordered I-S (R1) and R_o% values ranging from 0.40% to 0.57%, indicating lower levels of thermal maturity, in the immature to early mature stages of hydrocarbon generation. Thus, a gap of levels of thermal maturity is observed between the two formations.

Three evolutionary scenarios may be consistent with this present-day configuration. Nevertheless, geological features, mineralogical and paleothermal data allow us to discriminate

the most likely among them. Such scenarios differ in amount of burial, timing and mode of structural thickening and exhumation.

In the first model (Fig. 2.9) the Lercara unit represents an extensional structural high developed in the lowermost Jurassic time and inherited during the chain building. In this scenario, after the sedimentation of the Mufara Fm. (1.4 km), only a few meters of sediments of the Imerese succession deposited on it until the early Oligocene (Fig. 2.9A). During Oligocene-Langhian times, in front of the orogenic wedge a foredeep developed on top of this structure and ~1.3 km thick succession of the Numidian Flysch deposited. Shallow seated thrusts developed since Serravallian, as a consequence of the advancing orogenic wedge, leading to the tectonic thickening of the foredeep deposits and the emplacement of the Sicilide Complex onto the Numidian Flysch (Fig. 2.9A). Following, the Castellana Sicula Fm. deposited (~0.2 km) in a wedge-top setting until the end of the Serravallian onto the deformed substratum. At that time, the Mufara Fm. experienced a maximum burial of 4.2 km in agreement with thermal modelling constrained by paleothermal data (Fig. 2.9B). In the uppermost Tortonian, the onset of the activity of high angle transpressive faults (Event II) uplifted the area leading to the erosion of 3.2 km of the Tertiary to Triassic units (Fig. 2.9B). This process brought to the exhumation of the Mufara Fm. where nowadays the Numidian Flysch stratigraphically lies on top of the structural high and locally on the footwall of transpressive faults (Fig. 2.9A).

This scenario is consistent with an exhumation of 3.2 km for the Lercara high (located NW of Scillato wedge-top basin), whereas only 1.8 km were exhumed from the CRSSB high (located SE of Scillato wedge-top basin; Fig. 2.8). These amounts of exhumation are not strongly supported by paleocurrents direction reconstructed for the Scillato wedge-top basin that indicate a main source area for the wedge top sediments located to the E and SE (Gugliotta and Gasparo Morticelli 2012; Gugliotta et al., 2013) where low exhumation amounts have been calculated.

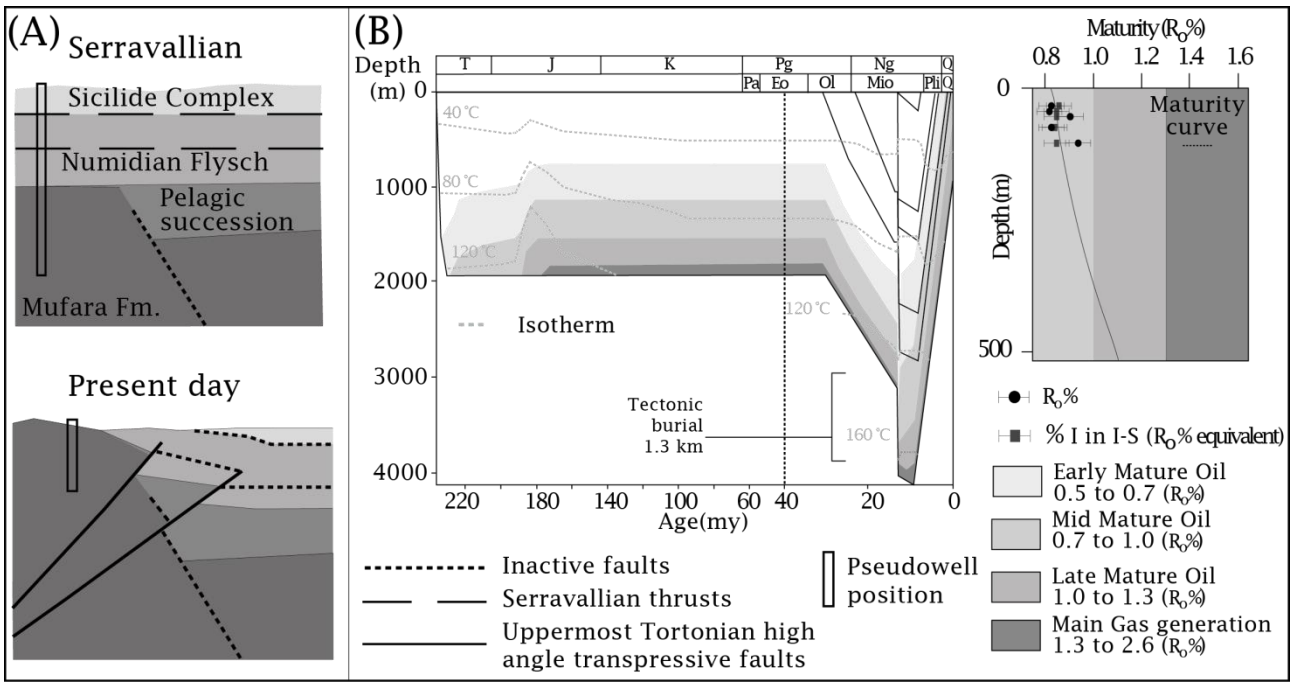

Figure 2.9 - (A) Simplified tectonic sketches showing Serravallian and present day setting of the Lercara unit considered as a structural high within the Imerese basin (not to scale) (B) Representative one-dimensional (pseudo-well) burial and thermal model for the Lercara unit. %I in I-S—illite content in mixed layers illite-smectite; R_o%—vitrinite reflectance data.

In the second model (Fig. 2.10), the Lercara unit experienced continuous deposition until Langhian time (~2 km) of pelagic facies deposits of the Imerese succession in a passive margin setting and of Numidian Flysch in foredeep facies. Since the Serravallian, the advancing orogenic wedge induced the development of shallow seated thrusts which led to the emplacement of thin thrust sheets made up of the Sicilide Complex (~0.3 km) onto the Numidian Flysch (Fig. 2.10A,B). The Castellana Sicula Fm. deposited (~0.2 km) in a wedge-top setting onto this deformed substratum. Since uppermost Tortonian time, high angle transpressive faults activity drove the exhumation of the Mufara Fm. resulting in 2.65 km of erosion (Fig. 2.10B) and a present-day configuration where Triassic deposits tectonically overlay younger Numidian Flysch succession (Fig. 2.10A).

Also in this scenario mean paleocurrents direction does not support exhumation amounts depicted in the previous scenario.

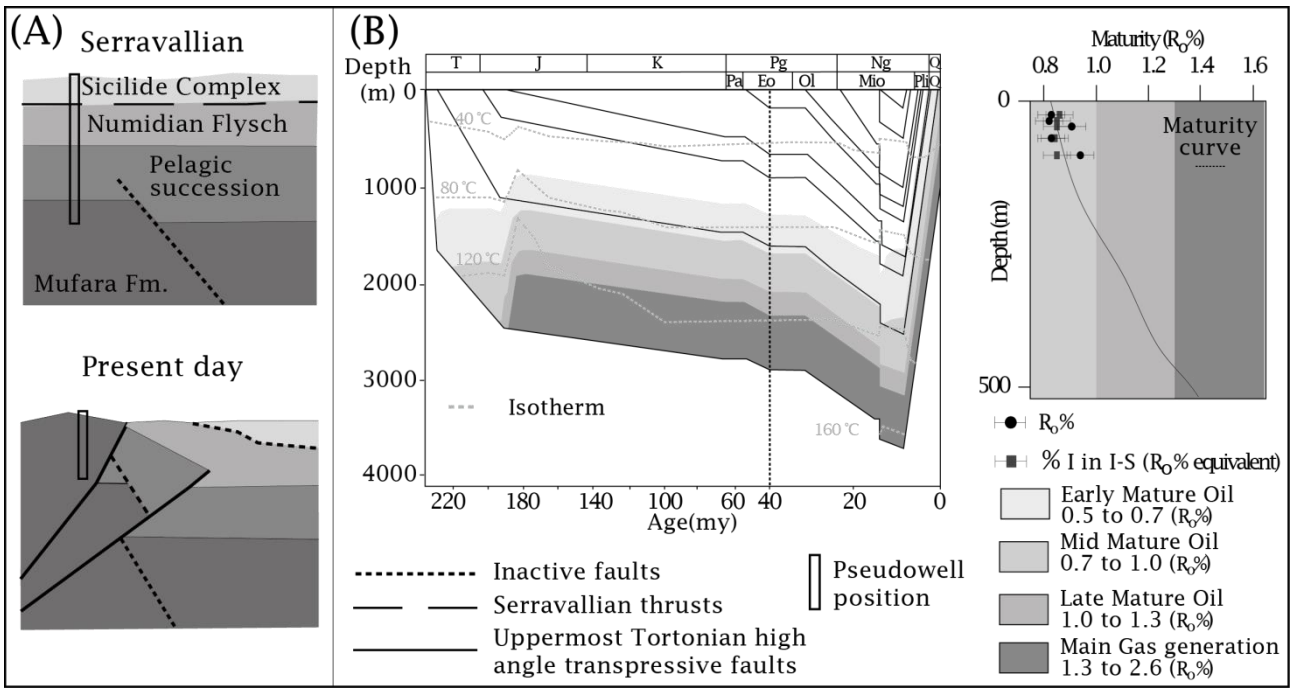

Figure 2.10 - (A) Simplified tectonic sketches showing Serravallian and present day setting of the Lercara unit considered as Imerese unit (not to scale) (B) Representative one-dimensional (pseudo-well) burial and thermal model for the Lercara unit. %I in I-S—illite content in mixed layers illite-smectite; R_o%—vitrinite reflectance data.

In the third scenario (Fig. 2.11), the Lercara unit experienced two different phases of exhumation. Continuous sedimentation of the Imerese succession occurred until the early Eocene in a passive margin setting and the Mufara Fm. experienced maximum burial of about 2.35 km at that time (Fig. 2.11A). During the Oligocene, a low-angle normal fault removed 1.35 km thick Triassic–Eocene succession, inducing isostatic footwall rebound responsible for the early exhumation of the Mufara Fm. (Fig. 2.11A,B). Following, the Numidian Flysch deposited both on the hangingwall and footwall blocks with changing thickness. In the hangingwall, where the Numidian Flysch is thicker, it was locally fed by the erosion of the Mufara Fm. During the Serravallian, the Sicilide Complex (0.3 km thick) thrust over the Numidian Flysch, followed by the deposition of the Castellana Sicula Fm. (0.1 km), burying the Mufara Fm. at depth of 2.2 km (Fig. 2.11B). Since the uppermost Tortonian, final exhumation occurred, driven by high angle transpressive faults (Event II), resulting in 1.2 km of erosion (Fig. 2.11A,B).

This scenario is consistent with the paleocurrent directions distribution and XRD analysis of the <2 μm grain-size fraction of sediments. In detail, mineralogical assemblage of the substratum

units highlights the occurrence of rectorite both in the Mufara Fm. and in the Numidian Flysch (Tab. 2.1) suggesting that the Mufara Fm. exhumed in the Oligocene, partially feeding the Numidian Flysch. Even if this scenario is consistent with paleothermal data, thermocronological constraints are required in order to confirm the age of the Mufara Fm exhumation in the Rasolocollo-Cerda area.

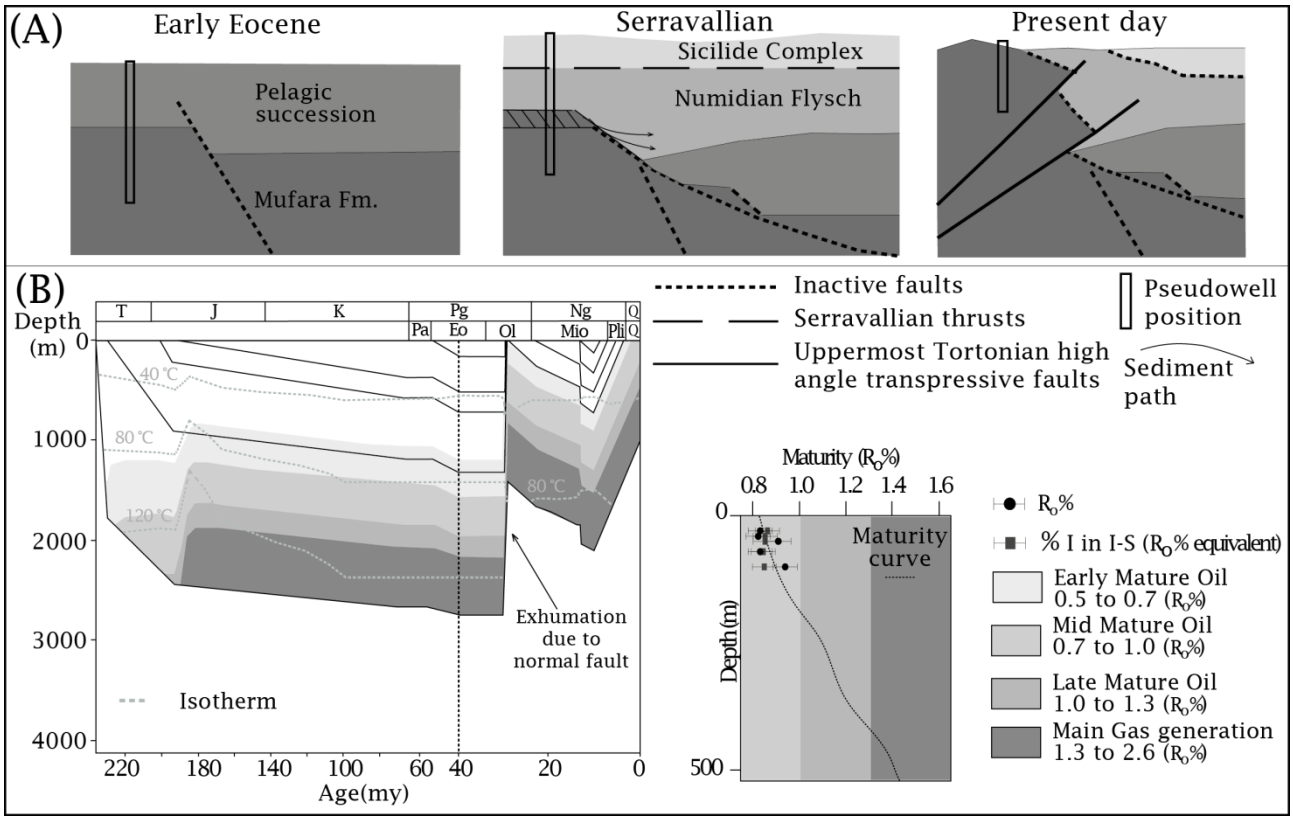

Figure 2.11 - (A) Simplified tectonic sketches showing Early Eocene, Serravallian and present day setting of the Lercara unit considering a low-angle normal fault acting during the Oligocene (not to scale) (B) Representative one-dimensional (pseudo-well) burial and thermal model for the Lercara unit. %I in I-S—illite content in mixed layers illite-smectite; R_o%—vitrinite reflectance data.

2.6.3. Source to sink system: insights into kinematic evolution of the belt

Paleothermal indicators, coupled with sedimentological and structural data (Gugliotta and Gasparo Morticelli 2012; Gugliotta et al., 2013), allow us to describe a source (deformed substratum) to sink (wedge-top) system evolution for the Scillato basin, identifying two main source areas feeding the wedge-top basin since Serravallian time.

The basal part of the wedge-top basin succession (Castellana Sicula Fm. and Terravecchia 1 member) shows a depocenter migration toward the NW (Event I) coherently with the main thrust

transport direction to the SW (Fig. 2.6C). The top of the succession (Terravecchia 2-3 and 1b members, late Tortonian) is accommodated in a ~NE-SW-trending asymmetric synform, whereas the Castellana Sicula Fm. and Terravecchia 1 member are deformed, as a result of the NE-SW-directed transpressive faults activity of the Event II (Fig. 2.6B, C).

The Terravecchia 1 member contains pebbles mainly made up of igneous and metamorphic rocks indicating a continental source area for sediments filling the basin. According to paleocurrents reconstruction, the source area was located to the NW of the Scillato basin and pebbles belong to the European domain, most likely Sardinia and Kabilo-Calabride crystalline basement (Gugliotta and Gasparo Morticelli, 2012; Gugliotta et al., 2013). The sandy-shaly portion of the Terravecchia 1 member contains indigenous fragments of organic matter and two populations of mixed layered phases. The population with low expandable mixed layers I-S (R1 80) represents the inherited fraction of sediments probably coming from the dismantling of the Numidian Flysch that was exhuming during Serravallian-Tortonian times in more internal areas to the NW (Di Paolo et al., 2014).

A different source area fed the Late Tortonian deposits of the Terravecchia 2-3 and 1b members. They contain high amounts of reworked organic and inorganic material. The inorganic fraction of sediments displays the occurrence of minerals coming from the Scillato basin margins such as mixed layers I-S with high illite content (R1 70-80) and rectorite that represent the detrital minerals filling the basin during the late Tortonian. Such a mineralogical assemblage has been detected in the Numidian Flysch succession exposed to the SE of the Scillato wedge-top basin along the CRSSB alignment that has been exhuming since the late Tortonian (Fig. 2.8). Reworked vitrinite macerals, as well, show R_o% values between 0.42% and 0.55%, similar to those measured for the Numidian Flysch (0.40% - 0.57%) of surrounding areas, strengthening this hypothesis. In addition, paleocurrents analysis identifies a source area for sediments, during the uppermost Tortonian, located to the SE of the Scillato wedge-top basin, corresponding to the

CRSSB alignment (Gugliotta and Gasparo Morticelli, 2012) and consistent with detrital mineral supply, identified by XRD analysis.

Coupling paleothermal and mineralogical data, 1D thermal and 3D geological modelling of both the Scillato wedge-top basin and its substratum, a new kinematic evolution scenario for this part of the Sicilian fold-and-thrust belt can be proposed (Fig. 2.12). From the Triassic to the early Eocene, passive margin conditions led to the deposition of the Imerese succession. Jurassic normal faults probably created horst and graben structures (Fig. 2.12A). Since the Oligocene time, low-angle extensional faults developed in a convergence setting detaching the Triassic–Eocene section of the Imerese succession from the Mufara Fm. (Fig. 2.12B) currently exposed along the CRSSB alignment. Isostatic footwall rebound led the Mufara Fm. to be exhumed, partially providing clasts and detrital minerals to the Numidian Flysch depositing in the hangingwall block. As a result, the hangingwall block corresponds to the CRSSB alignment where the Numidian Flysch is 1.8 km thick, and the footwall block corresponds to the Lercara unit where the Numidian Flysch is 0.4 km thick. Since Serravallian time, the advancing orogenic wedge generated shallow seated thrusts which brought the Sicilide Complex to thrust over the Numidian Flysch and deformed the Imerese substratum succession (Fig. 2.6B and 2.12 C). At that time, sediment fluxes moved parallel to the main thrusts direction (NW-SE) individuating a main source area for sediments located to the NW of the Scillato basin. As a result, the Castellana Sicula Fm. and Terravecchia 1 member deposited in a wedge-top setting. Since the uppermost Tortonian time, high angle transpressive faults cut the shallow seated thrusts (Fig. 2.6B) leading to the differential exhumation of the Imerese unit along the CRSSB alignment (Fig. 2.8A) and the Lercara unit in the Rasolocollo-Cerda area (Fig.12D). At that time, shift in source area for sediments from NW to E-ESE is recorded by the Terravecchia 2-3 and Terravecchia 1b members which are mainly fed by the erosion of the Sicilide complex and Numidian Flysch located along the CRSSB alignment.

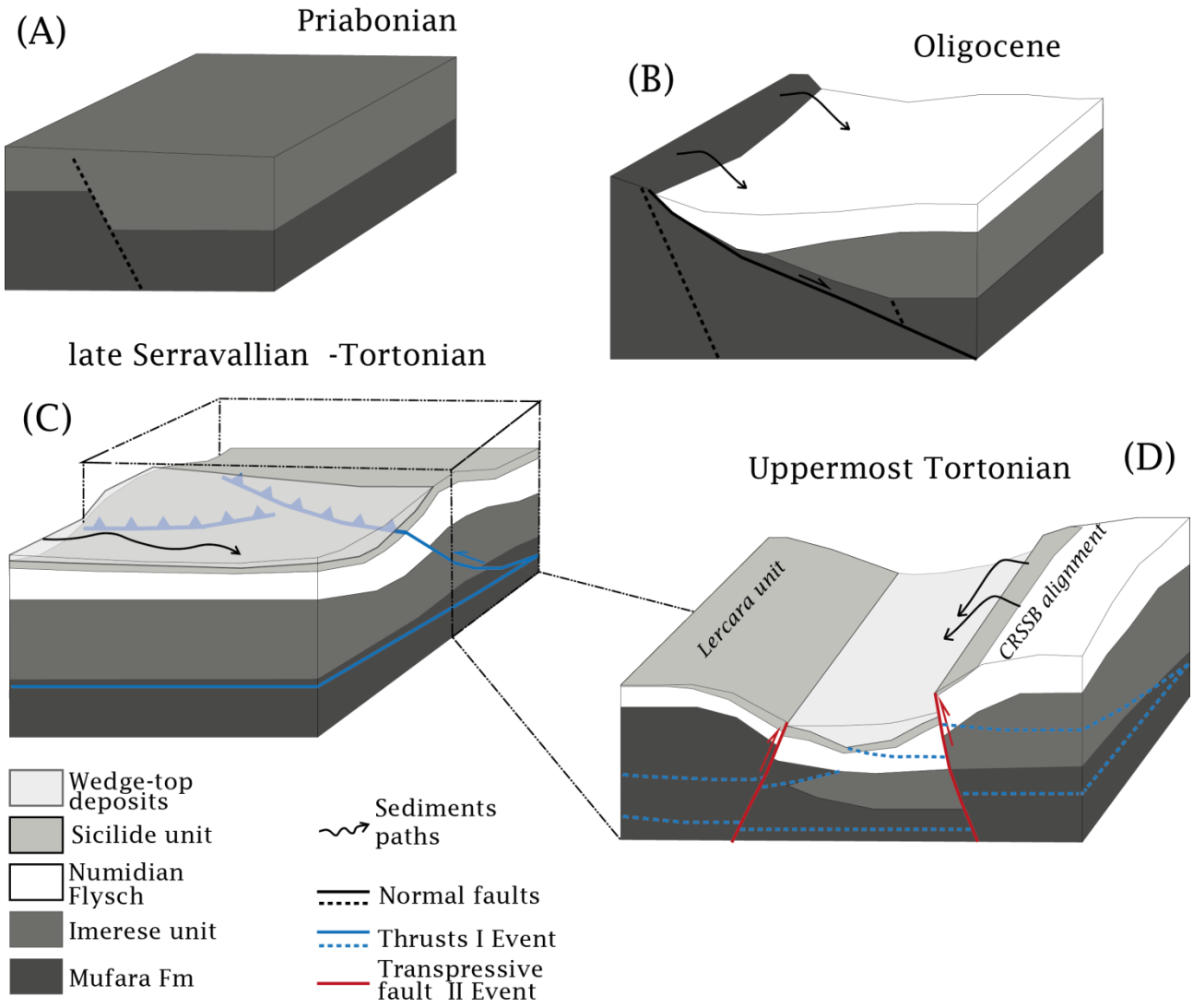

Figure 2.12 - Tectonic evolutionary model for the Sicilian fold-and-thrust belt in the study area (not to scale). (A) Passive margin setting during the late Eocene. (B) low angle-extensional tectonics generating exhumation of the upper Triassic Mufara formation which fed the Numidian Flysch during the Oligocene (C) thin skinned thrust tectonics of the Imerese units and onset of wedge-top basin sedimentation in Late Serravallian-Tortonian times (D) Model detail (dotted cube in C) showing high angle transpressive faults driving exhumation of the Imerese units and controlling wedge-top basin deposition during the latest Tortonian. Dotted lines indicate inactive faults.

2.7. Conclusions

Burial and thermal history of the Scillato wedge-top basin and its pre-orogenic substratum allowed us to define levels of thermal maturity of the Triassic to Tortonian succession in the Sicilian fold-and-thrust belt. The wedge-top basin fill experienced shallow burial (~2 km) and levels of thermal maturity in the immature stage of hydrocarbon generation and early diagenesis

whereas the pre-orogenic substratum experienced a maximum burial of 3.5 km in deep diagenetic conditions.

The integration of mineralogical and paleothermal data with 1D thermal and 3D geological modelling allowed us to reconstruct the Scillato wedge-top basin geometry and evolution through time in the framework of a source to sink system, unravelling the kinematic evolution of the Apennine-Maghrebian fold-and-thrust belt. In particular, an early phase of exhumation driven by low-angle extensional faults was detected during the Oligocene predating Neogene compression.

Chapter III - 3D structural modeling and restoration in fold-and-thrust belts: examples from the Kumeta and Busambra Mts., NW Sicily (Italy)

3.1 Abstract

Reflexion seismic data and field observation have been used to build a 3D geological interpretation of sub-surface block architecture of the structurally complex Kumeta and Busambra Mountains, NW Sicily, Italy. Available seismic profiles (13 lines) were interpreted in order to build the 3D geological model of the Trapanese unit of horizons and faults. A kinematic control of possible movements allow to discriminate between two downward alternative extrapolations of the major decollement faults developed during tectonics compression. Along strike variation of the structural style is recognised where pre-existing discontinuities (e.g. inherited normal faults) play an important role. In particular, south verging structures characterize the western part of the area whereas north verging structures characterize the northern and eastern part of the area. The full methodology, starts with building an initial 3D structural model setup and then checks kinematic movements through elastic block model restorations. It results in a consistent interpretation of the outcropping Kumeta and Busambra Mountains quantifying the shortening amount.

Therefore, albeit two different kinematic evolutionary scenarios can be envisaged, either a single step or a two-step thrust-fault deformation, coupling the 3D model reconstruction with the 3D geomechanical restoration only validates the scenario which involve the single step thrust-fault deformation model, defining less than 15% of shortening

3.2 Introduction

Uncertainty in seismic interpretation is a common feature especially in structurally complex settings such as fold-and-thrust belts where seismic reflection profiles often have low resolution images (Torvela and Bond, 2011; Totake et al., 2017). For this reason, different alternative

structural interpretations can be achieved (Bond et al., 2007; 2012; Bond, 2015) especially in fault zones where seismic reflection records are perturbed (Iacopini and Butler, 2011) and a way to constrain the most viable interpretation is mandatory. Restoration and structural balancing techniques represent an appropriate tool to validate or invalidate a structural interpretation (Dahlstrom 1969; Rowan and Kligfield, 1989 Egan et al., 1997; Groshong, 2006; Groshong et al., 2012; Lovely et al., 2012; Butler, 2013). Recently Bond et al., (2012), documented how seismic interpreters who validate their seismic interpretation sketching restoration, have higher probabilities to achieve a correct interpretation. Also, comparing different published regional cross sections in fold and thrust belt settings, Berthelon and Sassi, (2016) showed that forward structural modelling is an unavoidable step to validate a structural interpretation and that the "interpreters" should make clear on their interpreted cross section which are the faults trajectory paths that have a low or a high degree of uncertainty.

Thus a restorable geological cross-section is internally consistent and has a topologically consistent geometry. Conversely, an unrestorable geological cross-section is topologically impossible, so it is geologically unviable (Dahlstrom, 1969). In the oil and gas industry, in fact, restoration techniques are routinely used to validate structural models and are widely adopted to mitigate exploration risks.

In structurally complex areas, where along strike variations of shortening, structural style and thickness frequently occur (e.g., Aldega et al., 2018; Bigi et al., 2018; Carminati et al., 2016), 2D seismic interpretation and restoration are not always sufficient to discriminate which geometry and kinematics of the involved structures is the most appropriate since out-of-plane movements are not considered (Roure and Sassi, 1995; Deville and Sassi, 2006; Castelluccio et al., 2016; Tavani et al., 2018).

Coupling three-dimensional modelling with 3D restoration techniques (Royer et al., 2013), represents a good approach to easily detect inconsistencies in structural interpretations and it allows to describe the geometry and layout of rock units in three-dimensional space. This

approach allows to honour field observations, measurements, seismic interpretation and geological concepts (Plesch et al., 2007; Li et al., 2013, 2016; Shuwei et al., 2013; Bond, 2015;). Any 3D description of horizons and faults for which 3D restoration validates a kinematic scenario is therefore considered better. On the opposite, a 3D description for which a kinematic scenario is shown to be impossible probably needs to be revised.

The area of Kumeta and Busambra Mountains represents a school case sector of the Sicilian fold-and-thrust belt where structural style varies along-strike and high angle transpressive faults occur at different vergences. On the basis of field observations different authors (Roure et al., 1990; Tavarnelli et al., 2003; Avellone et al., 2010; Barreca and Maesano, 2012), proposed several kinematic evolutionary scenarios for the Mt. Kumeta and Mt. Busambra structures. A recent work by Albanese and Sulli, (2012), proposes a structural model for the Kumeta and Busambra Ridges that is strongly constrained by 2D seismic lines and field data. In their model the major faults are interpreted as the result of backthrusts development and the eastern Mt. Busambra structure is considered as a triangle zone.

In this work, we coupled interpreted seismic lines from this previous work (Albanese and Sulli, 2012) with an additional (original) interpretation of unpublished seismic lines to construct a water-tight 3D geological model. Computer geomodelling and 3D geomechanical restoration of the Kumeta and Busambra structures have been performed in order to: (1) reconstruct the surface and subsurface geometry of these structures; (2) improve pre-existing structural interpretation proposing a revised 3D structural model that sheds new light on the kinematic evolution of the Kumeta and Busambra structures in the framework of the Sicilian fold-and-thrust belt; (3) quantify the amount of shortening affecting the Trapanese unit.

3.3 Geological setting

The Sicilian fold-and-thrust belt (SFTB) is a segment of the Apennine-Maghrebian chain (Fig. 3.1) originated from the tectonic inversion of the former Africa continental passive margin (Roure et al., 1990; Catalano et al., 2007).

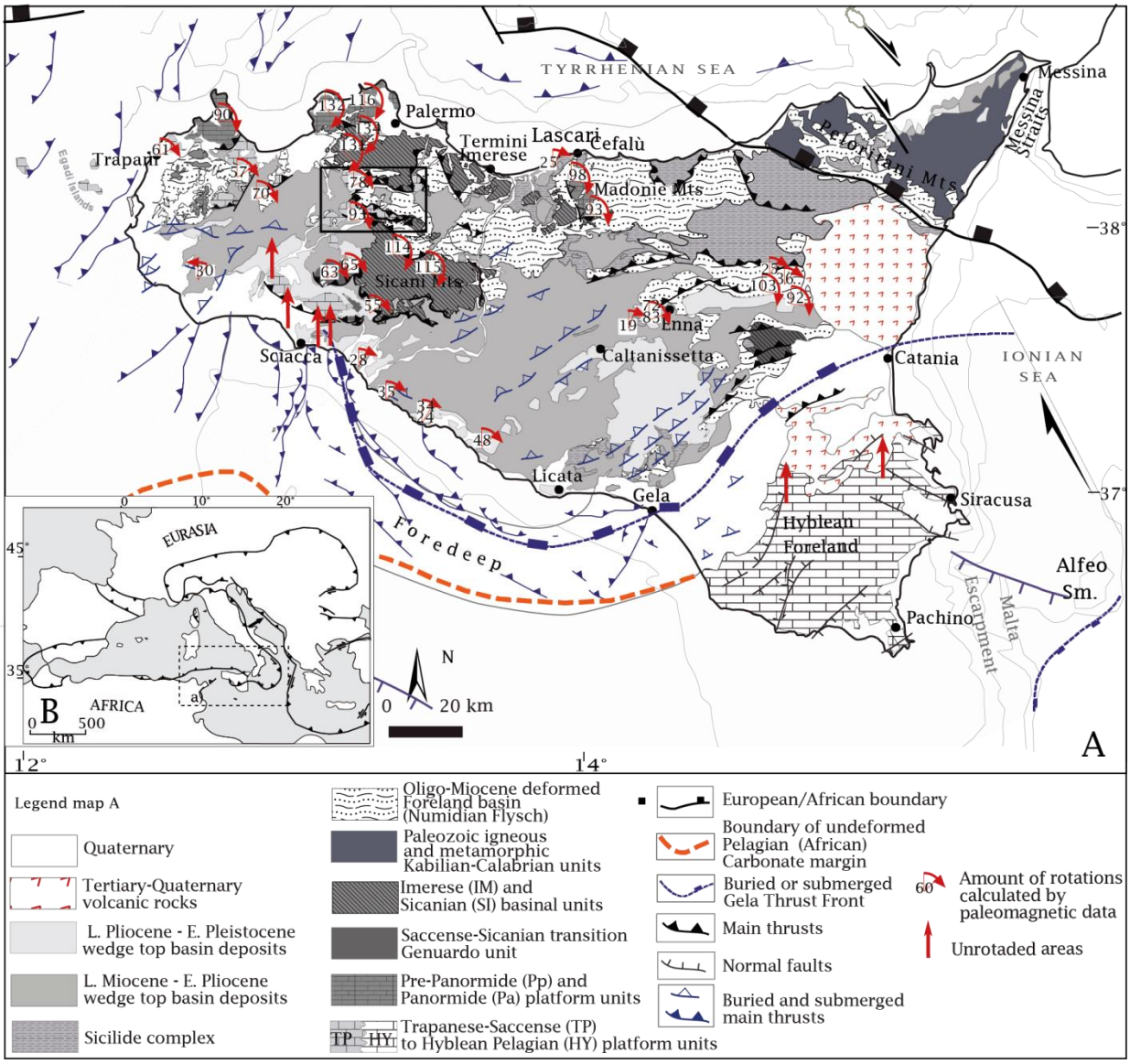

Figure 3.1 (A) Geological map of Sicily (modified after Gasparo Morticelli et al., 2015). The black rectangle indicates the study area. Palaeomagnetic data are from Channel et al., (1990), Grasso et al., (1987), Speranza et al., (2003; 2018). (B) Tectonic map of central Mediterranean area (modified after Gasparo Morticelli et al., 2015).

The SFTB has been developing since the early Miocene as a SSE-verging chain, resulting from the post-collisional convergence between Africa and Europe (Dercourt et al., 1986; Dewey et al., 1989; Catalano et al., 1996, 2000; Faccenna et al., 2004) and the rollback of the subduction hinge

of the Ionian lithosphere (Caputo et al., 1970; Doglioni et al., 1999; Faccenna et al., 2001). This tectonic process transports and deforms different paleogeographic domains, now stacked to form the tectonic wedge (Catalano et al., 1996, Speranza et al., 2018).

Its structurally highest tectonostratigraphic unit is derived from the deformation of the distal pre-orogenic domain (Sicilide Complex; Ogniben, 1960) and was generally involved in the Neotethyan Sicilian accretionary wedge (Monaco and Tortorici, 1995; Roure et al., 1990; Corrado et al., 2009). Tectonically beneath the Sicilide Complex, more external tectonostratigraphic units are present (e.g., Imerese, Sicanian and Trapanese units). They formed in part at the expense of the African continental paleomargin and consist of rootless units, derived mainly from shortened and rotated Mesozoic-Cenozoic basinal and platform successions (Fig. 3.2 A, Di Paolo et al., 2012, 2014; Catalano et al., 2013a; Gasparo Morticelli et al., 2015; Speranza et al., 2018).

The Imerese unit (Fig. 3.2 B), middle Carnian-lowermost Oligocene in age, is a 800-1400 m thick succession (Fig. 3.2 B) mainly constituted by alternating sandstones, limestones and shales (Mufara Fm.) followed by pelagic limestones, dolostones, radiolarites and marls. The Sicanian unit (Fig. 3.2 B) is a 900-1900 m thick succession made up of middle Triassic-lower Oligocene sandstones, shales, cherty limestones and marls passing upward to upper Oligocene-upper Miocene calcarenites and marls.

Both Sicanian and Imerese units are often detached from their original substratum and the basal detachment is represented by the Mufara Fm (Avellone et al., 2010). Further detachment levels in the Sicanian unit are within the Oligocene-lower Miocene and Jurassic to Cretaceous marls and shales (Avellone et al., 2010).

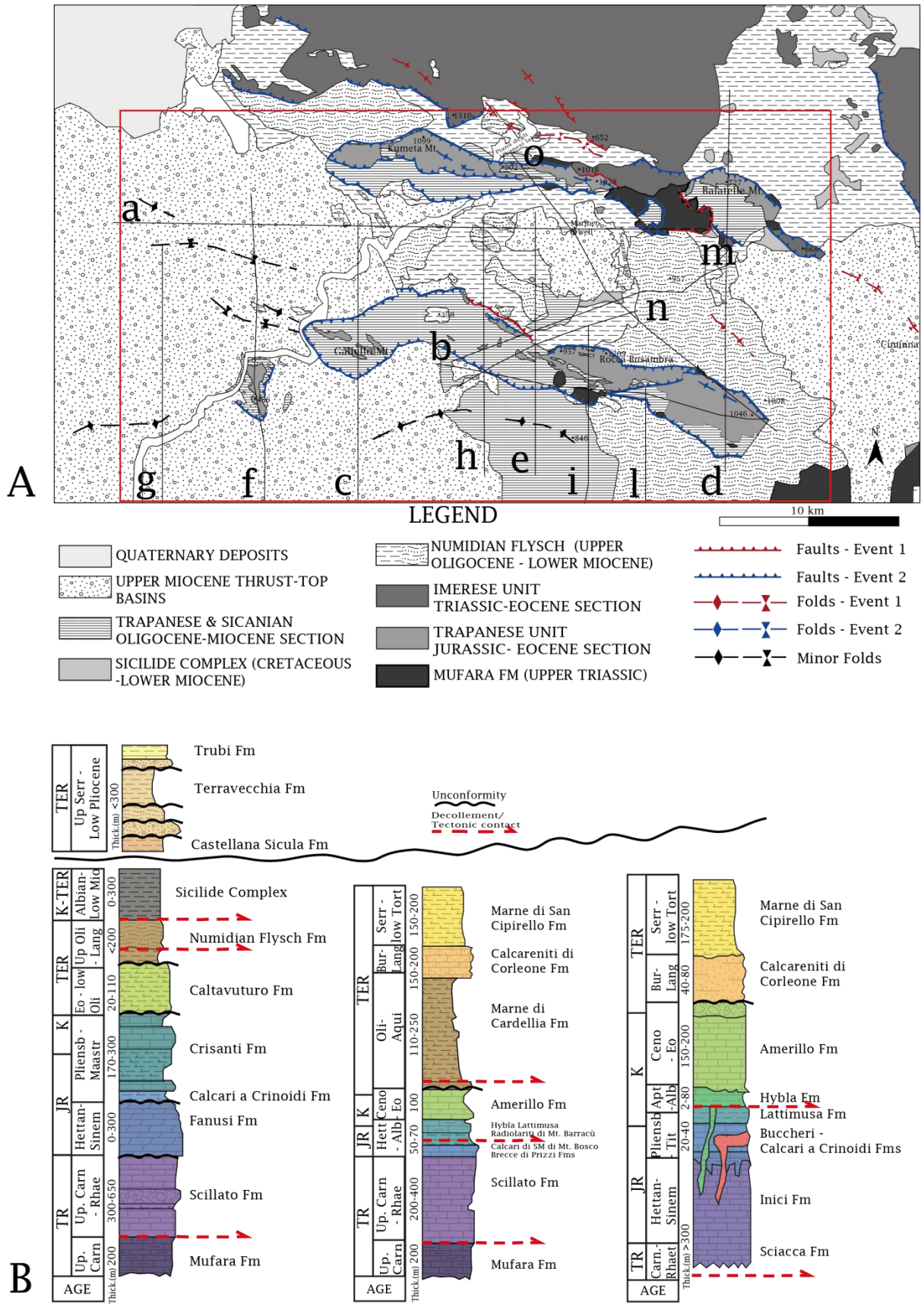

Figure 3.2 (A) Tectonic sketch map of the study area. Location of available seismic lines is also shown (a – o). (B) Simplified stratigraphic logs of the main tectonic units exposed in the study area (modified after Avellone et al., 2010). Carn-Carnian; Rhae—Rhaetian; Hettan—Hettangian; Sinem—Sinemurian; Pliensb—Pliensbachian; Tit—Tithonian; Apt—Aptian; Alb—Albian; Ceno—Cenomanian; Eo—Eocene; Oli—Oligocene; Aqui—Aquitanian; Bur—Burdigalian; Lang—Langhian; Serr—Serravallian; Tort—Tortonian; TR—Triassic; JR—Jurassic; K—Cretaceous; TER—Tertiary.

The Trapanese unit (Fig. 3.2 B) is an up to 5,000 m thick succession that can be subdivided into two sub-units. The lower Trapanese unit is characterized by upper Triassic-lower Jurassic shallow water limestones (Sciacca and Inici Fms) passing to middle Jurassic-Eocene pelagic carbonates and marls deposited on a seamount morphology (from the Calcari a Crionoidi to Amerillo Fms). The upper Trapanese unit is characterized by Burdigalian-lower Tortonian calcarenites and marls (Calcareniti di Corleone and Marne di San Cipirello Fms). The unit is detached from its original substratum. The basal detachment is localized within the Triassic evaporites/shales (Di Stefano et al., 2015). A shallower detachment is constituted by Cretaceous marls (Avellone et al., 2010).

The Numidian Flysch succession represents the earliest foredeep deposit at the onset of collisional tectonics (Grasso, 2001) and extensively crops out in the area (Fig. 3.2 A). The succession is constituted by sand-rich turbidites from 600 to 2000 m thick, which unconformably cover the Imerese unit and is often detached (Fig. 3.2 B) and tectonically thickened (Corrado et al., 2009; Pinter et al., 2017). Syn-tectonic upper Miocene-lower Pleistocene wedge top basins unconformably cover the aforementioned units (Gugliotta et al., 2014).

Two main thin-skinned tectonic events affecting the study area have been described so far (Oldow et al., 1990; Roure et al., 1990; Bello et al., 2000; Catalano et al., 2000; Avellone et al., 2010; Albanese and Sulli, 2012; Gugliotta et al., 2014; Gasparo Morticelli et al., 2015, 2017; Chapter II):

I) Since Serravallian time, deep-water units (Imerese and Sicanian units) were detached from their substratum thrusting over more external units constituted by thick carbonate platforms of the Trapanese unit (shallow seated event). This first event (faults in red in Fig. 3.2 A) of thrusting produced duplex geometries and major shortening.

II) Since the uppermost Tortonian, the ongoing compressional deformation shifted to deeper crustal levels involving thick carbonate platform and pelagic platform units (Trapanese unit) which are consequently detached from their substratum and

incorporated into the orogenic wedge. Deep seated thrusts (and backthrusts) deformed these units generating a further imbrication to the superimposed deep-water units and deformation of syn-tectonic basin successions (Avellone et al., 2010 Gasparo Morticelli et al., 2015, 2017). This second event (faults in blue in Fig. 3.2 A) has been characterized by high angle reverse to transpressive faults (Fig. 3.3 A,C) which join thrusts/backthrusts at depth (Avellone et al., 2010; Catalano et al., 2000; Albanese and Sulli, 2012; Gasparo Morticelli et al., 2017).

Structures generated during these two events are not coaxial due to vertical-axis clockwise rotations (progressively decreases towards the unrotated foreland; Fig. 3.1), linked to the Tyrrhenian sea evolution, affecting differentially the described units during their emplacement (Catalano et al., 1976; Channell et al., 1990; Oldow et al., 1990; Speranza et al., 1999, 2003, 2018).

3.3.1 The Trapanese unit and the development of the Kumeta and Busambra ridges

The Trapanese unit, exposed along the Mt. Busambra and Mt. Kumeta ridges, has been strongly affected by extensional tectonics before its involvement in the tectonic wedge. Basilone, (2009), on the basis of field mapping and structural analysis along the Mt. Busambra ridge, has defined several steps in the Sinemurian–earliest Miocene tectono-sedimentary evolution of the Trapanese unit. From the Sinemurian to the middle Jurassic, the Trapanese unit evolved from a Bahamian-type carbonate platform to a condensed pelagic platform facies (Di Stefano et al., 2002; Pavia et al., 2002) as a result of the activity of extensional faults that caused the drowning of carbonate platform units in the hangingwall blocks. Neptunian dykes and normal faults affecting the Inici Fm showing WNW-ESE to E-W orientation and volcanic episodes give evidences of the extensional tectonics (Fig. 3.3 B; Gasparo Morticelli et al., 2017; Avellone et al., 2010).

In the middle Jurassic, the Mt. Busambra and Mt. Kumeta ridges constituted two morphostructural highs that maintained their morphology at least until the early Cretaceous. At the same time, marginal areas rapidly subsided to basins and pelagic deposits directly onlapped

onto Jurassic stepped margins. During the early Cretaceous, a new volcanic input occurred in the Mt. Kumeta area represented by pyroclastic levels and pillow lavas intercalated within pelagic limestones (Basilone et al., 2010). During the late Cretaceous, Jurassic normal faults were partially reactivated by a new extensional tectonic pulse generating uplift of faulted carbonate blocks. Such an uplift produced widespread shallow-water carbonate-derived megabreccias (Fig. 3.3 C, Fig. 3.4 A) interlayered in the pelagic platform and deeper basin successions. Last minor tectonic pulses took place during the late Eocene producing widespread carbonate breccias and during the earliest Miocene generating a new tilted fault-block system which partially overprint previous extensional structures (Basilone, 2009).

3.3.2 Previous interpretations for the Kumeta and Busambra Mts.

The Kumeta and Busambra Mts. were deeply investigated by several authors who proposed highly different kinematic scenarios to explain their tectonic evolution mainly based on field observations and partially on seismic data. Roure et al., (1990) defined the Kumeta and Busambra structures exhumed as a consequence of N-dipping normal faults developed during the Pliocene. Analogously, Tavarnelli et al., (2003) explained the exhumation of these structures as a result of the activity of S-dipping normal faults since the late Pliocene. Di Stefano et al., (2002) evidenced that part of the displacement generated by the late Tortonian high angle transpressive faults which border the Mt. Kumeta structure is a paleotectonic heritage of the basin-swell Jurassic topography. Different authors (Ghisetti and Vezzani, 1984; Nigro 1998; Giunta et al., 2000b; Renda et al., 2000; Tortorici et al., 2001; Ghisetti et al., 2009; Barreca et al., 2010; Barreca and Maesano, 2012) pointed out the importance of Pliocene wrench tectonics. In detail, these authors individuated a crustal shear zone in western Sicily (named Mt. Kumeta-Alcantara fault system) along which transpressive right lateral movement occurred. According to these authors, the Kumeta and Busambra Mts. alignment corresponds to positive flower structures generated during the Pliocene strike-slip activity.

In contrast, for Catalano et al., (2000), Avellone et al., (2010) and Gasparo Morticelli et al., (2017), using a robust dataset of seismic lines and field data, it seems that the exhumation of the Kumeta and Busambra structures is the result of erosion driven by the development of thrusts and backthrusts and high angle transpressive faults which join them at depth, since uppermost Tortonian time. According to this last interpretation, Albanese and Sulli, (2012) described the Kumeta and Busambra Mts. as the result of a two-step tectonic evolution where S-verging thrusts development during the uppermost Tortonian was followed by backthrusting and "enucleation" of high angle transpressive faults. Since the latest Miocene, high angle transpressive faults and backthrusts led the exhumation of these structures.

Though several hypotheses have been proposed, most of them have been rejected as a consequence of new data acquisition. Firstly, field data (Avellone et al., 2010; Basilone, 2009; Barreca and Maesano 2012; Gasparo Morticelli 2017) clearly indicate that the faults bordering the Kumeta and Busambra Mts. structures are E-W to WNW-ESE striking reverse to transpressive high angle faults.

Furthermore, recent paleomagnetic data performed in the area by Speranza et al., (2018) show that strike-slip tectonics did not play a significant role in the genesis of the Kumeta and Busambra Mts. structures and that the transpressive movement is coeval to the thrusting/backthrusting phase (11 - 5 Ma).

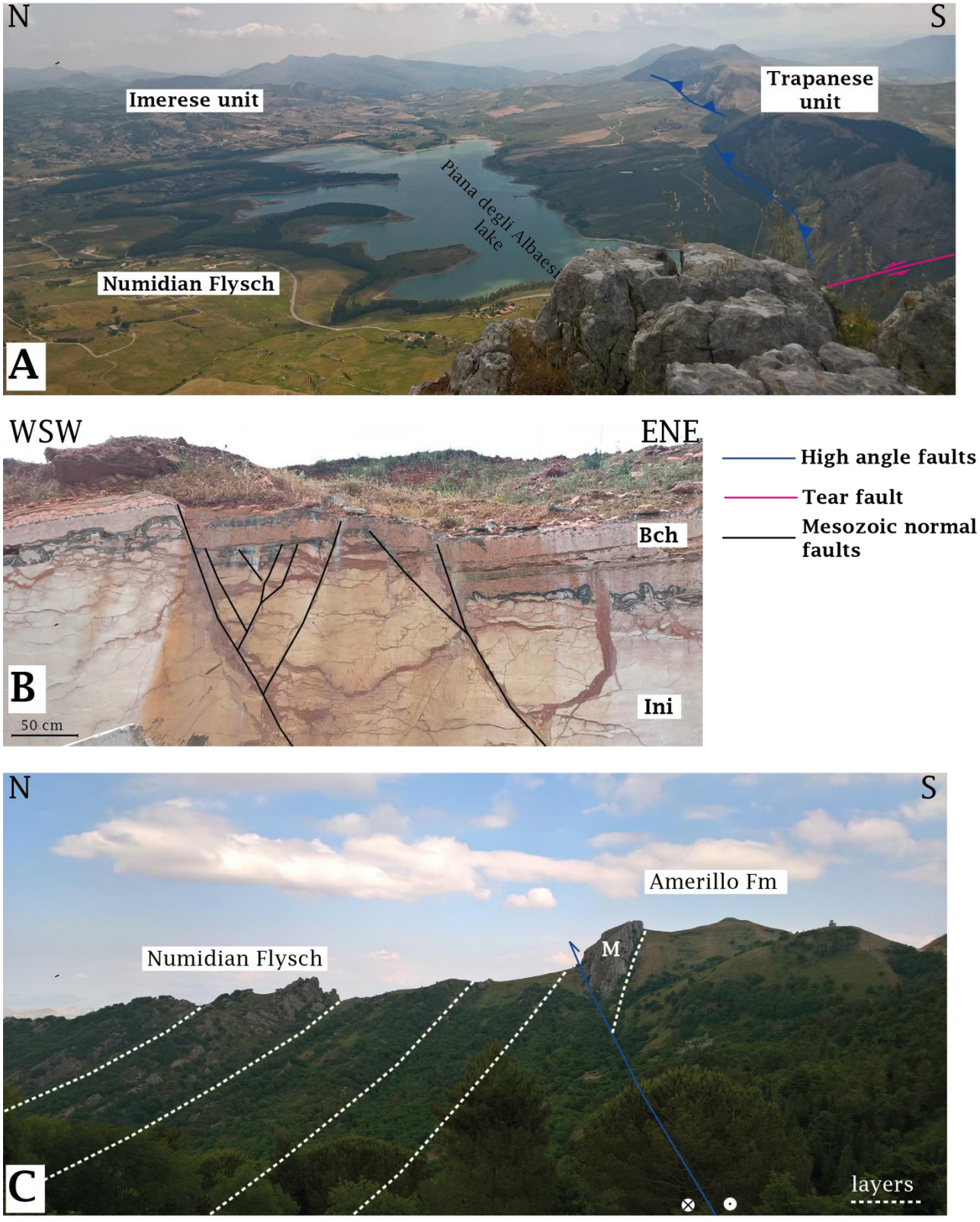

Figure 3.3 Main faults observed in the study area. (A) Panoramic view showing WNW-ESE- to E-W-trending high angle and NNE-SSW- trending tear faults characterizing the northern border of the Mt. Kumeta ridge. (B) WNW-ESE-trending Mesozoic normal faults along the Mt. Kumeta. (C) Panoramic view showing WNW-ESE-trending high angle transpressive fault characterizing the northern border of the Mt. Busambra ridge. Ini—Inici Fm.; Bch—Buccheri Fm.; M—Amerillo megabreccias.

3.4 Methods and Materials

3.4.1 Seismic Interpretation

Thirteen multichannel seismic reflection profiles (from different surveys by Eni/Agip from the 70's to the 90's) covering an area of ~ 900 km^2 are available (Fig. 3.2). Datum plane is the sea level. Eight seismic profiles are dip lines (perpendicular to the main structures), two are strike lines (parallel to the main structures) and three are oblique lines. Processed seismic lines (see Albanese and Sulli, 2012 for adopted parameters) result in data with a resolution of about tens of meters providing fair to good images of the shallower portion of the crust. The recording length is 7.0 s TWT with an effective penetration of 5 to 6 s TWT. In this work we focused our interpretation on the first 4s TWT as any deeper signal bears most of the time very misleading interpretations.

Calibration of the seismic lines was performed using well data (Marineo 1 well; Fig. 3.4 A, B) and geological maps (Catalano et al., 2010a, b). Seismic units were defined after identifying key reflectors (tops of interpreted horizons), seismic attributes (e.g., lateral continuity of the reflectors, amplitude and frequency of the signal) and thickness of seismic facies. Move software has been used to perform the seismic interpretation. Picked horizons are: top of lower and upper Trapanese unit; top of the Mesozoic overthrusting unit (Sicanian or Imerese units); top of Tertiary claystones/sandstones (Numidian Flysch). Major faults affecting the Trapanese unit were interpreted. Along strike, fault traces pertaining to the same fault surface were grouped assigning a common name (e.g. Fault_1, Fault_2, Fault_3).

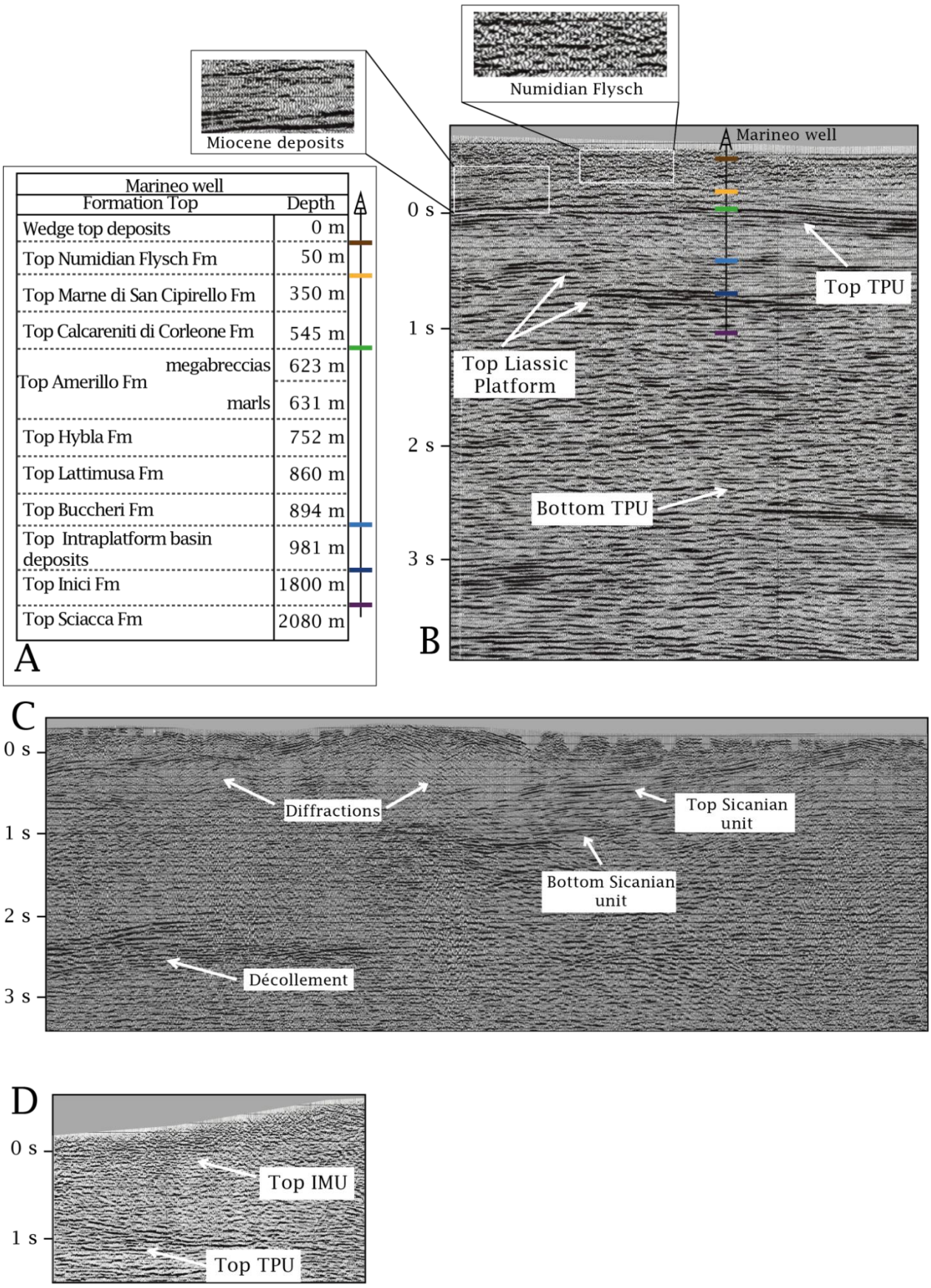

Figure 3.4 Main seismic units (B, C, D) calibrated by the Marineo well stratigraphy (A). See Fig. 3.2 A for well location.

3.4.2 3D Geological model reconstruction

Horizons and faults after a first check of consistency (no crossing between horizons) were exported as pointsets from Move software (.dat file) and imported in Skua-Gocad software in order to reconstruct a more refined water-tight 3D geological model.

A 3D model is said to be water-tight when every stratigraphic horizon is continuously defined over the area of interest and has clean intersections with either lateral boundaries, faults, unconformities or erosion surfaces (Caumon et al., 2004). Faults and horizons can be handled simultaneously in Skua software (Jayr et al., 2008). A chronological stratigraphic scale has been built using the selected horizons to guarantee that no horizon crossing occurred. The software interpolates the stratigraphic horizons according to the different types of stratigraphic sequences. The sequences might be conformable, unconformable, baselap or erosive.

As the main focus of this work is to define the deformation affecting the Trapanese unit, the tectonic boundary between this unit and the overthrusting units is assumed to be an unconformable boundary. This simplification strongly reduces the modelling computation time and model complexity (limited number of faults) without having a strong impact on the results.

A volume of interest (V.O.I., 24 km x 37 km x 5.5 s) has been defined to include the interpreted structures. It indicates the amount of three-dimensional space occupied by faults and horizons. After V.O.I. definition, a fault network that interpolates fault points and defines the branching relations of the various sets of faults is built. Once the V.O.I. is split into fault blocks bounded by the interpreted faults, the horizons are constructed, for each stratigraphic sequence. Horizons are defined as isovalues of a spatial varying function, representing the stratigraphic time in the faulted blocks. As a consequence, horizon-fault definitions are consistent and geometrical cuts on faults are clean. Building a water-tight model is also a good test for the quality of data. Whenever some data points are incorrectly interpreted, for example being assigned to the wrong side of a fault, the resulting time function becomes geologically incorrect. Thus, the possibility of consistently interpreting and building a water-tight model is a first step in the quality control

of the resulting model. In order to reduce the simulation time for building the 3D model at regional scale, a 300 x 150 m resolution for the horizon construction was selected and fault zones were drowned as single fault planes to reduce the number of small faults (length < 3km).

3.4.3 3D depth conversion

3D velocity cube was built using standard averaged velocity values based on DIX interval velocity analyses, extracted from the board on the seismic profiles. It has been used to convert 3D time to depth (Fig. 3.5). Average velocities used for the conversion are: 4.6 km/s for the lower Trapanese unit (until the Top Amerillo Fm); 3.1 km/s for the upper Trapanese unit (between Top Amerillo and Top Marne di San Cipirello Fms); 3.8 km/s for the deep-water limestone/siliciclastic deposits; 3.2 km/s for the Numidian Flysch and 2.7 km/ for the wedge-top basin deposits.

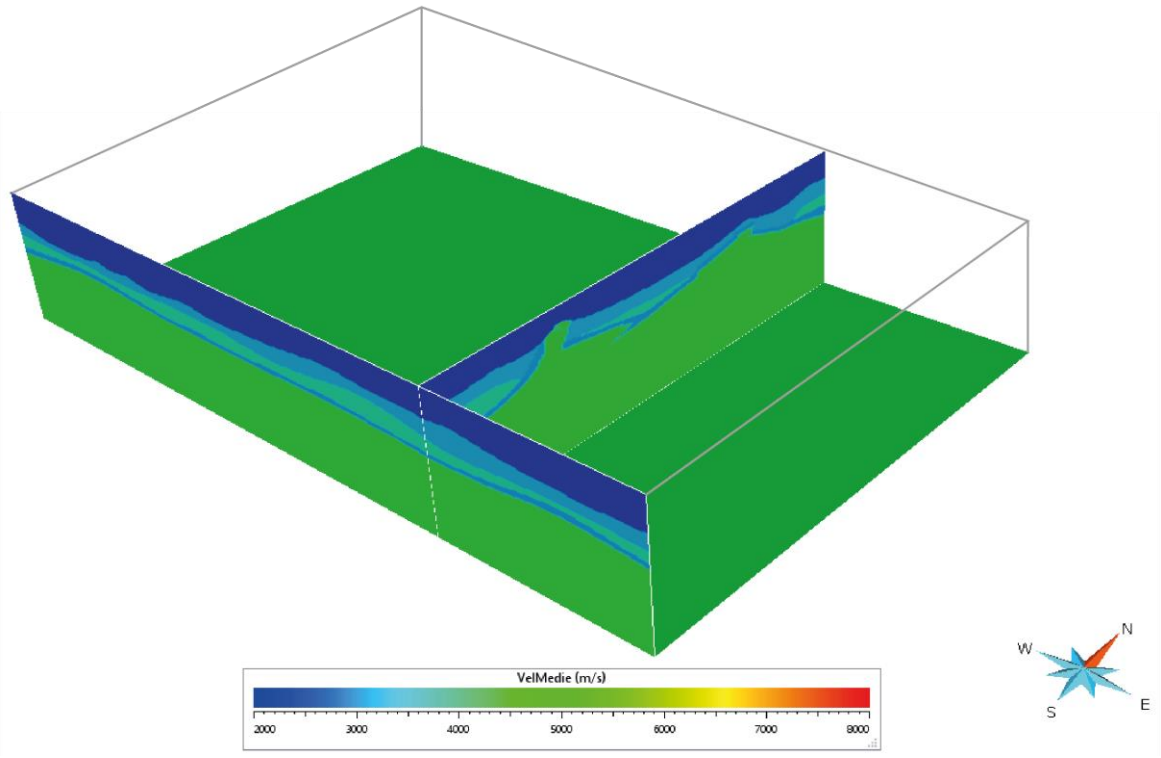

Figure 3.5 3D velocity model applied for performing depth conversion.

3.4.4 3D Restoration

Restoration technique aims at obtaining the pre-deformation geometry of the model. Thus, not-restorable models are geometrically and topologically inconsistent (Dahlstrom, 1969). A work stage of 3D geo-mechanical restoration was performed by using Kine3D-3 tool (Skua-Gocad software). The restoration computes the equilibrium of elastic forces on the water-tight earth model, once the model has several movement constraints. The basic assumption in Kine3D-3 is that geometry of horizons and faults in the past is approached by minimizing the strain energy of deformation of the various blocks, while giving some boundary on the faults and on the horizons and different types of rheology to the blocks (Plesch et al., 2007; Li et al., 2013, 2016; Shuwei et al., 2013; Al Fahmi et al., 2016;). While traditional 2D section balancing restores each unit separately in a stepwise approach, the 3D approach restores multiple fault blocks in one single step. Thus, the user input is limited to the definition of adequate boundary conditions (Moretti, 2008). The boundary conditions are:

i) faults are defined as two sided gliding contacts, during deformation the rock units in the hangingwall must be in contact with the ones in the footwall. This gliding contact is a first type of constraint for the energy minimization and makes sure that the fault blocks do not interpenetrate or get separated during deformation;

ii) the southern border of the model is set as a “pin” face (movement locked in x and y directions) whereas the eastern border, is considered as secondary pin face (locked movement in x direction). The main transport direction reconstructed for the Trapanese unit is towards S-SSE (Avellone et al., 2010; Gasparo Morticelli et al., 2017), thus the undeformed or less deformed part is located toward the S-SSE.

iii) the Amerillo horizon which represents the interpreted horizon with the clearest image must be flattened (z is fixed=0).

Assuming these boundary conditions, the restoration tool tries to find a solution for the 3D model minimizing the deformation energy. This approach is called geomechanic (Maerten and

Maerten, 2006; Moretti et al., 2006; Moretti, 2008; Guzofski et al., 2009; Durand-Riard et al., 2010; 2013) and only its geometric results are used here in order to define which interpretation is validated. Rheology is assumed as uniform for the entire model. According to the rock types involved, the chosen parameters are density of 2.8 g/cm^3, Poisson ratio of 0.3, Young module of 0.65x10^{11} Pa (Turcotte and Schubert, 2002).

3.5 Results and discussion

3.5.1 Seismic facies interpretation

We distinguished four seismic facies delimited by four seismic reflectors: the Trapanese unit (lower and upper), the Numidian Flysch, and deep-water limestones/siliciclastic deposits (Sicanian or Imerese units). Seismic reflectors has been calibrated using well data (Fig. 3.4) and field data (where the interpreted horizons crops out; Fig. 3.2)

The top of the lower Trapanese unit is delimited by the top of the Amerillo Fm (Fig. 3.4). In this case, the strong contrast of acoustic impedance (IA) due to the boundary between the Miocene calcarenites and marls (upper Trapanese unit) and the Cretaceous-Eocene limestones generates a high amplitude reflector, recognisable in all the seismic profiles. It is the clearest picked horizon, therefore, it represents a seismic marker.

The top of the upper Trapanese unit is delimited by the top of San Cipirello Fm. (Fig. 3.4). In seismic profiles, this reflector is interpreted as a tectonic boundary between the Trapanese and the overthrusting units. The lower Trapanese seismic facies is mainly transparent and locally replaced by high amplitude broken reflectors, indicating that the top of the Jurassic platform is often affected by Mesozoic normal faults (Fig. 3.4 A, Fig. 3.6 a). The bottom of the lower Trapanese unit is often discontinuous and locally marked by a package of high frequency reflectors with internal divergence, indicating that the unit is detached from its basement (Fig. 3.4 A, C). The upper Trapanese unit (between the top Amerillo and top San Cipirello Fms.)

seismic facies is characterised by reflection free bands. The total thickness of the Trapanese unit is 2.0 to 2.2s TWT.

The top of the Numidian Flysch is hard to identify as it is marked by low acoustic impedance contrast due to similar lithology between the Numidian Flysch and overlying wedge-top basins successions (Figs. 3.2, 3.4). This reflector was interpreted in a few seismic profiles, mainly toward the western part of the study area (lines a, b, c, e, e' in Figs.3.6, 3.7). Seismic facies (Fig. 3.4) is characterized by medium to high amplitude reflectors and it is locally transparent. The bottom of the Numidian Flysch is a tectonic contact with the Trapanese unit or an unconformable contact with the deep-water limestone-siliciclastic unit (Imerese or Sicanian unit) (Figs. 3.4, 3.6, 3.7). The overall thickness is about 0.3-0.7 s TWT.

The top of the deep-water limestones-siliciclastic unit is well defined in the southern part of the study area where it corresponds to the Sicanian unit widely cropping out in the Sicani Mts. area (Fig. 3.1). Top of the Sicanian limestones as well as the top of the lower Trapanese unit is characterized by high amplitude continuous reflectors (Fig. 3.4), due to the high acoustic impedance contrast with the overlying Oligocene-Miocene calcarenites and marls. The seismic facies is characterized by sub-parallel continuous and medium-high amplitude reflectors and it is locally transparent. The bottom of this unit is a tectonic contact with the underlying unit. Total thickness is about 0.5–1 s TWT.

In the eastern part of the study area between the Kumeta and Busambra Mts. (Fig. 3.7), a seismic unit with a facies similar to that observed for the deep-water limestones-siliciclastic unit, has been detected below the Numidian Flysch. Previous authors attributed this seismic facies to the Sicanian unit (Albanese and Sulli, 2012; Avellone, 2010; Catalano, 2000) without any constraint by either wells or field data. The thickness of the unit between the Kumeta and Busambra Mts. is 0.5-0.7 s TWT. In the northern part of the study area, only one seismic profile (Fig. 3.7 d, d') shows the deep-water limestones/siliciclastic unit overriding the Trapanese unit. There, average thickness of this seismic facies is about 0.8 s TWT and based on field data, it corresponds to the

Imerese unit (Fig. 3.4). Westward, between the Kumeta and Busambra Mts. only the Numidian Flysch overlying the Trapanese unit has been detected (Fig. 3.6 c).

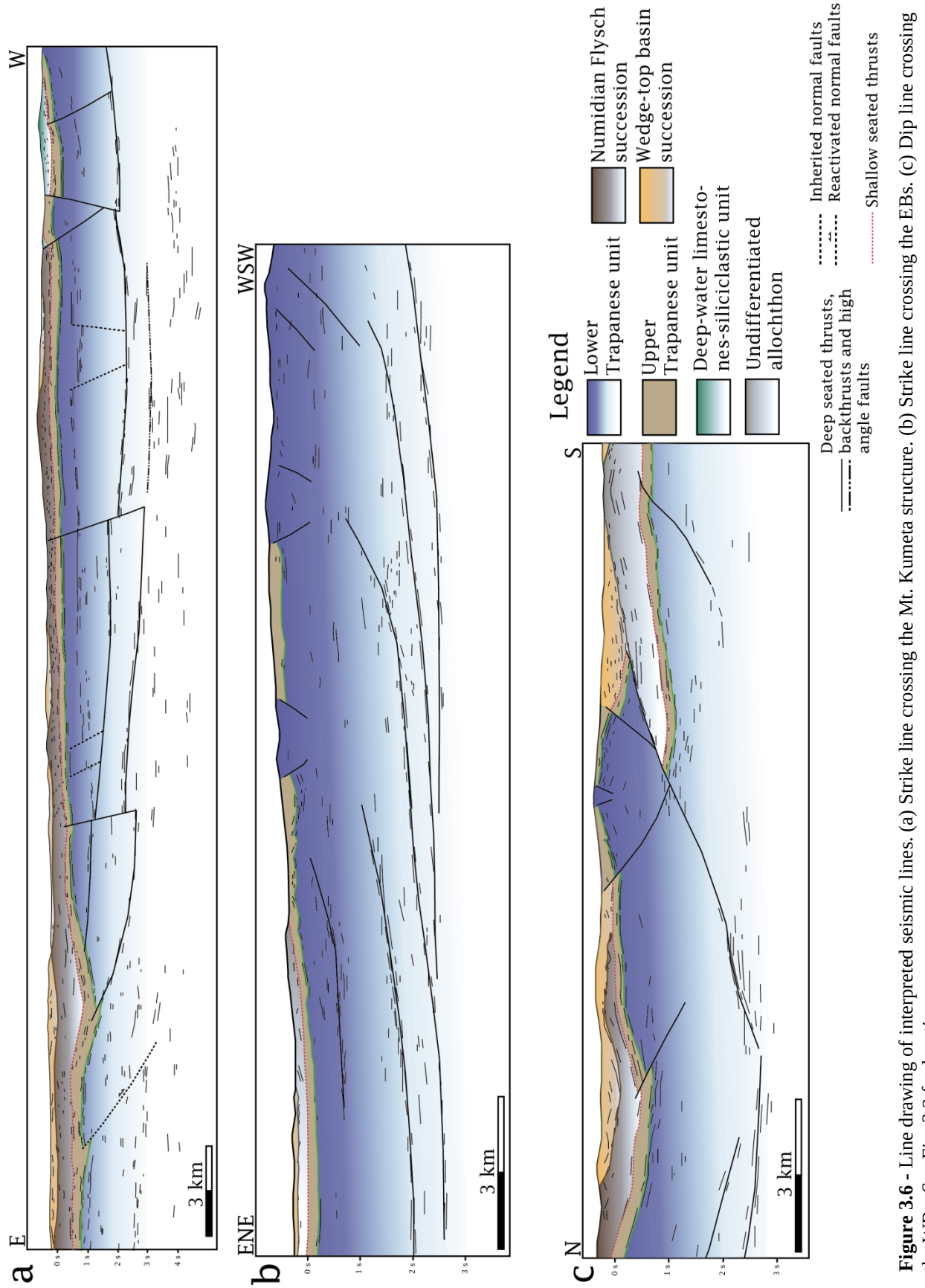

Figure 3.6 - Line drawing of interpreted seismic lines. (a) Strike line crossing the Mt. Kumeta structure. (b) Strike line crossing the EBs. (c) Dip line crossing the WBs. See Fig. 3.2 for location.

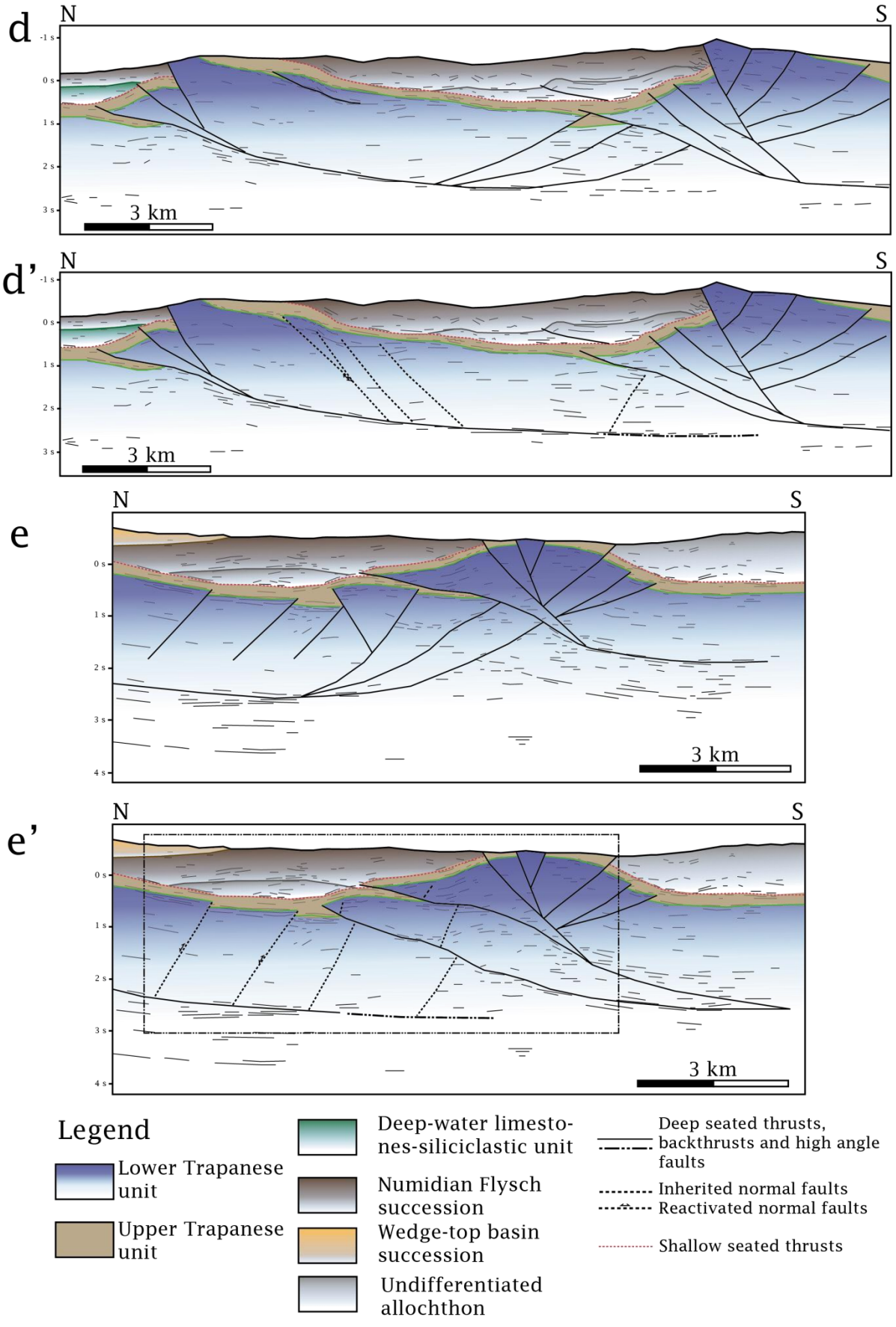

Figure 3.7 - Line drawing of interpreted N-S-trending seismic lines. (d, e) Structural interpretation based on previous structural model (Albanese and Sulli, 2012); (d', e') Structural interpretation proposed in this work. See Fig. 3.2 for location. Dotted rectangle indicate the seismic line detail shown in Fig. 3.9.

3.5.2 Previous structural model

We used seismic lines interpreted by Albanese and Sulli (2012) (Fig. 3.2 A lines c, e, f, g) as base for our structural interpretation (Fig. 3.6 c and Fig. 3.7 d, e). The remaining seismic lines available in the area (Fig. 3.2 A) were interpreted following the structural style depicted by these authors in order to reconstruct the 3D model. The Mt. Busambra structure can be subdivided into two different sectors: the western Mt. Busambra structure (WBs) covered by lines c, f, g (Fig. 3.2) and the eastern Mt. Busambra structure (EBs) covered by the remaining lines (Fig. 3.2). The Structural and kinematic model proposed by Albanese and Sulli, (2012) defines a first stage of deformation involving the Trapanese unit that was deformed by foreland verging thrusts during the late Tortonian. In the study area, thrusts linked to this first deformation involve the Mt. Busambra structure (Fig. 3.6 c and Fig. 3.7 d, e). The second stage of deformation involves the Mt. Kumeta and the EBs after the uppermost Tortonian time, when backthrusting associated with high angle transpressive faults occurred (Fig. 3.7 d, e). In detail, the foreland verging thrusts deforming the EBs gently rises and wedges bringing the backthrusts to be uplifted and passively carried up (Albanese and Sulli, 2012; Fig. 3.7 d, e). As a result, the eastern Mt. Busambra structure was interpreted as a triangle zone where the outcropping relief represents a passive-roof duplex.

Seismic lines (~E-W striking), crossing the EBs, show how backthrusts individuated in the N-S striking seismic lines correspond to different splays (Fig. 3.6 c) of an imbricate backthrust system. On the other hand, the Mt. Kumeta ridge is characterized by tear faults dissecting the backthrusts passing to a lateral ramp toward the west (Fig. 3.6 a). Inherited normal faults affecting the lower Trapanese unit are also recognisable along the Mt. Kumeta structure (Fig. 3.6 a).

Both ridges are bounded by ~E-W striking high angle transpressive to reverse faults (Fig. 3.3 A, C). In seismic profiles, these faults seem to join backthrusts at depth (Fig. 3.7 d, e).

Albanese and Sulli (2012) in their work, validated their structural interpretation by restoring four of the seismic lines proposed in this work (lines c, e, f, g in Fig. 3.2). As a result, they evaluated an increase of shortening for the Trapanese unit from the West (13.5%) to the East (19.3%). In this work, we further checked whether their structural model can be validated by a 3D geological model reconstruction and restoration.

In order to build the 3D model, extrapolation of different horizons and faults in areas uncovered by seismic lines is required. For this purpose, we used available geological cross-sections and field data (Avellone and Barchi, 2003; Avellone, et al., 2010; Catalano et al., 2010a, b; Gasparo Morticelli et al., 2017).

Five surfaces are represented in the 3D model (Fig. 3.8 B), from bottom to top these are: top of Amerillo Fm and top of Marne di San Cipirello Fm (which represent the top of the lower Trapanese unit and the top of the upper Trapanese unit, respectively); top of deep-water limestones/siliciclastic succession; top of the Numidian Flysch; topography.

The lowermost surface corresponds to the top Amerillo Fm that is exposed along the Mt. Kumeta and partially along the Mt. Busambra structures. The surface describes two large ramp anticlines (~5km wide) (Fig. 3.8 C, D; Kumeta and Busambra Mts. structures) with wavelength of about 7 km and a syncline in between the two. Along the high angle faults bordering the Kumeta and Busambra Mts. structures the Amerillo Fm is often eroded. As a result eroded area are identifiable in the model (Fig. 3.8 C). Top of Marne di San Cipirello Fm. almost mimics the Amerillo Fm. Differences are related to the amount of erosion that is higher for the San Cipirello Fm respect to the Amerillo Fm. The third surface consists of Top of deep-water limestones/siliciclastic succession that unconformably overlies the Trapanese unit. This surface extends only in the southern and central-eastern portions of the study area. Even though this horizon is interpreted also to the north of the Mt. Kumeta structure (Fig. 3.7 d, d'), the small amount and the quality of data does not allow to extrapolate this horizon there with confidence,

thus, it was disregarded in this reconstruction. The top of the Numidian Flysch surface, is represented only in the western part of the area.

Twenty-eight fault segments affecting the Trapanese unit are defined in the 3D model (Fig. 3.8 B). Due to the modelling method, some segments sometimes represent the same original fault, if a later deformation stage separates a first generation fault into several other segments. The Mt. Kumeta structure is characterized by SSW dipping backthrusts connected along hard linkages constituted by three NNE-SSW striking tear faults (Fig. 3.8 A). The dip angle of the Mt. Kumeta backthrusts varies from almost horizontal close to the basal décollement, up to 35° close to the surface. Foreland verging thrusts deform the Mt. Busambra structure as it follows (Fig. 3.8 A):

i) eastward (EBs) three thrusts are interpreted with dip angles varying from 10° to 45° (Fig. 3.8 A, C, D). Tip lines of these thrusts reach depths of 1-1.5 s TWT;

ii) westward (WBs) a ENE-WSW striking thrust which shows dip angles of 38° close to the surface (~0 s TWT) flattening at depth is interpreted.

Between eastern and western Mt. Busambra foreland verging thrusts (Fig. 3.8 A) a hard linkage (e.g. a tear fault) is suggested (Albanese and Sulli, 2012). The geological map of the area (Fig. 3.2) and field observations do not allow to clearly recognise such a tear fault. On the contrary, tear faults dissecting the Mt. Kumeta structure are clearly recognisable in the field (Fig. 3.3 A) and poorly defined in the seismic profiles (Fig. 3.6 a). Furthermore, the EBs is characterized by an imbricate system of backthrusts constituted by four SSW-dipping splays cutting and obliterating the foreland verging thrusts. Backthrust splays show a ramp-flat geometry where dip angles vary from almost horizontal close to décollement, up to 45° in the ramp portion and 20° in the flat one (Fig. 3.8 B, D).Thrusts and backthrusts are blind.

Ten reverse to transpressive E-W to WNW-ESE striking faults are displayed crossing the topography and partially branching the backthrusts (Fig. 3.8 B). Some of these faults do not join backthrusts at depths (Fig. 3.8 B) probably due to the applied simplification (grouping small faults). Reverse to transpressive faults dip angles vary from 45° to 70°.

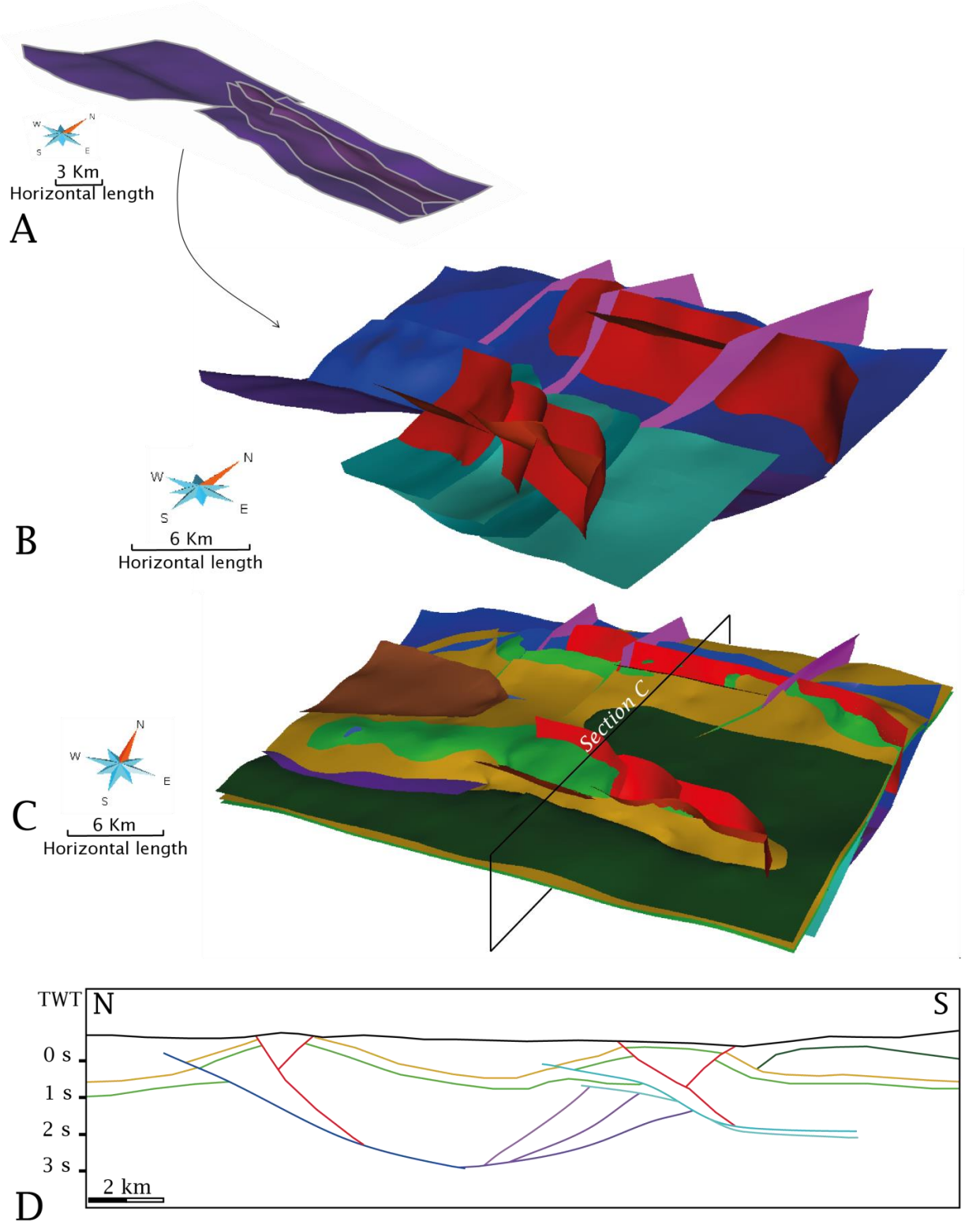

Figure 3.8 - 3D geological model based on the structural model by Albanese and Sulli (2012). (A) Detail of foreland verging thrusts characterizing the Mt. Busambra structure. (B) Detail of fault network. (C) Represented faults and horizons. (D) Cross-section extracted from the 3D model. Faults in blue correspond to the Mt. Kumeta backthrusts; faults in light blue correspond to the Mt. Busambra backthrusts; faults in purple correspond to the Mt. Busambra thrusts; faults in red correspond to the high angle transpressive to reverse faults; Green surface corresponds to the Amerillo Fm (top lower Trapanese unit); light brown surface corresponds to the San Cipirello Fm (top upper Trapanese unit); dark green surface corresponds to the limestone/siliciclastic deep-water unit; brown surface corresponds to the Numidian Flysch.

3D water-tight model reconstruction provides a first quality check of the seismic interpretation. The reconstructed water-tight 3D model reveals some inconsistencies between the seismic interpretation and lateral continuity of the structures along the Mt. Busambra ridge. In particular, 3D representation of the backthrust splays cannot perfectly fit the seismic interpretation. Cross-section D (Fig. 3.8) is extracted from the 3D model in the same position where line e (Fig. 3.7) is located. A single backthrust is recognisable in the seismic interpretation whereas two different backthrusts are represented in the cross-section. This mismatching is related to the lateral transition from a backthrust splay to the next one that is not taken into account in the 2D interpretation but must be considered when building a 3D geological model.

3D restoration provides a second quality check of the seismic interpretation. Before restoring the model, 3D depth conversion was performed. The resulting structural model, shows an increase in the fault dip angles: 35° to 40° for the Mt. Busambra thrust and backthrusts; 29° to 40° for the Mt. Kumeta backthrusts; 50° to 75° for the reverse to transpressive faults.

Resulting thickness for the different units is: 3.9 km for the lower Trapanese unit; 0.4 -0.9 km for the upper Trapanese unit (with maximum thickness values close to thrust termination, probably due to tectonic thickening); 0.6-2.0 km for the overthrusting unit with highest values between the Kumeta and Busambra Mts. ridges.

The restoration tool was not able to find a solution for this model, because the convergence towards a solution was never reached. In order to understand the geometrical issue of the model, we released the global convergence constraint of the equilibrium of forces, so that we got an approximated solution. This solution revealed that only some faults did prevent the restoration to reach full convergence. These faults are the foreland verging thrusts characterizing the EBs. Since these faults (EBs thrusts) were not restored, it was possible to assume that the geometrical issue which does not allow us to perform correctly the 3D restoration, was linked to these faults (located in the triangle zone)

In order to solve this issue and reconstruct a correct restored state, we performed the restoration in two steps. In the first step, we restored only the thrusts characterizing the EBs, which created the geometrical issue (Fig. 3.8 A). In the second step we performed the restoration of the rest of the model. Also in this case, no reliable solution could be found.

For this reason it was decided to re-interpret the seismic lines proposing a new structural model for the Kumeta and Busambra Mts.

3.5.3 New model

3D geological model and restoration show that seismic interpretation of the EBs is geometrically incorrect or inconsistent. Thus, a new interpretation of this portion of the study area is required. The new interpretation (Fig. 3.7 d', e') considers the EBs affected only by a backthrust system. Following this interpretation, a single-step deformation model is generated, considering the coexistence of thrusting to the west and backthrusting to the east forming the Mt. Busambra structure. Furthermore, in the new interpretation inherited normal faults affecting the Trapanase unit are depicted (Fig. 3.7 d', e') in order to explain diffraction and changing in the reflectors dip angles recognised in the seismic reflection profiles.

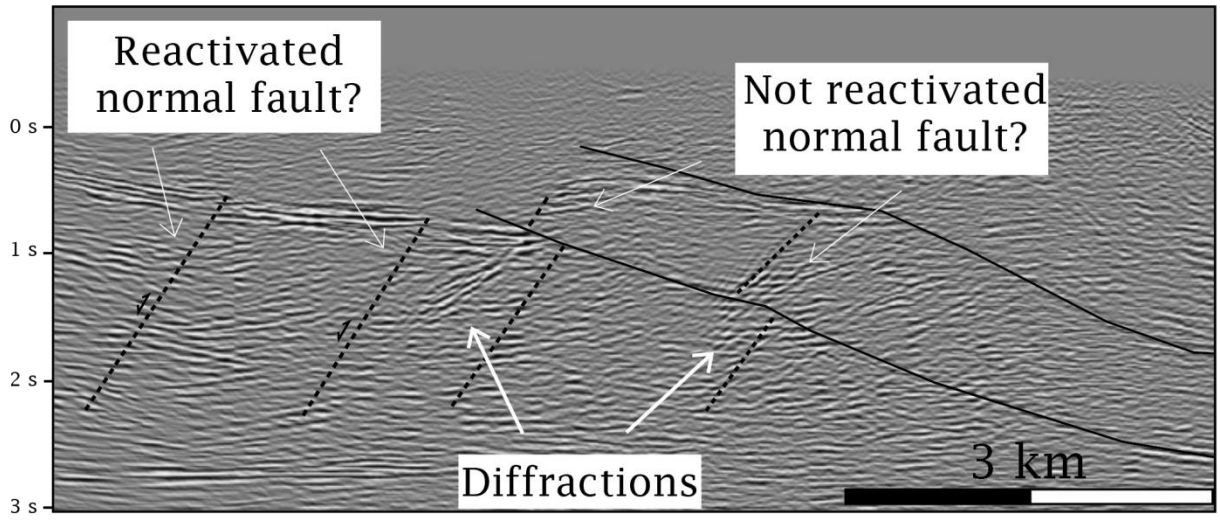

Figure 3.9 - Detail of seismic line e (Figs. 3.2, 3.7 e') showing backthrusts (black lines) and Mesozoic normal faults (dotted black lines) which are cut and partially inverted during the compressional phase affecting the Trapanese unit (double arrow).

These faults probably correspond to Mesozoic normal faults affecting the Trapanese unit passively carried up or partially cut by Neogene backthrusts (Fig. 3.7 d', e' and Fig. 3.9). Some of these faults could have been partially reactivated (Fig. 3.7 d', e').

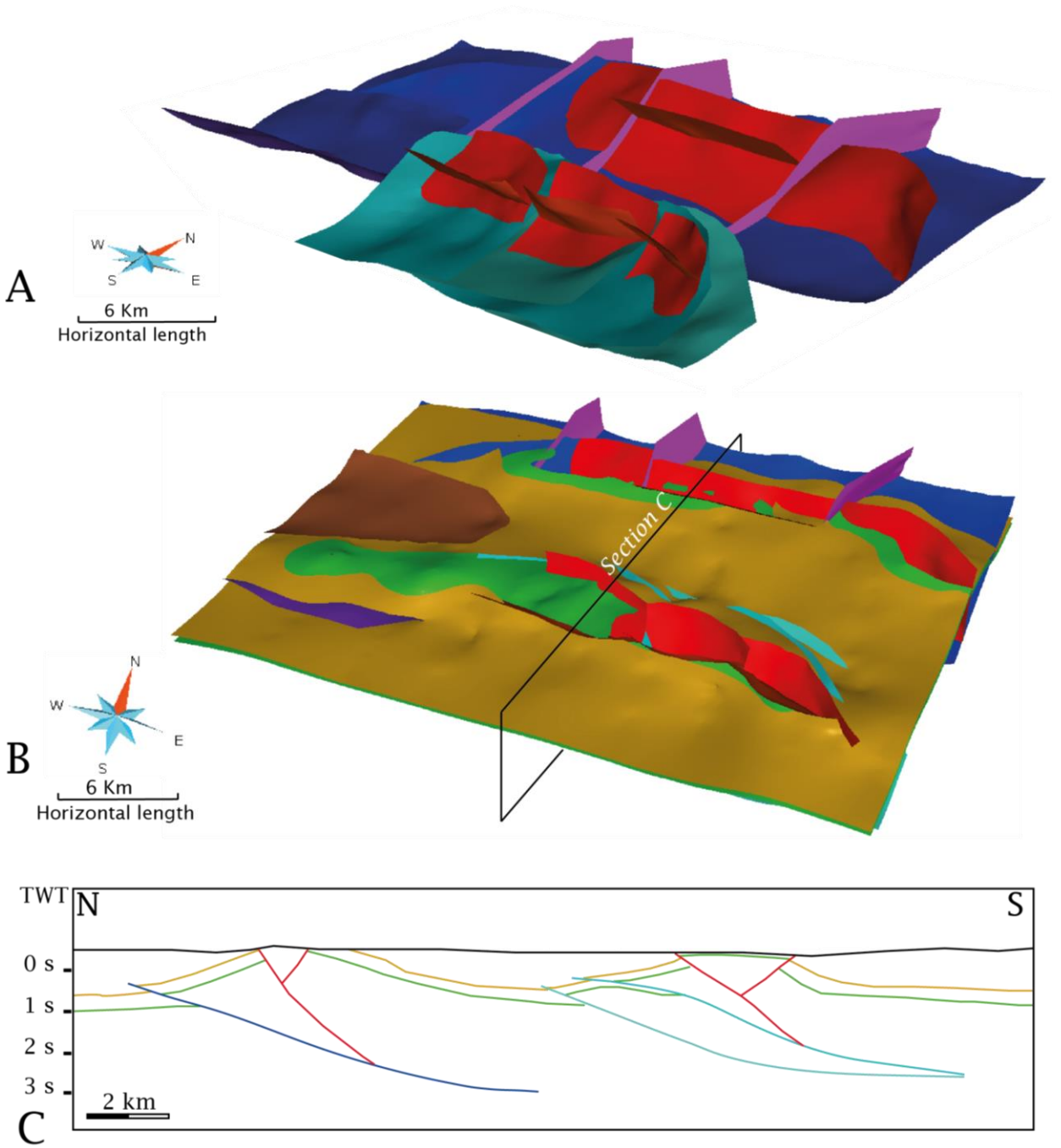

Figure 3.10 - 3D geological model based on the structural interpretation proposed in this work (A) Detail of fault network. (B) Represented faults and horizons. (C) Cross-section extracted from the 3D model. e faults in blue correspond to the Mt. Kumeta backthrusts; faults in light blue correspond to the Mt. Busambra backthrusts; faults in red correspond to the high angle transpressive to reverse faults; Green surface corresponds to the Amerillo Fm (top lower Trapanese unit); light brown surface corresponds to the San Cipirello Fm (top upper Trapanese unit); brown surface corresponds to the Numidian Flysch.

Four surfaces were represented in the 3D model, from bottom to top they are (Fig. 3.10 B): top of the Amerillo and top of the Marne di San Cipirello Fms. defining the lower and upper Trapanese unit; top of the Numidian Flysch and topography.

In this model we did not represent the top of deep-water limestones/siliciclastic surface because it does not impact on the modelling and restoration results.

Twenty-five fault segments affecting the Trapanese unit are also represented in the new 3D model (Fig. 3.10 A).

Differences between this new 3D structural model and the previous one mainly concern the Mt. Busambra structure. The EBs is only deformed by a backthrust system where lateral extension of the different splays is well represented. Splays dip angles vary from 38° close to the surface to almost horizontal reaching the décollement level. Cross-section extracted from the 3D model (Fig. 3.10 C) match the interpretation of the seismic line (Fig. 3.7 e') located in the same position. A soft linkage (e.g., folding) is considered to connect the WBs and EBs. Soft linkages connecting thrusts are recognised by different authors (Dashlstrom, 1969; Walsh et al., 1999; Watkins et al., 2017, Higgins et al., 2007, 2009; Bretis et al., 2011) in deep-water fold-and-thrust belts, in the frontal portion of fold-and-thrust belts and in siliciclastic successions. These linkages can explain accommodation of a relatively constant shortening amount within the fold-and-thrust belt (Watkins et al., 2017) even if changes in structural style occur along strike.

In the reconstructed 3D model, displacement is transferred between the thrust and backthrust zones defining an antithetic thrust fault linkage (Type 2 in Higgings at al. 2007). In this kind of linkage, two faults with opposite vergence grow with associated fault-propagation folds and converge laterally creating a continuous fold between the two faults (Fig. 3.11 A).

As a result, displacement along the thrust and backthrust decreases toward the linkage area. Along the Mt. Busambra structure (Fig. 3.11 B, C), the displacement of the backthrust system (Fig. 3.11 D) which gradually decreases toward the linkage area (west) can be noticed; a continuous fold is depicted in the linkage area (Fig. 3.11 E); a gradual increase of displacement

along the thrust is recognised moving westward. Thus, this configuration is in agreement with a soft linkage connecting thrust and backthrust (Higgins et al., 2007; Fig. 3.11 A and B).

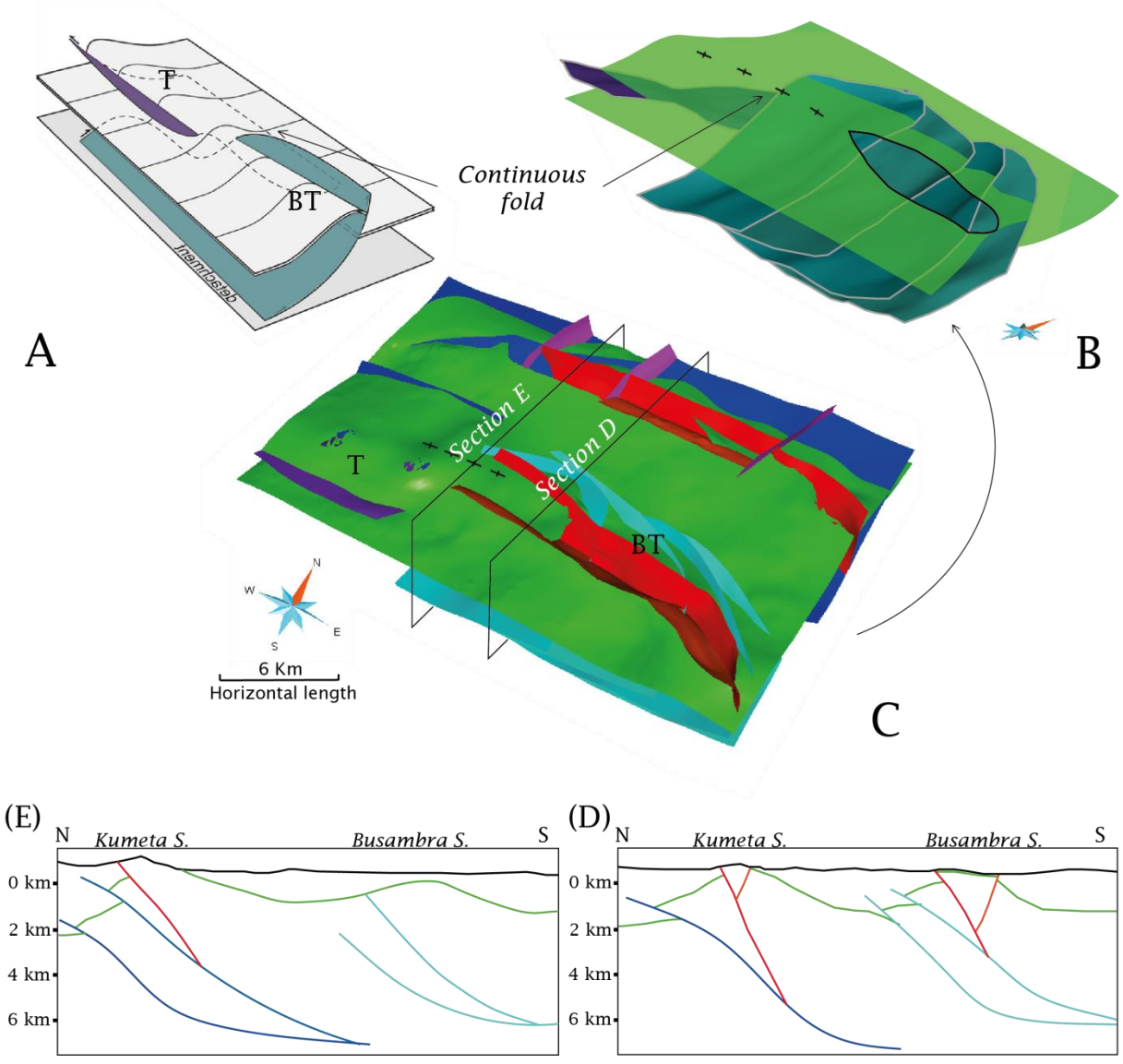

Figure 3.11 - Detail of the soft linkage connecting the WBs and EBs. (A) Type 2 antithetic soft linkage modified after Higgings et al., (2007). (B) Antithetic soft linkage proposed for the Mt. Busambra structure. (C) 3D model showing surface displacement variation along different faults for the Amerillo Fm (top of the lower Trapanese unit). (D, E) cross-sections extracted from the model showing displacement variation for the Amerillo Fm. Faults in blue correspond to the Mt. Kumeta backthrusts; faults in light blue correspond to the Mt. Busambra backthrusts; faults in red correspond to the high angle transpressive to reverse faults; Green surface corresponds to the Amerillo Fm.

3D restoration validates the 3D model (Fig. 3.12 A, A'), showing a dominant NNW-SSE elongation. Eroded portion of the Amerillo Fm horizon are preserved, showing holes in the 3D

restored model (Fig. 3.12 B, B'). Calculated amounts of shortening along are: ~13 % in the western portion of the study area and ~10% in the eastern portion. These data are in agreement with a larger tectonic transport observed by Albanese and Sulli (2012) in the WBs, with respect to the eastern one, that is revealed by buried WNW-ESE thrust fronts. Amount of shortening in the western sector of the area are consistent as well with previously reported values (13.5% in Albanese and Sulli, (2012); 13% in this work).

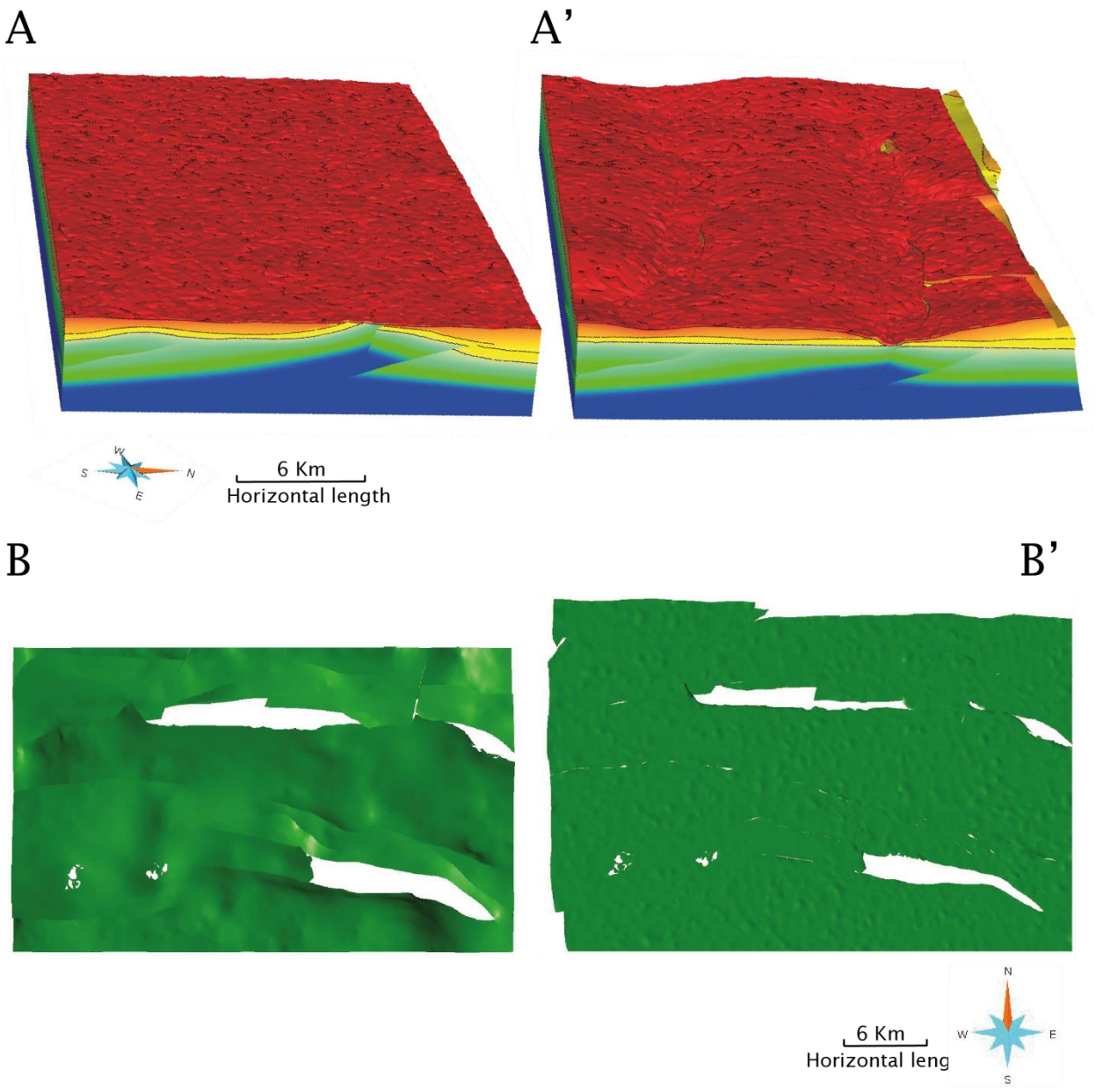

Figure 3.12 - 3D restoration performed for the 3D model in Fig. 3.10. (A) Deformed state. (A') Restored state. (B) Detail of the deformed state of the Amerillo Fm surface. (B') Detail of the restored state of the Amerillo Fm surface.

On the other hand, shortening amount evaluated by Albanese and Sulli (2012) in the eastern part (19.3 %) is much higher than the amount of shortening calculated in this work (10%). Such a difference can be explained with the absence of the triangle zone in our model. The maximum compression direction for the Trapanese unit (NNW-SSE oriented) is in agreement with directions evaluated by different authors using field data (Avellone et al., 2010; Gasparo Morticelli, 2017). Several assumptions (e.g., single fault representing a fault zone; lateral extrapolation of structures in poorly constrained areas) were needed to obtain a restorable water-tight representation of horizons and faults. Several parts of it are geometrical extrapolations, and it is probable that it will need to be revised if any new seismic becomes available in the area. 3D seismic would of course be of great help to improve the correct representation of horizons and faults. Until this becomes available, the 3D model presented here is the most consistent with all available data and kinematic reconstructions.

3.5.4 Impact of inherited structures

Occurrence of triangle zones and backthrusts are recognised worldwide (Medwedeff, 1992; MacKay, 1995; Zapata and Allmendinger, 1996; Burbank et al., 1999; Bello et al., 2000; Xu and Zhou, 2007; Cardello and Doglioni, 2015; Malz et al., 2016; Mahoney et al., 2017; Tibalti et al., 2017; Von Hagke and Malz, 2018). Development of such kinds of structures as well as their lateral variability are linked to several parameters widely investigated by means of numerical and analogue modelling (Costa and Vendeville, 2002; Bonini, 2007; Ruh et al., 2012; Dean et al., 2013; Likerman et al., 2013; Malz et al., 2016; Mahoney et al., 2017; Watkins et al., 2017). Main factors influencing backthrusts rather than forethrusts development are: i) basal friction coefficient, if very low it can promote backthrusts rather than forethrusts development; ii) thickness of the sedimentary cover and depth of basal décollement layer: thicker cover and décollement layers can promote backthrusting and triangle zone development; iii) inherited

mechanical weaknesses such as pre-thrusting normal faults, which can also affect lateral variation of thrusts spacing and their position.

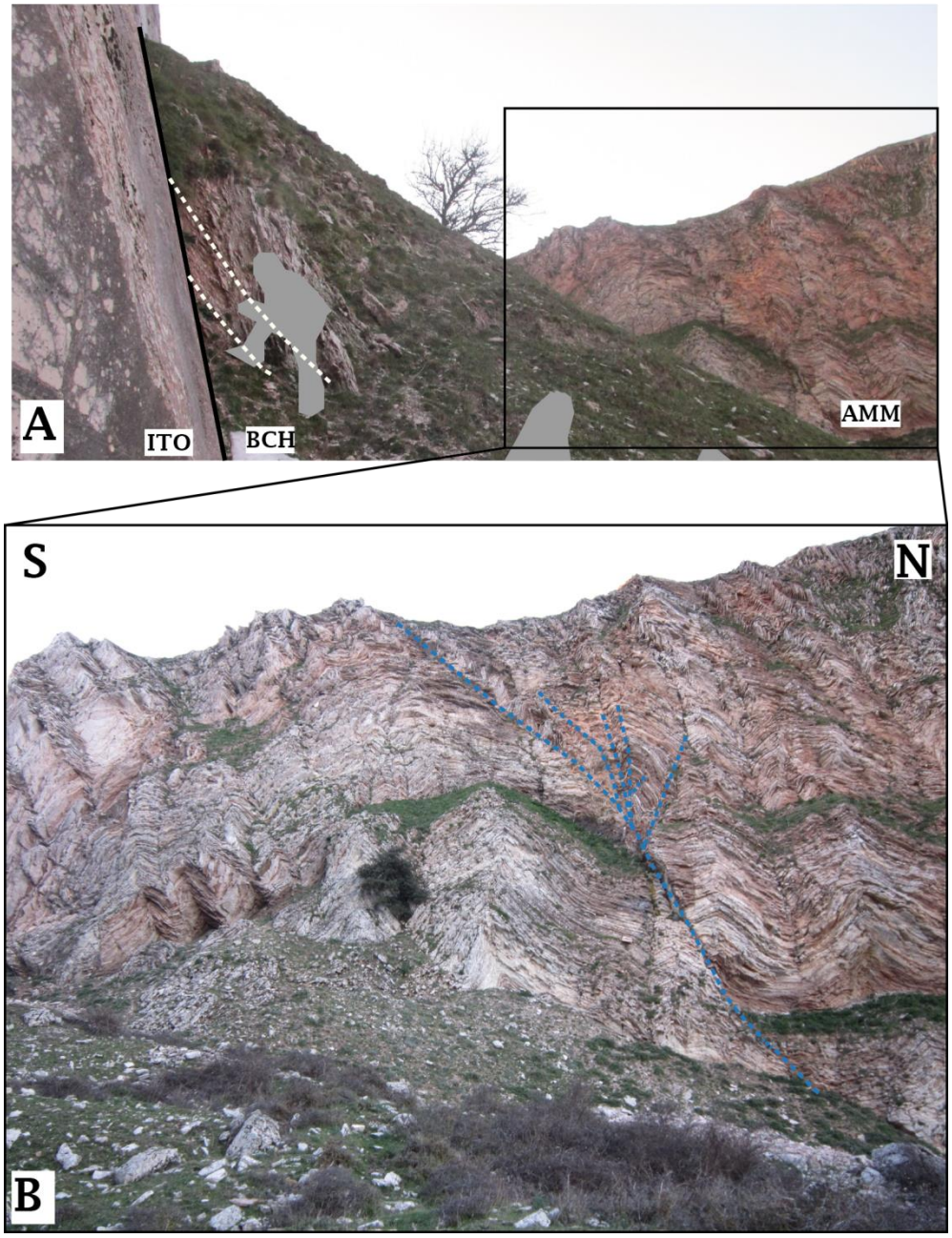

Figure 3.13 - Panoramic view showing Buccheri Fm (BCH) and Amerillo Fm (AMM) buttressing against the Calcari di Maraibito Fm (ITO; lateral facies variation of the Norian-Rhaetian Sciacca Fm). The contact between older limestones (ITO) and younger stratified micrites is represented by Mesozoic normal fault probably reactivated during compression. (B) Detail of upright chevron folds with sub-vertical axial planes characterizing the Amerillo Fm.

Influence of structural inheritance in the development of fold-and-thrust belts and especially in the along strike variation of structural style is widely documented as well (Butler et al., 2006;

Turner et al., 2010; Rodriguez-Roa and Wiltschko 2010; Calamita et al., 2011; Likerman et al., 2013; Pace and Calamita, 2014; Malz et al., 2016; Mahoney et al., 2017; Tibalti et al., 2017). In the study area, strong influence of inherited structures on the development of the Kumeta and Busambra Mts. ridges has been already demonstrated (Basilone, 2009; Avellone et al., 2010; Gugliotta et al., 2014 Gasparo Morticelli et al., 2017; Renda et al., 2000; Nigro and Renda, 2001; Di Stefano et al., 2002).

In particular, Albanese and Sulli, (2012) highlighted how differences of structural style between the eastern and western sector of the study area can be attributed to the irregular shape of the ancient continental margin. In detail, the authors describe a thick carbonate sequence in the eastern part of the area that prevent the forward propagation of the structures in that portion, favouring development of backthrusts. Other studies (Basilone, 2009; Basilone et al., 2010, 2014; Bertok and Martire, 2009; Di Stefano et al., 2002) demonstrate how the Kumeta and Busambra Mts. were two morphostructural highs during the Jurassic and their evolution was continuously affected by extensional faulting until the lowermost Cenozoic. As a consequence, various sets of inherited normal faults affecting the Trapanese unit are clearly recognised in the field (Fig. 3.3; Basilone et al., 2010; Avellone et al., 2010; Gasparo Morticelli et al., 2017). In addition, between the Kumeta and Busambra Mts. structures a Lower Jurassic intraplatform basin (Marineo basin) is described (Catalano and D'Argenio, 1982b; Basilone et al., 2016b) based on well (Marineo well Fig. 3.4 A,B) and seismic data.

Seismic interpretation, as well as field data, highlights the presence of various sets of inherited normal faults. In detail, they are E-W striking faults (Fig. 3.7 d' e') corresponding to the prevalent set recognised in the field and N-S- and NE-SW-striking faults recognised along the E-W oriented seismic line (Fig. 3.6 a). The first set of faults seems to be partially reactivated (as shown in the field Fig. 3.13) and/or cut by backthrusts. In the field, faults with similar orientation correspond to the high angle transpressive faults bordering the Kumeta and Busambra Mts.

The second set of faults probably correspond to the N-S or NE-SW striking inherited normal faults observed in the field. Such inherited faults have orientation similar to the tear faults dissecting the Mt. Kumeta structure. Thus, they may have influenced the tear faults development (Mahoney et al., 2017).

In addition, seismic interpretation along the two ridges (Figs. 3.6, 3.7) allows to define push-up inversion structures characterizing the hangingwall of the backthrusts. Such kind of structures are typical in inversion tectonics deforming carbonate platforms (Pace and Calamita, 2014). Thus, high angle transpressive faults bordering the two ridges, probably are the reactivation in transpression or partial reactivation of E-W striking inherited normal faults, as already pointed out by Avellone at al., (2010) and Gasparo Morticelli et al., (2017) and described by Calamita et al., (2011) in the Central Apennines, where structural highs made up of carbonate platform units crops out along shortcut anticlines. Thus, considering the Kumeta and Busambra Mts. as Mesozoic structural highs deformed by thrusting or backthrusting where Mesozoic (or Cenozoic) normal faults are partially reactivated and partially carried up or cut, we can define the Kumeta and Busambra Mts. as blind shortcut backthrusts (Fossen 2016; Granado et al., 2017) and the resulting structural configuration is consistent with the hypothesis pointed out also by Di Stefano et al., (2002) where part of the displacement along the outcropping Mt. Kumeta structure (and probably also the Mt. Busambra structure) could be inherited.

In addition, this configuration, strictly linked to inherited extensional deformation (Granado et al., 2017), can explain the complex distribution and representation in the 3D model of the high angle faults bordering the Kumeta and Busambra Mts. (Figs. 3.8 B and 3.10 A).

Following our interpretation, inherited mechanical weaknesses had a strong impact on the structural style affecting the Kumeta and Busambra Mts. and thus may have played an important role also in the preferential occurrence of hinterland verging structures rather than foreland verging ones.

According to the validated geological model, a single step tectonic model can be proposed for the Kumeta and Busambra Mts. evolution, where, high angle faults seem to have been activated in the same deformational event during which thrusts, backthrusts and tear faults developed and do not represent the expression of a late strike-slip tectonic. This hypothesis is supported by the evidence, in the seismic profiles (Figs.3.6 and 3.7), that high angle faults are located in the hangingwall of backthrusts and thrusts and do not cut them and by the limited amount of out-of-plane movement (4.5% of shortening in the E-W direction).

Thus, thrusts, backthrusts and high angle transpressive faults led to the exhumation of the Kumeta and Busambra Mts. since uppermost Tortonian time during the deformational event which involve the Trapanese unit.

3.5.5 Implication for hydrocarbon exploration

Since 1950, oil discovery in the Ragusa and Gela fields (Kafka and Kirkbride, 1960) encouraged oil exploration in Sicily. Stratigraphic correlation between the subsurface rocks belonging to the Hyblean succession and the outcropping Trapanese-Saccense successions led the oil and gas exploration to focus on the buried lower Mesozoic limestones of these units. Several wells mainly located using the gravimetric response of carbonate structural highs were mostly unsuccessful (Catalano et al., 2002). Main causes for dry wells could be related to the absence of the source rock, well described in the Hyblean foreland (Late Triassic Noto and Streppenosa Fms; Mattavelli and Novelli, 1990; Frixa et al., 2000) but not still found in the Trapanese and Saccense units. But dry wells could also due to incorrect structural model and erroneous definition of possible traps.

Therefore, definition of a correct structural model, especially in fold-and-thrust belt has large implications for hydrocarbon potential evaluation. In detail, definition of triangle zones is difficult because seismic resolution of steep beds is poor and rapid vertical and lateral changes in seismic velocity generate uncertainty (Jardin et al., 2007 Beche et al., 2007). Presence of a triangle zone such as that described by Albanese and Sulli, (2012) could represent a sub-thrust

trap favourable to hydrocarbons accumulation. Indeed, such kinds of hydrocarbon traps, are largely described in other areas worldwide such as the Oriente belt in Colombia, the southern Canadian FTB and Argentinian sub-Andes (Echavarria et al., 2003; Roeder, 2010). As structural interpretation in fold-and-thrust belt, especially underneath thrust faults is not always straightforward, evaluation errors can be made that may lead to unsuccessful investment for the oil industry A case history from East Venezuela basin described by Roeder, (2010), shows how structural interpretation which depicted the presence of structural traps underlying a thrust sheet changed after drilling a well, suggesting a completely different structural style (from thin- to thick- skinned thrusting). Obviously, new data acquisition and in this case post-mortem analysis allowed to improve geological interpretation but this is time consuming.

In this work we used 3D geological modelling and restoration techniques to discriminate a first reliable interpretation in a study area where the fairy quality of the seismic reflection profiles coupled with the complex structural setting (tectonic inversion of an ancient passive margin) allowed to propose more than one structural interpretation. In addition, such an approach allows to detect mistakes or inconsistency in seismic interpretation and to delineate key sectors or plays for hydrocarbon exploration, where it is challenging to focus on with further investigation and new data acquisition.

In detail, 3D geological model reconstruction and restoration provide a warning about the geometric reliability of models and therefore these techniques could be used in other study areas with similar complex structural settings in order to individuate mistakes and issues in structural interpretation.

3.6 Conclusions

3D geological model building allowed us to reconstruct the surface and subsurface geometry of the Kumeta and Busambra structures depicting lateral variations of the structural style. In particular:

- the Kumeta Mt. structure is characterized by WNW-ESE backthrusts with a transport towards the NNE linked by hard linkage (NNE-SSW to NE-SW tear faults);
- the Mt. Busambra structure is characterized by a more complex geometry where an imbricate backthrust system (sense of transport towards the NNE) converts into thrust (sense of transport towards the SSW) moving westward. In this case a soft linkage (fold) is suggested connecting the two structures (thrust and backthrust);
- WNW-ESE to E-W high angle transpressive to reverse faults characterized both the Kumeta and Busambra Mts.. These faults join thrusts at depth and probably reactivate or partially reactivate pre-existing normal faults.

Coupling 3D geological modelling with 3D restoration technique, allowed us to improve pre-existing structural interpretation. We are proposing a new validated 3D structural model that sheds new light on the kinematic evolution of the Kumeta and Busambra ridges in the framework of the Sicilian fold-and-thrust belt.

The proposed geometrically correct model considers a single stage evolution where thrust, backthrusts and high angle faults formed as a result of the Trapanese unit involvement in the orogenic wedge during the late Tortonian. Thus, variations in structural style affecting the Trapanese unit are not related to different tectonic events, but depend on the structural inheritance of Mesozoic and Cenozoic normal faults.

Calculated shortening amounts for the Trapanese unit vary from 10% in the eastern portion of the area and 13% in the western part. As a result, low levels of deformation affected the Trapaese unit internally which seems totally detached from its substratum and passively carried up onto more external units.

Chapter IV - Paleothermal data as a tool for kinematic reconstruction of the Sicilian fold-and-thrust belt: implication for the tectonics evolution and petroleum system of the Kumeta and Busambra Mts. area (Apennine-Maghrebian FTB)

4.1 Abstract

Organic matter optical analysis, X-ray diffraction on clay minerals and Rock-Eval pyrolysis techniques were performed on samples collected from the Imerese pelagic basin and the underlying Trapanese carbonate platform units in the Kumeta and Busambra Mts. area (Western Sicily). Resulting paleothermal and geochemical data were used to constrain 1D and 3D burial-thermal reconstructions in order to: 1) define maximum temperatures and burial that the investigated Triassic-Miocene units (Trapanese and Imerese) underwent; 2) provide new insights into the kinematic evolution of the SFTB 3) identify which stratigraphic intervals represent potential source rocks and where and when they reached the hydrocarbon generation stage improving knowledge of the petroleum system of the study area.

Paleo-thermal data (vitrinite reflectance, $T_{max,}$ illite content in mixed layers illite-smectite) and thermal modelling indicate levels of thermal maturity higher in the Imerese unit (located at higher structural level) than the Trapanese unit (located at lower structural level). Low burial amounts (1.2 -1.3 km), identified as allochthonous, occurred on top of the outcropping Trapanese unit. Additionally, 3D model available in the area indicate that the structural low between the Kumeta and Busambra structural highs hosted up to 1.9 km of sedimentary rocks indicating a complex distributions of the tectonic loads affecting the Trapanese unit. Thus, a new kinematic evolution scenario has been proposed, constrained by thermal data and taking into account such variability. Impact of the former Mesozoic configuration and inherited structures have been taken into account in the new kinematic model.

Rock-Eval data allowed to discriminate two main potential source rock levels for the Trapanese unit within the Cretaceous (oil prone) and Miocene (gas prone) formations. On the other hand,

paleothermal data from bitumen samples and 3D thermal model allowed us to define kitchen areas and to hypothesize other source rocks within the Triassic formations at the base of the Imerese and Trapanese units.

4.2 Introduction

Quantification of burial, exhumation and amount of tectonic thickening represents a crucial issue in the study of fold-and-thrust belts (FTBs). Different amount of shortening and tectonic styles (e.g. thick-skinned vs. thin skinned models, Tozer et al., 2002), indeed, determine different amount and modes of burial and exhumation and variable crustal thickening.

In order to reconstruct the original crustal thickening of the investigated FTB, forward structural and stratigraphic modelling (e.g. Butler et al., 1992; Schönborn 1999; Tozer et al., 2002; Hermoza et al., 2005) are widely adopted.

Nevertheless, erroneous interpretation can derive from these approaches especially in structurally complex areas such as collisional belts which are usually strongly affected by erosion and extensional tectonics (Roure et al., 2010). Thus, in these areas it is not always possible to exclude the assumption of the occurrence of allochthonous units subsequently eroded, using only structural and stratigraphic methods (among the others, Baby at al. 1992; Shonborn 1999; Tozer et al., 2002; Hirschmiller et al.2014; Gasparo Morticelli et. al 2015; Tavani et al., 2018).

On the other hand, key data sets to constrain burial and exhumation processes are found from the search of thermochronological indicators (e.g. fission tracks and U-Th/He dating on apatite and zircon crystals) and paleothermal indicators such as vitrinite reflectance (Ro%) and illite content in mixed layers illite-smectite (I% in I-S) (e.g., Corrado et al.,2002, 2009, 2010; Thomas et al., 2008; Di Paolo et al., 2012, 2014; Caricchi et al., 2014; Aldega et al., 2007, 2011, 2017; Zhu et al., 2018).

Therefore, combining quantitative thermal-burial history constraints with the kinematics of structural and stratigraphic evolution can reduce uncertainty in building critical time-temperature

curves necessary for a more complete understanding of thrust belts and mountains chains building (among the others, Aldega et al., 2018; Caricchi et al., 2014; Corrado et al., 2005, 2009; Di Paolo et al., 2012, 2014; Mazzoli et al., 2006, 2008; Labaume et al., 2016; Nakapelyukh et al., 2018; Zhang et al., 2018).

In addition, understanding the burial-thermal evolution of prospective areas in fold and thrust belts is aid in reducing exploration risk (Toro et al., 2004).

Paleothermal indicators and relative constrained thermal-burial histories, indeed, represent pieces of essential knowledge to better constrain the petroleum system (relationships between any potential source-rocks, reservoirs and cap-rocks formations) in complex areas such as FTBs. Goffey et al., (2010), in a general review on petroleum exploration in FTBs defined several levels of uncertainties in the petroleum potential evaluation of such complex areas. As a matter of fact, trap identification and, even more, the possibility to be hydrocarbon charged remain a major challenge.

On this point, well constrained kinematic evolution and thermal histories reconstruction coupled with paleothermal and geochemical data can reduce uncertainties in the timing and modes of hydrocarbon generation, expulsion and accumulation.

The Sicilian fold-and-thrust belt (SFTB) represents a structurally complex area showing along strike variations of amount and rates of shortening, tectonic transport and structural style (Lickorish et al., 1999; Catalano et al., 2002; 2013; Corrado et al., 2009; Aldega et al., 2011; Di Paolo et al., 2012; Gasparo Morticelli et al., 2015).

Even though amounts and rates of orogenic shortening and tectonic exhumation, as well as kinematic evolution are well constrained in the Eastern SFTB by means of thermal and thermochronological indicators (Corrado et al., 2009; Aldega et al., 2007, 2011; Di Paolo et al., 2012, 2014) no thermal data are available in the Kumeta and Busamba Mts. area, located in the Western SFTB. Lack of a well-defined dataset (e.g. high quality seismic profiles) and independent constraints (e.g. paleothermal data) allowed several authors to propose different

interpretations/models for the kinematic evolution of the SFTB in the study area (Kumeta and Busambra Mts. area) (Roure 1990; Tavarnelli et al., 2003; Avellone et al., 2010; Albanese and Sulli, 2012; Barreca and Maesano, 2012).

Thus, paleothermal data, linked with the structural record, may provide critical constraints necessary i) to reduce the number of possible interpretations, ii) defining a new kinematic evolution scenario of the study area.

SFTB represent an attractive area for petroleum exploration since it hosts different oil discoveries (e.g. Vega, Gela and Ragusa located along the Hyblean foreland; Granath and Casero, 2004) and bitumen occurrences recovered in the study area suggest the presence of source-rocks and thus, the existence of a petroleum system (Magoon and Dow, 1994). Granath and Casero, (2004) already described the occurrence of such bitumen in their work. Nevertheless, lack of thermal and geochemical data and uncertainties in the structural and kinematic model in the study area did not allow the authors (Granath and Casero, 2004) to define the petroleum system, the linked source rocks and potential kitchens distribution.

Therefore, in this work, paleothermal data coupled with 1D and 3D thermal modelling, have been performed to:

1) define maximum temperatures and burial that the investigated Triassic-Miocene units underwent;

2) provide new insights into the kinematic evolution of the SFTB;

3) identify which stratigraphic intervals represent potential source rocks and where and when they reached the hydrocarbon generation stage improving knowledge of the petroleum system characterizing the study area.

4.3 Geological Setting

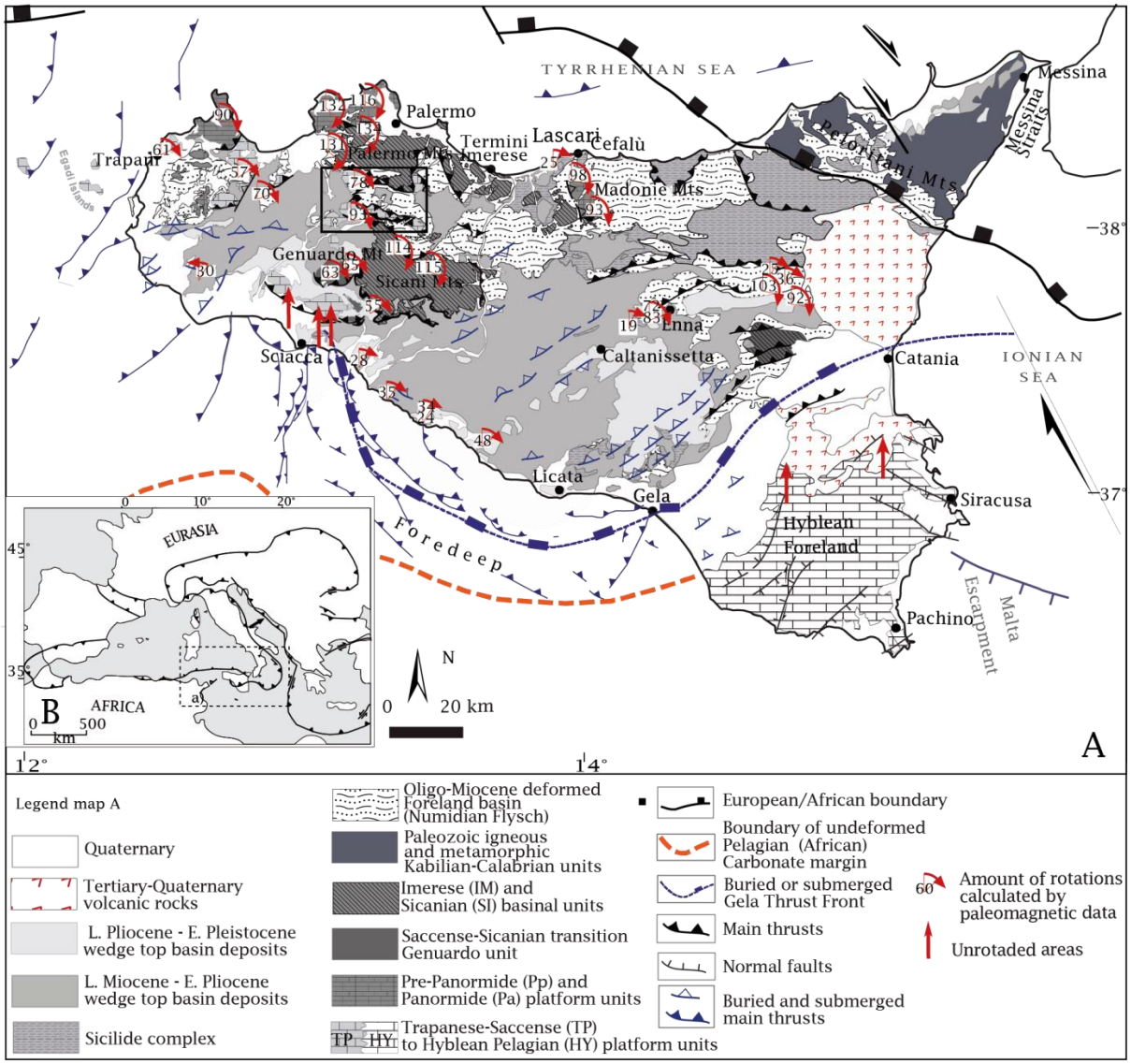

Figure 4.1 - (A) Geological map of Sicily (modified after Gasparo Morticelli et al., 2015). The black rectangle indicates the study area. Palaeomagnetic data are from Channel et al., (1990), Grasso et al., (1987), Speranza et al., (2003, 2018). (B) tectonic map of central Mediterranean area (modified after Gasparo Morticelli et al., 2015).

The Sicilian fold-and-thrust belt (SFTB) is a segment of the Apennine-Maghrebian chain developed as a SSE-verging chain (Fig. 4.1), resulting from the post-collisional convergence between Africa and Europe (Dercourt et al., 1986; Dewey et al., 1989; Catalano et al., 1996, 2000; Faccenna et al., 2004) and the rollback of the subduction hinge of the Ionian lithosphere (Caputo et al., 1970; Doglioni et al., 1999; Faccenna et al., 2001).

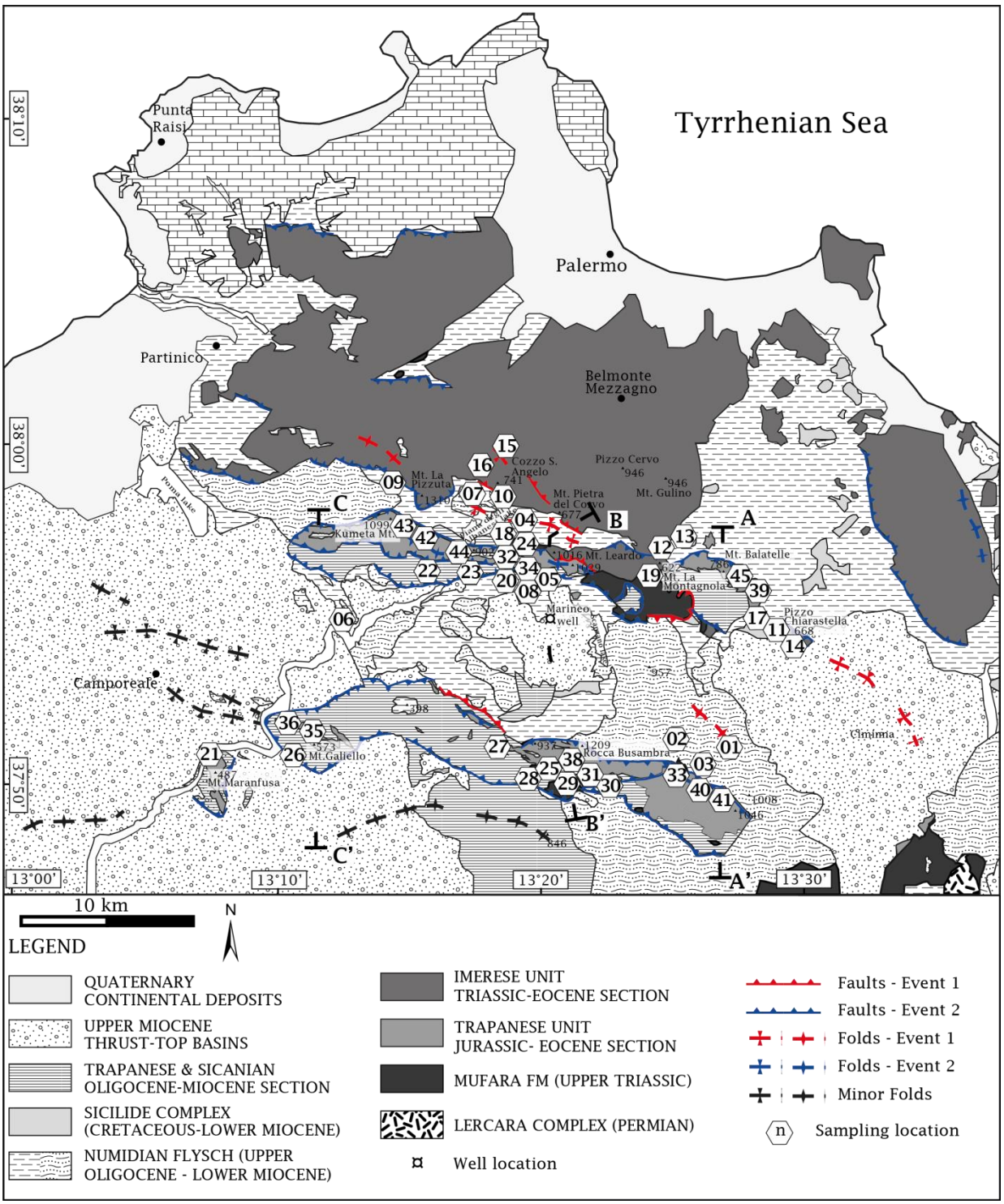

Figure - 4.2 Tectonic sketch map of the study area with sampling sites (modified after Catalano et al., 2010a, b). Location of cross-sections of Fig. 4.5 is shown. Red faults indicate I tectonic event (shallow seated) Blue faults indicate II tectonic event (deep seated).

Since the early Miocene, the advancing accretionary system involved different paleogeographical units belonging to the former African passive margin which subsequently form individual nappes of the SFTB. Four main thrust sheets involving distinct regional

décollements can be distinguished (Catalano et al., 2000; Bello et al., 2000; Avellone et al., 2010; Gasparo Morticelli et al., 2015).

The lowermost unit (and the most external) corresponds to the Mesozoic-Cenozoic carbonate to pelagic platform (Trapanese unit) detached from its original substratum and overthrusting the Hyblean foreland and the Pelagian offshore. The Trapanese unit succession is up to 5 km thick and characterized by upper Triassic-lower Jurassic shallow water limestones (Sciacca and Inici Fms.) passing to middle Jurassic-Eocene pelagic carbonates and marls deposited on a seamount morphology (from the Calcari a Crionoidi to the Amerillo Fms.) followed by Burdigalian-lower Tortonian calcarenites and marls (Calcareniti di Corleone and Marne di San Cipirello Fms.).

Mesozoic-Cenozoic deep-water limestones (Imerese and Sicanian units), located in a more internal position, tectonically overlie the Trapanese unit. The Imerese unit succession is 800-1400 m thick and mainly constituted by alternating sandstones, limestones and shales (Mufara Fm.) followed by pelagic limestones, dolostones, radiolarites and marls (from Fanusi to Caltavuturo Fms.) deposited in a passive margin setting.

The Sicanian unit succession is 900-1,900m thick and made up of middle Triassic-lower Oligocene sandstones, shales, cherty limestones and marls passing upward to upper Oligocene-upper Miocene calcarenites and marls.

Mesozoic rifting affected both carbonate platform and deep-water successions (Jenkyns 1970; Catalano and D'Argenio, 1978; 1982a; Abate et al., 1982; Di Stefano and Mindszenty, 2000; Di Stefano et al., 2002). As a result, extensive systems of neptunian dykes and normal faults affected the Trapanese unit and occurrence of condensed successions characterize both the Imerese (Pizzo Chiarastella area) and the Trapanese units. Evidences of this inherited extensional tectonics are well preserved in the field (Fig. 4.3A, B).

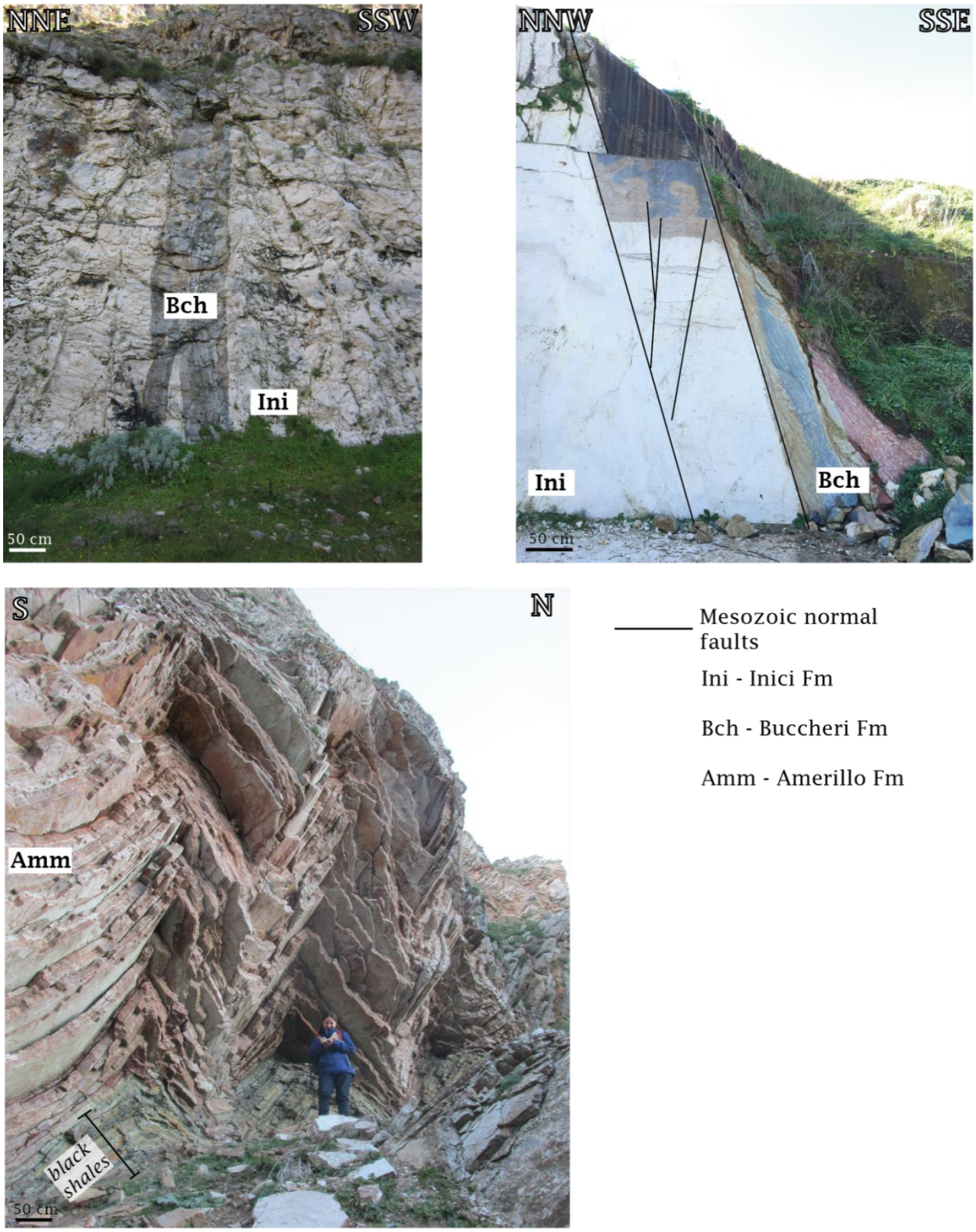

Figure 4.3 - Detail of extensional and compressional features recognised in the field. (A) Neptunian dykes affecting the Inici Fm.; (B) normal faults involving Inici and Buccheri Fms.; (C) Chevron faults characterizing the Amerillo Fm. and black shale level recognised in the same formation. Location of the site (C) is indicated in Fig. 4.5.

The highest tectonic units are the Numidian Flysch and Sicilide Complex. The Numidian Flysch succession represents the earliest foredeep deposit at the onset of collisional tectonics (Grasso,

2001). The succession is constituted by sand-rich turbidites from 600 to 2,000 m thick which unconformably covers the Imerese unit (Pinter et al., 2017) and is often detached and tectonically thickened (Corrado et al., 2009; Gugliotta et al., 2014; Gasparo Morticelli et al., 2015). The Sicilide Complex, derived from the deformation of distal pre-orogenic domain (Ogniben, 1960), is generally involved in the Neotethyan Sicilian accretionary wedge (Monaco and Tortorici, 1995; Roure et al., 1990; Corrado et al., 2009). In the study area the thickness of the Sicilide Complex does not exceed 0.3 km. Onto the aforementioned units, late Miocene–early Pleistocene clastic deposits unconformably seal the shortened tectonic units (Gugliotta et al., 2014). Tectonic emplacement was accomplished by differential clockwise rotations around vertical axis (Catalano et al., 1976; Channell et al., 1990; Speranza et al., 1999, 2003, 2018) which produced interference pattern at various scales.

Two different thin-skinned tectonic events (Oldow et al., 1990; Roure et al., 1990; Bello et al., 2000; Catalano et al., 2000; Avellone et al., 2010; Albanese and Sulli, 2012; Gasparo Morticelli et al., 2015 2017; Chapter II) can be distinguished and the timing of Neogene deformation is constrained by the age of the first unconformable deposits and by syn-tectonic basins successions (Avellone et al., 2011; Gugliotta and Gasparo Morticelli 2012; Gugliotta et al., 2014).

Since Serravallian time, deep-water units (Imerese and Sicanian units) together with the Numidian Flysch and Sicilide successions were detached from their substratum thrusting over the more external Trapanese unit (shallow seated event Avellone et al., 2010; Gasparo Morticelli et al., 2015; 2017). This first event (faults in red in Figs. 4.2 and 4.5; Fig. 4.4A) of thrusting produced duplex overthrust geometries and major shortening. Since the uppermost Tortonian, the ongoing compressional deformation shifted to deeper levels involving the thick carbonate platform-pelagic platform unit (Trapanese unit) which is consequently detached from its substratum and incorporated into the orogenic wedge forming south-verging imbricate fan (Gugliotta et al., 2014 Gasparo Morticelli et al., 2017). Deep seated thrusts (and backthrusts) deforming the Trapanese unit, generated a further imbrication to the superimposed deep-water

units and deformation of syn-tectonic basin successions (Fig. 4.5; Avellone et al., 2010; Gasparo Morticelli et al., 2015; 2017; Chapter II).

In the study area, this second tectonic event (faults in blue in Fig. 4.2; black faults in Fig. 4.5) is characterized by high angle reverse to transpressive faults (Fig. 4.4A, B) which join thrusts/backthrusts at depth (Fig. 4.5) and drive the exhumation of the Trapanese unit along the Kumeta and Busambra Mts. which thus nowadays represent two tectonic windows (Avellone et al., 2010; Catalano et al., 2000; Albanese and Sulli, 2012; Gasparo Morticelli et al., 2017).

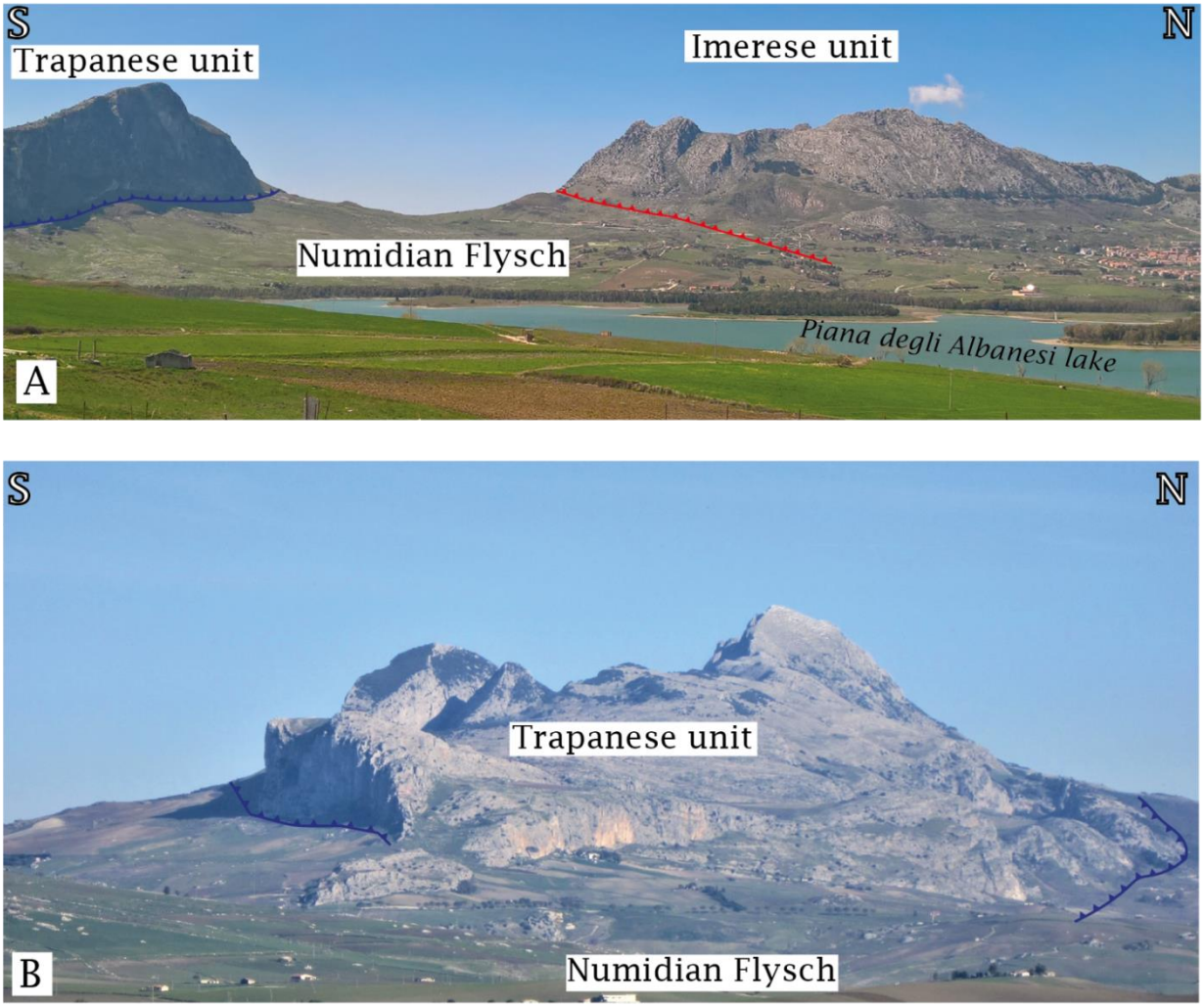

Figure 4.4 - Panoramic view showing (A) WNW-ESE- to E-W-trending high angle fault affecting the Trapanese unit along the Kumeta Mt. structure and NW-SE-trending fault affecting the Imerese succession; (B) WNW-ESE- to E-W-trending high angle faults affecting the Busambra structure. Red fault belongs to the first tectonic event. Blue faults belong to the second tectonic event.

4.4 Methods and Materials

4.4.1 Sampled structures

The Imerese and Trapanese successions were investigated along different thrust sheets. In Fig. 4.5, three structural cross-sections are showing the position and geological relationship between the sampled units. The Imerese succession was sampled along three different NW-SE oriented thrust sheets namely IW (Imerese West), IC (Imerese Central) and IE (Imerese East). IW corresponds to the most internal one (Fig. 4.5) and crops out along the northern border of the study area. It was sampled in the Cozzo S. Angelo area (Fig. 4.2). Southward, in a more external position, thrust sheets IC (Fig. 4.5) and IE crop out separated along strike by a structural high made up of the Trapanese unit (Fig. 4.2). The first thrust sheet (IC) is made up of a slightly condensed succession (thickness of 1.25 km) and was sampled in the La Montagnola area (Fig. 4.2). The latter (IE) is made up of a strongly condensed succession (0.75 km) and was sampled in the Pizzo Chiarastella area (Fig. 4.2).

Samples from the Trapanese succession were collected along the two ~30 km long WNW-ESE elongated Kumeta and Busambra Mts. structures (Fig. 4.2). The distribution of samples in different sites allowed to quantify the along strike variability, over a distance of ~ 10 km, of the tectonic and/or sedimentary burial affecting the Trapanese succession. Samples were collected from the easternmost termination of the Mt. Kumeta structure in the Mt. Balatelle area (Fig. 4.2; KE in Fig. 4.5) and in the Mt. Kumeta area (Fig. 4.2; KW in Fig. 4.5). Samples from the Busambra structure were collected in the Mt. Galiello and Mt. Maranfusa area (Fig. 4.2; BW in Fig. 4.5), in the Rocca Busambra area (Fig. 4.2; BC in Fig. 4.5) and along the eastern termination of the Mt. Busambra structure (Fig. 4.2; BE in Fig. 4.5A). The Numidian Flysch succession was sampled extensively in the area both in stratigraphic continuity with the Imerese unit and in the member tectonically detached, on top of the Trapanese unit.

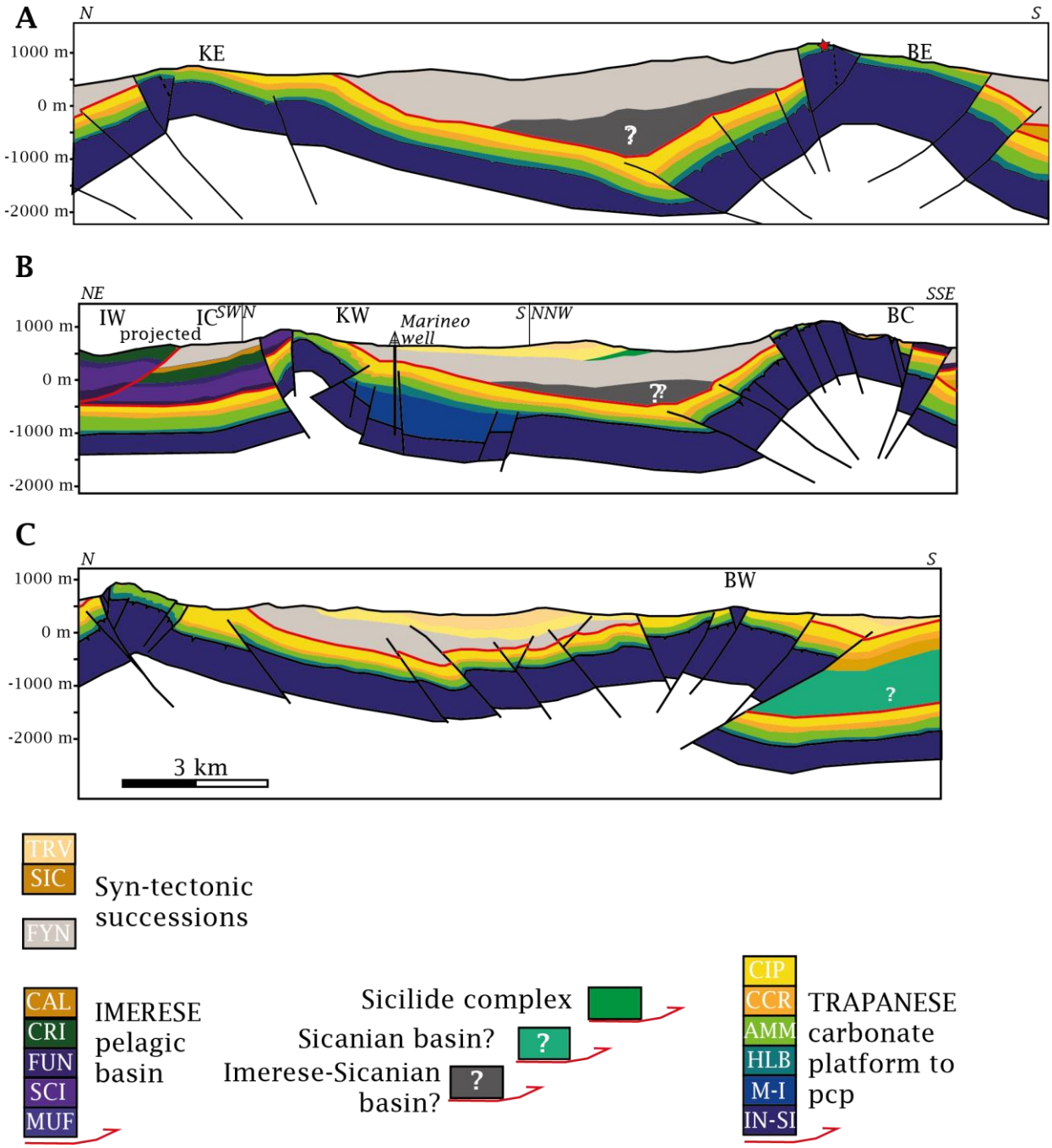

Figure 4.5 - Original and redrawn cross sections (see Fig. 4.2 for location) with projected pseudo-wells (KW, KE, BE, BC, BE, IW, IC) defined to evaluate burial-thermal histories (see text for explanations). Red lines indicate faults belonging to the first tectonic event. Black lines indicate faults belonging to the second tectonic event. Dotted lines indicate Mesozoic inherited faults. Red star indicates location of outcrop in Fig. 4.3 C.
TRV—Terravecchia Fm.; SIC—Castellana Sicula Fm.; SCX—Sicilide complex; FYN—Numidian Flysch Fm.; CAL—Caltavuturo Fm.; CRI—Crisanti Fm. ; FUN—Fanusi Fm.; SCI—Scillato Fm.; MUF—Mufara Fm.; CIP—Marne di San Cipirello Fm.; CCR—Calcareniti di Corleone Fm.; AMM—Amerillo Fm.; HLB—Hybla, Lattimusa, Calcari a Crinoidi and Buccheri Fms..; M-I—Marineo intra-platform basin; SIA—Sciacca and Inici Fms..; SI—Upper Triassic-Eocene Sicanian succession; S-I—Sicanian or Imerese succession.

4.4.2 Organic matter optical analysis

Organic matter optical analysis has been performed on dispersed organic matter from nineteen samples (Fig. 4.2, Tabs. 4.1, 4.2). Eleven samples were collected in the clayey-sandy portions of the Imerese and Numidian Flysch successions. Five samples were collected in the clayey-sandy portions of the Trapanese succession. Three samples correspond to bitumen found both in the Imerese and Trapanese successions. Whole-rock samples were crushed in an agate mortar, mounted in epoxy resin and polished according to standard procedures (Bustin et al., 1990). Vitrinite reflectance (R_o%) measurements were performed on randomly oriented grains using a Zeiss Axioplan microscope, under oil immersion (n=1.518) in reflected monochromatic non-polarized light. Three different reflectance standards (R_o = 0.426 %; 0.595% and 0.905%) were used for calibration. The number of measurements ranges from 15 in samples with small amount of organic matter to 50 for organic matter-rich samples. On each sample, measurements were carried out on unaltered, non-oxidized, and unfractured fragments of huminite-vitrinite fragments. Mean reflectance values were calculated using the arithmetic mean of these measurements.

Bitumen reflectance, measured on polished sections, was converted to equivalent vitrinite reflectance (R_{oeq} %) values by using published equation of Jacob, (1989): R_{oeq}% = 0.618 R_{obit}%+ 0.40.

4.4.3 X-ray diffraction (XRD) analysis

A suite of forty-one samples has been analysed by XRD analysis. In detail, samples come from (Fig. 4.2; Tabs. 4.1 and 4.2): claystones/siltstones of the Numidian Flysch; marls and shales of the Caltavuturo, Crisanti and Mufara Fms.; marls claystones and shales of the Marne di San Cipirello, Calcareniti di Corleone, Amerillo, Hybla and Buccheri Formations. Qualitative and semi-quantitative analyses of the <2 μm grain-size fraction (equivalent spherical diameter) were performed using a Scintag X1 X-ray system (CuKα radiation). After centrifugation, the suspension containing the <2 μm grain-size fraction was decanted, pipetted, and dried at room

temperature on glass slides to produce a thin highly oriented aggregate. Oriented air-dried samples were scanned from 1° to 48° 2θ with a step size of 0.05° 2θ and a count time of 4 s per step at 40 kV and 45 mA. The presence of expandable clays was determined for samples treated with ethylene glycol at 25 °C for 24 h. Ethylene glycol–solvated samples were scanned at the same conditions as air-dried aggregates, with a scanning interval of 1°–30° 2θ. Expandability measurements were determined according to Moore and Reynolds (1997) by using the Δ2θ method after decomposing the composite peaks between 9°–10° and 16°–17° 2θ with Pearson VII functions.

4.4.4 Pyrolysis

Rock-Eval pyrolysis has been performed on twenty seven samples from the Mufara, Scillato, Crisanti, Hybla, Numidian Flysch and Marne di San Cipirello Formations. The Rock–Eval 6 device operating at the IFP Energies Nouvelles (France) was used applying the ‘‘IFP basic method’’ temperature program for bulk source rocks described by Behar et al., (2001). Rock–Eval parameters as well, were calculated following procedures described in Behar et al., (2001). Free hydrocarbons (S_1) in the rock and the amount of hydrocarbons (S_2) and CO2 (S_3) expelled from pyrolysis of kerogen are also measured. Five samples provided reliable results (TOC higher than 0.5 %; Tab. 4.3).

4.4.5 Thermal modelling

The main assumptions for the thermal modelling are: (1) rock decompaction factors apply only to clastic deposits, according to Sclater and Christie’s method (1980); (2) sea-level changes are neglected, as thermal evolution is mainly affected by sediment thickness rather than by water depth (Butler, 1992b); (3) thrusting is considered instantaneous when compared with the duration of sedimentation, as generally suggested in theoretical models (Endignoux and Wolf, 1990; Sassi et al., 2007); (4) temperature was computed using surface temperature (10°C-18 °C) and heat flow at the base of the sedimentary pile. In detail, present-day heat flow of 55-65mWm^{-}

^{2} is extracted from borehole datasets (GeoThopica, http://geothopica.igg.cnr.it/), whereas paleo-heat flow values are evaluated using the correlation of vitrinite reflectance and mixed-layers I-S data based on the kinetic model of vitrinite maturation of Burnham and Sweeney (1989) and the kinetics of the I-S reaction determined by Hillier et al., (1995); and (5) thickness, lithology and age of sediments are from geological maps and well logs.

1D thermal modelling was performed along pseudowells from both the Trapanese and the Imerese units using BASIN MOD 1D software. Simplified burial and thermal history reconstructions of the Imerese unit have been performed along three different pseudo-wells corresponding to IW, IC and IE thrust sheets. 1D burial and thermal histories of the Trapanese unit are performed along five pseudo-wells, three along the Busambra Mt. structure (corresponding to BW, BC and BE) and two along the Kumeta Mt. structure (corresponding to KW and KE).

Numerical data were collected in order to reconstruct a 3D numerical representation of the area. These data include stratigraphic information from geological maps (Catalano et al., 2010a, b) and wells (e.g., Marineo well) and depth maps (imported as grid files) from the available 3D geometrical model (Chapter III). Depth maps, from the bottom to the top are: Topography (T), Top Numidian Flysch (NUM), Top Marne di San Cipirello Fm. (CIP) and Top Amerillo Fm. (AMM).

Since Top Marne di San Cipirello Fm. and Top Amerillo Fm. surfaces are affected by reverse faults, they have to be simplified due to the lack of an appropriate tool able to define reverse faults in the 3D thermal simulation. In detail, main problem is represented by the double depth values (z; z') assigned to a single position (x, y) in space, when a reverse fault cut a layer (overlap of the horizon along the fault). Grid maps reconstructed for thermal modelling cannot take into account such layer overlap. Thus it was necessary to modify the original geological maps using Skua-Gocad software. Specifically, in areas affected by reverse faults, the software

smoothed the maps defining a middle depth value between the footwall and the hangingwall of the fault in order to obtain a single depth value for the horizon and thus removing the fault.

The resulting 3D geometrical model is 21x33x8 km and contains 4 different layers. The two layers reconstructed for the Trapanese unit were further subdivided into seven different layers in order to obtain a more refined distribution of rock properties (e.g. lithology, thermal conductivity, porosity) along the Trapanese succession. Thickness of each layer was determined by well data, depth maps, extracted from the 3D model and/or geological maps (Catalano et. al 2010 a, b). Resulting model contains 9 layers corresponding to: Sciacca Fm.; Inici Fm.; Buccheri Fm. (including Calcari a Crinoidi, Buccheri and Lattimusa Fms.); Hybla Fm.; Amerillo Fm.; Calcareniti di Corleone Fm.; Marne di San Cipirello Fm.; Numidian Flysch succession (including both the Numidian Flysch and deep-water limestone unit); Wedge-top basin succession.

The basin structural evolution was reconstructed using backstripping techniques, taking into account the sediments compaction from porosity depth curves assigned to each lithology. The thermal maturity calculations were considered in the 3D simulations. Resulting simulation was consistent with the geological maps and thermal maturity data. 3D thermal modelling was performed only for the Trapanese unit using Temisflow software. Reverse faults were not included in the thermal model, so that its effect implies that thermal maturity simulated close to the thrust faults (max displacement 2.6 km) is slightly underestimated.

4.5 Results

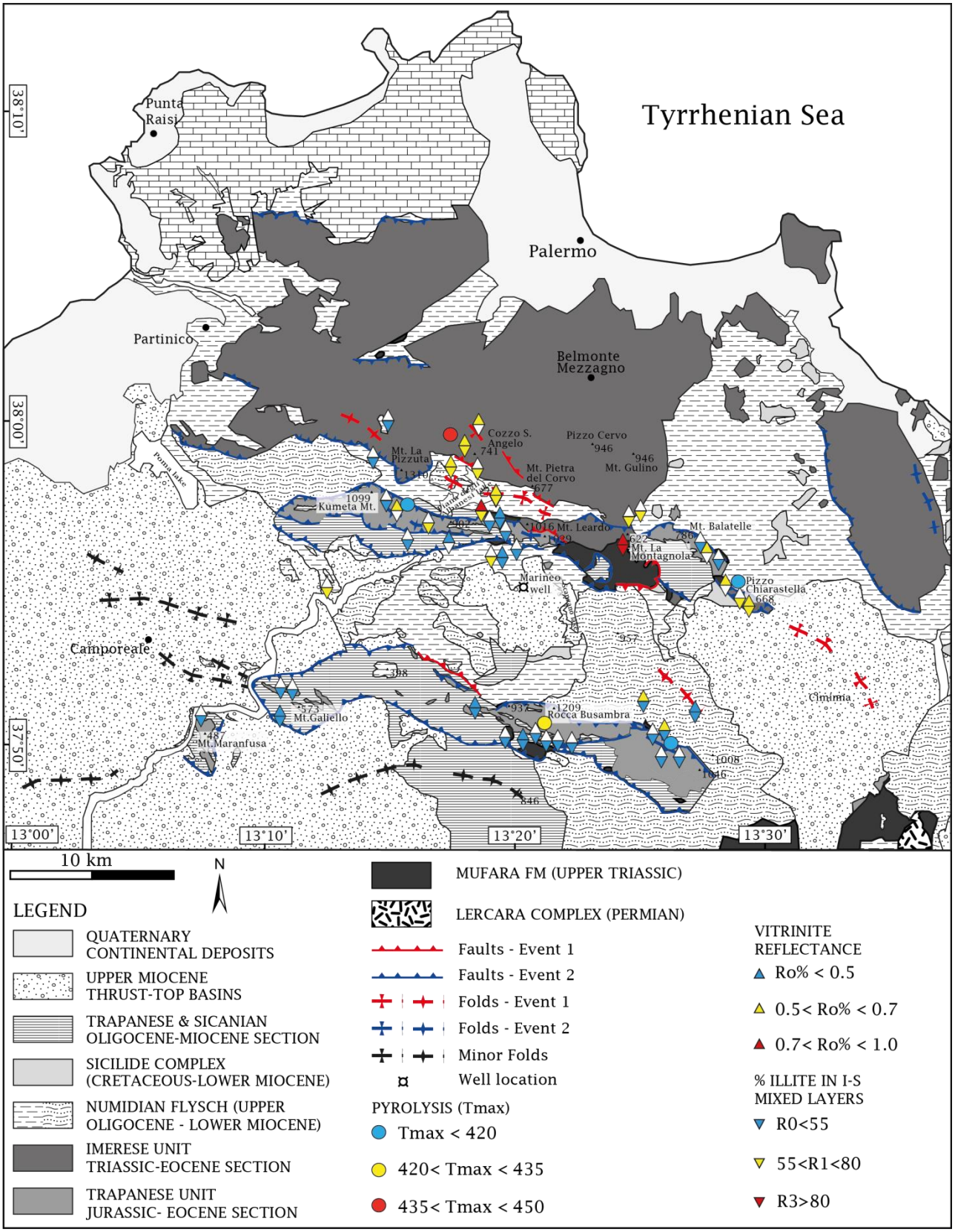

Figure 4.6 - Map distribution of Ro%, Tmax and illite content in mixed layers illite-smectite (%I in I-S) and stacking order data. White triangles indicate not-defined data.

4.5.1 Organic matter optical analysis

4.5.1.1 Imerese unit and Numidian Flysch

Numidian Flysch, Crisanti, Mufara and Scillato Fms. provided suitable results for the organic matter optical analysis (Tab. 4.1; Fig. 4.6).

Mufara Fm. contains macerals belonging to the vitrinite and inertinite groups. R_o% values range between 0.89% and 0.95% indicative for middle mature stages of hydrocarbon generation.

Bitumen reflectance measurements from the Scillato Fm. shows $R_{oeq\%}$ values of 0.69% (according to Jacob, (1989) equation) consistent with early to middle mature stages of hydrocarbon generation.

The Crisanti Fm. is abundant in organic matter that is mainly made up of macerals belonging to the vitrinite and inertinite groups. R_o% values of 0.58% and 0.68% (Fig. 4.8) attesting for early mature stages of hydrocarbon generation.

Organic matter in the Numidian Flysch Fm. is mainly made up of macerals which belong to the huminite-vitrinite and subordinately the inertinite groups. Pyrite, either finely dispersed or in small globular aggregates, is locally present. R_o% values ranging between 0.41% and 0.64% (Fig. 4.8) are indicative for immature to early mature stages for hydrocarbon generation.

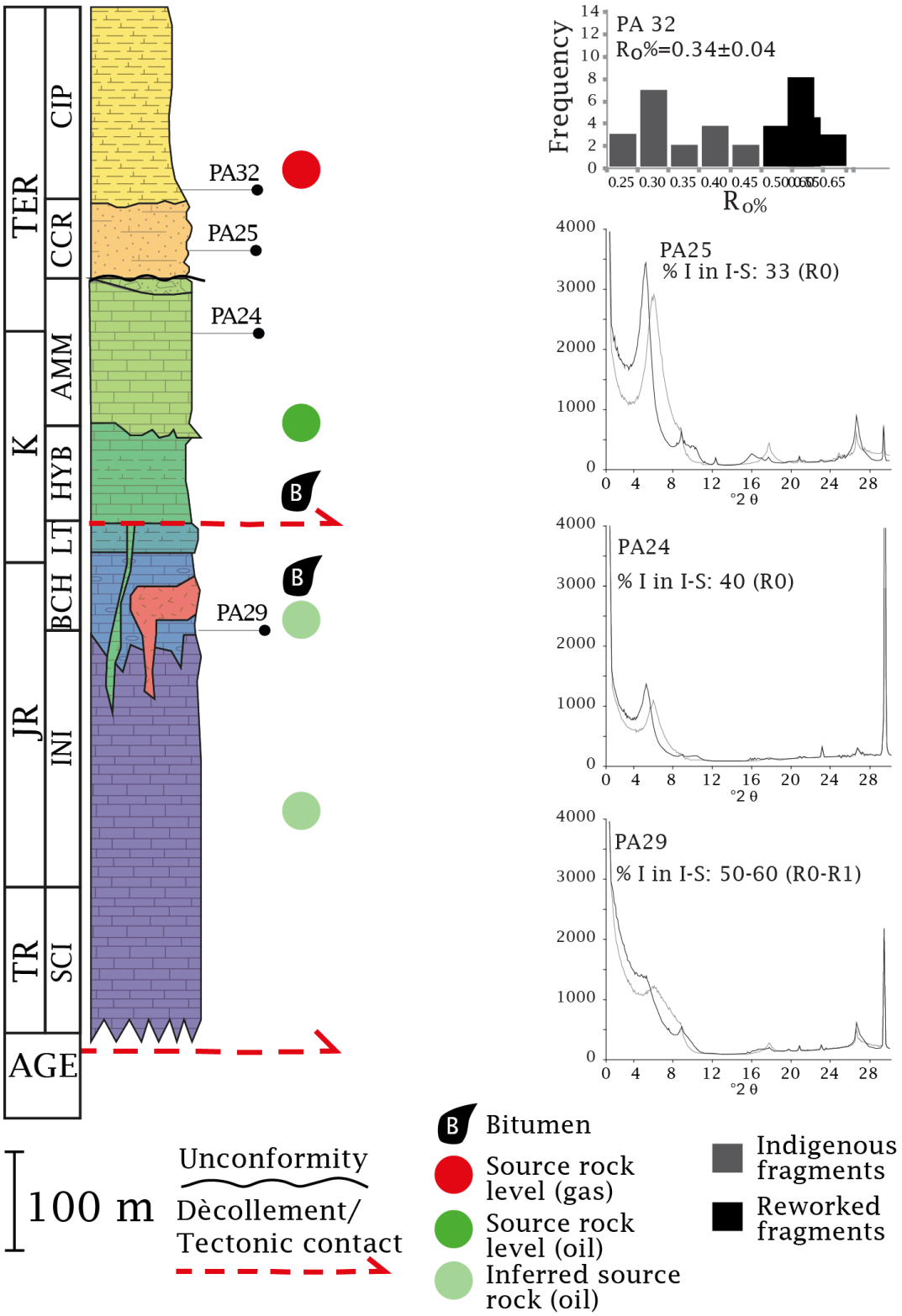

Figure - 4.7 Simplified stratigraphic columns of the Trapanese succession, with selected paleothermal results. In detail, representative histograms of vitrinite reflectance data and X-ray diffraction oriented patterns of the <2 μm grain-size fraction (grey lines indicate air-dried samples, black lines refer to ethylene glycol–solvated mounts). Values of vitrinite reflectance (Ro%), the illite content in mixed layers illite-smectite (%I in I-S) and the mixed layer illite-smectite stacking order (R parameters) are also reported per each sample. Main unconformities and detachment levels are indicated. TR—Triassic; JR—Jurassic; K—Cretaceous; TER—Tertiary; SCI—Sciacca Fm.; INI—Inici Fm.; BCH—Calcari a Crinoidi and Buccheri Fms.; LT—Lattimusa Fm. HYB—Hybla Fm.; AMM—Amerillo Fm.; CCR—Calcareniti di Corleone Fm.; CIP—Marne di San Cipirello Fm.

4.5.1.2 Trapanese unit

Marne di San Cipirello, Hybla, and Inici Fms. provided suitable results for the organic matter optical analysis (Tab. 4.2; Fig. 4.6).

Bitumen reflectance measurements from the Inici Fm. show R_{oeq}% value of 0.65% (according to Jacob, (1989) equation). Bitumen reflectance measurements from the Hybla Fm. show R_{oeq}% value of 0.61% (according to Jacob, (1989) equation). Measured values are consistent with the early mature stage of hydrocarbon generation for both the formations.

Organic matter in the Marne di San Cipirello Fm. is mainly made up of oxidized macerals belonging to the huminite-vitrinite and subordinately to the inertinite groups. Pyrite, either finely dispersed or in small globular aggregates, is locally present. Two populations of macerals are often identifiable, one population corresponds to the indigenous fraction, whereas the other is interpreted as reworked (Fig. 4.7). R_o% values for indigenous vitrinite fragments range between 0.34% and 0.47% and indicate the immature stage of hydrocarbon generation.

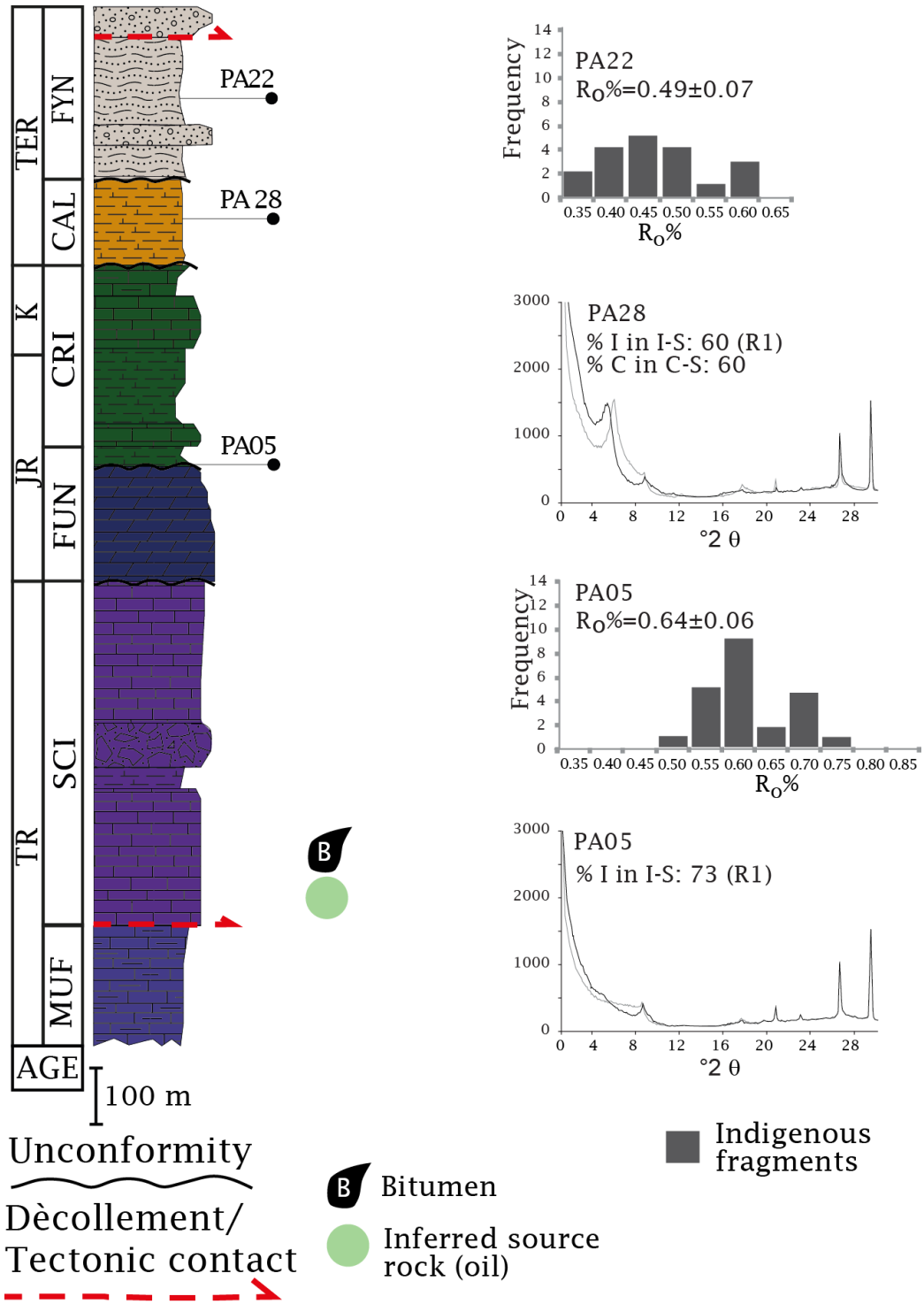

Figure 4.8 - Simplified stratigraphic columns of the Imerese succession, with selected paleothermal results. In detail, representative histograms of vitrinite reflectance data and X-ray diffraction oriented patterns of the <2 μm grain-size fraction (grey lines indicate air-dried samples, black lines refer to ethylene glycol–solvated mounts). Values of vitrinite reflectance (Ro%), the illite content in mixed layers illite-smectite (%I in I-S) and the mixed layer illite-smectite stacking order (R parameters) are also reported per each sample. Main unconformities and detachment levels are indicated. TR—Triassic; JR—Jurassic; K—Cretaceous; TER—Tertiary; MUF—Mufara Fm.; SCI—Scillato Fm.; FUN—Fanusi Fm.; CRI—Crisanti Fm.; CAL—Caltavuturo Fm.; FYN—Numidian Flysch Fm.

4.5.2 X-ray diffraction (XRD) analysis

4.5.2.1 Imerese unit and Numidian Flysch

X-ray diffraction analysis for the Imerese succession and the Numidian Flysch is listed in Tab. 4.1.

Clay minerals assemblage for the Mufara Fm. in sites 18 and 20 (Tab. 4.1) is mainly constituted by illite (13%-46%) mixed-layers I-S (16-26%), smectite (20-36%), kaolinite (8-27%) and chlorite (<8%), whereas site 19 shows a different clay minerals assemblage where the most abundant mineral is the mixed layer I-S (up to 93%), followed by kaolinite, mixed layers chlorite-smectite and chlorite (<3%).

Crisanti Fm. is characterized by illite (8-66%), mixed layers I-S (10-43%) and, in sites 13 and 14, kaolinite (up to 78%) and chlorite (<4%).

Caltavuturo Fm. is mainly composed by illite (39%-59%), mixed layers I-S (13-36%) and chlorite-smectite (11%-29%), and subordinately kaolinite and chlorite (<13%).

Numidian Flysch Fm. generally shows illite (12%-31%), mixed layers I-S % (6%-23%), kaolinite (46-80%) and chlorite (up to 14%). Sites 8, contains only 21% illite and 79% mixed-layers I-S.

Short range ordered structures (R1) passing to long-range ordered structures (R3) with illite content of 70-80% characterize the Mufara Fm.

Caltavuturo and Crisanti Fms. show short range ordered structures (R1) with illite contents of 60-78% (Fig. 4.8). Two samples (sites 13-14) of the Crisanti Fm. also present random ordered I-S (R0) with illite content of 20% interpreted as retrograde alteration.

Random ordered I-S (R0) with high expandability (40-50% of illite layers) and short range ordered structures (R1) with an illite content of 60-73% characterize the upper portion of the Numidian Flysch. For three samples in sites 5, 6 and 9, both populations (R0 and R1) coexist and the R1 population is interpreted as detrital since the R0 population represents the clearest signal in these samples.

Caltavuturo, Crisanti and Mufara Fms. experienced levels of thermal maturity from early diagenetic conditions to late diagenesis moving from younger to older units (Merriman and Frey, 1999, Aldega et al., 2007).

4.5.2.2 Trapanese unit

X-ray diffraction analysis for the Trapanese succession is listed in Tab. 4.2.

Clay minerals assemblage for the Buccheri Fm. is constituted by illite (36-42%), mixed-layers I-S (54-62%) and kaolinite (<4%).

Hybla Fm. is characterized by illite (49-55%), mixed-layers I-S (40-47%) and chlorite (<5%).

Amerillo Fm. is mainly composed by illite (20-23%), mixed-layers I-S (77-80%) in sites sampled along the Mt. Kumeta structure (sites 34 and 39 in Tab. 4.2) and illite (12-28%), mixed-layers I-S (10-70%), kaolinite (1-75%) and occasionally chlorite (<3%) along the Mt. Busambra structure (sites 33, 35-36 and 38). Site 38 presents also 29% of palygorskite.

Calcareniti di Corleone Fm. contains illite (up to 40%), mixed-layers I-S (51-56%) and kaolinite and chlorite (<5%). Marne di San Cipirello Fm. is mainly composed by illite (11-36%), mixed-layers I-S (11-30%), kaolinite (36-78%) and chlorite (<8%).

Buccheri Fm. shows the coexistence of both random -ordered I-S (R0) with high expandability (40-50% of illitic layers) and short range ordered structures (R1) with illite content 60-70% (Fig. 4.7). R1 structures are interpreted as reworked since R0 structures are prevailing.

Amerillo and Hybla Fms. show random ordered I-S (R0) with high expandability (33-55% of illite layers; Fig. 4.7) which are associated with short range ordered structures (R1) with an illite content of 65-75% in three sample sites (sites 35, 39 and 40). As well as the Buccheri Fm. the clearest signal is represented by R0 structures.

Random-ordered I-S (R0) with high expandability (33-40% of illite layers) characterize the Calcareniti di Corleone Fm. (Fig. 4.7).

Marne di San Cipirello Fm. shows random ordered I-S (R0) with high expandability (40-55% of illite layers) in some cases associated with short range ordered structures (R1) with an illite content of 75-78% which are interpreted as not indigenous component.

Buccheri, Amerillo, Hybla, Calcareniti di Corleone and Marne di San Cipirello Fms. experienced levels of thermal maturity in the early diagenetic conditions (Merriman and Frey, 1999, Aldega et al., 2007).

4.5.3 Pyrolysis

The total organic carbon (TOC) content and pyrolysis data (e.g., S_1, S_2, and T_{max}) were used to determine the amount and type of organic matter and the present-day hydrocarbon generation potential (Tab. 4.3). Among the analysed samples, five of them (Tab. 4.3) show a present-day TOC above 0.5 wt.%, thus, they can be considered potential source rocks with fair to good generative potential (Peters and Cassa, 1994). Two samples (sites 17 and 42) contain bitumen (Hybla and Scillato Fms.). Crisanti, Amerillo and Marne di San Cipirello Fms. have S_2 value between 0.05-0.67 mg HC/g rock indicating fair generative potential to 94.73 mg HC/g rock, indicating very high generative potential (Tab. 4.3). Hydrocarbon type index (HCI) indicates that Crisanti and Marne di San Cipirello Fms. are gas prone (HCI 0.14-0.65) whereas Amerillo Fm. (HCI 9.2) Hybla and Scillato Fms. (HCI 15.5-38.5) are oil prone (Hunt, 1996). HI values against OI values, indicate that Marne di San Cipirello Fm. (site 29; Fig. 4.7) corresponds to type III kerogen whereas Amerillo Fm. (site 40; Fig. 4.7) corresponds to type II kerogen (Tissot and Welte, 1978). Conversely, Crisanti Fm. contains an high amount of inert carbon (site 16 in Tab. 4.3) indicating fairy hydrocarbon generation potential which is confirmed by the production index value (0).

In general, both PI value and T_{max} value indicate that the analysed rocks are in the immature stage for the hydrocarbon generation (PI lower than 0.08 and/or T_{max} lower than ~430; Hunt, 1996).

Site	Pseudo -well	Sample	Coordinates	Formation	Age	R_o% (± s.d.)	X-ray analysis (<2μm)	%I in I-S and stacking order	%C in C-S
01		PA 11	37°51'48.08"N 13°27'8.82"E	Numidian Flysch	Late Oligocene – early Miocene		I_{14} I-S_{12} K_{70} Chl_4	R0 50 R1 80	
01		PA 12	37°51'45.37"N 13°27'1.29"E	Numidian Flysch	Late Oligocene – early Miocene	0.41±0.06			
02		PA 13	37°52'10.54"N 13°25'3.25"E	Numidian Flysch	Late Oligocene – early Miocene	0.60±0.06	I_{12} I-S_6 K_{80} Chl_2	R0 50	
03		PA 15	37°51'9.60"N 13°25'51.11"E	Numidian Flysch	Late Oligocene – early Miocene	0.55±0.07	I_{14} I-S_{12} K_{72} Chl_2	R0 50	
04	IW	PA 22	37°58'18.90"N 13°19'8.40"E	Numidian Flysch	Late Oligocene – early Miocene	0.49±0.07	I_{18} I-S_{22} K_{58} Chl_2	R1 65	
05		PA 26	37°56'48.00"N 13°19'44.60"E	Numidian Flysch	Late Oligocene – early Miocene		I_{19} I-S_{23} K_{56} Chl_2	R0 45 R1 75	
06		PA 75	37°55'26.3"N 13°12'24.5"E	Numidian Flysch	Late Oligocene – early Miocene		I_{18} I-S_{22} K_{46} Chl_{14}	R1 73	
07	IW	PA 58	37°59'34.6"N 13°17'29.8"E	Numidian Flysch	Late Oligocene – early Miocene	0.48±0.08	I_{21} I-S_{79}	R1 60	
08		PA 73	37°56'45.6"N 13°19'34.1"E	Numidian Flysch	Late Oligocene – early Miocene	0.40±0.07	I_{31} I-S_{12} K_{52} Chl_5	R0 40 R1 65	
09		PA 76?	37°59'40.4"N 13°14'08.8"E	Numidian Flysch	Late Oligocene – early Miocene		I_{18} I-S_{23} K_{55} Chl_4	R0 20 R1 65	
10	IW	PA 28	37°59'28.70"N 13°18'2.50"E	Caltavuturo	Late Paleocene-low Oligocene		I_{59} I-S_{30} C-S_{11}	R1 60	60
11	IE	PA 67	37°55'40"N 13°28'33.8"E	Caltavuturo	Late Paleocene-low Oligocene		I_{39} I-S_{36} C-S_{15} Chl_{10}	R1 78	80
12	IC	PA 71	37°57'35"N 13°24'23.6"E	Caltavuturo	Late Paleocene-low Oligocene		I_{45} I-S_{13} C-S_{29} K_{13}	R1 77	80
13	IC	PA 70	37°57'34.5"N 13°24'28.5"E	Crisanti	Up. Toarcian – Cretaceous		I_{51} I-S_{43} K_4 Chl_2	R0 20 R1 73	
14	IE	PA 66	37°55'38.4"N 13°28'39.2"E	Crisanti	Up. Toarcian – Cretaceous	0.58±0.06	I_8 I-S_{10} K_{78} Chl_4	R0 20 R1 75	
15	IW	PA 27	38° 0'31.50"N 13°18'10.10"E	Crisanti	Up. Toarcian – Cretaceous	0.68±0.08			
16	IW	PA 05	37°59'47.35"N 13°18'5.96"E	Crisanti	Up. Toarcian – Cretaceous	0.64±0.06	I_{66} I-S_{34}	R1 73	
17	IE	PA 65	37°55'48.6"N 13°28'20.2"E	Scillato	upper Carnian-Rhaetian	0.48±0.07* 0.69±0.07#			
18		PA 23	37°57'56.30"N 13°18'51.10"E	Mufara	Middle-upper Carnian	0.95±0.06	I_{46} I-S_{26} K_8 Sm_{20}	R1 75	
19	IC	PA 69	37°57'04.6"N 13°24'08.8"E	Mufara	Middle-upper Carnian	0.89±0.08	I-S_{93} K_3 C-S_3 Chl_1	R3 80	
20		PA 72	37°57'04.2"N 13°19'27.4"E	Mufara	Middle-upper Carnian		I_{13} I-S_{16} K_{27} Chl_8 Sm_{36}	R1 70	

Note: **R_o%—vitrinite reflectance; s.d.—standard deviation; I—illite; I-S—mixed-layer illite-smectite; C-S—mixed-layer chlorite-smectite; K—kaolinite; Chl—chlorite; Sm—Smectite; R parameter—mixed layer illite-smectite stacking order; %I in I-S—illite content in mixed layers illite-smectite; %C in C-S—chlorite content in mixed layers chlorite-smectite. Subscript numbers correspond to mineral weight percentage. *vitrinite reflectance of bitumen; # vitrinite reflectance equivalent obtained using Jacob (1989) equation.**

Table 4.1 - Organic matter maturity and clay mineralogy data from Imerese and Numidian Flysch successions.

Site	Pseudo -well	Sample	Coordinates	Formation	Age	R_o% (± s.d.)	X-ray analysis (<2μm)	%I in I-S and stacking order
21	BW	PA 18	37°51'19.78"N 13° 7'43.09"E	Marne di San Cipirello	Serravallian-low. Tortonian		I_{35} I-S_{27} K_{36} Chl_2	R0 40 R1 78
22	KW	PA 30	37°57'5.70"N 13°15'43.80"E	Marne di San Cipirello	Serravallian-low. Tortonian		I_{15} I-S_{30} K_{52} Chl_3	R0 50
23	KW	PA 31	37°57'2.80"N 13°17'31.40"E	Marne di San Cipirello	Serravallian-low. Tortonian	0.47±0.08		
24	KW	PA 32	37°57'47.00"N 13°19'8.00"E	Marne di San Cipirello	Serravallian-low. Tortonian	0.37±0.07	I_{23} I-S_{22} K_{53} Chl_2	R0 55
25	BC	PA 53	37°50'50.80"N 13°20'39.80"E	Marne di San Cipirello	Serravallian-low. Tortonian	0.36±0.05	I_{18} I-S_{20} K_{57} Chl_5	R0 35 R1 78
26	BW	PA 34	37°51'46.60"N 13°10'33.00"E	Marne di San Cipirello	Serravallian-low. Tortonian	0.34±0.06	I_{27} I-S_{22} K_{47} Chl_4	R0 45 R1 75
27	BC	PA 50	37°51'47.90"N 13°18'33.80"E	Marne di San Cipirello	Serravallian-low. Tortonian	0.37±0.05	I_{23} I-S_{13} K_{59} Chl_5	R0 50
28	BC	PA 52	37°50'54.60"N 13°19'48.90"E	Marne di San Cipirello	Serravallian-low. Tortonian		I_{11} I-S_{11} K_{78}	R0 45
29	BC	PA 54	37°50'53.90"N 13°20'44.70"E	Marne di San Cipirello	Serravallian-low. Tortonian		I_{36} I-S_{16} K_{40} Chl_8	R0 42
30	BE	PA 56	37°50'43.90"N 13°21'48.80"E	Marne di San Cipirello	Serravallian-low. Tortonian		I_{22} I-S_{23} K_{48} Chl_7	R0 40
31	BC	PA 57	37°50'50.10"N 13°21'2.60"E	Calcareniti di Corleone	Burdigalian-Langhian		I_{40} I-S_{51} K_8 Chl_1	R0 40
32	KW	PA 25	37°57'25.60"N 13°19'2.90"E	Calcareniti di Corleone	Burdigalian-Langhian		I_{39} I-S_{56} K_5	R0 33
33	BE	PA 14	37°51'8.02"N 13°25'47.39"E	Amerillo	Late Cretaceous-late Eocene		I_{15} I-S_{10} K_{75}	R0 45
34	KW	PA 24	37°57'33.40"N 13°18'44.20"E	Amerillo	Late Cretaceous-late Eocene		I_{20} I-S_{80}	R0 40
35	BW	PA 35	37°52'20.50"N 13°10'55.90"E	Amerillo	Late Cretaceous-late Eocene		I_{28} I-S_{70} K_2	R0 45 R1 65
36	BW	PA 37	37°52'22.50"N 13°10'52.00"E	Amerillo	Late Cretaceous-late Eocene		I_{12} I-S_{45} K_{40} Chl_3	R0 50
38	BC	PA 55	37°50'53.00"N 13°20'55.60"E	Amerillo	Late Cretaceous-late Eocene		I_{26} I-S_{44} K_1 Pal_{29}	R0 45
39	KE	PA 20	37°56'42.20"N 13°27'35.69"E	Amerillo	Late Cretaceous-late Eocene		I_{23} I-S_{77}	R0 33 R1 75
40	BE	PA 17	37°50'32.65"N 13°26'42.51"E	Hybla	up. Aptian-low. Albian		I_{49} I-S_{47} Chl_4	R0 45 R1 75
41	BE	PA 16	37°50'31.78"N 13°26'20.20"E	Hybla	up. Aptian-low. Albian		I_{55} I-S_{40} Chl_5	R0 40
42	KW	PA 03	37°58'16.11"N 13°14'50.39"E	Hybla	up. Aptian-low. Albian	0.34±0.07* 0.61±0.07#		
43	KW	PA 04	37°58'13.18"N 13°14'42.10"E	Hybla	up. Aptian-low. Albian		I_{54} I-S_{44} Chl_2	R0 40
44	KW	PA 29	37°57'31.90"N 13°16'39.40"E	Buccheri	Toarcian-Tithonian		I_{42} I-S_{54} K_4	R0 50 R1 60
45	KE	PA 19	37°56'48.96"N 13°27'19.17"E	Buccheri	Toarcian-Tithonian		I_{36} I-S_{62} K_2	R0 40 R1 70
45	KE	PA 19b	37°56'48.96"N 13°27'19.17"E	Inici	Hettangian-Sinemurian	0.40±0.04* 0.65±0.05#		

Note: **R_o%—vitrinite reflectance; s.d.—standard deviation; I—illite; I-S—mixed-layer illite-smectite; C-S—mixed-layer chlorite-smectite; K—kaolinite; Chl—chlorite; Pal—Palygoskite; R parameter—mixed layer illite-smectite stacking order; %I in I-S—illite content in mixed layers illite-smectite; %C in C-S—chlorite content in mixed layers chlorite-smectite. Subscript numbers correspond to mineral weight percentage. *vitrinite reflectance of bitumen; # vitrinite reflectance equivalent obtained using Jacob (1989) equation.**

Table 4.2 - Organic matter maturity and clay mineralogy data from Trapanese successions.

Site	Sample	S_1	S_2	S_3	T_{max}(°C)	TOC(%)	PI	HCI	HI	OI
29	PA54	0.01	0.67	1.04	433	0.59	0.015	0.65	114	176
40	PA17	2.15	94.73	10.34	410	22.00	0.02	9.2	431	47
16	PA05	0	0.05	0.37	452	0.64	0	0.14	8	58
42	PA03	0.57	8.47	0.22	420	1.19	0.06	38.5	712	18
17	PA65	20.64	293.2	18.92	417	59.21	0.07	15.5	504	33

Note: S_1—volatile hydrocarbon (HC) content, mg HC/g rock; S_2—remaining HC generative potential, mg HC/g rock; S_3—carbon dioxide yield mg CO_2/g rock; T_{max}—temperature at maximum S_2 peak; TOC—total organic carbon wt%; PI—production index $S_1/(S_2 + S_2)$ HCI—hydrocarbon type index S_2/ S_3; HI—hydrogen index S_2*100/TOC, mg HC/g TOC; OI—oxigen index S_3*100/TOC, mg CO_2/g TOC

Table 4.3 – Rock-Eval pyrolysis results of selected samples.

4.5.4 1D Thermal modelling

4.5.4.1 Imerese unit

Reconstructed burial and thermal evolution for the Imerese unit (Fig. 4.9 A) began during the middle Triassic and continued until the lowermost Oligocene times. During the Oligocene, a depositional hiatus characterized the area associated with the end of the passive margin sedimentation and the onset of the syn-orogenic Numidian Flysch deposition. Sedimentary thickness for the Numidian Flysch varies from 1.3 km on top of the more internal thrust sheet (IW; Fig. 4.9 B,C) to 0.9 km above the IC and IE (Fig. 4.9 D, E) thrust sheets. During the Serravallian, the Imerese unit and Numidian Flysch were incorporated into the advancing orogenic wedge and stacked up into thrust sheets tectonically buried by more internal units (mainly represented by Numidian Flysch and Sicilide complex) (Gugliotta et al., 2014). Tectonic as well as sedimentary burial, varies as a function of the investigated thrust sheets (Fig. 4.9 B, D). Low amount of tectonic burial is recorded by the IW thrust sheet (0.8 km; Fig. 4.9 B), whereas IC and IE thrust sheets were buried by a 1 km thick allochthonous unit (Fig. 4.9 D). Since late Serravallian time, wedge-top basin successions deposited onto the deformed IC and IE thrust sheets (0.3km; Fig. 4.9 D), whereas a depositional hiatus characterized the IW thrust sheet (Fig. 4.9 B). At that time, the base of the Imerese succession underwent similar maximum burial of 3.45km toward the West (IW; Fig. 4.9 A) and the east (IC). The base of the condensed Imerese succession corresponding to the easternmost tectonic unit was buried at maximum depths of 2.95km (IE; Fig. 4.9 D). IC and IE tectonic units experienced similar tectonic burials albeit the base of the succession reached different maximum depth. This discrepancy is due to the different sedimentary thickness characterizing the investigated successions (IC, slightly condensed succession, 1.25km thick whereas IE, strongly condensed succession, 0.75km thick). During the Tortonian, the Imerese unit and its tectonic cover thrusted over the more external platform to pelagic platform units (Trapanese unit).

Since the uppermost Tortonian, deformation involved the buried Trapanese unit leading to the exhumation of the overlying allochthonous units (Imerese, Numidian Flysch and wedge-top basin successions). Amounts of erosion, constrained by paleothermal data, are: 1.6km for the internal IW thrust sheet (Fig. 4.9 A) and 1.9km to 2.0km for the more external IC and IE (Fig. 4.9 C) thrust sheets respectively.

4.5.4.2 Trapanese unit

Reconstructed burial and thermal evolution for the Trapanese unit (Fig. 4.10 A) begins during the late Triassic with deposition of shallow water limestones of the Sciacca and Inici Fms until the lower Jurassic. Since the end of Sinemurian, platform drowning led to the sedimentation of limestones and radiolarites of the Calcari a Crinoidi and Buccheri Fms. in a pelagic condensed platform setting. From the end of the Jurassic until the Eocene, the sedimentation of limestones and marls of the Lattimusa, Hybla and Amerillo Fms. occurred. A sedimentary hiatus characterizes the end of the Paleogene (Fig. 4.10 A). Since the Aquitanian, the area was involved in the collisional process leading flexural accommodating series corresponding to the Calcareniti di Corleone and Marne di San Cipirello Fms. to be unconformably deposited until the lowermost Tortonian (Fig. 4.10 A, B, D). During the Tortonian time, the advancing orogenic wedge brought more internal units (mainly made up of Numidian Flysch and Sicilide complex) to stack up onto the Trapanese succession. Reconstructed thickness of the overthrusting unit is in the same range along the Mt. Kumeta structure and the Mt. Busambra structure (1.3 and 1.2 km respectively; Fig. 4.10B, D). As a result, maximum burial experienced at the base of the Trapanese succession is ~ 5 km (Fig. 4.10B D). By the end of Tortonian, the Trapanese unit was involved in the orogenic wedge and thrusts, backthrusts and associated high angle transpressive faults deformed it. As a consequence, the Trapanese unit and the overthrusting tectonic units, began to be exhumed. The modelled thickness of the removed succession above the Trapanese unit along the

Kumeta and Busambra Mts. is 1.2-1.3km. No significant variation of tectonic burial have been identified along strike for both structures.

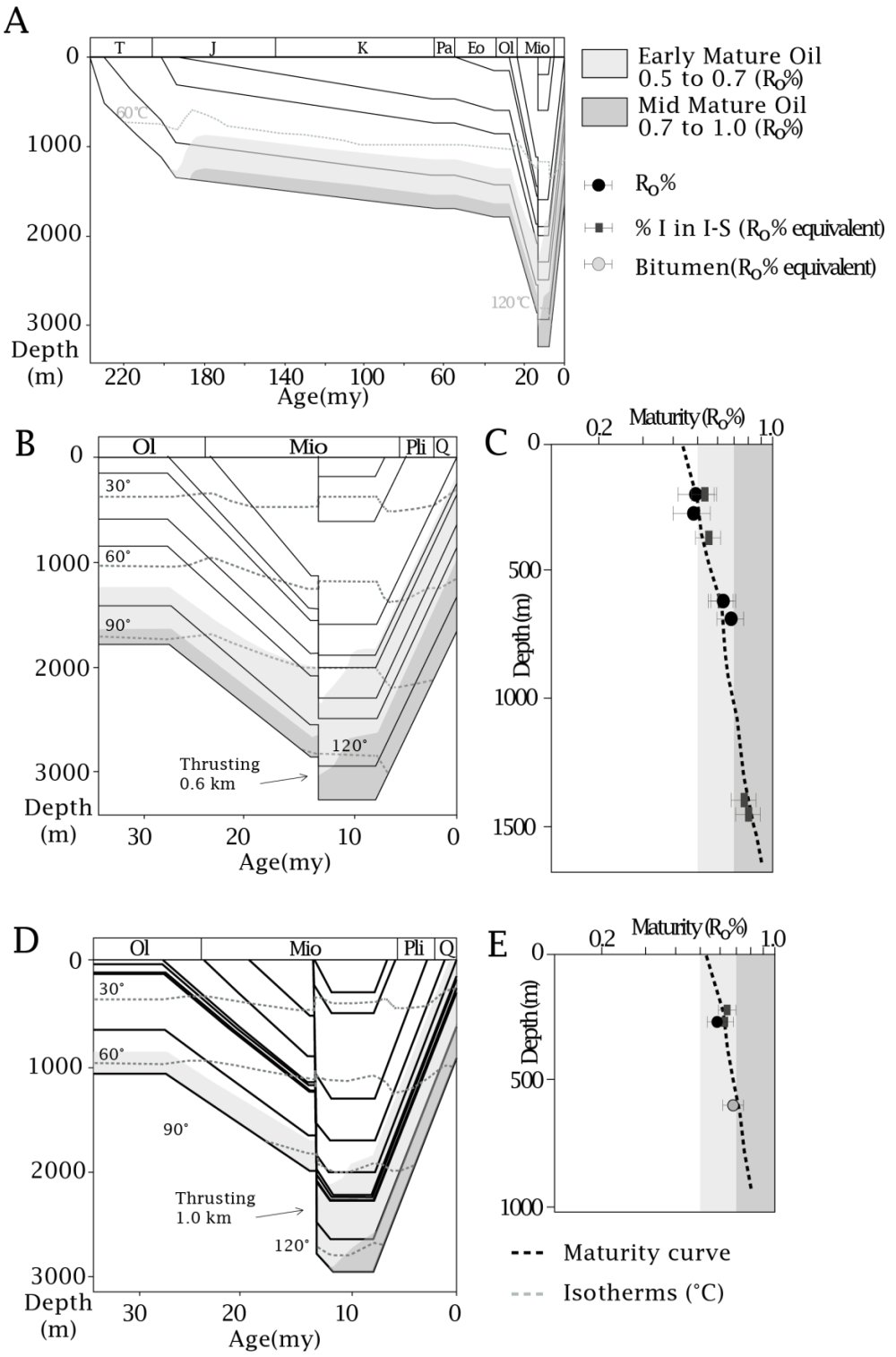

Figure 4.9 - (A) Representative one-dimensional burial and thermal model of the Imerese unit along IW pseudo-well (see text for explanations). (B) Detail of one-dimensional burial and thermal model of the Imerese unit along IW pseudo-well for the last ~35Ma and (C) simulated thermal maturity. (D) Detail of one-dimensional burial and thermal model of the Imerese unit along IE pseudo-well (see text for explanations) for the last ~35Ma and (E) simulated thermal maturity. %I in I-S—illite content in mixed layers illite-smectite; Ro%—vitrinite reflectance data; Bitumen Ro%—vitrinite reflectance equivalent after Jacob, (1989).

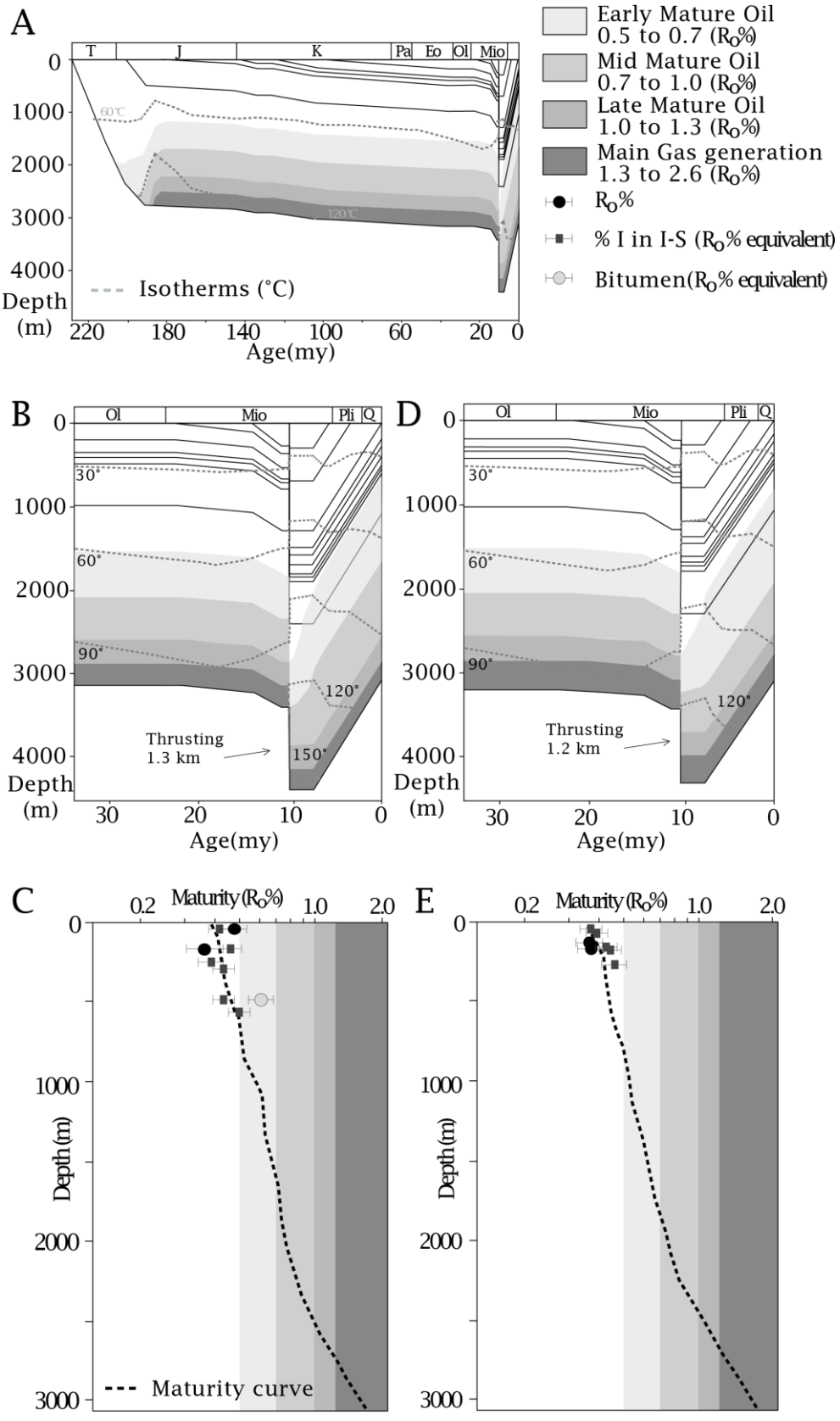

Fig. 4.10 A) Representative one-dimensional burial and thermal model of the Trapanese unit along KW pseudo-well (see text for explanations). (B) Detail of one-dimensional burial and thermal model of the Trapanese unit along KW pseudo-well for the last ~35Ma and (C) simulated thermal maturity. (D) Detail of one-dimensional burial and thermal model of the Trapanese unit along BC pseudo-well (see text for explanations) for the last ~35Ma and (E) simulated thermal maturity. %I in I-S—illite content in mixed layers illite-smectite; Ro%—vitrinite reflectance data; Bitumen Ro%—vitrinite reflectance equivalent after Jacob, (1989).

4.5.5 3D Thermal modelling

1D burial and thermal histories computed for different pseudo-wells located along the Kumeta and Busambra Mts. structures (Trapanese unit) has been incorporated into the 3D simulation.

Thus, thickness of the overthrusting units was modelled along the Kumeta and Busambra Mts. structures according to the results of the 1D thermal models (Fig. 4.10).

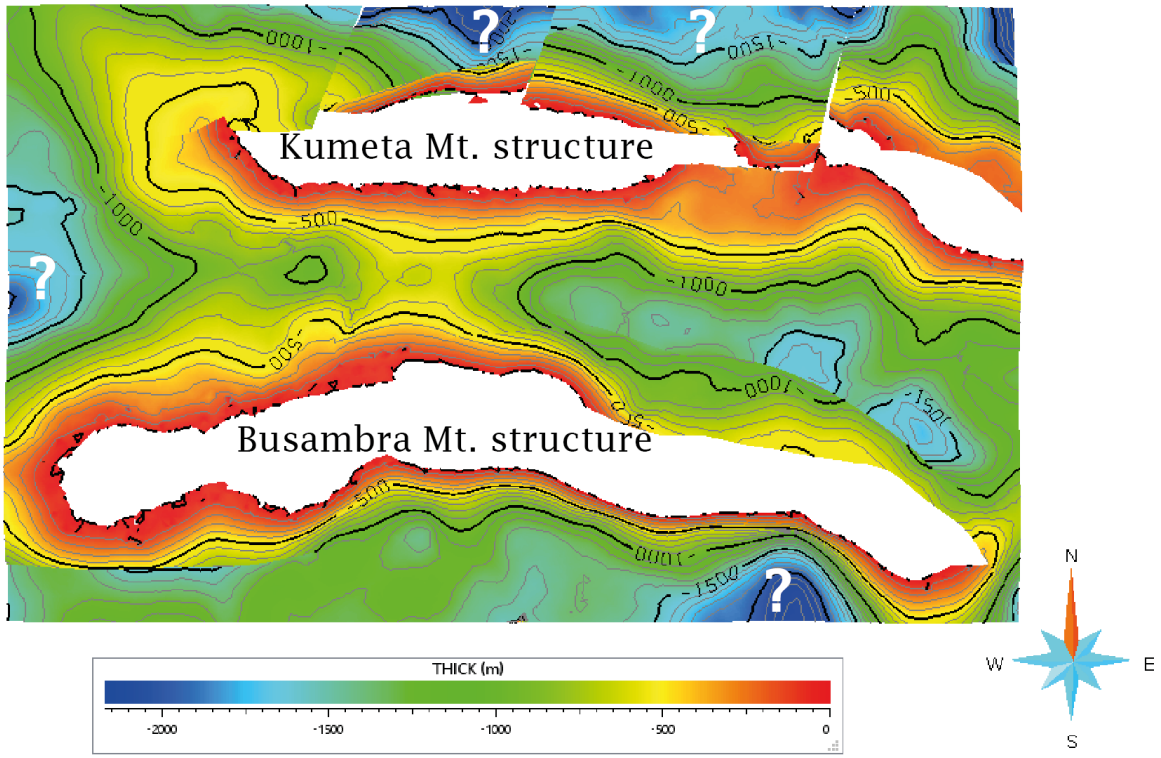

Figure 4.11 - Map showing the present-day allochthonous units thickness variation. Values extrapolated close to the border of the model are poorly constrained.

Nevertheless, the lack of paleothermal data in the area comprised between the Kumeta and Busambra Mts. structures did not allow determining with high precision levels of thermal maturity and amount of tectonic loading experienced by the Trapanese unit in this area.

Thus, the maximum thickness of the overthrusting units in the area between the Kumeta and Busambra Mts. has been indirectly derived from the amount of erosion along the two ridges.

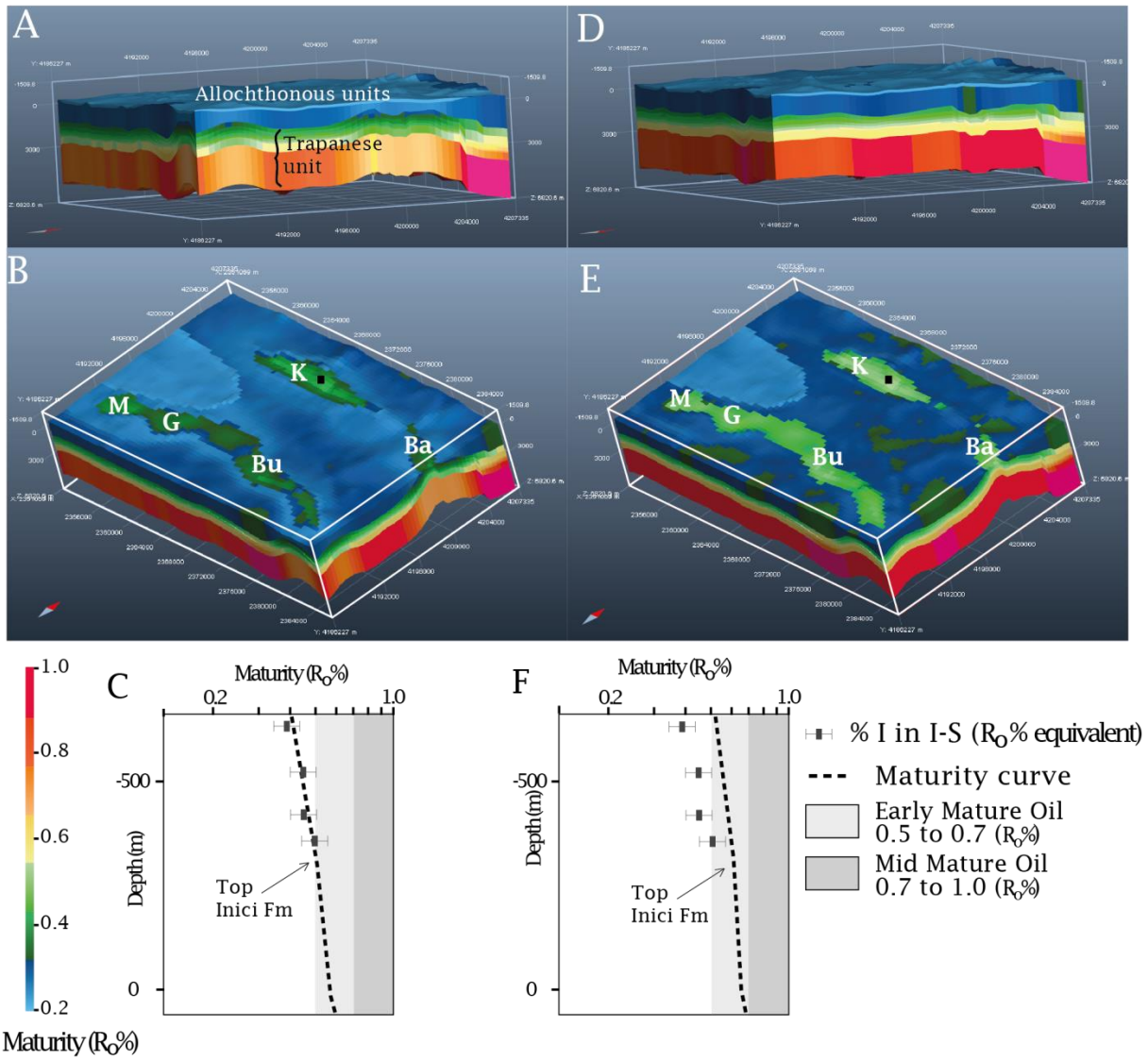

Figure 4.12 - Results of the 3D simulation performed for the Trapanese unit. 3D view of results from the simulation which considers variable thickness of the allochthonous units before (A) and after (B) the allochthonous erosion. 3D view of results from the simulation which considers constant thickness of the allochthonous units before (D) and after (E) the allochthonous erosion. Thermal maturity distribution is expressed in Ro% (vitrinite reflectance) values. (C) 1D pseudo-well extracted from the model (B); (F) 1D pseudo-well extracted from the model (E). Black square indicate pseudo-wells (C and F) position. K— Mt. Kumeta; Ba— Mt. Balatelle; M— Mt. Maranfusa; G— Mt. Galiello; Bu— Mt. Busambra; %I in I-S—illite content in mixed layers illite-smectite.

Considering that the modelled amount of eroded thickness (1.2-1.3 km) of the allochthonous units above the Kumeta and Busambra Mts. is similar or lower than the present day thickness of the allochthonous unit preserved between the two structures (from ~0.7 to ~1.9 km;, Figs. 4.7, 4.11) the expected amount of erosion between the two structures should have been very low and therefore can be neglected. As a result, the present-day thickness of the allochthonous units is

considered as maximum thickness in this area. According to this conclusive remark the simulated thermal maturity for the Trapanese unit is shown in Fig. 4.12 (A, B, C).

The base of the succession, represented by the Sciacca Fm. (Fig. 4.13 A) enters the oil window at the end of Eocene, after the deposition of the Amerillo Fm., and experienced middle to late stages of hydrocarbon generation after the emplacement of the allochthonous units during the Tortonian time (Fig. 4.13 B).

Inici (Fig. 4.13 C), Buccheri and Lattimusa, Hybla and Amerillo Fms. (Fig. 4.13 D) entered the oil window in areas surrounding the Kumeta and Busambra Mts. after the emplacement of allochthonous units during the Tortonian time. At that time, also the Calcareniti di Corleone and San Cipirello Fms. entered the oil window (maximum R_o% simulated 0.5%) in narrow areas between the two ridges. The Inici Fm., in particular, experienced levels of thermal maturity consistent with the onset of the early mature stage of oil generation (R_o% ~0.5 %) in narrow portions along the Kumeta and Busambra Mts. structures (Fig. 4.13 C).

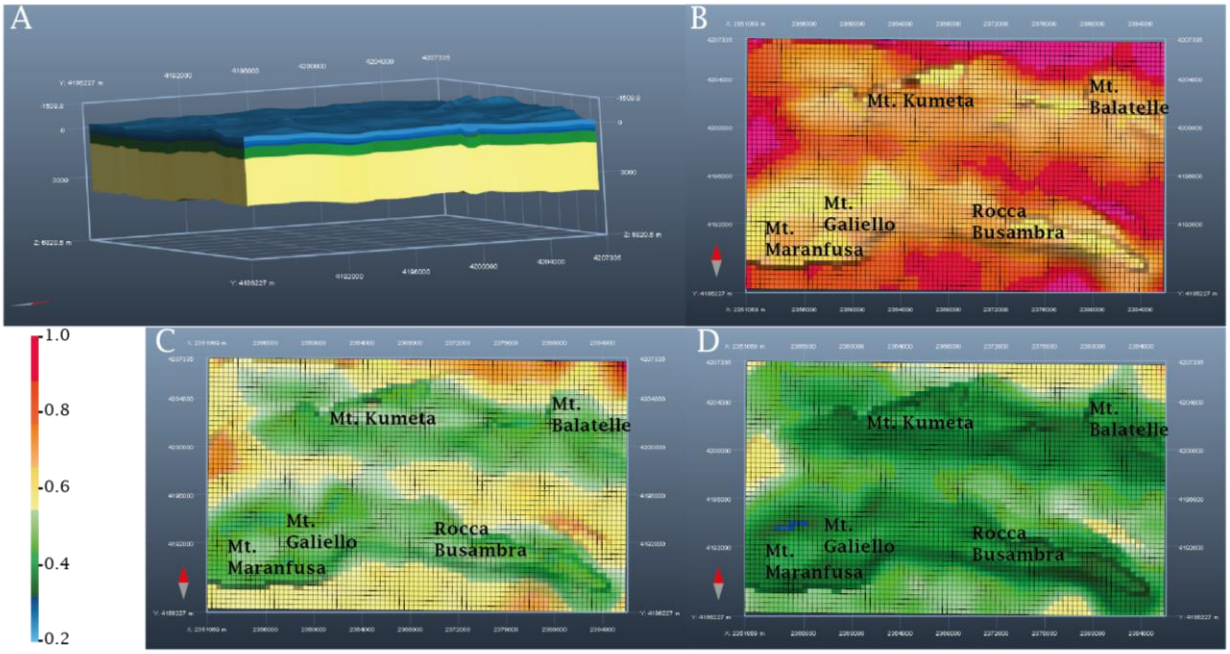

Figure 4.13 - Results of the 3D simulation performed for the Trapanese unit. Thermal maturity distribution expressed in Ro% (vitrinite reflectance) values. (A) 3D reconstruction at the end of Eocene time showing the basal Sciacca Fm. (yellow layer) entering in the oil window (Ro%: 0.6%) after the deposition of the Amerillo Fm. (light blue layer). (B) Map of the Sciacca Fm. showing the present-day thermal maturity distribution. (C) Map of the Inici Fm. showing the present-day thermal maturity distribution. (D) Map of the Amerillo Fm. showing the present-day thermal maturity distribution. Key areas location is also indicated.

Allochthonous thickness and thermal maturity distribution resulting from the reconstructed burial-thermal history imply a complex tectonic history able to justify such differences in allochthonous emplacement. Thus, in order to test a less complex tectonic scenario, a different 3D thermal simulation was performed (Fig. 4.12 D, E). In this case, 1.9km of maximum thickness of the allochthonous unit was assumed and maintained constant for the whole area.

Resulting tectonic history considers the advancing allochthonous units homogeneously emplacing above the Trapanese unit since the Tortonian time. Starting from the latest Tortonian, the Trapanese unit, involved in the deformation began to exhume along the Kumeta and Busambra Mts. structures.

The resulting present-day configuration is characterized by a variable thickness of the allochthonous units in the study area due to differential erosion.

Nevertheless, the simulated thermal maturity according with this last reconstruction, is higher than the measured thermal maturity (Fig. 4.12 F).

4.6 Discussion

4.6.1 Paleothermal data as a tool for kinematic reconstruction of the Sicilian fold-and-thrust belt

Paleothemal data coming from the Imerese and Trapanese successions show considerable differences in levels of thermal maturity. The entire Imerese succession experienced levels of thermal maturity ranging from immature-early mature to mid-mature stages of oil generation (Fig. 4.9). On the contrary, the Trapanese succession experienced levels of thermal maturity in the immature stage for the oil generation in the investigated Miocene-Jurassic section (Fig. 4.10). 1D burial and thermal histories (Fig. 4.10) as well as the 3D thermal modelling (Fig. 4.12 A, B, C) performed for the Trapanese unit show how only the thick carbonate platform (Sciacca Fm. up to 2.0km thick) experienced high level of thermal maturity in the oil and gas generation stages, along the Kumeta and Busambra Mts.

In detail, comparing paleothermal data coming from time-equivalent formations, we observe: the Caltavuturo Fm. (Imerese unit) characterized by R1 structures with an illite content of 60-78% (Fig. 4.8) suggesting levels of thermal maturity consistent with early to late diagenetic conditions; Amerillo Fm. (Trapanese unit) characterized by R0 structures with an illite content of 33-50% (Fig. 4.7), indicating lower levels of thermal maturity, consistent with early diagenetic conditions and the immature stage of oil generation.

Several authors (Catalano et al., 2000; Avellone et al., 2010; Albanese and Sulli 2012; Gasparo Morticelli et al., 2015; 2017) described two tectonic events affecting the study area. During the first tectonic event of latest Serravallian-Tortonian, deep-water basin successions (Imerese and Sicanian units) together with the Numidian Flysch and Sicilide Complex thrust over the Trapanese unit. During the second tectonic event of latest Tortonian-Pliocene, high angle transpressive faults deformed deeper structural levels affecting the Trapanese unit (and re-deforming the allochthonous units) which is subsequently exhumed along the Kumeta and Busambra Mts. structures.

In the Termini Imerese area, ~30 km to the east of the study area (Fig. 4.1), Catalano et al., (2013a) indicate a carbonate platform (ascribed to the Trapanese unit) deeply buried by the Imerese and Sicanian units at depths of 5-6 km, interpreting a deep crustal seismic profile (SI.RI.PRO.). In the same area, in chapter II, ~1.8 km of eroded overburden atop the Imerese unit has been calculated.

Coupling both information, the original thickness of the allochthonous units overlying the carbonate platform unit (Trapanese unit) could have reached about 7km.

The southern Apennine as well as Sicily, display a paleogeographic configuration composed by platform units (Apennine platform, Apulian platform) alternated with a deep-water basin (Lagonegro basin). In detail, the Apulian Platform is exposed in Mt. Alpi structure, that was tectonically buried at depths in excess of ~5km during the early Pliocene (Corrado et al., 2002; 2005; Mazzoli et al., 2006, 2008). Maximum tectonic burial affecting the Apulian platform is in

the same order of magnitude of the maximum tectonic burial affecting the carbonate platform ascribed to Trapanese unit) in the Termini-Imerese area (according to Catalano and co-authors, (2013a)' interpretation).

Tectonic load affecting the Apulian platform in the Mt. Alpi area was subsequently removed off during two tectonic events: 1). a late Pliocene deep-seated thrusting event associated with the coeval activity of low angle extensional faults in the uppermost allochthonous units and 2). a middle Pleistocene deep-seated steep extensional faulting event (Mazzoli et al., 2006, 2008).

As a result, the Apulian platform nowadays crops out as a tectonic window along Mt. Alpi structure as well as the Trapanese unit crops out along the Kumeta and Busambra Mts.

Nevertheless, some substantial differences exist between the two areas.

In the Kumeta and Busambra Mts. area, reconstructed maximum thickness of Imerese thrust sheets (IC and IE) varies between 2.95 and 3.35 km, whereas the thickness of the Sicanian unit is 900-1,900 m, measured in the field (Avellone et al., 2010). On the other hand, maximum burial affecting the two investigated structures (Kumeta and Busambra Mts.) is ~ 1.2-1.3 km indicating that: i) thickness of the two deep-water units is higher than the tectonic burial measured along the two structures, thus such deep-water units could not have been totally emplaced above the Trapanese unit, in disagreement with previous tectonic models (among the others Catalano et al., 2000; Avellone et al., 2010; Barreca et al., 2010) ; ii) tectonic overburden reconstructed along the Kumeta and Busambra Mts. area is much lower than the tectonic overburden observed both in the Termini-Imerese and in the Mt. Alpi area.

Thus, albeit similarities are recognisable between the central sector of the SFTB (~6.8 km of tectonic burial above the underlying platform unit) and the southern Apennine (~5 km of tectonic burial above the underlying platform unit), a different kinematic evolution should characterize the Western sector of the SFTB (1.2-1.3 km of tectonic burial above the underlying platform unit).

3D geological (Chapter III) and thermal models performed in the study area highlighted a heterogeneous distribution of the allochtonous units emplaced atop the Trapanese unit.

Present-day allochthonous units preserved between the Mt. Kumeta and Mt. Busambra structures, indeed, are highly variable in term of thickness (Fig. 4.11) and lithology (Fig. 4.5).

In detail, limestones characterizing the easternmost part of the area, pinch out westward (Fig. 4.5). The Numidian Flysch, as well, gets thinner westward whereas syn-tectonic succession which unconformably covers the Numidian Flysch thicken westward (Fig. 4.5 C). In general, the thickness of the allochthonous units decreases westward (between the Kumeta and Busambra Mts.) from ~ 1.9 km to ~ 1 km (Figs. 4.5, 4.11).

Limestones overthrusting the Trapanese unit between the Kumeta and Busambra Mts. structures were ascribed to the Sicanian unit (Albanese and Sulli, 2012) on the base of similarities with the Sicanian seismic facies (Chapter III).This unit widely crops out to the south, in the Sicani Mts. area (Fig. 4.1) and according with seismic interpretation (Albanese and Sulli 2012; Chapter III) it overthrusts the Trapanese unit along its southern border.

Based on field data, the Imerese unit overthrusts the Trapanese unit to the north of the study area along NW-SE striking thrusts (Avellone et al., 2003; 2010; Gasparo Morticelli et al., 2017). On the other hand, thrusts involving the Trapanese unit are mainly striking WNW-ESE (Chapter III). As a result, the emplacement of the Imerese unit is oblique with respect to the Kumeta and Busambra Mts. structures. Differences in thrust orientation are mainly due to differential clockwise rotation affecting the two units during the two thrusting events (~130° of rotation for the Imerese unit and ~80° of rotation for the Trapanese unit; see Speranza et al., 2018, for a review).

Numidian Flysch widely crops out in the study area and coherently with the Imerese unit is deformed with NW-SE oriented major folds (Fig. 4.2). At a larger scale, Numidian Flysch outcrops are missing to the SW of the Mt. Busambra structure (Granath and Casero 2004; Pinter

et al., 2017) where wedge-top basin successions (mainly represented by the Castellana Sicula and Terravecchia Fms.) are widely exposed (Catalano et al., 2002; Gugliotta et al., 2014).

3D thermal modelling simulated assuming a constant thickness of 1.9 km of allochthonous units atop the Trapanese unit results in levels of thermal maturity higher than those recorded by paleothermal indicators on the Kumeta and Busambra Mts. structures (Fig. 4.12 D, E, F).

Thus, a new kinematic evolutionary scenario able to justify the heterogeneous distribution of the allochthonous units has been proposed (Fig. 4.14).

Since uppermost Oligocene time, the Numidian Flysch deposited onto the Imerese unit and partially onto the internal portion of the Trapanese unit which was probably constituted by a transitional facies between the thick carbonate platform (Trapanese unit) and the thinner deep-water basin (Imerese unit). Such a kind of transitional unit was already described in the area. To the south of the Mt. Busambra structure, indeed, a transitional succession between the Trapanese platform and Sicanian basin units crops out (Mt. Genuardo unit; Chiari et al., 2008). At that time, an extensive depositional hiatus is recorded for the external Trapanese unit (Fig. 4.14 A).

Since Burdigalian time, the Numidian Flysch sedimentation continued on top of more internal units, whereas the Calcareniti di Corleone Fm. sedimentation occurred above a more external Trapanese unit, where the Kumeta and Busambra Mts. already acted as two morpho-structural highs. Following, the Imerese unit together with the Numidian Flysch succession were deformed whereas the Sicilide Complex thrust over the aforementioned units.

Since late Serravallian time, the Castellana Sicula Fm. was unconformably deposited above a growing orogenic belt (composed by the deformed Imerese unit, the Numidian Flysch and Sicilide Complex), passing laterally to the Marne di San Cipirello Fm. that has been deposited in more external sectors (foredeep depozone and foreland ramp) above the Trapanese unit (Gugliotta et al., 2014) draping the Kumeta and Busambra morpho-structural highs (Fig. 4.14 B). Paleo-high morphology probably was still preserved at that time due to the repeated extensional tectonic phases affecting these two structures from the Late Triassic until the lower Miocene

time (Basilone, 2009; Basilone et al., 2010) and differential compaction (Carminati and Santantonio, 2005) between such paleo-structural highs and adjacent paleo-structural lows.

During the Tortonian, the advancing orogenic wedge together with the Castellana Sicula Fm. was emplaced, as a single large thrust sheet, on top of the internal portion of the Trapanese unit.

On the other hand, thicker external portion of the Trapanese unit and secondarily, the Kumeta and Busambra paleo-structural highs partially prevented thrust propagation.

Thus, only the most external thrust sheets, constituted by the Numidian Flysch, Sicilide Complex and wedge-top/foredeep deposits could overthust the Kumeta and Busambra Mts. structures (Fig. 4.14 C). Vergence of the allochthonous units was oblique (NW-SE striking) in respect to the morpho-structural highs elongation (WNW-ESE) as indicated by differential clockwise rotations (Speranza et al., 2018).

As a result, the Imerese unit was stuck by the Kumeta paleo-high morphology to the North but it could further propagate south-westward, on top of a paleo-structural low which at that time characterized the area between the Kumeta and Busambra Mts. structures. (Fig. 4.14 C'). The transition to the late Tortonian is marked by a regionally extended unconformity (Gugliotta et al., 2014) which cut the tectonic units and the upper Serravallian-lower Tortonian wedge-top to foredeep successions (Fig. 4.14 C). Following, the Terravecchia Fm. deposited in a wedge-top setting, above the most external portion of the allochthonous units (Fig. 4.14 C).

Since the uppermost Tortonian time, deformation affected the thicker carbonate platform-pelagic platform (Trapanese unit) resulting in internal complex deformation (Chapter III) and the onset of exhumation along the Kumeta and Busambra structures. As a consequence, the allochthonous units were affected by further deformation and exhumation as well as the Trapanese unit, resulting in the present day configuration (Fig. 4.14 D).

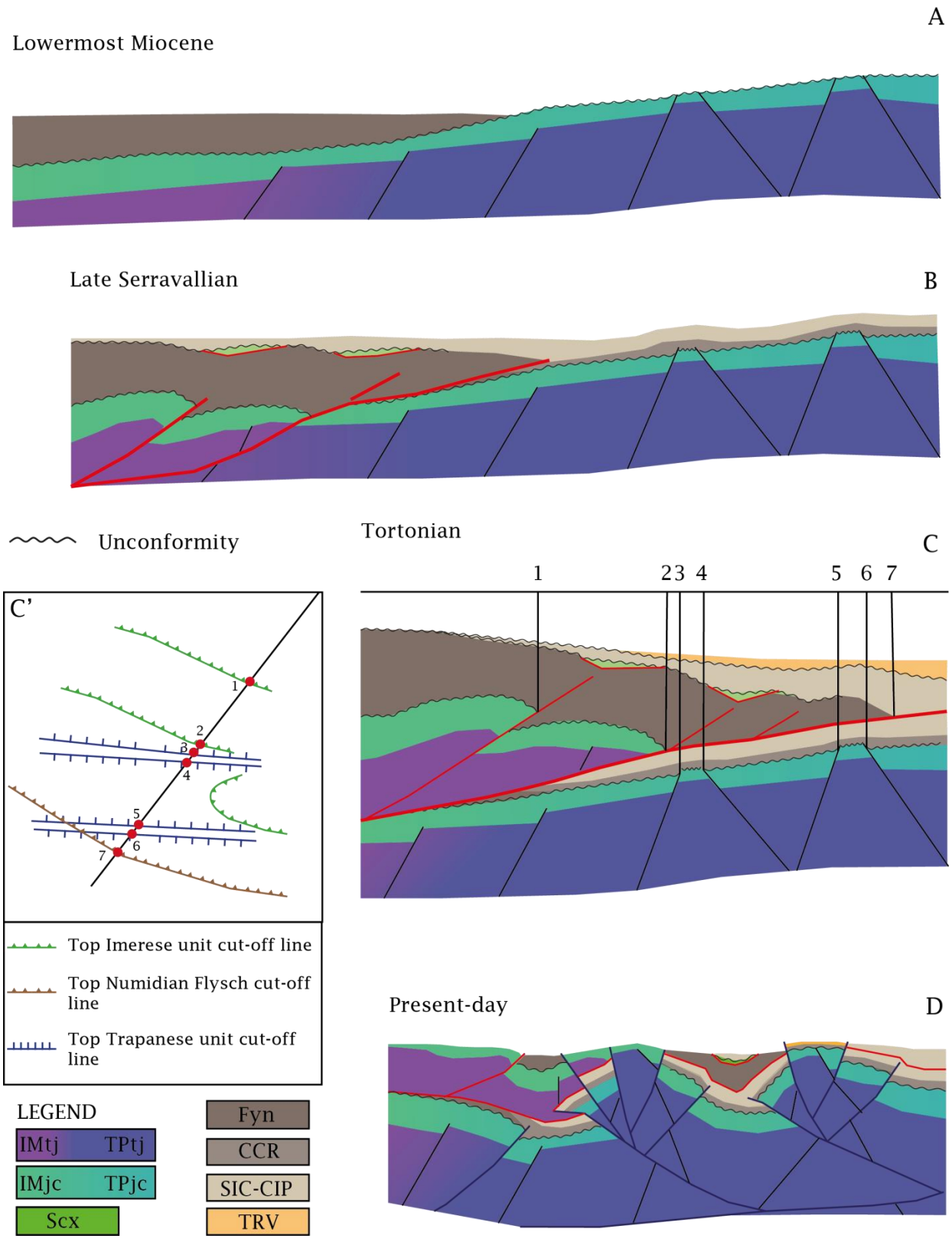

Figure 4.14 - Tectonic evolutionary model of the Sicilian fold-and-thrust belt proposed for the study area (not to scale). (A) Numidian Flysch deposition above the Imerese unit and external Trapanese unit in a foredeep setting during the lowermost Miocene. (B) Deformation affected internal units (Imerese, Numidian Flysch and Sicilide complex successions) during late Serravallian time. Sedimentation of Castellana Sicula and Marne di San Cipirello Fms. in a wedge-top to foredeep setting occurred at that time. (C) Emplacement of deformed Imerese, Numidian Flysch and wedge-top basin successions (allochthonous units) on top of the external Trapanese unit during the Tortonian time. Sedimentation of Terravecchia Fm. occurred at that time. (C') Cut-offs map of some noteworthy horizons. 1,2 - cut-off point of the top of the Imerese succession against thrust; 3,4,5,6 - cut-off point of the top of

the Trapanese succession against normal fault; 7 - cut-off point of the top Numidian Flysch against thrust. The Imerese unit is stuck in the northern portion of the area, whereas it propagates to the SW in correspondence of the paleo-structural low located between the Kumeta and Busambra Mts. The Numidian flysch overthrusts both the Kumeta and Busambra ridges.(D) Present-day configuration showing the deformed Trapanese unit and the re-deformation of the allochthonous units. IMtj—Imerese Triassic-lowest Jurassic succession; TPtj—Trapanese Triassic-lowest Jurassic succession; IMjc—Imerese lower Jurassic-lowermost Oligocene succession; TPjc—Trapanese lower Jurassic-late Eocene succession; Scx—Sicilide complex (Cretaceous-lower Miocene); Fyn—Numidian Flysch succession (upper Oligocene-lower Miocene); CCR—Calcareniti di Corleone Fm. (Aquitanian-Langhian); SIC-CIP—Castellana Sicula (Serravallian-Tortonian)-Marne di San Cipirello (late Langhian-early Tortonian) Fms.; TRV—Terravecchia Fm. (Tortonian).
Black lines correspond to Mesozoic normal faults; red lines correspond to the first tectonic event; blue lines correspond to the second tectonic event. Bold lines correspond to active faults.

4.6.2 Implications for hydrocarbon exploration

Oil exploration in Sicily started in the 1950 with oil discoveries in the Ragusa and Gela fields (Kafka and Kirkbride, 1960). Stratigraphic correlations between the subsurface rocks belonging to the Hyblean succession and the outcropping Trapanese-Saccense successions led the oil and gas exploration to focus on the buried lower Mesozoic limestones of these units. Nevertheless several drilled wells, mainly located using gravimetric response of carbonate structural highs, were mostly unsuccessful (Catalano et al., 2002). The main causes of failure can be related either i) to the absence of proper source rocks within the Trapanese and Saccense units, that on the contrary, were well defined in the Hyblean foreland (Late Triassic Noto and Streppenosa Fms.; Mattavelli and Novelli 1990; Frixa et al., 2000; Fantoni et al., 2008) or ii) to an incorrect structural model and fairy definition of potential traps.

Rock-Eval pyrolysis analysis performed in this work allowed to individuate potential source levels in the study area (Tab. 4.3; Fig. 4.7).

The Crisanti Fm. is the only formation of the Imerese unit which may contain possible source intervals (TOC > 0.5%) but it has fairy hydrocarbon generation potential as indicated by extremely low S_2 (0.05 mg HC/g) and related HI (8 mg HC/g TOC).

The Scillato Fm., belonging to the Imerese unit, is characterized by limestones with occurrence of bitumen filling pores and fractures in the sampled site (site 17 in Fig. 4.2; Fig. 4.8).

Since no potential source rocks are described for the Imerese unit, it is possible to hypothesize that this bitumen came from mature source rocks located within the underlying Trapanese unit.

On the other hand, vitrinite reflectance equivalent value measured on solid bitumen (R_{oeq}% ~0.7) indicates levels of thermal maturity compatible with the mid mature stage of oil generation. In addition, such a value is consistent with the simulated levels of thermal maturity experienced by the Scillato Fm. in the study area (Pizzo Chiarastella area, Fig. 4.9 E). Thus, according to thermal modelling, the source rock generating the bitumen could have been contained within the Scillato Fm. as bitumen has similar levels of thermal maturity than those recorded by the Scillato Fm.

The Streppenosa Fm. which is time equivalent to the Scillato Fm. (Trincianti et al., 2015), contains one of the most important source rocks in Sicily. In addition, Basilone et al., (2016a), described a strong facies variability within the Scillato Fm., highlighting the presence of a black-shales level informally called "Bivona facies", recorded in the Bivona 3 well drilled in the eastern Sicani Mts. area (Fig. 4.1). Thus, the presence of a localized levels rich in organic matter within the Scillato Fm. could justify the occurrence of bitumen found in the formation (Fig. 4.8).

Hydrocarbon expulsion/migration postdates the Miocene compression for both the hypotheses (source within the Trapanese or Imerese successions) and thus postdate the development of structural traps related to compression (such as 4-way closure anticlines). Seal rocks able to preserve hydrocarbon accumulations, are widespread along the succession (Crisanti claystones, Caltavuturo marls, Numidian flysch basal claystones).

Two fair to good potential source rocks intervals are identified for the Trapanese unit (Fig. 4.7).

Black shales found within the Amerillo Fm. (Fig. 4.3 C) represent a very good potential source rock with a TOC value of 22%. The investigated level is oil prone with high generative potential (S_2 = 94.73 mg HC/g; HI= 431mg HC/g TOC) and in the sampled site it is immature (T_{max}= 410 and PI= 0.06) as depicted also by XRD analysis (R0 I-S with 45% of illite layers).

The Marne di San Cipirello Fm. represents a fairy to good potential source rock (TOC of 0.59%) gas prone and immature in the sampled site as indicated also by XRD analysis (R0 I-S with 42% of illite layers).

Bitumen has been recovered in both Hybla and Inici Fms. along the Mt. Kumeta structure. Measured vitrinite reflectance equivalent value is 0.61% for the bitumen within the Hybla Fm. and 0.65% for the bitumen within the Inici Fm. (Tab. 4.2). In both samples measured R_{oeq}% is higher than the R_o% simulated for the respective reservoir rocks (Fig. 4.10 C).

Between the aforementioned potential source rocks detected for the Trapanese unit, only the black shales within the Amerillo Fm. may generate oil and bitumen.

Thermal maturity reached by the Amerillo Fm. is consistent with the immature stages of oil generation, along the Kumeta and Busambra Mts. structures and it might have experienced higher levels of thermal maturity, consistent with early mature stage of hydrocarbon generation, in the nearby narrow structural low between the two structures (Fig. 4.13 D). Such a higher thermal maturity simulated between the Kumeta and Busambra Mts., is linked to the higher thickness of the allochthonous units, still preserved there. As a logical consequence, hydrocarbon expulsion/migration would have post-dated the emplacement of the allochthonous units.

Nevertheless, the extremely reduced thickness (lower than 1m; Fig. 4.3C) of this black shales level makes the origin of bitumen from the Amerillo Fm., unlikely.

The Inici Fm., in the study area, is characterized by a lower Jurassic intra-platform basin facies (Marineo basin; Catalano and D'Argenio 1982b; Basilone et al., 2016b) drilled by the Marineo 1 well, located between the Kumeta and Busambra Mts. structures (Figs. 4.2, 4.7). Intra-platform basins represent areas of accumulation of excellent source rocks due to the common anoxic condition developed in such kinds of basins (Parrish and Curtis, 1982; Droste, 1990). In addition, in the Peri-adriatic region several source rocks derived from Triassic and Liassic intra-platform basins are described (Zappaterra, 1994). The Marineo 1 well, encountered levels of bituminous black shale along the Marineo intra-platform basin. Thus, the Inici Fm. could effectively contain the source rock that generated the bitumen remains, observed in the field.

In the study area, the Inici Fm. reached levels of thermal maturity (R_o% 0.55-0.65 in Fig. 4.13 C) consistent with the oil generation and in the same range of thermal maturity shown by the

sampled bitumen (R_{oeq}% 0.61-0.65). Such a thermal maturity is mainly reached in areas surrounding the Kumeta and Busambra Mts. (Fig. 4.13 C), as a consequence of the tectonic burial given by the emplacement of the allochthonous units during the Tortonian.

Late Triassic Streppenosa and Noto Fms. are stratigraphically correlated with the Sciacca Fm. and they represent the main source rocks for the Gela, Ragusa and Vega oil fields discovered along the Hyblean foreland (Mattavelli and Novelli, 1990; Zappaterra 1994; Frixa et al., 2000; Fantoni et al., 2008). Thus, source rock levels contained within the Sciacca Fm. can be envisaged. Levels of thermal maturity consistent with the oil generation were experienced by the Sciacca Fm. immediately after the deposition of the Amerillo Fm. (Fig. 4.13 A). Therefore, in this case, hydrocarbon generation predates the emplacement of allochthonous units (pre-Miocene in age). Levels of thermal maturity consistent with vitrinite reflectance equivalent values measured in the bitumen samples (R_{oeq}% 0.61-0.65) are reached by the Sciacca Fm. at depth, also along the Kumeta and Busambra structures (Figs. 4.10 and 4.13 B).

Therefore, to explain bitumen occurrence in the outcropping Inici and Hybla Fms., source rock levels could be contained in the subsurface within both the Inici and the Sciacca formations (Fig. 4.7). Data available in this work do not allow to define with extreme accuracy which formation contains the source rock and what is the effective source rock distribution. Despite that, one should point out that if the source rock were within the Inici Fm., hydrocarbons expelled during the late Miocene, could have migrated northward (from the Marineo intraplatform basin toward the Mt. Kumeta structure) in order to be accumulated along the Mt. Kumeta structure. In alternative, if the source rock were within the Sciacca Fm., hydrocarbon expulsion occurred after the late Eocene (Amerillo Fm. deposition) and migration should have been vertical. In this second case occurrence of structural traps linked to the compression (such-us 4-way closure anticlines) is questionable. Formations with sealing proprieties able to preserve hydrocarbon accumulations exists for both the hypotheses (Hybla marls, San Cipirello marls).

At the moment both hypotheses presented for the Trapanese and Imerese successions can be reliable, but further data should confirm it (e.g. biomarker analyses).

4.7 Conclusions

Thermal and structural modelling constrained by clay mineral-based geothermometers, organic matter optical analysis and Rock-Eval pyrolysis allowed us to define levels of thermal maturity experienced by the Imerese and Trapanese units in the SFTB.

The Imerese unit experienced maximum burial between 1.9-2.2km (overburden mainly represented by Numidian Flysch, Sicilide complex and wedge-top basin successions) at the top of the succession (Caltavuturo Fm.) and associated levels of thermal maturity consistent with the early-mid hydrocarbon generation stages.

The Trapanese unit experienced maximum burial between 1.2 and 1.3km (overburden mainly represented by allochthonous Numidian Flysch and wedge-top basin successions) at the top of the succession (Marne di San Cipirello Fm.) and associated levels of thermal maturity consistent with the immature stages of hydrocarbon generation.

As maximum thickness of the allochthonous units (1.2-1.3 km) atop the Trapanese unit, along the Kumeta and Busambra Mts. structures, is much lower than that expected from previous geometric and kinematic reconstructions (Imerese and Sicanian units, more than 5 km thick; e.g. Catalano et al., 2000; Avellone et al., 2010; Barreca et al., 2010) and the allochthonous units 3D distribution is quite variable, a new evolutionary scenario has been proposed invoking a major role for inheritance of passive margin structural elements into the thrust belt anatomy.

In the kinematic evolution proposed in this work, the allochthonous units (Imerese unit Numidian Flysch and syn-tectonic succession) propagate toward the south-west (present-day orientation) overthrusting the Trapanese unit. The increasing thickness of the Trapanese unit and inherited paleo-high morphology of the Kumeta and Busambra Mts. (elongated E-W to WNW-ESE, present day orientation) partially prevent the allochthonous propagation toward the south-

west. As a result, only to the Numidian Flysch and syn-tectonic successions could overthrust the Kumeta and Busambra Mts. structures. Following, since the uppermost Tortonian the Trapanese unit is involved in the orogenic wedge and began to exhume resulting in the Kumeta and Busambra Mts. tectonic windows.

In addition, paleothermal and geochemical data presented in this work coupled with the original 3D thermal model allowed also to individuate various potential source rock intervals throughout the Trapanese succession and to define eventual kitchen areas:

(i) black shales contained in the Amerillo Fm. (TOC of 22%) which are oil prone. This level is in the immature stage of oil generation along the Kumeta and Busambra Mts. structures as depicted by Rock-Eval pyrolysis (T_{max}= 410°C and PI= 0.06) and XRD analysis on clay minerals (R0 I-S with 45 % of illitic layers) whereas it is in the early stage of hydrocarbon generation in the structural low located between the two positive structures;

(ii) Marne di San Cipirello Fm. (TOC of 0.59%) which is gas prone. This formation is in the immature stage for hydrocarbon generation along the Kumeta and Busambra Mts. structures (R0 I-S with an illite content of 35-55% and R_o% values of 0.34-0.47%) and in the early stage for hydrocarbon generation in a narrow area between the two positive structures.

Since bitumen found along Trapanese and Imerese successions show different reflectance values, we infer potential source rocks located within the upper Triassic- lower Jurassic Trapanese platform and upper Triassic Imerese pelagic limestones.

5.1 Geometric and kinematic implications at a regional scale

5.1.1 The Sicilian Fold-and-thrust belt: comparison between Western, Central and Eastern Sicily paleothermal, structural and paleomagnetic data

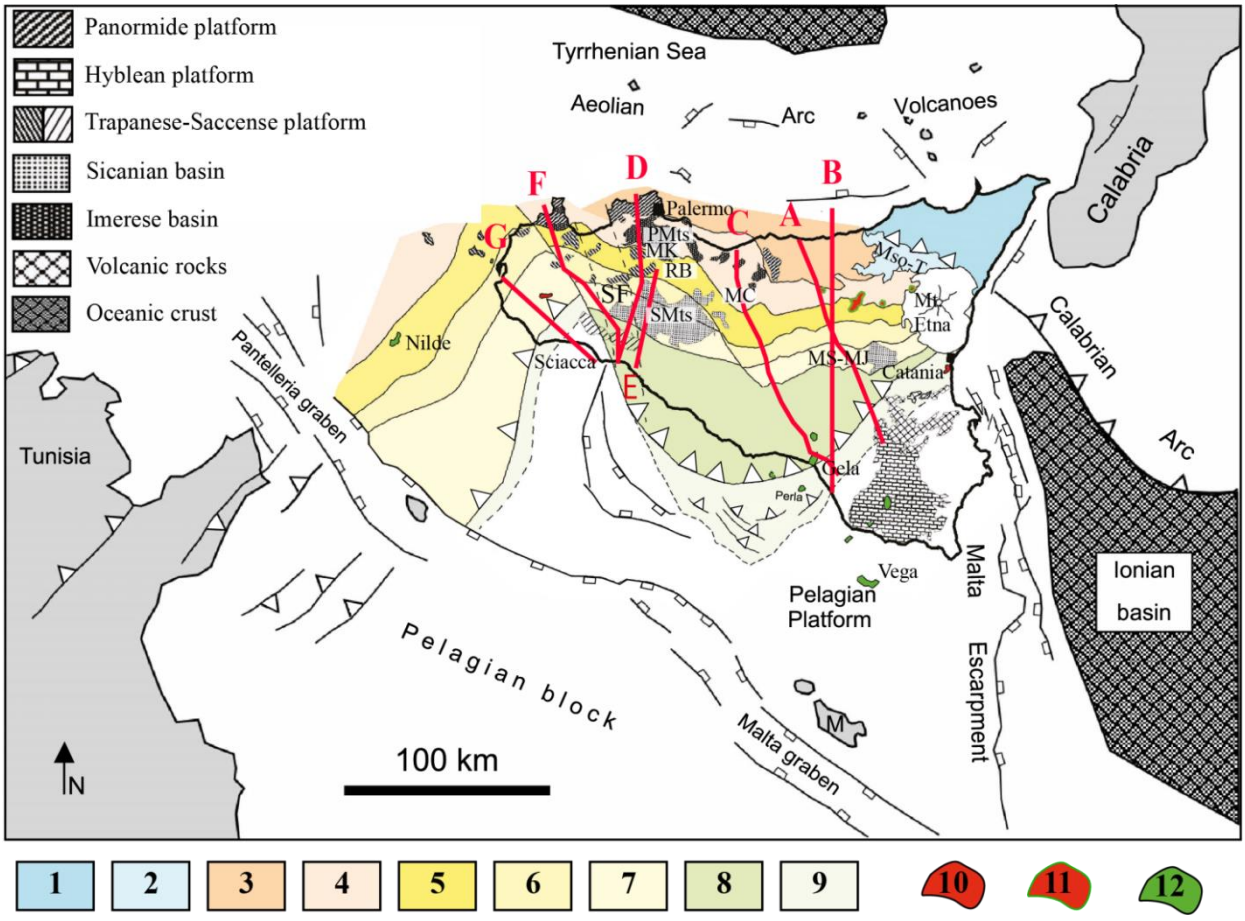

Figure 5.1 - Tectonic sketch map of the Sicilian region with a detailed sketching of the southward progression of foredeep basins (flysch deposits). Hydrocarbon field extensions: 10 biogenic gas; 11 gas-condensate; 12 predominantly oil, and Mesozoic rocks outcrops are also shown. Trace of the geological cross-sections A-E are indicated. 1 Peloritan crystalline terrain of European origin; 2 Mt. Soro flysch; 3 inner Numidian flysch and related Panormide platform rocks; 4 outer Numidian flysch and related Imerese domain basinal deposits; 5 inner Messinian foredeep; 6 central Messinian foredeep; 7 outer Messinian foredeep; 8 Gela nappe; 9 Gela foredeep and the Carla trough (Tunisian trough). PMts--Palermo Mts.; MK--Mt. Kumeta; RB--Mt. Rocca Busambra; SF--Segesta fault zone; SMts--Sicani Mts.; MS-MJ--Mt. Scalpello-Mt. Judica; Mso-T-- Mt. Soro and Troina. Modified after Granath and Casero (2004). See Fig. 5.2 for chronostratigraphic detail of each described unit.

The Sicilian Fold-and-Thrust belt (SFTB) is a key sector in the central Mediterranean basin, linking the Apennines and Calabria with the Maghrebides in North Africa through Tunisia (Fig. 5.1; Tricart et al., 1994, Casero and Roure, 1994; Catalano et al., 1996).

Figure 5.2 - Chronostratigraphic columns of the SFTB main stratigraphic domains (modified after Catalano et al., 2013b). Miocene–Pleistocene deformed foreland and wedge-top basin successions, progressively involved in the deformation, are also shown.

Several authors investigated the SFTB defining different structural styles for the belt: from early Miocene thin-skinned thrusting and limited involvement of the basement during the late Pliocene (Roure et al., 1990; Guarnieri et al., 2002; Finetti et al., 2005; Catalano et al., 2013a; Gasparo Morticelli et al., 2015) to widespread strike-slip tectonics rooted at deep structural levels (Ghisetti and Vezzani, 1984; Nigro 1998; Giunta et al., 2000b; Renda et al., 2000; Tortorici et al., 2001; Ghisetti et al., 2009; Barreca and Maesano, 2012) have been widely described.

Moreover, complex geometry characterizes the transition between the Western and the Central-Eastern portions of the SFTB. Some authors (Casero and Roure, 1994; Di Stefano et al., 2015) pointed out the presence of an important shear zone, mainly characterised by strike-slip kinematics, which must have displaced these two sectors of the chain (Fig. 5.1; Segesta fault zone, according to Casero and Roure, 1994).

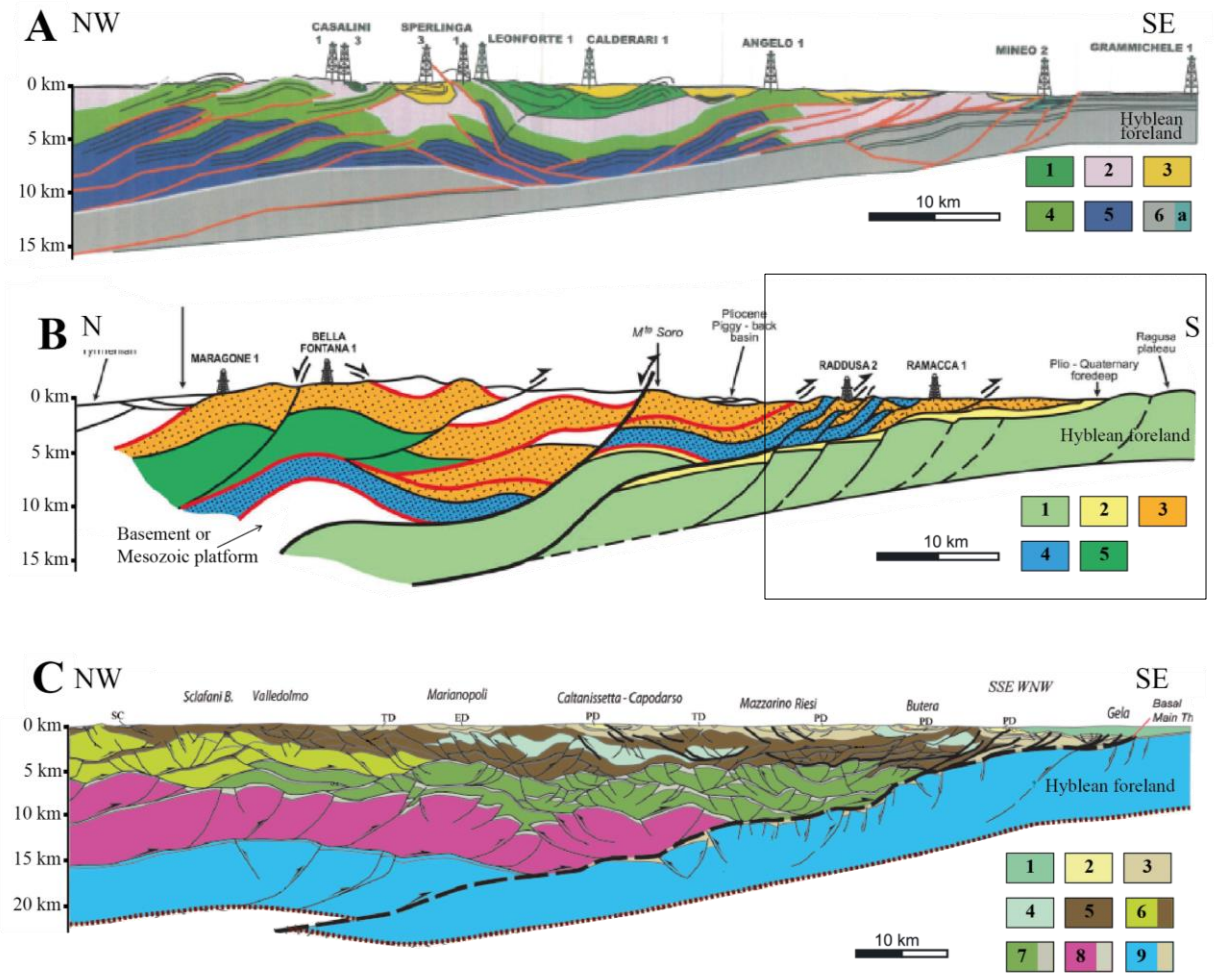

Figure 5.3 - Geological sections across Eastern-Central Sicily (traces in Fig. 5.1). A) Cross-section after Bello et al., (2000). 1 Far travelled Numidian Flysch (Oligocene - Miocene); 2 Sicilide Complex (Cretaceous-Eocene); 3 Late Tortonian - Pliocene syn-tectonic successions; 4 Numidian Flysch (Oligocene-Miocene); 5 Imerese-Sicanian (Triassic-Miocene); 6 Hyblean unit (Triassic – Pleistocene) and (a) late Pliocene-early Pleistocene clastic successions. B) Cross-section after Roure et al., (2012). 1 Hyblean unit; 2 Pliocene succession; 3 Miocene flysch; 4 Imerese unit; 5 Panormide unit (Triassic-Miocene). Black square indicates the portion of the cross-section equivalent to the one restored by Butler et al., (1992) C) Cross-section, modified after Catalano et al., (2013a). 1 Pleistocene foreland succession; 2 Pliocene- Pleistocene wedge-top successions; 3 upper Miocene-Pliocene successions; 4 detached Sicilide Complex; 5 detached Numidian Flysch; 6 Imerese unit; 7 Sicanian unit (Triassic-Miocene); 8 Trapanese unit (Triassic-Miocene); 9 Hyblean unit.

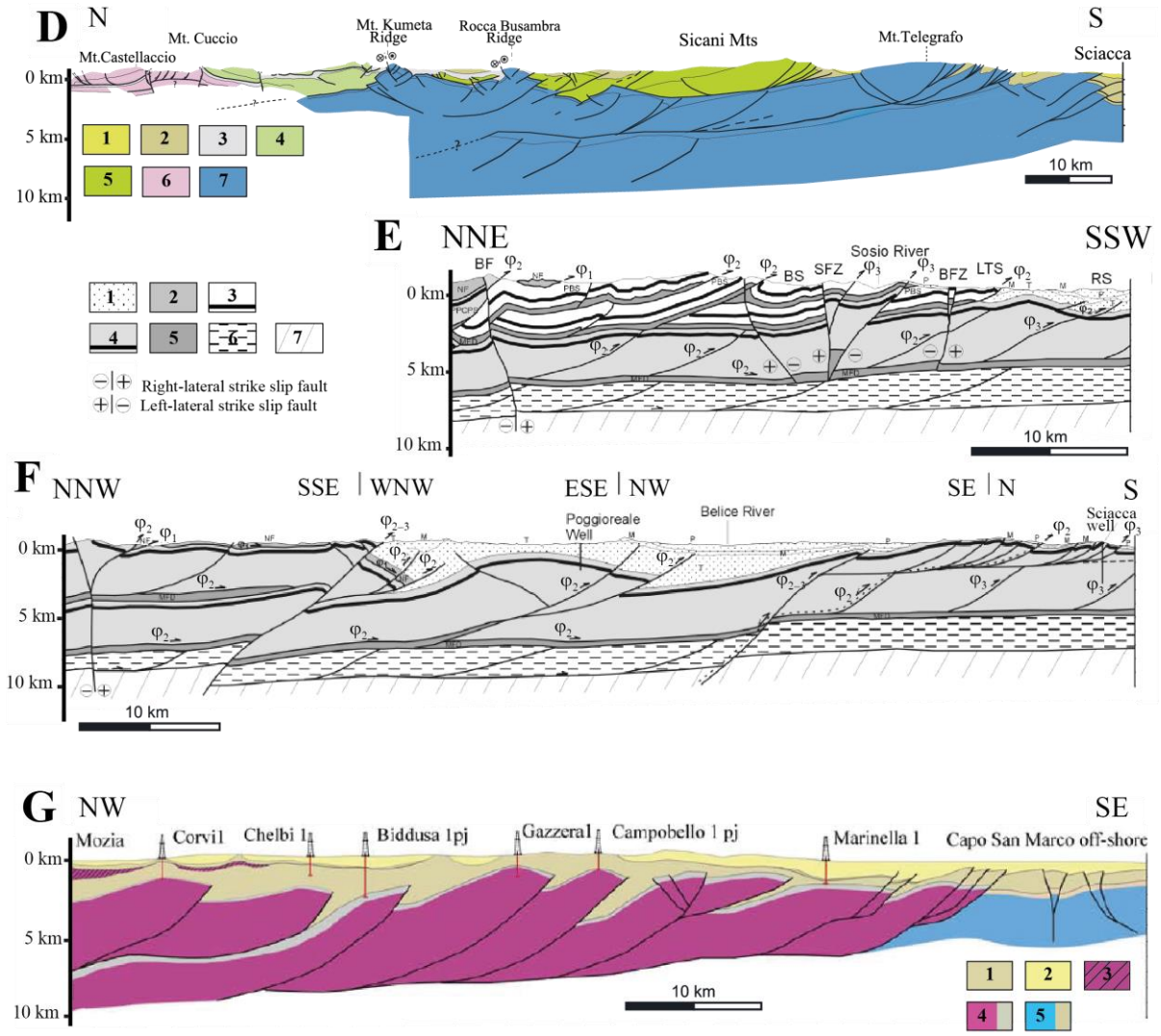

Figure 5.4 - Geological section crossing Western Sicily (traces in Fig. 5.1). D) Cross section modified after Catalano et al., (2000) and Speranza et al., (2018). 1 middle Pliocene-Pleistocene successions; 2 middle Miocene-lower Pliocene successions; 3 upper Oligocene-lower Miocene foredeep basin successions; 4 Imerese unit; 5 Sicanian unit; 6 Panormide unit; 7 Trapanese-Saccense unit. E) and F) Cross sections modified after Tortorici et al., (2001). 1 late Miocene-early Pleistocene clastic successions; 2 Numidian Flysch; 3 Sicanian unit; 4 Trapanese-Saccense unit; 5 Mufara Fm. (upper Triassic) detachment level; 6 Permian-early Triassic successions; 7 Basement. G) Cross-section modified after Catalano et al., (2013b). 1 lower Miocene-early Pliocene wedge-top basin successions; 2 lower Pliocene-early Pleistocene wedge-top basin successions;3 Pre-Panormide unit; 4 Trapanese-Saccense unit; 5 Hyblean unit.

Each structural style described in different time span and/or interpretations implies different amounts of shortening, with highly varying calculations in the literature. Among the others, Butler et al., (1992) evaluated ~38 km (along a cross-section 40km long) of maximum shortening within the Gela nappe (black square in Fig. 5.3 B); Di Paolo et al., (2012) as well, evaluated shortening amounts between 12.3km and 23.9km along three sections (between 50km and 52.2km long respectively) located in Eastern Sicily (e.g. 15.4km on a length of 51km, along

section A in Fig. 5.3); Tortorici et al., (2001) evaluated shortening not exceeding ~70km in western Sicily (along cross-sections in Fig. 5.4 E, F, ~47km and ~75km long respectively) and Gasparo Morticelli et al., (2015) evaluated ~112km of shortening for the Central Sicily (along cross section in Fig. 5.3 C, ~117km long). Furthermore, comparing geological sections reconstructed by various authors, it is possible to observe differences in structural styles moving from the east (Fig. 5.3) to the West (Fig. 5.4) of the SFTB. Major uncertainties regard: the role exerted by strike-slip tectonics (major role in Fig. 5.4 E and F; minor role in Fig. 5.4 D and G); the interpretation of the sections at depth concerning the position of the crystalline basements (along the northern border of the SFTB). Some authors propose that the basement is located at depths deeper than 10km (Fig. 5.3 and Fig. 5.4 D, G), among them, Catalano et al., (2013a, b), Speranza et al., (2018) and partly Roure et al., (2012) propose a carbonate platform doubling (Fig. 5.3 B and C, Fig. 5.4 D and G); conversely, Bello et al., (2000) and Tortorici et al., (2001) interpreted a shallower depth for the top of crystalline basement (~ 10 km; Fig. 5.3 A and Fig. 5.4 E and F). These different interpretations, of course, imply big differences in regional shortening calculation.

Thus, difference in shortening among the end member interpretations proposed in literature can be of one order of magnitude (e.g., tens of km vs. hundreds of km) and cannot be acceptable as along-strike changes. Such differences root in the evidence (underlined in Chapter III) that multiple interpretations are allowed when poor quality seismic line datasets are available. That's why independent cross check of structural style reconstructions can be of great help adopting thermal maturity investigations and thermal modelling (e.g. Corrado et al., 2005, 2009; Aldega et al., 2017, 2018), as well as a comparison among multiple seismic interpretations (e.g. Tozer et al., 2002; Shiner et al., 2004; Butler et al., 2004, 2018; Bond et al., 2007; Bond, 2015).

Paleothermal data presented in this thesis (chapters II and IV) show that the Imerese domain, detached at the base of the Triassic Mufara Fm., is deformed in thin-skinned style and experienced levels of thermal maturity in early to late stages of hydrocarbon generation in both

the study areas (Termini-Imerese and Kumeta and Busambra Mts.). Moreover, the Trapanese domain (platform to pelagic platform unit) experienced lower levels of thermal maturity than the Imerese unit, mainly in the immature stage of hydrocarbon generation.

In a wider framework, time equivalent formations (Caltavuturo Fm., Scaglia limestones and Amerillo Fm.) collected along the Imerese, Imerese-Sicanian and Trapanese units in this thesis in the Western and Central SFTB and in previous works in the Eastern SFTB (Aldega et al., 2007, 2011; Corrado et al., 2009; Di Paolo et al., 2012, 2014) show that (Fig. 5.5):

- the highest values of thermal maturity are recorded by the Imerese unit collected in the Palermo Mts. (e.g., Caltavuturo Fm.: R1 I-S with 60-78 % of illite content) and in the Termini-Imerese area (e.g. Caltavuturo Fm.: R1 I-S with 78% of illite content) (cfr. Chapters II and IV);
- a lower level of thermal maturity is detected in the Imerese-Sicanian unit, extensively cropping out in the eastern Sicily (e.g., Scaglia limestones: R0 and R1 I-S with 55% to 70% of illite content in the Mt. Judica area at the rear of the Hyblean foreland) (cfr. Aldega et al., 2007; Di Paolo et al., 2012, 2014);
- the lowest level of thermal maturity is recorded by the Trapanese unit, located in the Kumeta and Busambra Mts. area (e.g., Amerillo Fm.: R0 I-S with 33 to 50 % of illite content) (cfr. chapter IV).

Thus the thermal maturity of the Imerese and Imerese-Sicanian units, always confined in diagenesis, slightly decreases eastward, but it is always substantially higher than the thermal maturity experienced by the Trapanese unit. This difference between the Imerese-Sicanian and the Trapanese units in the Kumeta and Busambra Mts. (Western Sicily) area indicates a different tectonic and thermal history for these units.

Coupling these results with available structural and paleomagnetic data can help in building a robust kinematic reconstruction for the SFTB.

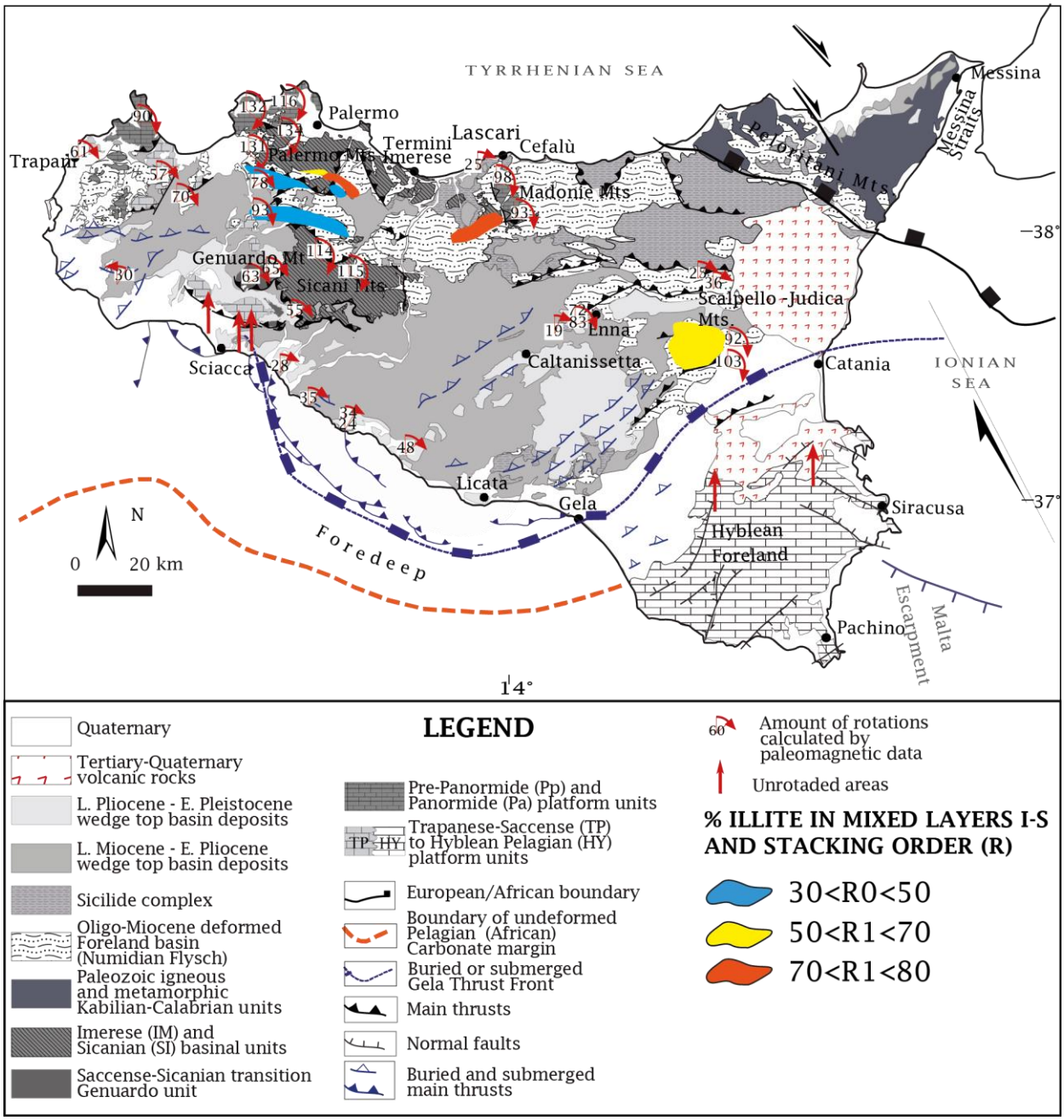

Figure 5.5 - Geological map of Sicily (modified after Gasparo Morticelli et al., 2015) showing: amount of clockwise rotations concerning different Mesozoic and Cenozoic units; thermal maturity distribution (expressed in %I in mixed layers illite-smectite) of the time equivalent Amerillo, Scaglia limestones and Caltavuturo Fms. Palaeomagnetic data are from Channel et al., (1990), Grasso et al., (1987), Speranza et al., (2003; 2018).

Geometrically, the Imerese unit cropping out in the Palermo Mts. thrusts above the Trapanese unit, whereas the Imerese-Sicanian unit (in the Mt. Judica area) directly thrusts onto the Hyblean foreland (Fig. 5.3 A, B).

High allochthony is recognised for the Imerese-Sicanian unit located in eastern Sicily since it directly overlies the Hyblean foreland (Bello et al., 2000) and it record ~100° of clockwise rotation during thrusting (Fig. 5.5 ;Speranza et al., 2003).

In Western Sicily, paleomagnetic data indicate differences in clockwise rotation between the portions of the two units studied in this thesis (Imerese unit ~130°and Trapanese unit ~80° resulting in ~50° of differential rotation). This evidence indicates, as well, high allochthony of the Imerese unit (Fig. 5.5) .

Seismic interpretation presented in Chapter III shows a detachment level at the base of the Trapanese unit. This evidence coupled with paleomagnetic data, indicates an allochthonous origin for this unit, as well as for the Imerese unit. Moreover, low levels of thermal maturity experienced by the Trapanese unit exclude the possibility of thick tectonic units overthrusting it for long time spans (Chapter IV). Maximum tectonic overburden, as modelled in chapter IV, is 1.2 -1.3 km thick.

Previous kinematic reconstructions (Catalano et al., 2000; Avellone et al., 2010; Barreca et al., 2010, 2012; Gasparo Morticelli et al., 2015) described deep-water basins (Imerese and Sicanian units) overthrusting platform units (Trapanese unit). According to such reconstructions, Kumeta and Busambra Mts. are defined as tectonic windows and between the two ridges remnants of the Sicanian unit were mapped (Catalano et al., 2000; Barreca et al., 2010; Albanese and Sulli, 2012).

In the Termini-Imerese study area, located ~35 km to the East of the Kumeta and Busambra Mts. area, the interpretation of the SIRIPRO; crustal seismic profile (Catalano et al., 2013a) shows that the Trapanese unit is buried below 5 to 6 km of Imerese and Sicanian thrust sheets (Fig. 5.3 C). Thermal data collected in this area (Chapter II) allowed us to reconstruct 1.8 km of Numidian Flysch previously overlying the Imerese unit, thus, the maximum tectonic burial which affected the Trapanese unit in this area is about 6.8 km, in agreement with Catalano et al.'s interpretation (2013a).

Conversely, thermal data collected in the Kumeta-Busambra area (Chapter IV) allowed us to evaluate 1.2-1.3 km of tectonic burial, affecting the Kumeta and Busambra tectonic windows (Trapanese unit) contrasting with previous interpretations.

Miuccio et al., (2000), in a stratigraphic review of different wells drilled along the SFTB, hypothesize the easternmost extension of the Trapanese unit, located in the Cerda 2 well area (Fig. 5.6), ~15 km west of the SIRIPRO profile. In this work, the authors, evaluated ~2.3 km of present-day tectonic burial affecting the Trapanese unit encountered in the Cerda 2 well. Thus, amount of tectonic burial does not differ substantially from the one evaluated in the Kumeta and Busambra Mts. (1.2-1.3 km) area and it is still much lower than that postulated in the Termini-Imerese area (6.8 km).

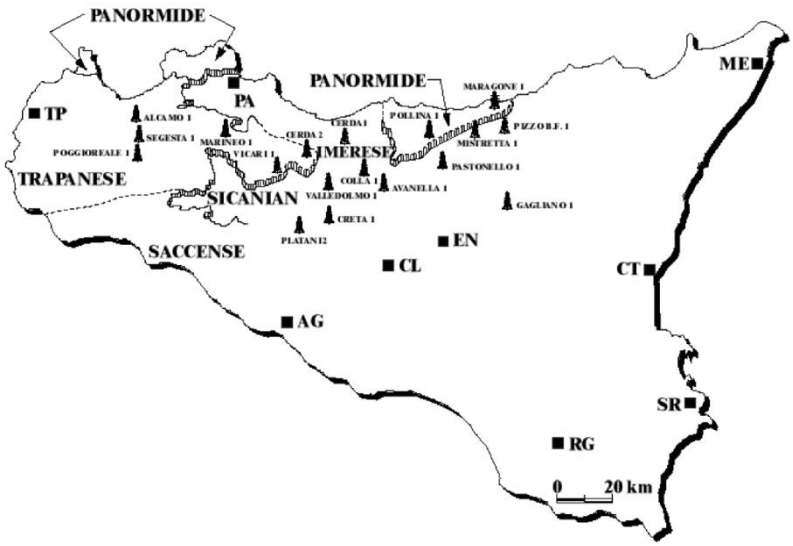

Figure 5.6 - Extension of the Triassic Platform domain in the present structural location (after Miuccio et al., 2000).

Such a high difference in tectonic burial affecting the Trapanese unit in the central and western sector of the SFTB could be explained postulating a crustal discontinuity between the two sectors, such as the regional fault described by Roure and Casero (1994) and Di Stefano et al., (2015). Absence of field evidences supporting this hypothesis make this configuration unlikely.

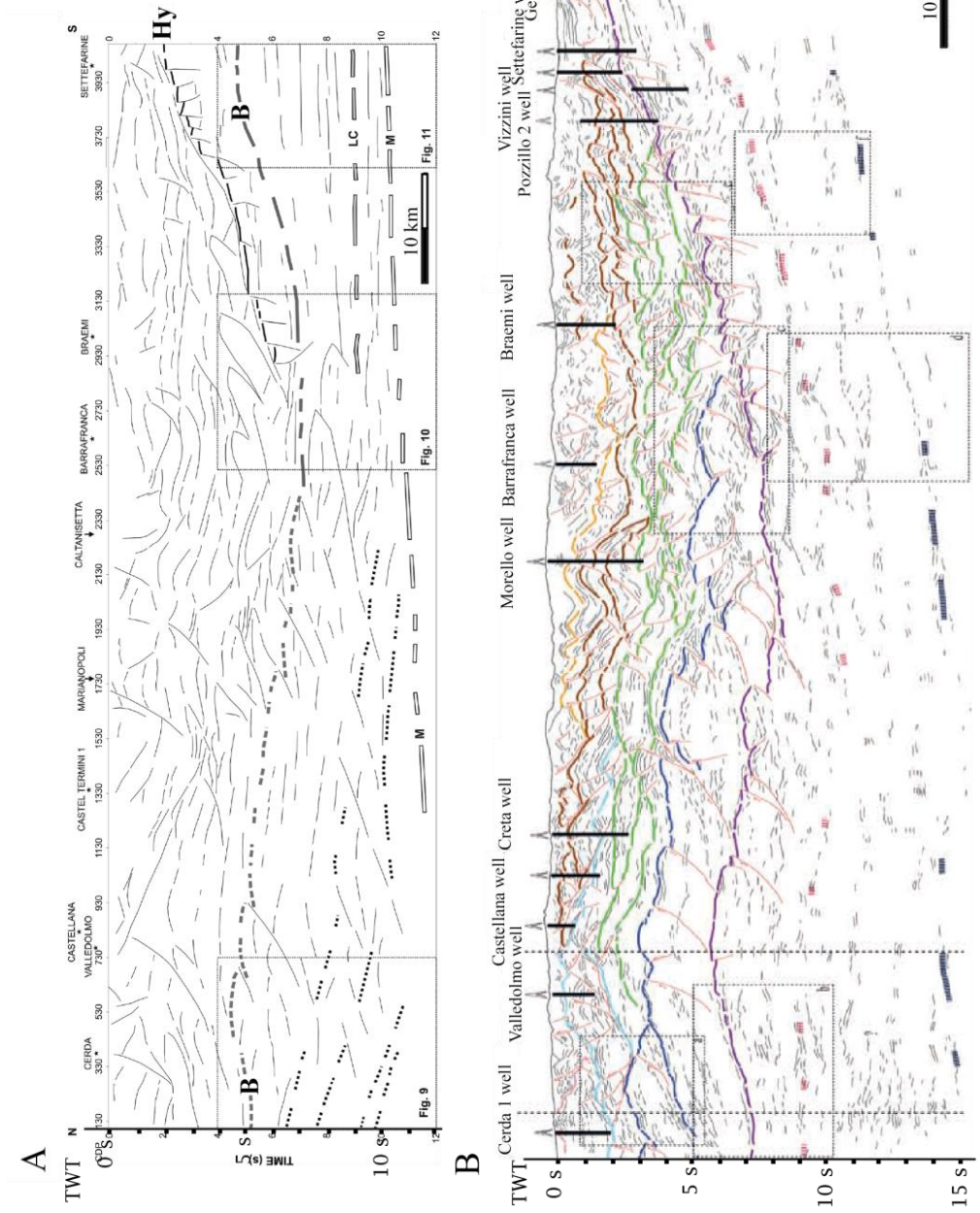

Figure 5.7 - (A) Line-drawing of the SIRIPRO profile (after Giustiniani et al., 2018) with highlighted the Moho interface (M), top of lower crust (LC), of basement (B), of Hyblean shelf (Hy). Dotted lines denote the presence of Tyrrhenian crustal structures, dipping south, and of lower crust lenses. Stars indicates the position of wells for HC exploration. Arrows indicate towns. (B) Line drawing of the SIRIPRO profile (after Catalano et al., 2013) and interpretation of the main horizons. Wells are also indicated.

On the other hand, a recent work from Giustiniani et al., (2018) proposed a re-processed version of the SIRIPRO profile and provided a new interpretation where the crystalline basement is located at significantly shallower depths than those estimated by the interpretation by Catalano et

al., (2013a). In the first interpretation (Catalano et al., 2013a), below the Cerda 1 well, the crystalline basement is at ~9s TWT (Fig. 5.7 B). On the contrary, in the recent work from Giustiniani et al., (2018) the position of the basement is located at ~5s TWT below the Cerda 1 well (Fig. 5.7 A). According to this second interpretation, the doubling of the platform (Trapanese unit overthrusting the Hyblean platform) is questionable.

Taking into account these pieces of evidence and the reconstruction by Bello et al., (2000) in Eastern Sicily (Fig. 5.3 A) it is possible to hypothesize a similar configuration for the Eastern and Central Sicily.

In this case, in Central Sicily (Termini-Imerese area), the deformed Hyblean platform should directly underlie the Imerese and Sicanian tectonic units as well as in Eastern Sicily without the occurrence of a further carbonate platform unit (Trapanese unit) in between the two. Thus, the Trapanese unit, cropping out along the Kumeta and Busambra Mts. and to the West (as shown in Fig. 5.1), probably disappears moving eastward, as shown by Miuccio et al., 2000 (Fig. 5.6) and in agreement with the most consolidated paleogeographic reconstructions (Catalano and D'Argenio 1978, 1982b; Montanari et al., 2000; Zarcone et al., 2010).

Moving from the Kumeta-Busambra Mts. to the west, the Trapanese unit probably overthrusts the Hyblean carbonate platform as shown by different reconstructions, summarised in Fig. 5.4.

In summary, integrating paleoethermal, structural, tectonic, paleomagnetic data, the main implication regarding the SFTB anatomy are:

- all the investigated units are allochthonous;
- - the Imerese unit directly overthrust the deformed Hyblean unit in central Sicily (Termini-Imerese area), resulting in a shallower position of the basement;
- - strike-slip tectonic play a minor role respect to thin-skinned thrusting

5.1.2 The SFTB in the Western Mediterranean

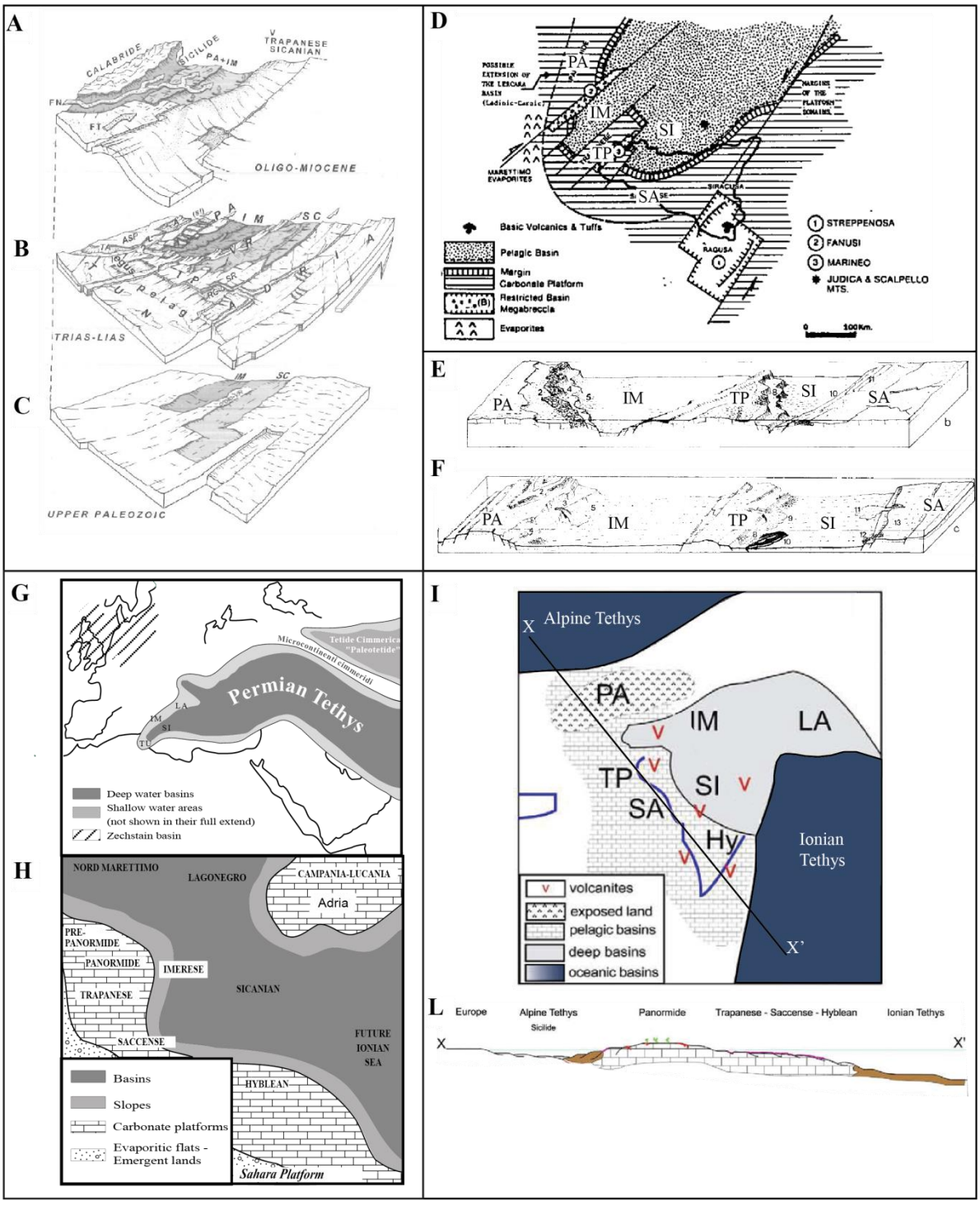

Figure 5.8 - Paleogeographic reconstructions of the Sicilian pre-compressional paleogeography proposed by various authors. A), B) and C) Evolution of Sicilian domain and subdomains during Oligo-Miocene times, Triassic-Liassic and upper Paleozoic, respectively. TUN--Tunisia; PA--Panormide unit; TP--Trapanese unit; IM--Imerese unit; SC--Sicanian unit; FN--Numidian Flysch; FT--Fortuna formation (after Montanari et al., 2000). D) Palinspastic map of Sicily (modified after Catalano and D'Argenio, 1982b) showing the occurrence of infraliassic strike-slip tectonics (e.g. Ragusa basins) PA--Panormide; IM--Imerese unit; TP--Trapanese unit; SI--Sicanian unit; SA--Saccense. E) and F) Paleogeographic reconstruction of Sicily (modified after Catalano and D'Argenio, 1978) during the Norian-middle Liassic and middle Cretaceous-early Eocene times, respectively. PA--Panormide; IM--Imerese unit; TP--Trapanese unit; SI--Sicanian unit; SA--Saccense. G) and H) Reconstruction of the Sicilian continental margin during middle Permian and late Triassic times, respectively (modified after Catalano et al., 1996). TU--Shallow-water

deposits of Tunisia, partly with pelagic influx; SI- Sicanian unit; LA-shallow-water middle and upper Permian Lagonegro domain (southern Apennines) and its possible prolongation in the Imerese domain of Sicily (IM). I) Paleogeographic reconstruction of the central Mediterranean area during middle Jurassic time and L) cross-section showing the relationship among different domains (modified after Zarcone et al., 2010). A bridge between the Panormide platform (PA) and the Apennine Carbonate platform is considered in this reconstruction. IM--Imerese unit; TP--Trapanese unit; SI--Sicanian unit; SA--Saccense; LA--Lagonegro basin; Hy--Hyblean unit.

Paleogeographic reconstructions (Figs. 5.8, 5.9) slightly differ from one another. The main differences are: the position of the Imerese and Sicanian basin respect to the Trapanese unit as some of the reconstructions propose the location of the pelagic basins to the north of the Trapanese unit (Fig. 5.8 H and Fig. 5.9) and some others propose the Trapanese unit located between the two pelagic basins (Fig. 5.8 A-G, I and L); the paleogeographic connection between the Panormide and Apennine platform which is still matter of debate (Catalano et al., 1996; Rosembaum et al., 2004; Zarcone et al., 2010; Tavani et al., 2013).

Nevertheless, all the proposed reconstructions generally show thick carbonate platform successions extending in the western-southwestern sector (Hyblean-Pelagian structural units), whereas in the eastern zone deepwater sediments (Imerese-Sicanian units) have been accumulated during the Permian and Mesozoic until Tertiary times. The Kumeta and Busambra Mts. area probably corresponds to the transitional area between these two domains where deep-water basins interdigitate thick carbonate platforms. This kind of configuration (Fig. 5.8 D, E and F) has been already described by Catalano and D'Argenio (1978, 1982b) and is partially responsible of the structural complexity recognised in this sector.

A recent work from Speranza et al., (2018) shows a paleogeographic scheme at the Oligocene-Miocene boundary with superimposed original faults and fold directions (back-rotated) deforming the Imerese-Panormide and Trapanese units. In this work (Fig. 5.9), the Imerese and Trapanese units show the same original direction of the main faults, ~NNE-SSW to NE-SW oriented, whereas, the original direction of the Panormide-to-Imerese paleogeographic margin is ~NW-SE oriented. Projecting the back-rotated tear (secondary) faults dissecting the Kumeta structure (reconstructed in Chapter III) onto this reconstruction, it is possible to observe that

these faults have similar orientation of the Imerese-Panormide paleogeographic margin (Fig. 5.9). In the Chapter III, we already pointed out how such tear faults orientation is consistent with inherited normal faults orientation.

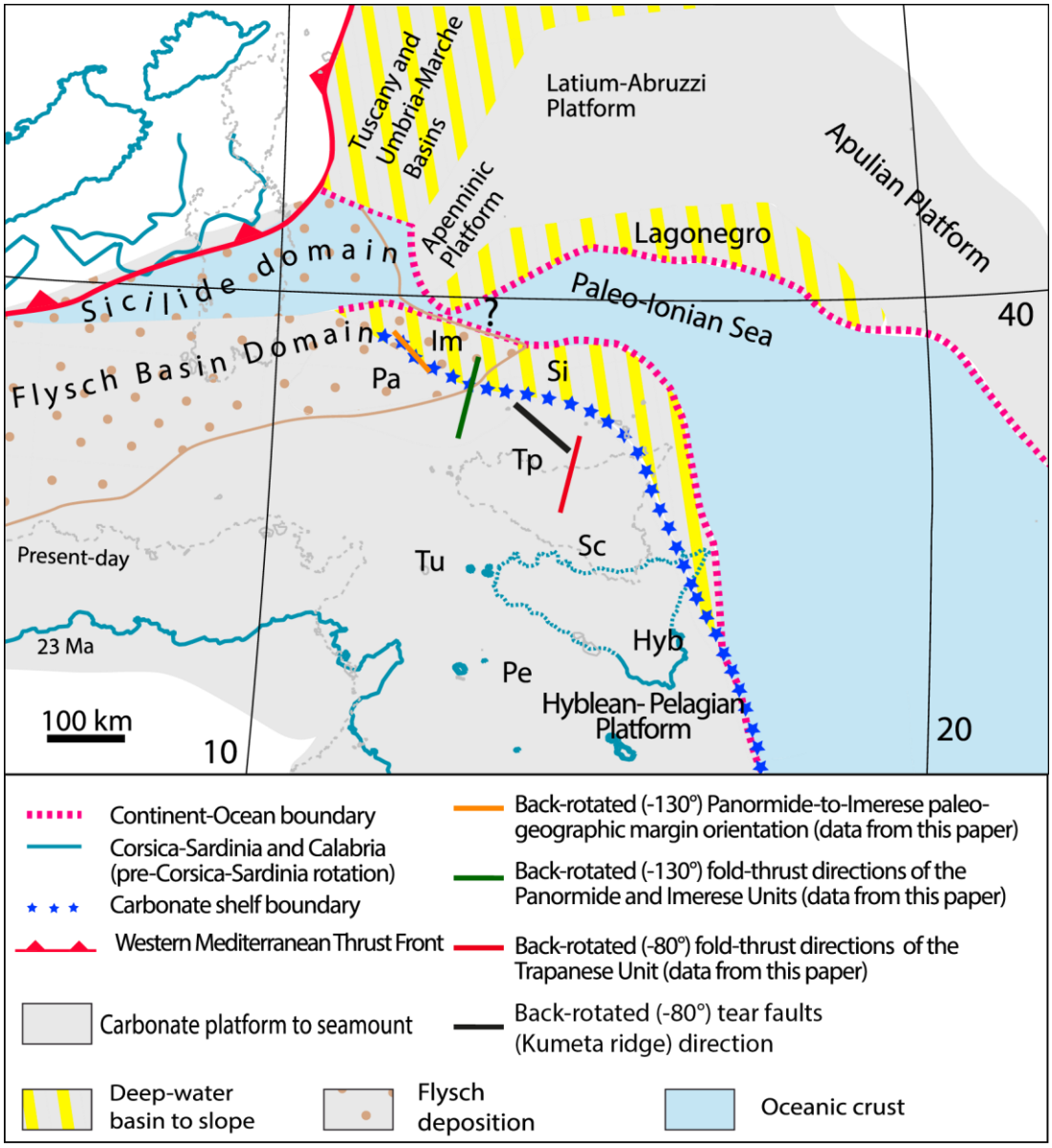

Figure 5.9 - Paleogeographic reconstruction of the central Mediterranean domain at 23 Ma (Oligo-Miocene boundary). Back-rotated trend of main faults affecting the Imerese (Im), Panormide (Pa) and Trapanese (Tp) units are also shown. Pe-Pelagian domain; Hyb-Hyblean domain; Sc-Saccense domain; Tu-Tunisia; Sc-Sciacca. (modified after Speranza et al., 2018).

Since the original direction of main faults affecting the Trapanese unit during the Neogene compression show the same orientation of the Mesozoic normal faults, partially reactivating

these last faults (Chapter III), I suggest that the NNE-SSW to NE-SW striking faults probably corresponds to inherited lineaments.

Therefore, inherited normal faults show two main directions (before rotation): ~NNE-SSW to ~NE-SW and ~NW-SE. Some Authors (Catalano and D'Argenio 1982b; Basilone et al., 2016b) highlighted the relevance of transtensional tectonics during the development of different intraplatform basins (Cala Rossa basin, Palermo Mts.; Marineo basin, Kumeta and Busambra Mts.; Streppenosa basin, Hyblean foreland) recognised in the SFTB and in general affecting the Trapanese unit in the Kumeta and Busambra Mts. area (Longhitano et al., 1995). Thus, the two described fault sets (~NNE-SSW to ~NE-SW and ~NW-SE) could represent the expression of a transtensional regime affecting the southern Tethyan margin during the late Triassic-early Jurassic times (Catalano and D'Argenio 1978; Basilone et al., 2016b).

Normal faults linked to the Mesozoic spreading with ~NW-SE trend have been described also in Tunisia (Dhahri and Boukadi, 2010; Raulin et al., 2011) and, more in general, are parallel to transform faults affecting the northern border of Africa since the late Triassic-Lower Jurassic (Fig. 5.10 A; Frizon de Lamotte et al., 2011). These faults have often been reactivated and, in the Maghrebian domain, they border various segments of present-day mountain belt (Frizon de Lamotte et al., 2011).

As well as NW-SE-trending faults, ~NE-SW- trending faults are also mapped in Tunisia (Fig. 5.10 B; Bracène and Frizon de Lamotte, 2002; Buaziz et al., 2002; Frizon de Lamotte et al., 2009; Dhahri and Boukadi, 2010; Melki et al., 2010; Rigane and Gourmelen, 2011), ascribed to the Mesozoic rifting phase and they were often reactivated and inverted during later contractional events (Gahnmi et al., 2016).

Thus, these two sets of Mesozoic faults defined in this thesis in Sicily, harmonically complete a regional framework, extensively described for the North African belts (Frizon de Lamotte et al., 2009, 2011). They correspond to inherited normal faults and weakness zones which played an important role in the SFTB building, as partially pointed out in the Chapter III.

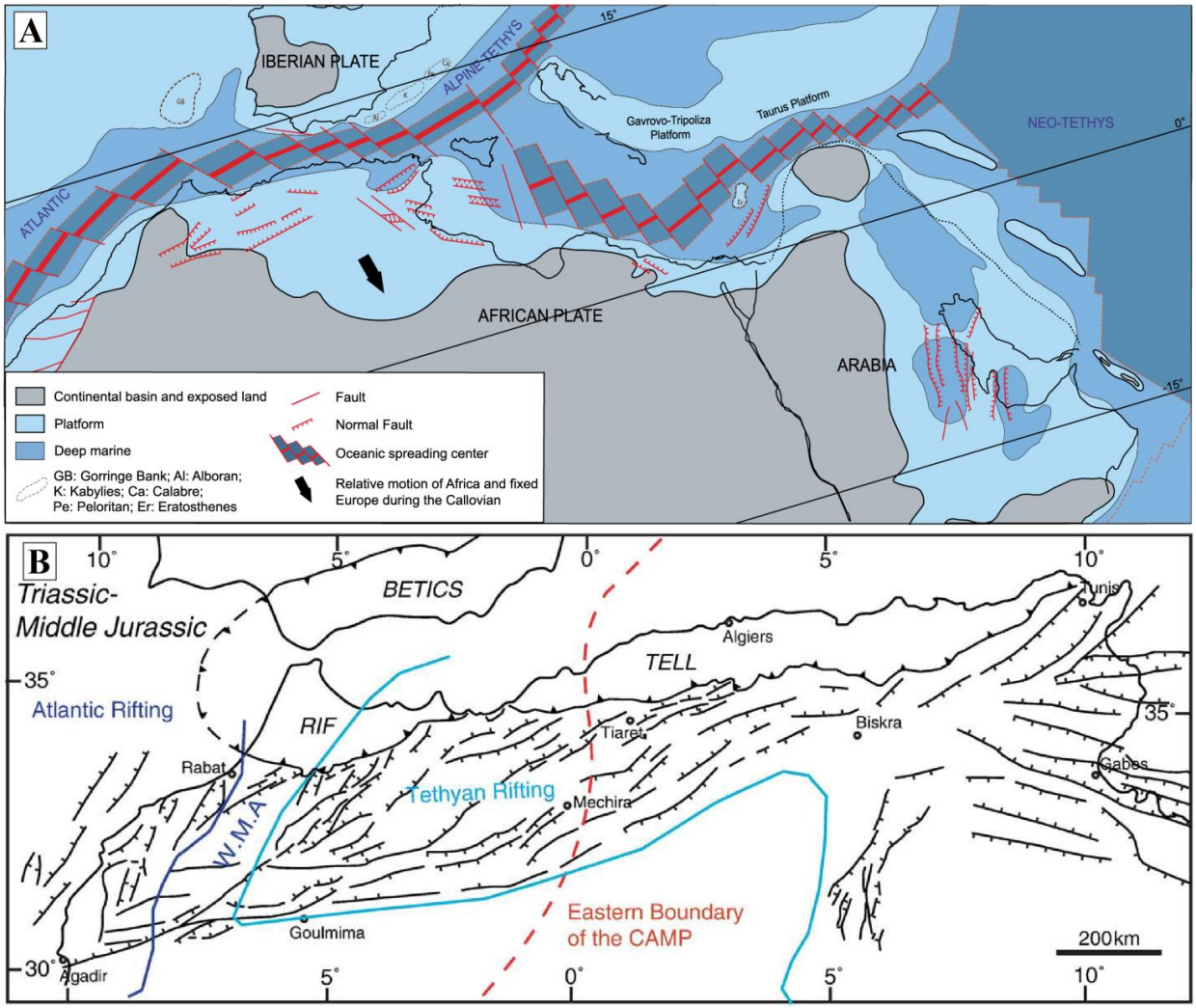

Figure 5.10 - A) Paleotectonic map of north Africa and Arabia for Callovian time, when basin domain was widespread in the Sicilian area, showing main transform and normal faults directions (after Frizon de Lamotte et al., 2011). B) Map of the main Triassic-Jurassic faults affecting north Africa. CAMP-Central Atlantic Magmatic Province (after Frizon de Lamotte et al., 2009).

In summary:

- Original fault directions (back-rotated) are consistent with Mesozoic normal fault directions;
- Detected original fault directions are consistent with inherited Mesozoic faults recognised along the North Africa belts.

5.1.3 Kinematic evolution of Western SFTB

Considering the complex paleogeographic setting which characterizes the study area, it is possible to envisage along-strike and along-dip variations of mechanical proprieties for the Imerese, Sicanian and Trapanese units, especially for their basal detachment level. It is constituted by the clayey portion of the Mufara Fm. in the deep-water basins (Imerese and Sicanian), whereas it is only hypothesized at the base of the Sciacca shallow water limestones, in the Trapanese unit (Triassic evaporites or claystones?) (Di Stefano et al., 2015).

Thus, as already described through analogues modelling (among the others: Corrado et al., 1998a; Li and Mitra, 2017; Borderie et al., 2018), such mechanical differences could explain the along strike variation of structural style, the orogen curvature (Costa and Speranza, 2003) and the higher propagation of thrusts in the eastern sector (Termini Imerese, e.g., "viscous" area) than that recorded in the western one (Kumeta-Busambra, e.g., "frictional" area).

Speranza et al., 2018 proposed a detailed kinematic evolution for the Central-Western SFTB supported by paleomagnetic data. According to these authors a stepwise decrease of rotation values in the progressively more external nappes is envisaged (in agreement also with Oldow et al., 1990). Moreover, the Imerese unit, which shows greater clockwise rotations (~130°), overthrust the Sicanian unit (~110° of clockwise rotation) and the detached Amerillo Fm. which overlie the Kumeta and Busambra Mts. structures (~110° of clockwise rotation) and subsequently thrust over the Trapanese unit (~80° of clockwise rotation).

Tectonic burial reconstructed in this thesis for the Trapanese unit in the Kumeta and Busambra Mts. area is about 1.2-1.3 km thick which is in disagreement with the mentioned tectonic model (see Chapter IV). In addition, thermal data coming from the Amerillo (R0 I-S with 33-50 % of illite content), Hybla (R0 I-S with 33-50 % of illite content) and Buccheri (R0 I-S and R0-R1 I-S with 40% and 50-60% of illite content respectively) Fms (Chapter IV) show a slightly increase of thermal maturity as function of depth.

Thus, albeit the Amerillo Fm. is often detached from the underlying substratum, this evidence is probably linked to a localized effect due to the heterogeneous mechanical proprieties of the Trapanese succession (Chapter III). In this context, the Hybla Fm. (underlying the Amerillo Fm.) corresponds to a secondary detachment level (according also to Avellone et al., 2010) rather than to regional detachment level, as described in Speranza et al., (2018).

Paleomagnetic data collected along the Sicanian succession were performed on samples from the Amerillo Fm. (Channel et al., 1990). The Amerillo Fm., belonging to the Sicanian unit, as well as the Amerillo Fm. belonging to the Trapanese unit shows 110° of clockwise rotation (speranza et al., 2018).

The higher amount of rotation of the Amerillo Fm. than that recorded for the underlying rock bodies is probably due to local effects in the Trapanese unit. The same explanation can be considered for the Sicanian unit cropping out in the Sicani Mts. Taking into account this consideration, it is possible to hypothesize a similar rotation for both the Sicanian and Trapanese units, where higher values of rotation (~110°) are related to local deformation effects and does not represent the rotation of the units at regional scale. Avellone et al., (2010), already pointed out that shallow seated deformation involving the Sicanian unit cropping out to the south of the Kumeta and Busambra Mts. area was partially coeval with the deep-seated deformation involving the Trapanese unit in the Kumeta and Busambra Mts. area.

In summary, the Sicanian unit could not have overthrust the Trapanese unit (Chapter IV), its deformation is almost coeval with the deep seated structures affecting the Trapanese unit and it shows similar amount of clockwise rotation observed for the Trapanese unit in the Kumeta and Busambra Mts. area (Amerillo Fm.). Therefore, it is possible to consider the Trapanese and Sicanian units likely pertaining to adjacent paleogeographic domains such as the Panormide and Imerese ones.

According to this reconstruction, both these units are involved into the orogenic wedge and internally deformed (Trapanese unit Chapter III) since the latest Tortonian and then they were emplaced above the more external Saccense-Hyblean domain.

Subsequently (early Pliocene?), deep-seated structures affecting the Saccense-Hyblean unit, further deformed the overlying Sicanian units (Avellone et al., 2010). The final configuration is similar to the one described by Tortorici et al., (2001; Fig. 5.4 E) where the Trapanese unit is internally gently deformed (in agreement with less than 15% of shortening, calculated in Chapter III), partially overthrust the Sicanian unit (seismic lines in Chapter III) and generally thrust together with the Sicanian unit onto a more external platform unit (Saccense-Hyblean unit). In contrast with Tortorici et al.'s interpretation (2001), the occurrence of widespread strike-slip systems, internally deforming the main thrust sheets is not confirmed by our reconstruction (Chapter III).

In summary:

- Chain building is strongly influenced by the former paleogeographic configuration
- The Sicanian unit did not overthrust the Trapanese unit in the Kumeta and Busambra Mts. area, instead, the Sicanian and Trapanese unit probably represent contiguous paleogeographic domains.
- Thin-skinned thrusting probably affected the Trapanese and the Sicanian units at the same moment, involving detachment levels located at different depths.

5.2 3D modelling strengths and limitations

3D geomodelling techniques are widely used in geological exploration to describe and characterize underground reservoirs, ore bodies, aquifers, and mitigate natural hazards (Royer et al., 2013). Furthermore, restoration, as well as backstripping techniques, are widely adopted in oil and gas industry, in order to: reconstruct the original setting of the investigated successions; validate 3D model reconstruction and define petroleum systems (including timing of

hydrocarbon generation and expulsion); convert the 3D models into 4D models (where the fourth dimension is represented by the time). For such purposes, 3D geomechanical restoration techniques, as well as 3D thermal modelling, have been developed. Unless 3D modelling represents a powerful tool, the use of this technique in the academia is still limited.

Main limitations of this technique are: i) the high amount of data (often not available in the academia) and knowledge necessary to build and constrain a 3D model; ii) the high computing power required to run 3D models; iii) the high natural complexity, hard to be represented in simplified models (e.g. branching faults (Y faults), thin or pinched out horizons; Durand-Riard et al., 2013; Pellerin et al., 2015).

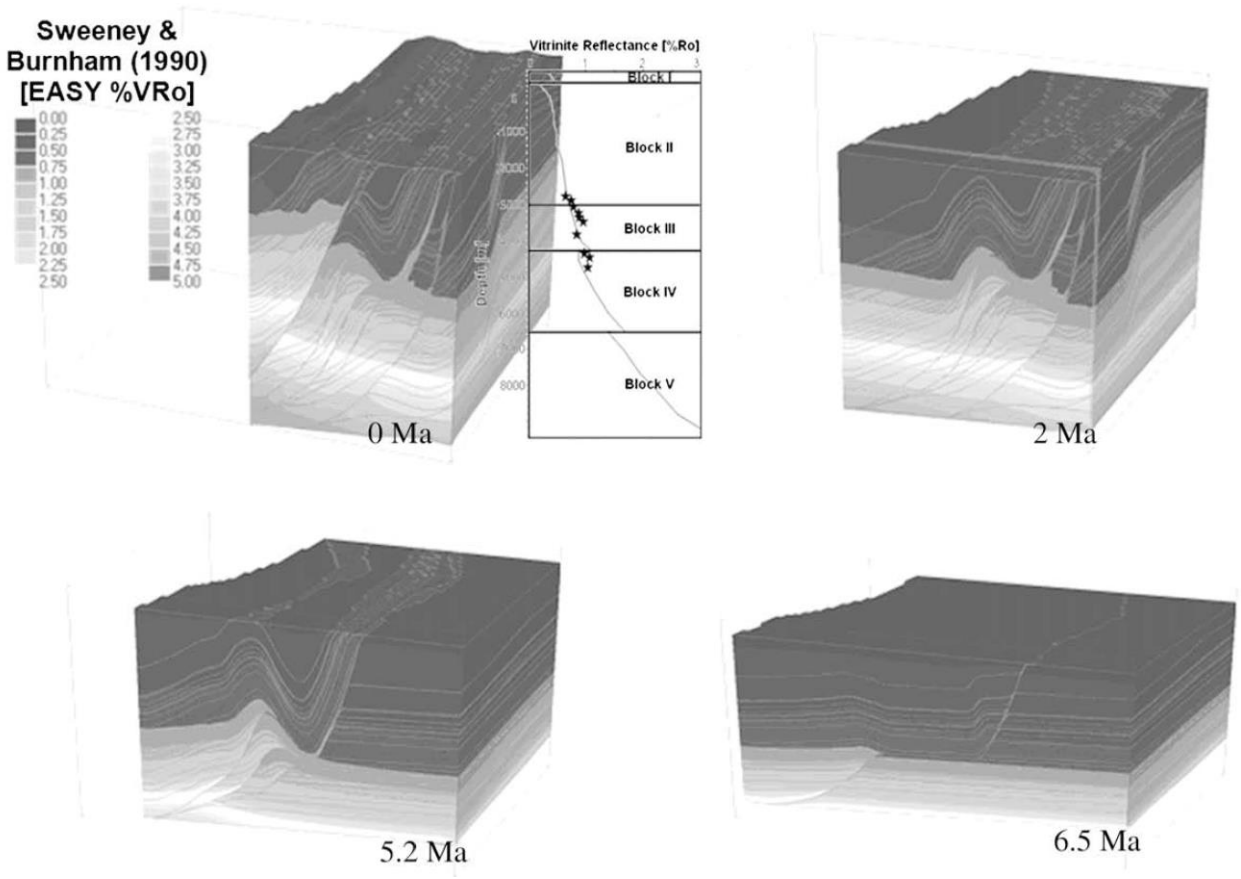

Figure 5.11 - Example of a 3D thermal model showing the development of vitrinite reflectance through time: at 6.5 Ma, 5.2 Ma, 2 Ma and at present-day situation (after Baur et al., 2009). 1D extraction of a calibration well is also shown. The extraction shows measured vitrinite reflectance data (stars) and the calculated maturity trend (solid line).

Over the years, several improvements have been made, drastically reducing computing time and allowing to represent (3D geological modelling) and validate (3D restoration) increasingly complex structures (Durand-Riard et al., 2010, 2013; Shuwei et al., 2013; Li et al., 2013, 2016).

Despite that, 3D thermal models have been mainly developed in simple areas in extensional settings (e.g.:Bayer et al., 1997; Romero-Sarmiento et al., 2013; Teles et al., 2014; Sachse et al., 2016; Goldbach et al., 2017; Olaruet al., 2018), but are still poorly adopted in structurally complex areas such as fold-and-thrust belt. Indeed, in this case, only one example is available (Baur et al., 2009), showing the 3D thermal model of the Bolivian fold-and-thrust belt that is affected by an almost cylindrical deformation (Fig. 5.11).

Main limitations in developing the 3D thermal modelling technique in complex setting are represented by: technical problems as well as the ones regarding 3D geological modelling; limited availability of data (such as paleothermal data) from the subsurface (well data), necessary to constrain the 3D thermal reconstruction.

For these reasons, various authors adopted a different approach in complex areas, either defining 2D thermal models along representative cross-sections (e.g. Schneider, 2005; Hardebol et al., 2009; Gusterhuber et al., 2014; Neumaier et al., 2014; Roure et al., 2014) or coupling 2D balanced cross-sections with 1D thermal modelling focused on key areas (e.g. Baby et al., 1995; Parra et al., 2011; Labaume et al., 2016).

This approach, until now represent a viable solution able to validate structural models using independent constraints (as shown in Chapters II and IV) and to describe the petroleum system of the area (in case of petroleum exploration).

Main limitations of this approach are: i) the lack of a refined maturity distribution of the investigated succession in the area; ii) difficulties in representing lateral variations of stratigraphic and thermal properties; iii) inability to define the expulsion and migration path of hydrocarbon (in the three dimensions) from the kitchen to the reservoir.

Therefore, in this project, the methodological aim was to overcome these limitations, building a fully 3D thermal model. Nevertheless, software limits (e.g. taking into account reverse faults) and lack of paleothermal constraints in areas where the investigated succession is not cropping out (subsurface), forced me to simplify the reconstructions on the base of some basic assumptions (Chapter IV).

In detail, two different 3D models were reconstructed in this work.

The first 3D model (Chapter II) located in the Termini-Imerese area, was mainly based on field data and geological cross-sections. Subsurface data in this area were represented by Cerda 1 well (Chapter II) and the SIRIPRO deep crustal reflection profile (Fig. 5.3 C). The main target was to reconstruct the deformed Imerese unit (cropping out along the Cervi, Sclafani Bagni, Rocca di Sciara Mts. and San Calogero Mts.). The 3D representation shown in Chapter II allowed me to constrain the structural model at depth and to reconstruct geometrically correct surfaces. 3D geological model reconstruction, indeed, constitutes a first validating tool to verify the geometrical reliability of the structures. 3D restoration of this model and 3D thermal modelling were not proposed for this first area. Main reasons of this choice are linked to: the absence of strong geometrical constraints in subsurface (e.g. different seismic profiles, well data); high structural complexity (two tectonic events affecting the Imerese unit, doubling of the unit which could not be simplified).

The second 3D model (chapter III, IV) located in the Kumeta and Busambra Mts. area, has a less complex geometry and more geometrical constraints. In this area Marineo 01 well and 13 seismic profiles were available to constrain the model at depth (Chapter III).

The main target was to reconstruct the deformed Trapanese unit (cropping out along the Kumeta and Busambra Mts. structures; Chapter III).

From a kinematic point of view, two tectonic events also affected this area as well as the Termini-Imerese area: the first event involved the Imerese unit whereas the second event involved the Trapanese unit and passively re-deformed the Imerese unit.

Thus, whereas the Imerese unit is affected by both the tectonic events (double fault sets; Chapter II) the Trapanese unit was affected only by the second tectonic event. In addition, the degree of deformation internally affecting the Trapanese unit is rather small (< 15%; Chapter III). Thus the complexity of this model is lower than the complexity of the first model (Termini-Imerese area).

In Chapter III, it is shown how the 3D modelling gave me a first warning about geometrical inconsistencies, whereas the 3D restoration allowed me to discriminate the correct interpretation of the area. Thus coupling the two tools represents a powerful way to define a geometrically correct and validated model.

Once the model was validated, the lower complexity of this model respect to the Termini-Imerese model, allowed me to apply some simplifications necessary to perform the 3D thermal modelling as shown in Chapter IV.

Despite the simplifications, the 3D thermal model provided me significant information about the thermal maturity distribution of the different formations (also at depth) and allowed me to define kitchens where potential source rock levels reached the hydrocarbon generation stage.

The complex case histories investigated in this project allowed me to define some limitations of 3D modelling in complex areas. In particular, I highlighted that more than one deformation phase involving a first generation of faults cut and displaced by a second generation of faults are difficult to be represented and hard to restore, requiring long computation time. High number of faults represented in the model, drastically increases the computation time, as well. Thus, I had to simplify the structural model and reduce the number of represented faults, maintaining only the most important ones (see Chapter II and III for simplification explanations).

In general it is still difficult to handle situations characterized by both complex stratigraphic setting (e.g. strong lateral facies variation) and complex structural setting (e.g. many reverse faults, complex deformation) thus different simplifications are necessary. Problems and simplifications presented in this work (Chapters II, III, IV) may be considered in 3D modelling

with similar complexity and they may represent technological challenges and case studies for people interested in software development.

Models reconstructed in this project are still rough but they represent a valuable starting point that can be refined through technical improvement and new data acquisition. 3D and 4D models, indeed, provide significant knowledge and improvements in understanding geological background (Royer et. al. 2013), as well as faults connectivity, but they are never complete. They need to be continuously up-dated through the acquisition of new data (e.g. new seismic lines, well data) which allow us to better constrain the model, and to make new ideas arise.

The mixed approach adopted in this work (1D, 2D and 3D) allowed me to review and validate (or invalidate) the structural interpretations proposed in previous literature. Thus, a recommended workflow for the validation of structural models in complex areas (fold-and-thrust belt) is finally proposed (Fig. 5.12).

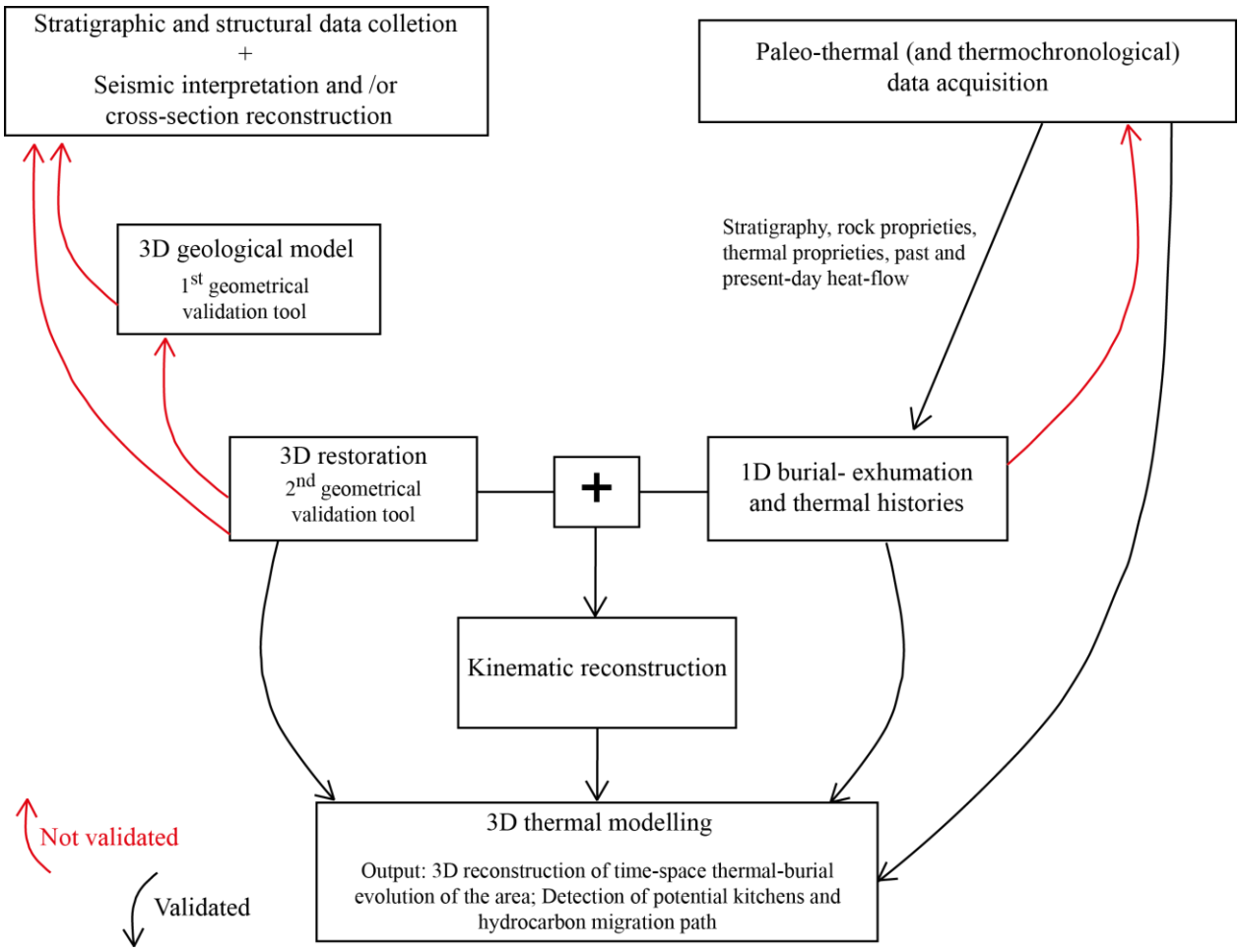

Figure 5.12 - Workflow showing the adopted methods to validate structural-kinematic model of the investigated areas.

6.1 Concluding remarks

This thesis fills a gap of analytical paleothermal data in the Italian panorama (see Corrado et al., 2010 for a review) proposing a multi-method approach of optical, geochemical and X-ray diffraction analysis for the study of the organic and inorganic fraction of sediments in western and central Sicily. A further novelty is the 3D representation and restoration of subsurface architecture in complex fold-and-thrust belt areas coupled with 1D and 3D thermal modelling. The main results allowed me to revise and integrate existing literature concerning the Sicilian fold-and-thrust belt anatomy and kinematics.

Here, the original paleothermal data and the numerical thermal-maturity modelling allowed to quantify the tectonic loads experienced by the sedimentary successions in western and central Sicily (~1.2-1.3 km vs ~6.8 km of allochthonous units onto the underlying carbonate platform unit, respectively) in order to improve previous tectonic interpretations (Chapter II and IV).

The reconstruction of two 3D geological models is proposed in order to visualize and describe along-strike variations of structural style. The geomechanical modelling approach used for the 3D restoration performed on the 3D model for the Kumeta and Busambra Mts. allow me to discuss and validate the fault architecture that I proposed with my new structural interpretation.

The amount of shortening along NNW-SSE direction is quite low (<15%) for the Trapanese unit.

For the 3D geological model performed in the Termini-Imerese area (Chapter II) the modelling methodology I have used, allowed me to reconstruct the complex geometry of this sector where two sets of faults are widely recognised: NW-SE-striking thrusts developed in the early Miocene which bring to the piling up of the different Imerese and Numidian Flysch thrust sheets; NE-SW-striking high angle transpressive faults developed during the latest Tortonian-early Pleistocene which led to the exhumation of the Imerese unit.

For the 3D geological model performed in the Kumeta and Busambra Mts. area my modelling allowed me to depict along strike variations of the structural style. In particular:

- the Mt. Kumeta structure is characterized by WNW-ESE backthrusts with a transport towards the NNE linked by hard linkages (NNE-SSW to NE-SW tear faults);
- the Mt. Busambra structure is characterized by a more complex geometry where an imbricate backthrust system (sense of transport towards the NNE) converts into thrust (sense of transport towards the SSW) moving westward. In this case soft linkages (folds) are suggested connecting the two structures (thrust and backthrust);
- WNW-ESE to E-W high angle transpressive to reverse faults characterized both the Kumeta and Busambra Mountains. These faults join thrusts at depth and probably reactivate pre-existing normal faults.

Mesozoic paleogeography influences the geometry of Cenozoic orogenic structures confirming the relevance of inherited structures (Chapter III). In detail, when Cenozoic vertical axis rotation is removed, two sets faults are recognised: a set of ~NNE-SSW to ~NE-SW and a second set of ~NW-SE striking faults. These two sets of faults are consistent with major Mesozoic structures described in Tunisia and, more in general, along north Africa.

Integration of paleothermal data, numerical modelling and available paleomagnetic data leads to indicate that the Sicilian fold-and-thrust belt is characterized by a thin-skinned tectonic style with high allochthony for the tectonic units derived from different paleogeographic domains.

As a secondary goal, data presented in this thesis allowed me to improve the knowledge concerning the petroleum system in the Kumeta and Busambra Mts. area. Different potential source rock levels are suggested within the Imerese and Trapanese Mesozoic-Cenozoic successions. In addition, 3D thermal-maturity modelling have strongly served to suggest and define possible kitchen areas related to these source rock levels.

In the oil and gas industry, the 3D geological modelling reconstruction and restoration proposed in this work (Chapter II) offer a "quickest and fast" approach to constrain/validate a structural interpretation (preventing possible unsuccessful exploration) before acquiring new data (which represent additional investments) in areas with a sparse, incomplete or debatable database (such as the Kumeta and Busambra Mts. area). This advanced workflow also is helpful to define interesting areas (possible traps) which unavoidably need further investigation.

Such an advanced workflow can be now recommended for validating structural models where structural and paleothermal input data are intimately connected and quantified using 1D to 3D numerical computer approaches.

6.2 Future perspectives

As it generally happens, the work proposed in this thesis does not represent just an end point. In fact, it is a starting point toward a re-evaluation of well-known areas through a new approach.

The 3D approach, as mentioned in the Chapter V, is still poorly developed for several reasons (Chapter V). Nevertheless, I think that it will be a common approach in the future, after technical improvements regarding the calculation velocity and the possibility to represent more and more complex geological setting.

In this thesis I demonstrated, indeed, that this approach did not represent only a way to visualize and describe a complex area but also a way to assemble variable data and documents in order to validate (or invalidate) geological concepts, interpretations and pre-existing models, in poorly constrained areas. 3D restoration, in particular, is able to exclude inconsistent interpretations and to individuate critical parts of the reconstructed model.

The combined approach of 3D geometrical model and paleothermal data represents the novelty introduced in this thesis. It provides, in turn, a new way to improve the geological knowledge of the investigated area. Chapter IV, indeed, outline how this combined approach allowed me to

highlight the role played by the inherited structures in the tectonic load distribution (preserved or now eroded) above the Trapanese unit.

Thus, several end points are reached in this thesis (even more than expected), as largely discussed above, but at the same time, the results obtained in this work represent a base (or starting point) on which we can make further improvements. In detail, new data acquisition (geometrical: e.g. new seismic data, re-processing of existing data; thermal: e.g. new low-temperature thermocronological data) and software improvements (e.g. representation of increasing number of fault in regional scale models; easy representation of reverse faults in 3D thermal models) can bring to further conclusions and to a more refined description of the area.

In conclusion, going on in this project, I would like to suggest three future lines of research:

i) Mapping the thermal maturity distribution of the deep-water units through new paleothermal data acquisition in the Sicani Mts. area (Sicanian unit) and between the Termini-Imerese and Kumeta and Busambra Mts. area (Imerese unit). Mapping the thermal maturity distribution of the "platform" units through new paleothermal data acquisition in the Mt. Palermo and Madonie Mts. area (Panormide unit) and to the west of Kumeta and Busambra Mts. area (Trapanese unit). A complete knowledge of the thermal maturity acquired by the involved units can be an aid in constraining the kinematic evolution of the entire Sicilian fold-and-thrust belt.

ii) 3D geometrical model reconstruction and 3D geomechanical restoration at a bigger scale, from Tunisia offshore toward the eastern Sicily (using a lower resolution, e.g. mapping only the tops of most important units and not top formations). As a result, I would expect to verify and describe the validity of the model, the evolution of differential rotations and (if the model is validated) the pre-compressional paleogeographic (and geometric) distribution of the different units.

iii) Continue to develop and improve software workflow methodology able to perform 3D thermal simulation in complex areas since, behind the primary scope represented by the

petroleum system modelling (oil and gas industry), it represents a quality-control tool in the kinematic evolution description of the investigated area.

References cited

Abate, B., Catalano, R., D'Argenio B., Di Stefano, E., Di Stefano, P., Lo Cicero, G., Montanari, L., Pecoraro, C., and Renda, P., 1982, Evoluzione delle zone di cerniera tra piattaforme carbonatiche e bacini nel Mesozoico e nel Paleogene della Sicilia occidentale. In: Catalano, R., and D'Argenio, B., (eds.), Guida alla Geologia della Sicilia Occidentale, Guide geologiche regionali, Società Geologica Italiana, Suppl. A, no. 26, p. 53-81.

Albanese, C., and Sulli, A., 2012, Backthrusts and passive roof duplexes in fold-and-thrust belts: The case of Central-Western Sicily based on seismic reflection data: Tectonophysics, no. 514, p. 180-198.

Aldega, L., Corrado, S., Grasso, M., Maniscalco, R., 2007, Correlation of diagenetic data from organic and inorganic studies in the Apenninic-Maghrebian fold-and-thrust belt: a case study from Eastern Sicily: The Journal of Geology, no. 115 (3), p. 335-353.

Aldega, L., Corrado, S., Di Paolo, L., Somma, R., Maniscalco, R., Balestrieri, M.L., 2011, Shallow burial and exhumation of the Peloritani Mts. (NE Sicily, Italy): insight from paleo-thermal and structural indicators: Geological Society of America Bulletin, no. 123, p. 132-149.

Aldega, L., Carminati, E., Scharf, A., Mattern, F. and Al-Wardi, M., 2017, Estimating original thickness and extent of the Semail Ophiolite in the eastern Oman Mountains by paleothermal indicators: Marine and Petroleum Geology, no. 84, p. 18-33.

Aldega, L., Bigi, S., Carminati, E., Trippetta, F., Corrado, S. and Kavoosi, M. A., 2018, The Zagros fold-and-thrust belt in the Fars province (Iran): II. Thermal evolution: Marine and Petroleum Geology, no. 93, p. 376-390.

Al-Fahmi, M.M., Plesch, A., Shaw, J.H., and Cole, J.C., 2016, Restorations of faulted domes: AAPG Bulletin, no. 100(2), p. 151-163.

Allen, P.A., 2008, From landscapes into geological history: Nature, no. 451, p. 274-276.

Allen, P.A. and Allen, J.R., 2013, Basin Analysis, principle and application to petroleum play assessment: Wiley-Blackwell, Third edition, p. 619.

Álvarez Marrón, J., 1995, Three dimensional geometry and interference of fault-bend folds: examples from the Ponga Unit, Variscan Belt: Journal of Structural Geology, no. 17, p. 549- 560.

Andreucci, B., Castelluccio, A., Corrado, S., Jankowski, L., Mazzoli, S., Szaniawski, R., and Zattin, M., 2015, Interplay between the thermal evolution of an orogenic wedge and its retro-wedge basin: An example from the Ukrainian Carpathians: GSA Bulletin, no. 127(3-4), p. 410-427.

Avellone, G. and Barchi, M.R., 2003, Le pieghe minori nelle Unità Imeresi e Trapanesi dei Monti di Palermo e il loro significato nell'evoluzione tettonica dell'area: Bollettino della Società Geologica Italiana, no. 122, p. 277-294.

Avellone, G., Barchi, M.R., Catalano, R., Gasparo Morticelli, M. and Sulli, A., 2010, Interference between shallow and deep-seated structures in the Sicilian belt, Italy: Journal of the Geological Society, London, no. 167, p. 109–126.

Avellone, G., Gennaro, C., Gugliotta, C., Barchi, M.R. and Agate M., 2011, Tectono-stratigraphic evolution of a basin generated by transpression: The case of the Early Pliocene Lascari Basin (northern Sicily): Italian Journal of Geosciences, no. 130, p. 93–105.

Baby, P., Hérail, G., Salinas, R., and Sempere, T., 1992, Geometry and kinematic evolution of passive roof duplexes deduced from cross section balancing example from the foreland thrust system of the southern Bolivian Subandean Zone: Tectonics, no. 11 (3), p. 523e536.

Baby, P., Moretti I., Guillier, B., Limachi, R., Mendez, E., Oller, J., and Specht., M., 1995, Petroleum system of the northern and central Bolivian Sub–Andean Zone. In: Tankard AJ, Suárez RS, Welsink HJ (eds.) Petroleum basins of South America: AAPG Memories, p. 445–458.

Balsamo, F., Aldega, L., De Paola, N., Faoro, I., and Storti, F., 2014, The signature and mechanics of earthquake ruptures along shallow creeping faults in poorly lithified sediments: Geology, 42(5), 435-438.

Barnes, J.B. and Heins, W.A., 2008, Plio-Quaternary sediment budget between thrust belt erosion and foreland deposition in the central Andes, southern Bolivia: Basin Research, p. 1-19.

Barreca, G., Maesano, F.E., and Carbone, S., 2010, Tectonic evolution of the Northern Sicanian-Southern Palermo Mountains range in Western Sicily: insight on the exhumation of the thrust involved foreland domains: Italian journal of geosciences, no. 129(3), p.429-440.

Barreca, G., and Maesano, F.E., 2012, Restraining stepover deformation superimposed on a previous fold-and-thrust-belt: A case study from the Mt.Kumeta–Rocca Busambra ridges (western Sicily, Italy): Journal of Geodynamics, no. 55, p. 1-17.

Barreca, G., and Monaco, C., 2013, Vertical-axis rotation in the Sicilian belt: New structural constrains from the Madonie Mts. (Sicily, Italy): Italian Journal of Geoscience, no. 132(2), p. 407–421.

Basilone, L., 2009, Mesozoic tectono-sedimentary evolution of Rocca Busambra in western Sicily: Facies, no. 55(1), p. 115.

Basilone, L., Morticelli, M.G., and Lena, G., 2010, Mesozoic tectonics and volcanism of Tethyan rifted continental margins in western Sicily: Sedimentary Geology, no. 226(1-4), p. 54-70.

Basilone, L., Frixa, A., Trincianti, E., and Valenti, V., 2016a. Permian-Cenozoic deep-water carbonate rocks of the Southern Tethyan Domain. The case of Central Sicily: Italian Journal of Geosciences, no. 135(2), p. 171-198.

Basilone, L., Sulli, A., and Morticelli, M.G., 2016b, Integrating facies and structural analyses with subsidence history in a Jurassic–Cretaceous intraplatform basin: Outcome for paleogeography of the Panormide Southern Tethyan margin, NW Sicily, Italy: Sedimentary geology, no. 339, p. 258-272.

Basin Mod® 1-D for WindowsTM, 1996, A Basin Analysis Modeling System version 5.4 Software: Denver, Platte River Associates, 386 p.

Baur, F., Di Benedetto, M., Fuchs, T., Lampe, C., and Sciamanna, S., 2009, Integrating structural geology and petroleum systems modeling–A pilot project from Bolivia's fold and thrust belt: Marine and Petroleum Geology, no. 26(4), p. 573-579.

Bayer, U., Scheck, M., and Koehler, M., 1997, Modeling of the 3D thermal field in the northeast German basin: Geologische Rundschau, no. 86(2), p. 241-251.

Bêche, M., Kirkwood, D., Jardin, A., Desaulniers, E., Saucier, D., and Roure, F., 2007, 2D Depth seismic imaging in the Gaspé Belt, a structurally complex fold and thrust belt in the Northern Appalachians, Québec, Canada: In Thrust Belts and Foreland Basins, p. 75-90. Springer, Berlin, Heidelberg.

Behar, F., Beaumont, V., and Penteado, H.D.B., 2001, Rock-Eval 6 technology: performances and developments: Oil & Gas Science and Technology, no. 56(2), p. 111-134.

Bello, M., Franchino, A. and Merlini, S., 2000, Structural model of eastern Sicily: Memorie della Società Geologica Italiana, no. 55, p. 61–70.

Berthelon, J., and Sassi, W., 2016, A discussion on the validation of structural interpretations based on the mechanics of sedimentary basins in the northwestern Mediterranean fold-and-thrust belts: Bulletin de la Société géologique de France, no. 187(2), p. 83-104.

Bertok, C., and Martire, L., 2009, Sedimentation, fracturing and sliding on a pelagic plateau margin: the Middle Jurassic to Lower Cretaceous succession of Rocca Busambra (Western Sicily, Italy): Sedimentology, no. 56(4), p. 1016-1040.

Bianchi, F., Carbone, S., Grasso, M., Invernizzi, G., Lentini, F., Longaretti, G., Merlini, S. and Mostardini, F., 1989, Sicilia orientate: profilo geologico Nebrodi-Iblei: Memorie della Società Geologica Italiana, no. 38, p. 429-458.

Bigi, S., Conti, A., Casero, P., Ruggiero, L., Recanati, R., and Lipparini, L., 2013, Geological model of the central Periadriatic basin (Apennines, Italy): Marine and Petroleum Geology, no. 42, p. 107-121.

Bigi, S., Carminati, E., Aldega, L., Trippetta, F., and Kavoosi, M.A., 2018, Zagros fold and thrust belt in the Fars province (Iran) I: Control of thickness/rheology of sediments and pre-thrusting tectonics on structural style and shortening: Marine and Petroleum Geology, no. 91, p. 211-224.

Bonanno, E., Bonini, L., Basili, R., Toscani, G., and Seno, S., 2017, How do horizontal, frictional discontinuities affect reverse fault-propagation folding?: Journal of Structural Geology, no. 102, p. 147-167.

Bond, C.E., Gibbs, A.D., Shipton, Z.K., and Jones, S., 2007, What do you think this is?``Conceptual uncertainty"in geoscience interpretation: GSA today, no. 17(11), p. 4.

Bond, C.E., Lunn, R.J., Shipton, Z.K., and Lunn, A.D., 2012, What makes an expert effective at interpreting seismic images?: Geology, no. 40(1), p. 75-78.

Bond, C.E., 2015, Uncertainty in structural interpretation: Lessons to be learnt: Journal of Structural Geology, no. 74, p. 185-200.

Bonini, M., 2007, Deformation patterns and structural vergence in brittle–ductile thrust wedges: an additional analogue modelling perspective: Journal of Structural Geology, no. 29(1), p. 141-158.

Bouaziz, S., Barrier, E., Soussi, M., Turki, M. M., and Zouari, H., 2002, Tectonic evolution of the northern African margin in Tunisia from paleostress data and sedimentary record: Tectonophysics, no. 357(1-4), p. 227-253.

Boutelier, D., Gagnon, L., Johnston, S., and Cruden, A., 2018, Buckling of orogens: Insights from analogue modelling: Journal of Structural Geology. DOI: 10.1016/j.jsg.2018.02.005.

Boyer, S.E. and Elliott, D., 1982, Thrust system: AAPG Bulletin, no. 66, p. 1196–1230.

Bracène, R., and Frizon de Lamotte, D., 2002, The origin of intraplate deformation in the Atlas system of western and central Algeria: from Jurassic rifting to Cenozoic–Quaternary inversion: Tectonophysics, no. 357(1-4), p. 207-226.

Bretis, B., Bartl, N., and Grasemann, B., 2011, Lateral fold growth and linkage in the Zagros fold and thrust belt (Kurdistan, NE Iraq): Basin Research, no. 23(6), p. 615-630.

Brocquet, P. 1968, Etude géologique de la région des Madonies, (Sicile). PhD thésis, Lille, 1-553.

Burbank, D.W., McLean, J.K., Bullen, M., Abdrakhmatov, K.Y., and Miller, M.M., 1999, Partitioning of intermontane basins by thrust-related folding, Tien Shan, Kyrgyzstan: Basin Research, no.11 (1), p. 75-92.

Burnham, A.K., and Sweeney, J.J., 1989, A chemical kinetic model of vitrinite maturation and reflectance: Geochimica et Cosmochimica Acta, no. 53, p. 2649–2657.

Bustin, R.M., Barnes, M.A., and Barnes, W.C., 1990, Determining levels of organic diagenesis in sediments and fossil fuels, in McIleareath, I.A., and Morrow, D.W., eds., Diagenesis: St. John's, Canada, Geoscience Canada Reprint, 4th series, p. 205–226.

Butler, R.W.H., 1992a, Evolution of Alpine fold-thrust complexes: a linked kinematic approach, in S. Mitra and G. Fisher, eds., Structural geology of fold and thrust belts: Baltimore, Johns Hopkins University Press, p. 29–44.

Butler, R.W.H., 1992b, Hydrocarbon maturation, migration and tectonic loading in the western Alps, in England, W.A., and Fleet, A.J., eds., Petroleum Migration: Geological Society of London Special Publication, no. 59, p. 227–244.

Butler, R.W.H., Grasso, M., and La Manna, F., 1992, Origin and deformation of the Neogene–Recent Maghrebian foredeep at the Gela Nappe, SE Sicily: Journal of the Geological Society, no. 149(4), p. 547-556.

Butler, R.W.H, and Grasso, M., 1993, Tectonic controls on base-level variations and depositional sequences within thrust-top and foredeep basins: examples from the Neogene thrust belt of central Sicily: Basin Research, no. 5, p. 137-151.

Butler, R.W.H., Mazzoli, S., Corrado, S., De Donatis, M., Di Bucci, D., Gambini, R., Naso, G., Nicolai, C., Scrocca, D., Shiner, P., and Zucconi, V., 2004, Applying thick-skinned tectonic models to the Apennine thrust belt of Italy – Limitations and implications, in McClay, K.R., ed., Thrust tectonics and hydrocarbon system: American Association of Petroleum Geologist Memoir, no. 82, p. 647–667.

Butler, R.W., Tavarnelli, E., and Grasso, M., 2006, Structural inheritance in mountain belts: an Alpine–Apennine perspective: Journal of Structural Geology, no. 28(11), p. 1893-1908.

Butler, R.W., 2013, Area balancing as a test of models for the deep structure of mountain belts, with specific reference to the Alps: Journal of Structural Geology, no. 52, p. 2-16.

Butler, R.W.H., Bond, C.E., Cooper, M.A., and Watkins, H., 2018, Interpreting structural geometry in fold-thrust belts: Why style matters: Journal of Structural Geology, no. 114, p. 251-273.

Caputo, M., Panza, G.F. and Postpischl, D., 1970, Deep structure of the Mediterranean Basin: Journal of Geophysical Research, no. 75, p. 4919-4923.

Cardello, G.L., and Doglioni, C., 2015, From mesozoic rifting to Apennine orogeny: the gran Sasso range (Italy): Gondwana Research, no. 27(4), p. 1307-1334.

Caricchi, C., Aldega, L., and Corrado, S., 2014, Reconstruction of maximum burial along the Northern Apennines thrust wedge (Italy) by indicators of thermal exposure and modeling: Geological Society of American Bulletin, no. 127, p. 428-442.

Caricchi, C., Aldega, L., Barchi, M. R., Corrado, S., Grigo, D., Mirabella, F., and Zattin, M., 2015, Exhumation patterns along shallow low-angle normal faults: an example from the Altotiberina active fault system (Northern Apennines, Italy): Terra nova, no. 27(4), p. 312-321.

Carminati, E., and Santantonio, M., 2005, Control of differential compaction on the geometry of sediments onlapping paleoescarpments: Insights from field geology (Central Apennines, Italy) and numerical modelling: Geology, no. 33(5), p. 353-356.

Carminati, E., Aldega, L., Bigi, S., Minelli, G., and Shaban, A., 2016, Not so simple “simply-folded Zagros”: The role of pre-collisional extensional faulting, salt tectonics and multi-stage thrusting in the Sarvestan transfer zone (Fars, Iran): Tectonophysics, no. 671, p. 235-248.

Casero, P., and F. Roure, 1994, Neogene deformations of the Sicilian-North African plate boundary. in PeriTethyan Platforms, F. Roure, ed.: Technip Editions, Paris, p. 27-50.

Castelluccio, A., Mazzoli, S., Andreucci, B., Jankowski, L., Szaniawski, R., and Zattin, M., 2016, Building and exhumation of the Western Carpathians: New constraints from sequentially restored, balanced cross sections integrated with low-temperature thermochronometry: Tectonics, no. 35(11), p. 2698-2733.

Catalano, R., Channell, J., D’argenio, B., and Napoleone, G., 1976, Mesozoic paleogeography of the Southern Apennines and Sicily: Memorie della Società` Geologica Italiana, no. 15, p. 95-118.

Catalano, R., and D’Argenio, B., 1978, An essay of palinspastic restoration across western Sicily: Geologica Romana, no. 17, p. 145-159.

Catalano, R. and D'argenio, B., 1982a, Schema geologico della Sicilia occidentale, in: Catalano, R. and D'argenio, B. (eds.) Guida alla Geologia della Sicilia Occidentale: Guide Geologiche Regionali, Memorie della Società Geologica Italiana, Supplement A, no. 24, p. 9–41

Catalano, R., and D'Argenio, B., 1982b, Infraliassic strike-slip tectonics in Sicily and Southern Apennines: Rendiconti della Società Geologica Italiana, no. 5, p. 5-10.

Catalano, R., D'argenio, B. and Torelli, L., 1989, From Sardinia Channel to Sicily Straits. A geologic section based on seismic and field data, in: Boriani, A., et al., (eds.) The Lithosphere in Italy. Advances in Earth Science Research, Atti Accademia Nazionale Lincei, no. 80, p. 109–127.

Catalano, R., Di Stefano, P. and Kozur, H., 1991, Permian circumpacific deep-water faunas from the Western Tethys (Sicily, Italy) - new evidence for the position of the Permian Tethys: Palaeogeography, Palaeoclimatology, Palaeoecology, no. 87, p. 75-108.

Catalano, R., Di Stefano, P., Sulli, A. and Vitale, F.P., 1996, Paleogeography and structure of the Central Mediterranean: Sicily and its offshore area: Tectonophysics, no. 260, p.291-323.

Catalano, R., Franchino, A., Merlini, S. and Sulli, A., 2000, Central western Sicily structural setting interpreted from seismic reflection profiles: Memorie della Società Geologica Italiana, no. 55, p. 5–16.

Catalano, R., Merlini, S., and Sulli, A., 2002, The structure of western Sicily, central Mediterranean: Petroleum Geoscience, no. 8(1), p. 7-18.

Catalano, R., Avellone, G., Basilone, L., Gasparo Morticelli, M., and Lo Cicero, G., 2010a, Note illustrative della Carta Geologica d'Italia alla scala 1:50.000. Foglio 608 "Caccamo" e carta geologica allegata. ISPRA, Servizio Geologico d'Italia, Roma.

Catalano, R., Avellone, G., Basilone, L., and Sulli, A., 2010b, Note illustrative della Carta Geologica d'Italia alla scala 1:50.000. Foglio 607 "Corleone" e carta geologica allegata. ISPRA, Servizio Geologico d'Italia, Roma.

Catalano, R., Avellone, G., Basilone, L., Contino, A., Agate, M., Gugliotta, C., Di Maggio, C., Di Stefano, E., Gennaro, C., Arnone, M., Sulli, A., Di Maio, D., Mancuso, M., Abate, B., Gasparo Morticelli, M., 2011, Note illustrative della Carta Geologica d'Italia alla scala 1:50.000 sheets 609-596"Termini Imerese – Capo Plaia", con allegata carta geologica in scala 1:50.000 (2a), ISPRA- Servizio Geologico D'Italia.

Catalano, R., Valenti, V., Albanese, C., Accaino, F., Sulli, A., Tinivella, U., Gasparo Morticelli M., Zanolla C. and Giustiniani M., 2013a, Sicily's fold/thrust belt and slab rollback: The

SI.RI.PRO. seismic crustal transect: Journal of Geological Society, London, no. 170, p. 451-464.

Catalano, R., Agate, M., Albanese, C., Avellone, G., Basilone, L., Gasparo Morticelli, M., Gugliotta, C., Sulli, A., Valenti, V., Gibilaro, C., and Pierini, S., 2013b, Walking along a crustal profile across the Sicily fold and thrust belt: Geological Field Trips, no.5.

Catalano, S., De Guidi, G., Romagnoli, G., Torrisi, S., Tortorici, G. and Tortorici, L., 2007, The migration of plate boundaries in SE Sicily: Influence on the large-scale kinematic model of the African promontory in southern Italy: Tectonophysics, no. 449, p. 41–62.

Caumon, G., Lepage, F., Sword, C. H., and Mallet, J. L., 2004, Building and editing a sealed geological model: Mathematical Geology, no. 36(4), p. 405-424.

Channell, J.E.T., Catalano, R., and D'Argenio, B., 1980, Paleomagnetism and deformation of the Mesozoic continental margin of Sicily: Tectonophysics, no. 61, p. 391– 407.

Channell, J.E.T., Oldow, J.S., Catalano, R. and D'argenio, B., 1990, Paleomagnetically determined rotations in the western Sicilian fold and thrust belt: Tectonics, no. 9, p. 641-660.

Chiari, M., Di Stefano, P., and Parisi, G., 2008, New stratigraphical data on the Middle-Late Jurassic biosiliceous sediments from the Sicanian basin, Western Sicily (Italy): Swiss journal of geosciences, no. 101(2), p. 415-429.

Cifelli, F., Mattei, M., and Rossetti, F., 2007, Tectonic evolution of arcuate mountain belts on top of a retreating subduction slab: The example of the Calabrian Arc: Journal of Geophysical Research, no. 112(B9).

Cifelli, F. and Mattei, M., 2010, Curved orogenic systems in the Italian peninsula: A paleomagnetic review: Journal of Virtual Explorer, no. 36, p. 1-23.

Colletta, B., Letouzey, J., Pinedo, R., Ballard, J. F., and Balé, P., 1991, Computerized X-ray tomography analysis of sandbox models: Examples of thin-skinned thrust systems: Geology, no. 19(11), p. 1063-1067.

Corrado, S., Di Bucci, D., Naso, G., and Faccenna, C., 1998a, Influence of palaeogeography on thrust system geometries: an analogue modelling approach for the Abruzzi–Molise (Italy) case history: Tectonophysics, no. 296(3-4), p. 437-453.

Corrado, S., Di Bucci, D., Naso, G., Giampaolo, C., Adatte, T., 1998b, Application of organic matter and clay mineral studies to the tectonic history of the Abruzzo-Molise-Sannio area, Central Apennines, Italy. Tectonophysics, no. 285 (1-2), p. 167-181.

Corrado, S., Invernizzi, C., and Mazzoli, S., 2002, Tectonic burial and exhumation in a foreland fold and thrust belt: the Monte Alpi case history (Southern Apennines, Italy): Geodinamica Acta, no. 15(3), p. 159-177.

Corrado, S., Aldega, L., Di Leo, P., Giampaolo, C., Invernizzi, C., Mazzoli, S., and Zattin, M., 2005, Thermal maturity of the axial zone of the southern Apennines fold-and-thrust belt (Italy) from multiple organic and inorganic indicators: Terra Nova, no. 17(1), p. 56-65.

Corrado, S., Aldega, L., Balestrieri, M.L., Maniscalco, R. and Grasso, M., 2009, Structural evolution of the sedimentary accretionary wedge of the Alpine system in Eastern Sicily: Thermal and thermochronological constraints: Geological Society of America Bulletin, no. 121, p. 1475–1490.

Corrado, S., Aldega, L., and Zattin, M., 2010, Sedimentary vs. tectonic burial and exhumation along the Apennines (Italy): Journal of Virtual Explorer, no. 36.

Costa, E., and Vendeville, B.C., 2002, Experimental insights on the geometry and kinematics of fold-and-thrust belts above weak, viscous evaporitic décollement: Journal of Structural Geology, no. 24(11), p. 1729-1739.

Costa, E., and Speranza, F., 2003, Paleomagnetic analysis of curved thrust belts reproduced by physical models: Journal of Geodynamics, no. 36(5), p. 633-654.

D'Adda, P., Longoni, R., Magistroni, C., Meda, M., Righetti, F., Cavozzi, C., Nestola, Y., and Storti, F., 2017, Extensional reactivation of a deep transpressional architecture: Insights from sandbox analogue modeling applied to the Val d'Agri basin (Southern Apennines, Italy): Interpretation, no. 5(1), SD55-SD66.

Dahlstrom, C.D.A., 1969, Balanced cross sections: Canadian Journal of Earth Sciences, no. 6(4), p. 743-757.

Dean, S.L., Morgan, J.K., and Fournier, T., 2013, Geometries of frontal fold and thrust belts: Insights from discrete element simulations: Journal of Structural Geology, no. 53, p. 43-53.

DeCelles, P.G., Giles, K.A., 1996, Foreland basin systems: Basin Research, no. 8, p. 105-123.

Dercourt, J., Zonenshain, L.P., Ricou, L.E., Kazmin, V.G., Le Pichon, X., Knipper, A.L., Grandjacquet, C., Sbortshikov, I.M., Geyssant, J., Lepvrier, C., Pechersky, D.H., Boulin, J., Sibuet, J.C., Savostin, L.A., Sorokhtin, O., Westphal, M., Bazhenov, M.L., Lauer, J.P. and Biju-Duval, B., 1986, Geologic evolution of the Tethys belt from the Atlantic to the Pamirs since the Lias: Tectonophysics, no. 123, p. 241-315.

Deville, E., and Sassi, W., 2006, Contrasting thermal evolution of thrust systems: An analytical and modeling approach in the front of the western Alps: AAPG bulletin, no. 90(6), p. 887-907.

Dewey, J.F., Helman, M.L., Turco, E., Hutton, D.H.W. and Knott, S.D., 1989, Kinematics of the western Mediterranean. In: Coward, M.P. (Ed.), Alpine Tectonics: Geological Society Special Publication, no. 45, p. 265-283.

Dhahri, F., and Boukadi, N., 2010,. The evolution of pre-existing structures during the tectonic inversion process of the Atlas chain of Tunisia: Journal of African Earth Sciences, no.56(4-5), p. 139-149.

Di Domenica, A., Bonini, L., Calamita, F., Toscani, G., Galuppo, C., and Seno, S., 2014, Analogue modeling of positive inversion tectonics along differently oriented pre-thrusting normal faults: An application to the Central-Northern Apennines of Italy: GSA Bulletin, no. 126(7-8), p. 943-955.

Di Paolo, L., Aldega, L., Corrado, S., and Mastalerz, M., 2012, Maximum burial and unroofing of Mt. Judica recess area in Sicily: Implication for the Apenninic–Maghrebian wedge dynamics: Tectonophysics, no. 530, p. 193-207.

Di Paolo, L., Olivetti, V., Corrado, S., Aldega, L., Balestrieri, M. L. and Maniscalco, R., 2014, Detecting the stepwise propagation of the Eastern Sicily thrust belt (Italy): insight from thermal and thermochronological constraints: Terra Nova, no. 26, p. 363–371.

Di Stefano, P. and Gullo, M., 1997, Permian deposits of Sicily: a review: Geodiversitas, no. 19 (2), p 193-202.

Di Stefano, P., and Mindszenty, A., 2000, Fe–Mn-encrusted “Kamenitza” and associated features in the Jurassic of Monte Kumeta (Sicily): subaerial and/or submarine dissolution?: Sedimentary Geology, no. 132(1-2), p. 37-68.

Di Stefano, P., Galácz, A., Mallarino, G., Mindszenty, A., and Vörös, A., 2002, Birth and early evolution of a Jurassic escarpment: Monte Kumeta Western Sicily: Facies, no. 46(1), p. 273.

Di Stefano, P., McRoberts, C., Renda, P., Tripodo, A., Torre, A. and Torre, F., 2012, Middle Triassic (Ladinian) deep-water sediments in Sicily: new findings from the Madonie Mountains. Riv. It. Paleont. Strat., no. 118, p. 235-246.

Di Stefano, P., Favara, R., Luzio, D., Renda, P., Cacciatore, M.S., Calò, M., Napoli, G., Parisi, L., Todaro, S., and Zarcone, G., 2015, A regional-scale discontinuity in western Sicily revealed by a multidisciplinary approach: A new piece for understanding the geodynamic puzzle of the southern Mediterranean: Tectonics, no. 34(10), p. 2067-2085.

Doglioni, C., Harabaglia, P., Merlini, S., Mongelli, F., Peccerillo, A. and Piromallo, C., 1999, Orogens and slab vs. their direction of subduction: Earth Science Reviews, no. 45, p. 167-208.

Dotare, T., Yamada, Y., Adam, J., Hori, T., and Sakaguchi, H., 2016, Initiation of a thrust fault revealed by analog experiments: Tectonophysics, no.684, p. 148-156.

Droste, H., 1990, Depositional cycles and source rock development in an epeiric intra-platform basin: the Hanifa Formation of the Arabian peninsula: Sedimentary Geology, no. 69(3-4), p. 281-296.

Durand-Riard, P., Caumon, G., and Muron, P., 2010, Balanced restoration of geological volumes with relaxed meshing constraints: Computers and Geosciences, no. 36(4), p. 441-452.

Durand-Riard, P., Guzofski, C., Caumon, G., and Titeux, M.O., 2013, Handling natural complexity in three-dimensional geomechanical restoration, with application to the recent evolution of the outer fold and thrust belt, deep-water Niger Delta: AAPG bulletin, no. 97(1), p. 87-102.

Echavarria, L., Hernández, R., Allmendinger, R., and Reynolds, J., 2003, Subandean thrust and fold belt of northwestern Argentina: Geometry and timing of the Andean evolution: AAPG bulletin, no. 87(6), p. 965-985.

Egan, S.S., Buddin, T.S., Kane, S.J., and Williams, G.D., 1997, Three-dimensional modelling and visualisation in structural geology: new techniques for the restoration and balancing of volumes. In Proceedings of the 1996 Geoscience Information Group Conference on Geological Visualisation: Electronic Geology Special Volume, no. 1, p. 67-82.

Egbue, O., and Kellogg, J., 2012, Three-dimensional structural evolution and kinematics of the Piedemonte Llanero, Central Llanos foothills, Eastern Cordillera, Colombia: Journal of South American Earth Sciences, no. 39, p. 216-227.

Ellis, S., Schreurs, G., and Panien, M., 2004, Comparisons between analogue and numerical models of thrust wedge development: Journal of Structural Geology, no. 26(9), p. 1659-1675.

Endignoux, L., and Wolf, S., 1990, Thermal and kinematic evolution of thrust basins: A 2D numerical model, in Letouzey, J., ed., Petroleum Tectonics in Mobile Belts: Paris, Edit. Technip, p. 181–192.

Faccenna, C., Funiciello, F., Giardini, D. and Lucente, F.P., 2001, Episodic back-arc extension during restricted mantle convection in the central Mediterranean: Earth and Planetary Science Letters, no. 187, p. 105-116.

Faccenna, C., Piromallo, C., Crespo-Blanc, A., Jolivet, L. and Rosetti, F., 2004, Lateral slab deformation and the origin of the western Mediterranean arcs: Tectonics, no. 23, p. 1-21.

Fantoni, R., Bertello, F., and Franciosi, R., 2008, Reservoirs and source rocks in Mesozoic carbonate units of Italy: Rendiconti della Società Geologica Italiana, no. 3(1), p. 365-366.

Ferrer, O., McClay, K., and Sellier, N.C., 2017, Influence of fault geometries and mechanical anisotropies on the growth and inversion of hanging-wall synclinal basins: insights from sandbox models and natural examples: Geological Society, London, Special Publications, no. 439(1), p. 487-509.

Finetti, I.R., Lentini, F., Carbone, S., Del Ben, A., Di Stefano A., Forlin, E., Guarnieri, P., Pipan, M. and Prizzon, A., 2005, Geological Outline of Sicily and Lithospheric Tectono-Dynamics of its Tyrrhenian Margin from new CROP seismic data, in: Finetti I.R. (Ed.), CROP PROJECT: Deep seismic exploration of the Central Mediterranean and Central Italy, Elsevier, Amsterdam , 794 p.

Flügel, E., Di Stefano, P. and Senowbari-Daryan, B., 1991, Microfacies and depositional structure of allochtonous carbonate base-of-slope deposits: the Late Permian Pietra di Salomone megablock, Sosio valley (Western Sicily): Facies, no. 25, p. 147-186.

Fossen, H., 2016, Structural geology. Cambridge University Press.

Frank, T., Tertois, A.-L., and Mallet, J.-L., 2007, 3-D reconstruction of complex geological interfaces from irregularly distributed and noisy point data: Computers and Geosciences, v. 33, no. 7, p. 932–943.

Frixa, A., Bertamoni, M., Catrullo, D., Trincianti, E., and Miuccio, G., 2000, Late Norian-Hettangian paleogeography in the area between wells Noto 1 and Polpo 1 (SE Sicily): Memorie della Società Geologica Italiana, no. 55, p. 279-284.

Frizon de Lamotte, D., Leturmy, P., Missenard, Y., Khomsi, S., Ruiz, G., Saddiqi, O., Guillocheau, F., and Michard, A., 2009, Mesozoic and Cenozoic vertical movements in the Atlas system (Algeria, Morocco, Tunisia): an overview: Tectonophysics, no. 475(1), p. 9-28.

Frizon de Lamotte, D., Raulin, C., Mouchot, N., Wrobel-Daveau, J. C., Blanpied, C., and Ringenbach, J. C., 2011, The southernmost margin of the Tethys realm during the Mesozoic and Cenozoic: Initial geometry and timing of the inversion processes: Tectonics, no. 30(3).

Garver, J. J., Brandon, M. T., Roden-Tice, M. and Kamp, P. J. J., 1999, Exhumation history determined by detrital fission-track thermochronology: Geological Society, London, Special Publications, no. 154, p. 283-304.

Gasparo Morticelli, M., Valenti, V., Catalano, R., Sulli, A., Agate, M., Avellone, G., Albanese, C., Basilone, L., and Gugliotta, C., 2015, Deep controls on Foreland Basin System evolution along the Sicilian Fold and Thrust Belt: Bulletin de la Société géologique de France, no. 186, p. 273-290.

Gasparo Morticelli, M., Avellone, G., Sulli, A., Agate, M., Basilone, L., Catalano, R., and Pierini, S., 2017, Mountain building in NW Sicily from the superimposition of subsequent thrusting and folding events during Neogene: structural setting and tectonic evolution of the Kumeta and Pizzuta ridges: Journal of Maps, no. 13(2), p. 276-290.

GeoThopica, Banca Dati Nazionale Geotermica, CNR: http://geothopica.igg.cnr.it/

Ghanmi, M. A., Ghanmi, M., Aridhi, S., Salem, M. S. B., and Zargouni, F., 2016, Role of tectonic inheritance in the instauration of Tunisian Atlassic fold-and-thrust belt: Case of Bouhedma–Boudouaou structures: Journal of African Earth Sciences, no. 119, p. 1-16.

Ghisetti, F., and Vezzani, L., 1984, Thin-skinned deformations of the western Sicily thrust belt and relationships with crustal shortening; mesostructural data on the Mt. Kumeta-Alcantara fault zone and related structures: Bollettino della Societa Geologica Italiana, no. 103(1), p. 129-157.

Ghisetti, F.C., Gorman, A.R., Grasso, M., and Vezzani, L., 2009, Imprint of foreland structure on the deformation of a thrust sheet: The Plio-Pleistocene Gela Nappe (southern Sicily, Italy): Tectonics, no. 28(4), p. 1-16.

Giunta, G., Nigro, F., and Renda, P., 2000a, Extensional tectonics during Maghrebides chain building since late Miocene: examples from Northern Sicily: Annales Societatis Geologorum Poloniae, no. 70, p. 81-98.

Giunta, G., Nigro, F., Renda, P., and Giorgianni, A., 2000b, The Sicilian-Maghrebides Tyrrhenian margin; a neotectonic evolutionary model: Bollettino della Società geologica italiana, no. 119(3), p. 553-565.

Giustiniani, M., Tinivella, U., and Nicolich, R., 2018, Crustal structure of Central Sicily: Tectonophysics, no. 722, p. 299-313.

Goffey, G. P., Craig, J., Needham, T., and Scott, R., 2010, Fold–thrust belts: overlooked provinces or justifiably avoided?: Geological Society, London, Special Publications, no.348(1), p. 1-6.

Goldbach, M., Geršlová, E., Misz-Kennan, M., and Nehyba, S., 2017, Thermal maturity of Miocene organic matter from the Carpathian Foredeep in the Czech Republic: 1D and 3D models: Marine and Petroleum Geology, no. 88, p. 18-29.

Granado, P., Ferrer, O., Muñoz, J.A., Thöny, W., and Strauss, P., 2017, Basin inversion in tectonic wedges: Insights from analogue modelling and the Alpine-Carpathian fold-and-thrust belt: Tectonophysics, no. 703, p. 50-68.

Granath, J. W., and P. Casero, 2004, Tectonic setting of the petroleum systems of Sicily, in Deformation, Fluid Flow and Reservoir Appraisal in Foreland Fold-and-Thrust Belts,

AAPG Hedberg Ser., vol. 1, R. Swennen, F. Roure, and J. Granath eds., pp. 391–411, American Association of Petroleum Geologists, Tulsa, Okla

Grasso, M., Manzoni, M. and Quintili, A., 1987, Misure magnetiche sui Trubi della Sicilia orientale: Possibili implicazioni stratigrafiche e strutturali: Memorie della Società Geologica Italiana, no. 38, p. 459–474.

Grasso, M., 2001. The Apenninic–Maghrebian orogen in southern Italy, Sicily and adjacent areas: Tectonophysics, no. 343, p. 135–163.

Groshong Jr, R.H., 2006, 3-D structural geology (pp. 305-371): Springer-Verlag Berlin Heidelberg.

Groshong Jr, R., Bond, C., Gibbs, A., Ratcliff, R., and Wiltschko, D., 2012, Preface: Structural balancing at the start of the 21st century: 100 years since Chamberlin: Journal of Structural Geology, no. 41, p. 1-5.

Guarnieri P., Carbone S. and Di Stefano A., 2002, The Sicilian orogenic belt: a critical tapered wedge?: Bollettino della Società Geologica Italiana., no. 121(2), p. 221-230.

Guarnieri, P., 2004, Structural evidence for deformation by block rotation in the context of transpressive tectonics, northwestern Sicily (Italy): Journal of Structural Geology, no. 26, p. 207-219.

Gugliotta, C. 2012. Inner vs. outer wedge-top depozone “sequences” in the Late Miocene (late Tortonian-early Messinian) Sicilian Foreland Basin System; new data from the Terravecchia Formation of NW Sicily: Journal of Geodynamics, no. 55, p. 41–55.

Gugliotta, C. and Gasparo Morticelli, M. 2012, Using high-resolution stratigraphy and structural analysis to constrain polyphase tectonics in wedge-top basins: Inferences from the late Tortonian Scillato Basin (central–northern Sicily): Sedimentary Geology, no. 273–274, p. 30–47.

Gugliotta, C., Agate, M. and Sulli, A., 2013, Sedimentology and sequence stratigraphy of wedge-top clastic successions: Insights and open questions from the upper Tortonian Terravecchia Formation of the Scillato Basin (central–northern Sicily, Italy): Marine and Petroleum Geology, no. 43, p. 239–259.

Gugliotta, C., Gasparo Morticelli, M., Avellone, G., Agate, M, Barchi, M.R., Albanese, C., Valenti, V. and Catalano, R. , 2014, Middle Miocene – Early Pliocene wedge-top basins of NW Sicily (Italy): Constraints for the tectonic evolution of a “non-conventional” thrust belt, affected by transpression: Journal of Geological Society, London, no. 171, p. 211-226.

Guo, J., Wei, X., Long, G., Wang, B., Fan, H., and Xu, S., 2017, Three-dimensional structural model of the Qaidam basin: Implications for crustal shortening and growth of the northeast Tibet: Open Geosciences, no. 9(1), p. 174-185.

Gusterhuber, J., Hinsch, R., and Sachsenhofer, R. F., 2014, Evaluation of hydrocarbon generation and migration in the Molasse fold and thrust belt (Central Eastern Alps, Austria) using structural and thermal basin models: AAPG bulletin, no.98(2), p. 253-277.

Guzofski, C.A., Mueller, J.P., Shaw, J.H., Muron, P., Medwedeff, D.A., Bilotti, F., Rivero, C., 2009. Insights into the mechanisms of fault-related folding provided by volumetric structural restorations using spatially varying mechanical constraints. AAPG Bulletin, no. 93 (4), p. 479-502.

Hardebol, N. J., Callot, J.P., Bertotti, G., and Faure, J. L., 2009, Burial and temperature evolution in thrust belt systems: Sedimentary and thrust sheet loading in the SE Canadian Cordillera: Tectonics, no. 28(3).

Hermoza, W., Brusset, S., Baby, P., Gil, W., Roddaz, M., Guerrero, N., and Bolaños, R., 2005, The Huallaga foreland basin evolution: Thrust propagation in a deltaic environment, northern Peruvian Andes: Journal of South American Earth Sciences, no. 19(1), p. 21-34.

Higgins, S., Davies, R.J., and Clarke, B., 2007, Antithetic fault linkages in a deep water fold and thrust belt: Journal of Structural Geology, no. 29(12), p. 1900-1914.

Higgins, S., Clarke, B., Davies, R.J., and Cartwright, J., 2009, Internal geometry and growth history of a thrust-related anticline in a deep water fold belt: Journal of Structural Geology, no. 31(12), p. 1597-1611.

Hillier, S., Màtyàs, J., Matter, A., and Vasseur, G., 1995, Illite/smectite diagenesis and its variable correlation with vitrinite reflectance in the Pannonian Basin: Clays and Clay Minerals, no. 43, p. 174–183.

Hirschmiller, J., Grujic, D., Bookhagen, B., Coutand, I., Huyghe, P., Mugnier, J. L., and Ojha, T., 2014, What controls the growth of the Himalayan foreland fold-and-thrust belt?: Geology, no. 42(3), p. 247-250.

Hunt, J. M., 1996, Petroleum Geochemistry and Geology: W. H. Freeman, San Francisco.

Iacopini, D., and Butler, R.W., 2011, Imaging deformation in submarine thrust belts using seismic attributes: Earth and Planetary Science Letters, no. 302(3-4), p. 414-422.

Jacob, H., 1989, Classification, structure, genesis and practical importance of natural solid oil bitumen (“migrabitumen”). International Journal of Coal Geology, no. 11(1), p. 65-79.

Jardin, A., Chaker, R., and Krzywiec, P., 2007, Understanding seismic propagation through triangle zones. In Thrust Belts and Foreland Basins, p. 63-74: Springer, Berlin, Heidelberg.

Jayr, S., Gringarten, E., Tertois, A.L., Mallet, J.L. and Dulac, J.C., 2008, The need for a correct geological modelling support: the advent of the UVT-transform: First Break, no. 26, p. 73-79.

Jenkyns, H. C., 1970, Growth and disintegration of a carbonate platform: Neues Jahrbuch für Geologie und Paläontologie, Monatshefte, p. 325-344.

Jirman, P., Geršlová, E., Kalvoda, J., and Melichar, R., 2018, 2D Basin modelling in the eastern Variscan fold belt (Czech republic): influence of thrusting on patterns of thermal maturation: Journal of Petroleum Geology, no. 41(2), p. 175-188.

Jolivet, M., Labaume, P., Monie, P., Brunel, M., Arnaud, N. and Campani, M., 2007, Thermochronology constraints for the propagation sequence of the south Pyrenean basement thrust system (France-Spain): Tectonics, no. 26, p. 1-17.

Kafka, F.T., and Kirkbride R.K., 1960, The Ragusa Oil Field (Sicily) In: Excursion in Sicily. Petr. Expl. Soc. Libya, Tripoli, p.61-85.

Kozur, H.W., Krainer, K. and Mostler, H., 1996, Ichnology and sedimentology of the Early Permian deep-water deposits from the Lercara-Roccapalumba area (Western Sicily, Italy). Facies, no. 34, p.123-150.

Labaume, P., Meresse, F., Jolivet, M., Teixell, A., and Lahfid, A., 2016, Tectonothermal history of an exhumed thrust-sheet-top basin: An example from the south Pyrenean thrust belt: Tectonics, no. 35(5), p. 1280-1313.

Li, J., and Mitra, S., 2017, Geometry and evolution of fold-thrust structures at the boundaries between frictional and ductile detachments: Marine and Petroleum Geology, no., 85, p. 16-34.

Li, Y., Jia, D., Plesch, A., Hubbard, J., Shaw, J.H., and Wang, M., 2013, 3-D geomechanical restoration and paleomagnetic analysis of fault-related folds: An example from the Yanjinggou anticline, southern Sichuan Basin: Journal of Structural Geology, no. 54, p. 199-214

Li, Y., Wei, D., Chen, Z., Jia, D., Ma, D., Wang, Y., Cui J., and Shen, S., 2016, Multiphase deformation deduced from 3D construction and restoration: Implication for the hydrocarbon exploration in the mountain front of the Northern Tianshan: Marine and Petroleum Geology, no. 77, p. 916-930.

Lickorish, W.H., Grasso, M., Butler, R.W.H., Argnani, A., and Maniscalco, R., 1999, Structural styles and regional tectonic setting of the “Gela Nappe” and frontal part of the Maghrebian thrust belt in Sicily: Tectonics, no. 18(4), p. 655-668.

Likerman, J., Burlando, J.F., Cristallini, E.O., and Ghiglione, M.C., 2013, Along-strike structural variations in the Southern Patagonian Andes: insights from physical modeling: Tectonophysics, no. 590, p. 106-120.

Liu, S., and Dixon, J. M., 1991, Centrifuge modelling of thrust faulting: structural variation along strike in fold-thrust belts: Tectonophysics, no. 188(1-2), p. 39-62.

Longhitano, S., Montanari, L., Punturo, R., 1995, Tematiche genetiche sui Filoni nettuniani della Rocca Busambra (Sicilia occidentale): Bollettino delle sedute della Accademia gioenia di scienze naturali in Catania, no. 28, p. 113–145.

Lovely, P., Flodin, E., Guzofski, C., Maerten, F., and Pollard, D.D., 2012, Pitfalls among the promises of mechanics-based restoration: Addressing implications of unphysical boundary conditions: Journal of Structural Geology, no. 41, p. 47-63.

MacKay, M.E., 1995, Structural variation and landward vergence at the toe of the Oregon accretionary prism: Tectonics, no. 14(6), p. 1309-1320.

Maerten, L., and Maerten, F., 2006, Chronologic modeling of faulted and fractured reservoirs using geomechanically based restoration: Technique and industry applications: AAPG Bulletin, no. 90, p. 1201-1226.

Magoon, L. B., and W. G. Dow, 1994, The petroleum system, in L. B. Magoon and W. G. Dow, eds., The petroleum system— from source to trap: AAPG Memoir, no. 60, p. 3–24.

Mahoney, L., Hill, K., McLaren, S., and Hanani, A., 2017, Complex fold and thrust belt structural styles: Examples from the Greater Juha area of the Papuan Fold and Thrust Belt, Papua New Guinea: Journal of Structural Geology, no. 100, p. 98-119.

Malz, A., Madritsch, H., Meier, B., and Kley, J., 2016, An unusual triangle zone in the external northern Alpine foreland (Switzerland): Structural inheritance, kinematics and implications for the development of the adjacent Jura fold-and-thrust belt: Tectonophysics, no. 670, p. 127-143.

Mattavelli, L., and Novelli, L., 1990, Geochemistry and Habitat of the Oils in Italy (1): AAPG Bulletin, no. 74(10), p. 1623-1639.

Mattioni, L., Sassi, W., and Callot, J.P., 2007, Analogue models of basin inversion by transpression: role of structural heterogeneity: Geological Society, London, Special Publications, no. 272(1), p. 397-417.

Mascle G.H., 1979, Etude géologique es Monts Sicanis, Sicile. Rivista Italiana di Paleontologia e stratigrafia, XVI, p. 1-431.

Mazzoli, S., Aldega, L., Corrado, S., Invernizzi, C., Zattin, M., and Butler, R.W.H., 2006, Pliocene-quaternary thrusting, syn-orogenic extension and tectonic exhumation in the

Southern Apennines (Italy): Insights from the Monte Alpi area: Geological Society Of America, Special Paper, no. 414, p. 55-77.

Mazzoli, S., D'errico, M., Aldega, L., Corrado, S., Invernizzi, C., Shiner, P., and Zattin, M., 2008, Tectonic burial and "young"(< 10 Ma) exhumation in the southern Apennines fold-and-thrust belt (Italy): Geology, no. 36(3), p. 243-246.

McClay, K.R., 1995, The geometries and kinematics of inverted fault systems: a review of analogue model studies: Geological Society, London, Special Publications, no. 88(1), p. 97-118.

McClay, K., and Bonora, M., 2001, Analog models of restraining stepovers in strike-slip fault systems: AAPG bulletin, no. 85(2), p. 233-260.

Medwedeff, D.A., 1992, Geometry and kinematics of an active, laterally propagating wedge thrust, Wheeler Ridge, California, in Mitra, S., and Fisher, G.W., eds., Structural geology of fold and thrust belts: Baltimore, Maryland, Johns Hopkins University Press, p. 3–28.

Melki, F., Zouaghi, T., Chelbi, M. B., Bedir, M., and Zargouni, F., 2010, Tectono-sedimentary events and geodynamic evolution of the Mesozoic and Cenozoic basins of the Alpine Margin, Gulf of Tunis, north-eastern Tunisia offshore: Comptes Rendus Geoscience, no. 342(9), p. 741-753.

Merriman, R.J. and Frey, M., 1998, Patterns of very low-grade metamorphism in metapelitic rocks, in Frey, M., and Robinson, D., eds., Low grade metamorphism: Blackwell, Oxford, UK. 61-107.

Michael, N.A., Carter, A., Whittaker, A.C. and Allen, P.A., 2014, Erosion rates in the source region of an ancient sediment routing system: comparison of depositional volumes with thermochronometric estimates: Journal of the Geological Society, London, no. 171, 2014, p. 401–412.

Miuccio, G., Frixa, A., and Bertamoni, M., 2000, The Trapanese Structural Domain in the Termini Imerese Mountain area (Sicily): Memorie della Società Geologica Italiana, no. 55, p. 227-234.

Molli, G., Carlini, M., Vescovi, P., Artoni, A., Balsamo, F., Camurri, F., Clemenzi, L., Sorti, F., and Torelli, L., 2018, Neogene 3-D structural architecture of the north-west Apennines: The role of the low-angle normal faults and basement thrusts: Tectonics, no. 37, p. 2165–2196.

Montanari, L., 2000, Paleogeography of Sicily: importance of stratigraphy. Memorie della Societa` Geologica Italiana, no. 55, p. 211–217.

Moore, D.M., and Reynolds, R.C., Jr., 1997, X-Ray Diffraction and the Identification and Analysis of Clay Minerals: Oxford, Oxford University Press, 378 p.

Monaco, C., and Tortorici, L., 1995, Tectonic role of ophiolite-bearing terranes in the development of the Southern Apennines orogenic belt: Terra Nova, no. 7(2), p. 153-160.

Monaco, C. and De Guidi, G., 2006, Structural evidence for Neogene rotations in the eastern Sicilian fold and thrust bel: Journal of Structural Geology, no. 28, p. 561-574.

Moretti, I., Lepage, F., Guiton, M., 2006, KINE3D: a New 3d restoration method based on a mixed approach linking geometry and geomechanics: Oil Gas Technology, no. 61 (2), p. 277-289.

Moretti, I., 2008, Working in complex areas: new restoration workflow based on quality control, 2D and 3D restorations: Marine and Petroleum Geology, no. 25, p. 205-218.

Nigro, F., 1998, Neotectonic events and kinematics of rhegmatic-like basins in Sicily and adjacent areas. Implications for a structural model of the Tyrrhenian openning: In Annales Societatis Geologorum Poloniae , no. 68(1), p. 1-21.

Nakapelyukh, M., Bubniak, I., Bubniak, A., Jonckheere, R., and Ratschbacher, L., 2018, Cenozoic structural evolution, thermal history, and erosion of the Ukrainian Carpathians fold-thrust belt: Tectonophysics, no. 722, p. 197-209.

Neumaier, M., Littke, R., Hantschel, T., Maerten, L., Joonnekindt, J. P., and Kukla, P., 2014, Integrated charge and seal assessment in the Monagas fold and thrust belt of Venezuela: AAPG bulletin, no.98(7), p. 1325-1350.

Nigro, F. and Renda, P., 1999, Evoluzione geologica ed assetto strutturale della Sicilia centro settentrionale: Bollettino della Società Geologica Italiana, no. 118, p. 375-388.

Nigro, F. and Renda, P. 2000. Un modello di evoluzione tettono-sedimentaria dell'avanfossa neogenica siciliana: Bollettino della Società Geologica Italiana, no. 119, p. 1913–1930.

Nigro, F., and Renda, P., 2001, Oblique slip thrusting in the Maghrebide chain of Sicily: Bollettino della Società geologica italiana, no. 120(2-3), p. 187-200.

Ogniben, L. 1960. Nota illustrativa dello schema geologico della Sicilia nordorientale: Rivista Mineraria Siciliana, no. 64–65, p. 183–222.

Olaru, R., Krézsek, C., Rainer, T. M., Ungureanu, C., Turi, V., Ionescu, G., and Tari, G., 2018, 3D Basin Modelling of Oligocene–Miocene Maikop Source Rocks Offshore Romania and in The Western Black Sea: Journal of Petroleum Geology, no.41(3), p. 351-365.

Oldow, J.S., Channell, J.E.T., Catalano, R. and D'argenio, B., 1990, Contemporaneous thrusting and large-scale rotations in the western Sicilian fold and thrust belt: Tectonics, no. 9, p. 661-681.

Pace, P., and Calamita, F., 2014, Push-up inversion structures v. fault-bend reactivation anticlines along oblique thrust ramps: examples from the Apennines fold-and-thrust belt (Italy): Journal of the Geological Society, no. 171, p. 227-238.

Parra, M., Sánchez, G.J., Montilla, L., Guzmán, O.J., Namson, J., and Jácome, M.I., 2011, The Monagas fold–thrust belt of eastern Venezuela. part I: structural and thermal modelling: Marine and Petroleum Geology, no.28(1), p. 40-69.

Parrish, J.T., and Curtis, R.L., 1982, Atmospheric circulation, upwelling, and organic-rich rocks in the Mesozoic and Cenozoic eras: Palaeogeography, palaeoclimatology, palaeoecology, no. 40(1-3), p. 31-66.

Pavia, G., Martire, L., Canzoneri, V., and D'Arpa., C., 2002. General Field Trip Guide (12–22 September 2002). An Introduction to the Jurassic geology of Western Sicily. In Santantonio, M., ed., 6th International Symposium on the Jurassic System: General Field Trip Guidebook, p. 1–316.

Pellerin, J., Caumon, G., Julio, C., Mejia-Herrera, P., and Botella, A., 2015, Elements for measuring the complexity of 3D structural models: Connectivity and geometry: Computers & Geosciences, no. 76, p. 130-140.

Peters, K.E., and Cassa, M.R., 1994, Applied source rock geochemistry. In: Magoon, L.B., Dow, W.G., Eds., The Petroleum System— From Source to Trap: American Association of Petroleum Geologists Memoir, no. 60, p. 93-117.

Pinter, P. R., Butler, R.W.H., Hartley, A.J., Maniscalco, R., Baldassini, N. and Di Stefano, A., 2016, The Numidian of Sicily revisited: a thrust-influenced confined turbidite system: Marine and Petroleum Geology, no. 78, p. 291-311.

Pinter, P.R., Butler, R.W.H., Hartley, A.J., Maniscalco, R., Baldassini, N., and Di Stefano, A., 2017, Tracking sand-fairways through a deformed turbidite system: the Numidian (Miocene) of Central Sicily, Italy: Basin Research, no. 30(3), p. 480-501

Plesch, A., Shaw, J.H., and Kronman, D., 2007, Mechanics of low-relief detachment folding in the Bajiaochang field, Sichuan Basin, China: AAPG bulletin, no. 91(11), p. 1559-1575.

Qayyum, M., Spratt, D.A., Dixon, J.M., and Lawrence, R.D., 2015, Displacement transfer from fault-bend to fault-propagation fold geometry: an example from the Himalayan thrust front: Journal of Structural Geology, no.77, p. 260-276.

Raulin, C., Frizon de Lamotte, D., Bouaziz, S., Khomsi, S., Mouchot, N., Ruiz, G., and Guillocheau, F., 2011, Late Triassic–early Jurassic block tilting along E–W faults, in southern Tunisia: New interpretation of the Tebaga of Medenine. Journal of African Earth Sciences, no. 61(1), p. 94-104.

Reiners, P. W. and Ehlers, T. A., 2005, Low-temperature thermochronology: techniques, interpretations, and application, Ed., PW Reiners, TA Ehlers. Washington: The Mineralogical Society of America.

Renda, P., Tavarnelli, E., Tramutoli, M., and Gueguen, E., 2000, Neogene deformations of Northern Sicily, and their implications for the geodynamics of the Southern Tyrrhenian Sea margin: Memorie della Società Geologica Italiana, no. 55, p. 53-59.

Rigane, A., and Gourmelen, C., 2011, Inverted intracontinental basin and vertical tectonics: The Saharan Atlas in Tunisia: Journal of African Earth Sciences, no. 61(2), p. 109-128.

Rodriguez-Roa, F.A., and Wiltschko, D.V., 2010, Thrust belt architecture of the central and southern Western Foothills of Taiwan: Geological Society, London, Special Publications, no. 348(1), p. 137-168.

Romero-Sarmiento, M.F., Ducros, M., Carpentier, B., Lorant, F., Cacas, M.C., Pegaz-Fiornet, S., Wolf, S., Rohais, S., and Moretti, I., 2013, Quantitative evaluation of TOC, organic porosity and gas retention distribution in a gas shale play using petroleum system modeling: Application to the Mississippian Barnett Shale: Marine and Petroleum Geology, no. 45, p. 315-330.

Rosenbaum, G., Lister, G.S., and Duboz, C., 2004, The Mesozoic and Cenozoic motion of Adria (central Mediterranean): a review of constraints and limitations: Geodinamica Acta, no. 17(2), p. 125-139.

Roure, F., Howell, D.G., Muller, C. and Moretti, I., 1990, Late Cenozoic subduction complex of Sicily: Journal of Structural Geology, no. 12, p. 259-266.

Roure, F., and Sassi, W., 1995, Kinematics of deformation and petroleum system appraisal in Neogene foreland fold-and-thrust belts: Petroleum Geoscience, no. 1(3), p. 253-269.

Roure, F., Andriessen, P., Callot, J. P., Faure, J. L., Ferket, H., Gonzales, E., Guilhaumou N., Lacombe O., Malandain J., Sassi W., Schneider, F., Swennen, R., and Vilasi, N., 2010, The use of palaeo-thermo-barometers and coupled thermal, fluid flow and pore-fluid pressure modelling for hydrocarbon and reservoir prediction in fold and thrust belts: Geological Society, London, Special Publications, no. 348(1), p. 87-114.

Roure, F., Casero, P., and Addoum, B.,2012, Alpine inversion of the North African margin and delamination of its continental lithosphere: Tectonics, no. 31(3).

Roure, F., 2014, Crustal architecture, thermal evolution and energy resources of compressional basins (André Dumont medallist lecture 2013): Geologica Belgica, no. 17/2, p. 182–194.

Rowan, M.G., and Kligfield, R., 1989, Cross section restoration and balancing as aid to seismic interpretation in extensional terranes: AAPG bulletin, no. 73(8), p. 955-966.

Royer, J.J., Mejia, P., Caumon, G., and Collon-Drouaillet, P., 2013, 3and 4D Geomodeling Applied to Mineral Resources Exploration-A New Tool for Targeting Deposits: In EGU General Assembly Conference Abstracts, no. 15.

Ruh, J. B., Kaus, B.J., and Burg, J.P., 2012, Numerical investigation of deformation mechanics in fold-and-thrust belts: Influence of rheology of single and multiple décollements: Tectonics, no. 31(3), p. 1-23.

Sachse, V.F., Anka, Z., Littke, R., Rodriguez, J.F., Horsfield, B., and Di Primio, R., 2016, Burial, temperature and maturation history of the Austral and Western Malvinas Basins, Southern Argentina, based on 3D basin modelling: Journal of Petroleum Geology, no. 39(2), p. 169-191.

Sadeghi, S., Storti, F., Yassaghi, A., Nestola, Y., and Cavozzi, C., 2016, Experimental deformation partitioning in obliquely converging orogens with lateral variations of basal décollement rheology: Inferences for NW Zagros, Iran: Tectonophysics, no. 693, p. 223-238.

Sassi, W., Graham, R., Gillcrist, R., Adams, M., and Gomez, R., 2007, The impact of deformation timing on the prospectivity of the Middle Magdalena sub-thrust, Colombia: Geological Society, London, Special Publications, no. 272(1), p. 473-498.

Schito, A., Andreucci, B., Aldega, L., Corrado, S., Di Paolo, L., Zattin, M., Szaniawski, R., Jankowski, L., and Mazzoli, S., 2018, Burial and exhumation of the western border of the Ukrainian Shield (Podolia): a multi-disciplinary approach: Basin Research, no. 30, p. 532-549.

Schneider, F., 2005, Understanding the diagenetic evolution of potential reservoirs in fold/thrust belts: an example from eastern Venezuela: Geological Society, London, Petroleum Geology Conference series, no. 6(1), p. 1359-1366.

Schönborn, G., 1999, Balancing cross sections with kinematic constraints: The Dolomites (northern Italy): Tectonics, no. 18(3), p. 527-545.

Sclater, J.G., and Christie, P.A.F., 1980, Continental stretching: An explanation of post–Mid-Cretaceous subsidence on the central North Sea Basin: Journal of Geophysical Research, no. 85, p. 3711–3739.

Shiner, P., Beccacini, A., and Mazzoli, S., 2004, Thin-skinned versus thick-skinned structural models for Apulian carbonate reservoirs: constraints from the Val d'Agri Fields, S Apennines, Italy: Marine and Petroleum Geology, no. 21(7), p. 805-827.

Shuwei, G., Dengfa, H., Yongliang, L.E.I., and Zhuxin, C., 2013, Kinematic classification, structural modeling and prospective fields of the foreland thrust belts in Midwest China: Petroleum Exploration and Development, no. 40(1), p. 69-83.

Sømme, T.O., Helland-Hansen, W., Martinsenw, O.J. and Thurmondw, J.B.,2009, Relationships between morphological and sedimentological parameters in source-to-sink systems: a basis for predicting semi-quantitative characteristics in subsurface systems: Basin Research, no. 21, p. 361–387.

Speranza, F., Maniscalco, R., Mattei, M., Di Stefano, A., Butler, R. W. H. and Funiciello, R., 1999, Timing and magnitude of rotations in the frontal thrust system of southwestern Sicily: Tectonics, no.18, p. 1178-1197.

Speranza, F., Maniscalco, R., and Grasso, M., 2003, Pattern of orogenic rotations in central-eastern Sicily: implications for the timing of spreading in the Tyrrhenian Sea: Journal of the Geological Society, London, no. 160, 183-195.

Speranza, F., Hernandez-Moreno, C., Avellone, G., Gasparo Morticelli, M., Agate M., Sulli A., and Di Stefano, E., 2018, Understanding paleomagnetic rotations in Sicily: Thrust vs. strike-slip tectonics: Tectonics, no. 37 (4), 1138-1158.

Sweeney, J.J., and Burnham, A.K., 1990, Evaluation of a simple model of vitrinite reflectance based on chemical kinetics: AAPG Bulletin no. 74, p. 1559–1570.

Tanner, D. C., Behrmann, J. H., and Dresmann, H., 2003, Three-dimensional retro-deformation of the Lechtal Nappe, northern Calcareous Alps: Journal of Structural Geology, no. 25(5), p. 737-748.

Tavani, S., Parente, M., Puzone, F., Corradetti, A., Gharabeigli, G., Valinejad, M., Morsalnejad, D., and Mazzoli, S., 2018, The seismogenic fault system of the 2017 M w 7.3 Iran–Iraq earthquake: constraints from surface and subsurface data, cross-section balancing, and restoration: Solid Earth, no. 9(3), p. 821.

Tavarnelli, E., Renda, P., Pasqui, V., and Tramutoli, M., 2003, The effects of post-orogenic extension on different scales: an example from the Apennine–Maghrebide fold-and-thrust belt, SW Sicily: Terra Nova, no. 15(1), p. 1-7.

Teles, V., Fornel, A., Houel, P., Delmas, J., Mengus, J.M., Michel, A., and Maurand, N., 2014, Coupling basin and reservoir simulators for an improved CO2 injection flow model: Energy Procedia, no. 63, p. 3665-3675.

Thomas, W.A., Kanda, R.V., O'Hara, K.D., and Surles, D.M., 2008, Thermal footprint of an eroded thrust sheet in the southern Appalachian thrust belt, Alabama, USA: Geosphere, no. 4(5), p. 814-828.

Tibaldi, A., Alania, V., Bonali, F.L., Enukidze, O., Tsereteli, N., Kvavadze, N., and Varazanashvili, O., 2017, Active inversion tectonics, simple shear folding and back-thrusting at Rioni Basin, Georgia: Journal of Structural Geology, no. 96, p. 35-53.

Tissot, B.P., and Welte, D.H., 1978, Petroleum Formation and Occurrence: Springer-Verlag, New York.

Toro, J., Roure, F., Bordas-Le Floch, N., Le Cornec-Lance, S., and Sassi, W., 2004, Thermal and kinematic evolution of the Eastern Cordillera fold and thrust belt, Colombia, in Swennen, R., Roure, F., and Granath, J.W., eds., Deformation, fluid flow, and reservoir appraisal in foreland fold and thrust belts: American Association of Petroleum Geologists, Hedberg Series, no. 1, p. 79–115.

Tortorici, L., Monaco, C., Mazzoli, S., and Bianca, M., 2001, Timing and modes of deformation in the western Sicilian thrust system, southern Italy: Journal of Petroleum Geology, no. 24(2), p. 191-211.

Torvela, T., and Bond, C.E., 2011, Do experts use idealised structural models? Insights from a deepwater fold–thrust belt: Journal of Structural Geology, no. 33(1), p. 51-58.

Totake, Y., Butler, R.W.H., and Bond, C.E., 2017, Structural validation as an input into seismic depth conversion to decrease assigned structural uncertainty: Journal of Structural Geology, no. 95, p. 32-47.

Tozer, R.S.J., Butler, R.W.H., and Corrado, S., 2002, Comparing thin-and thick-skinned thrust tectonic models of the Central Apennines, Italy: EGU Stephan Mueller Special Publication Series, no. 1, p. 181-194.

Tozer, R.S.J., Butler, R.W.H., Chiappini, M., Corrado, S., Mazzoli, S., and Speranza, F., 2006, Testing thrust tectonic models at mountain fronts: where has the displacement gone?: Journal of the Geological Society, no. 163(1), p. 1-14.

Tricart, P., Torelli, L., Argnani, A., Rekhiss, F., and Zitellini, N., 1994, Extensional collapse related to compressional uplift in the Alpine Chain off northern Tunisia (Central Mediterranean): Tectonophysics, no. 238(1-4), p. 317-329.

Trincianti, E., Frixa, A., and Sartorio, D., 2015, Palynology and stratigraphic characterization of subsurface sedimentary successions in the Sicanian and Imerese Domains—Central Western Sicily: Review of Palaeobotany and Palynology, no. 218, p. 48-66.

Turcotte, D., L., and Schubert, G., 2002, Geodynamics (Second Edition): Cambridge University Press, Cambridge, p. 1-476.

Turner, S.A., Cosgrove, J.W., and Liu, J.G., 2010, Controls on lateral structural variability along the Keping Shan Thrust Belt, SW Tien Shan Foreland, China: Geological Society, London, Special Publications, no. 348(1), p. 71-85.

Turrini, C., Bosica, B., Ryan, P., Shiner, P., Lacombe, O., and Roure, F., 2018, 3D structural and thermal modelling of Mesozoic petroleum systems in the Po Valley Basin, northern Italy: Petroleum Geoscience, no. 24(2), p. 172-196.

Vignaroli, G., Rossetti, F., Theye, T., and Faccenna, C., 2008, Styles and regimes of orogenic thickening in the Peloritani Mountains (Sicily, Italy), New constraints on the tectono-metamorphic evolution of the Apennine belt: Geological Magazine, no. 145, p. 552–569.

Von Hagke, C., and Malz, A., 2018, Triangle zones–Geometry, kinematics, mechanics, and the need for appreciation of uncertainties: Earth-Science Reviews, no. 177, p. 24-42.

Walsh, J.J., Watterson, J., Bailey, W.R., and Childs, C., 1999, Fault relays, bends and branch-lines: Journal of Structural Geology, no. 21(8-9), p. 1019-1026.

Watkins, H., Bond, C.E., and Butler, R.W.H., 2014, Identifying multiple detachment horizons and an evolving thrust history through cross-section restoration and appraisal in the Moine Thrust Belt, NW Scotland: Journal of Structural Geology, no. 66, p. 1-10.

Watkins, H., Butler, R.W.H., and Bond, C.E., 2017, Using laterally compatible cross sections to infer fault growth and linkage models in foreland thrust belts: Journal of Structural Geology, no. 96, p. 102-117.

Whitchurch, A.L., Cartera Sinclair, H.D., Duller, R.A., Whittaker, A.C. And Allen, P.A., 2011, Sediment routing system evolution within a diachronously uplifting orogen: insights from detrital zircon thermochronological analyses from the south-central pyrenees: American Journal of Science, no. 311, p. 442–482.

Xu, C., and Zhou, X.Y., 2007, Seismic interpretation of the Kelasu triangle zone in the southern Tian Shan foothills, northwestern China: AAPG bulletin, no. 91(2), p. 161-171.

Zapata, T.R., and Allmendinger, R.W., 1996, Thrust-front zone of the Precordillera, Argentina: a thick-skinned triangle zone: AAPG bulletin, no. 80(3), p. 359-381.

Zappaterra, E., 1994, Source-rock distribution model of the Periadriatic region: AAPG bulletin, no. 78(3), p. 333-354.

Zarcone, G., Petti, F.M., Cillari, A., Di Stefano, P., Guzzetta, D. and Nicosia, U., 2010, A possible bridge between Adria and Africa: New palaeobiogeographic and stratigraphic constraints on the Mesozoic palaeogeography of the Central Mediterranean area: Earth Science Review, no. 103, p. 154–162.

Zattin, M., Andreucci, B., Jankowski, L., Mazzoli, S. and Szaniawski, R., 2011, Neogene exhumation in the Outer Western Carpathians: Terra Nova, no. 23, p. 283–291.

Zhang, X., Pease, V., Carter, A., Kostuychenko, S., Suleymanov, A., and Scott, R., 2018, Timing of exhumation and deformation across the Taimyr fold–thrust belt: insights from apatite fission track dating and balanced cross-sections, In: Pease, V. and Coakley, B. (eds.) Circum-Arctic Lithosphere Evolution: Geological Society, London, Special Publications, no. 460, p. 315-333.

Zhu, C., Qiu, N., Liu, Y., Xiao, Y., and Hu, S., 2018, Constraining the denudation process in the eastern Sichuan Basin, China using low-temperature thermochronology and vitrinite reflectance data: Geological Journal. DOI: 10.1002/gj.3191.

APPENDIX

Legend

Organic matter optical analysis- vitrinite reflectance (from IV to XX)

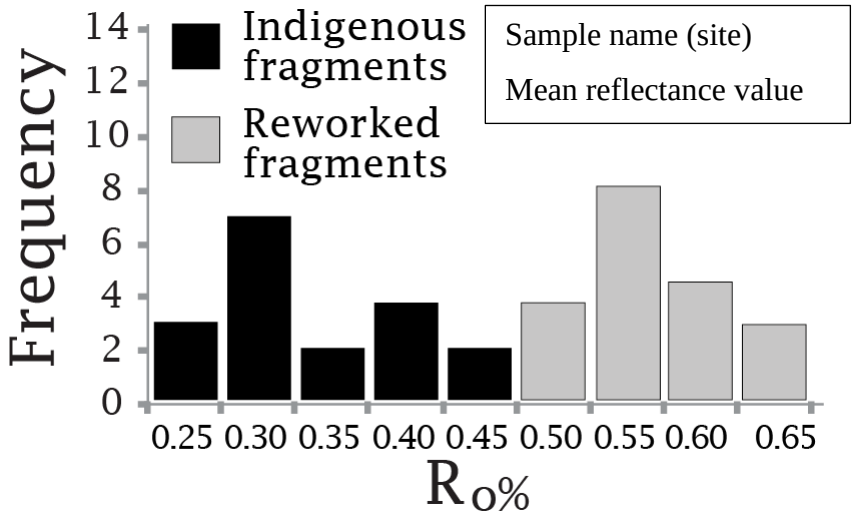

Ro% meas. – single measurement on vitrinite maceral

X-ray diffraction on (<2 μm) clay minerals (from XXI to XLIII)

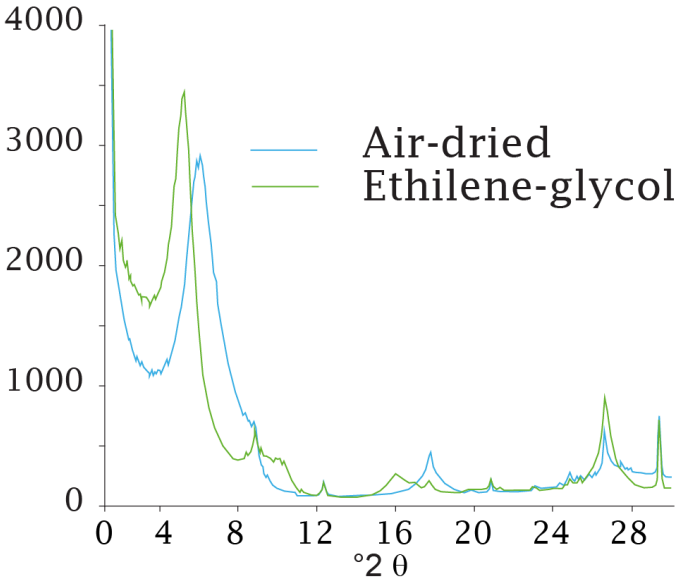

Rock-Eval analysis (XLIV)

Low-temperature thermochronology (U-Th)/He on apatite (XLV)

WEDGE TOP BASIN AND ITS DEFORMED SUBSTRATUM (Termini-Imerese area)

Site	Sample	Coordinates	Formation	Age	Optical analysis	XRD analysis	Pyrolysis	(U-Th)/apatite
01	PM22	37°53'12.78"N 13°53'34.20"E	Terravecchia 1b	up. Tortonian-low. Messinian	IV	XXI		
02	PM23	37°52'56.28"N 13°53'16.55"E	Terravecchia 1b	up. Tortonian-low. Messinian	IV	XXI		
03	PM28	37°52'37.18"N 13°52'58.36"E	Terravecchia 1b	up. Tortonian-low. Messinian	V	XXI		
04	PM29	37°53'4.24"N 13°52'11.28"E	Terravecchia 2-3	up. Tortonian-low. Messinian	V	XXII		
05	PM25	37°51'58.04"N 13°52'33.68"E	Terravecchia 2-3	up. Tortonian-low. Messinian	VI	XXII		
06	PM14	37°53'13.90"N 13°51'43.15"E	Terravecchia 2-3	up. Tortonian-low. Messinian	VI	XXII		
07	PA10	37°51'35.30"N 13°52'23.52"E	Terravecchia 2-3	up. Tortonian-low. Messinian	VI	XXIII		
08	PM18-19	37°51'44.71"N 13°53'25.29"E	Terravecchia 2-3	up. Tortonian-low. Messinian	VII	XXIII		
09	PA08	37°50'56.37"N 13°52'42.47"E	Terravecchia 1	up. Tortonian-low. Messinian	VII	XXIII		
10	MF5	37°50'58.33"N 13°52'34.42"E	Terravecchia 1	up. Tortonian-low. Messinian	VII	XXIV		
11	MF6	37°50'44.98"N 13°53'14.10"E	Castellana Sicula	up. Serravallian-low. Tortonian	VIII	XXIV		
12	PA44	37°49'50.00"N 13°51'49.20"E	Numidian Flysch	up. Oligocene-low. Miocene	VIII		XLIV	
13	PA60	37°48’53.8’’ 13°55’36.8’’	Numidian Flysch	up. Oligocene-low. Miocene	VIII	XXIV		
14	PA43	37°48'44.40"N 13°51'10.80"E	Numidian Flysch	up. Oligocene-low. Miocene		XXV		
15	PM35	37°50'22.40"N 13°54'34.50"E	Numidian Flysch	up. Oligocene-low. Miocene	IX	XXV	XLIV	XLV
16	PM34	37°50'3.51"N 13°53'50.35"E	Numidian Flysch	up. Oligocene-low. Miocene	IX	XXV		
17	MF4	37°49'52.81"N 13°53'36.23"E	Numidian Flysch	up. Oligocene-low. Miocene	X	XXVI		
18	PA45	37°49'37.70"N 13°53'32.20"E	Caltavuturo	up. Paleocene - low. Oligocene		XXVI		
19	PA41	37°49'4.40"N 13°51'19.70"E	Caltavuturo	up. Paleocene - low. Oligocene		XXVI		
20	PA46	37°51'36.70"N 13°54'50.60"E	Crisanti	up. Toarcian - Albian		XXVII		
21	PA40	37°49'13.80"N 13°51'23.90"E	Crisanti	up. Toarcian - Albian		XXVII		
22	PA47	37°51'38.20"N 13°54'52.20"E	Crisanti	up. Toarcian - Albian	X	XXVII	XLIV	
23	PA39	37°49'22.90"N 13°51'23.30"E	Crisanti	up. Toarcian - Albian	XI	XXVIII	XLIV	
24	PM1	37°54'19.59"N 13°50'39.61"E	Mufara	middle-upper Carnian	XI	XXVIII		
25	PM2	37°54'23.67"N 13°51'10.38"E	Mufara	middle-upper Carnian	XI	XXVIII	XLIV	
26	PM6	37°54'37.82"N 13°50'19.79"E	Mufara	middle-upper Carnian	XII	XXIX	XLIV	
27	PM7	37°54'34.72"N 13°49'59.63"E	Mufara	middle-upper Carnian	XII	XXIX		
28	PM5	37°54'43.68"N 13°50'30.19"E	Mufara	middle-upper Carnian	XIII	XXIX		

IMERESE UNIT AND NUMIDIAN FLYSCH (Kumeta and Busambra Mts. area)

Site	Sample	Coordinates	Formation	Age	Optical analysis	XRD analysis	Pyrolysis	(U-Th)/apatite
01	PA 11	37°51'48.08"N 13°27'8.82"E	Numidian Flysch	Late Oligocene – early Miocene		XXX		XLV
01	PA 12	37°51'45.37"N 13°27'1.29"E	Numidian Flysch	Late Oligocene – early Miocene	XIII			
02	PA 13	37°52'10.54"N 13°25'3.25"E	Numidian Flysch	Late Oligocene – early Miocene	XIV	XXX		
03	PA 15	37°51'9.60"N 13°25'51.11"E	Numidian Flysch	Late Oligocene – early Miocene	XIV	XXX		
04	PA 22	37°58'18.90"N 13°19'8.40"E	Numidian Flysch	Late Oligocene – early Miocene	XIV	XXXI	XLIV	XLV
05	PA 26	37°56'48.00"N 13°19'44.60"E	Numidian Flysch	Late Oligocene – early Miocene		XXXI		
06	PA 75	37°55'26.3"N 13°12'24.5"E	Numidian Flysch	Late Oligocene – early Miocene		XXXI		
07	PA 58	37°59'34.6"N 13°17'29.8"E	Numidian Flysch	Late Oligocene – early Miocene	XV	XXXII		
08	PA 73	37°56'45.6"N 13°19'34.1"E	Numidian Flysch	Late Oligocene – early Miocene	XV	XXXII		
09	PA 76?	37°59'40.4"N 13°14'08.8"E	Numidian Flysch	Late Oligocene – early Miocene		XXXII		
10	PA 28	37°59'28.70"N 13°18'2.50"E	Caltavuturo	Late Paleocene-low Oligocene		XXXIII		
11	PA 67	37°55'40"N 13°28'33.8"E	Caltavuturo	Late Paleocene-low Oligocene		XXXIII		
12	PA 71	37°57'35"N 13°24'23.6"E	Caltavuturo	Late Paleocene-low Oligocene		XXXIII		
13	PA 70	37°57'34.5"N 13°24'28.5"E	Crisanti	Up. Toarcian – Cretaceous		XXXIV	XLIV	
14	PA 66	37°55'38.4"N 13°28'39.2"E	Crisanti	Up. Toarcian – Cretaceous	XVI	XXXIV	XLIV	
15	PA 27	38° 0'31.50"N 13°18'10.10"E	Crisanti	Up. Toarcian – Cretaceous	XVI		XLIV	
16	PA 05	37°59'47.35"N 13°18'5.96"E	Crisanti	Up. Toarcian – Cretaceous	XVI	XXXIV	XLIV	
17	PA 65	37°55'48.6"N 13°28'20.2"E	Scillato	upper Carnian-Rhaetian	XVII		XLIV	
18	PA 23	37°57'56.30"N 13°18'51.10"E	Mufara	Middle-upper Carnian	XVII	XXXV	XLIV	XLV
19	PA 69	37°57'04.6"N 13°24'08.8"E	Mufara	Middle-upper Carnian	XVII	XXXV	XLIV	
20	PA 72	37°57'04.2"N 13°19'27.4"E	Mufara	Middle-upper Carnian		XXXV	XLIV	

TRAPANESE UNIT (Kumeta and Busambra Mts. area)

Site	Sample	Coordinates	Formation	Age	Optical analysis	XRD analysis	Pyrolysis	(U-Th)/apatite
21	PA 18	37°51'19.78"N 13° 7'43.09"E	Marne di San Cipirello	Serravallian-low. Tortonian		XXXVI		
22	PA 30	37°57'5.70"N 13°15'43.80"E	Marne di San Cipirello	Serravallian-low. Tortonian		XXXVI		
23	PA 31	37°57'2.80"N 13°17'31.40"E	Marne di San Cipirello	Serravallian-low. Tortonian	XVIII			
24	PA 32	37°57'47.00"N 13°19'8.00"E	Marne di San Cipirello	Serravallian-low. Tortonian	XVIII	XXXVI		
25	PA 53	37°50'50.80"N 13°20'39.80"E	Marne di San Cipirello	Serravallian-low. Tortonian	XIX	XXXVII		
26	PA 34	37°51'46.60"N 13°10'33.00"E	Marne di San Cipirello	Serravallian-low. Tortonian	XIX	XXXVII	XLIV	
27	PA 50	37°51'47.90"N 13°18'33.80"E	Marne di San Cipirello	Serravallian-low. Tortonian	XIX	XXXVII		
28	PA 52	37°50'54.60"N 13°19'48.90"E	Marne di San Cipirello	Serravallian-low. Tortonian		XXXVIII		
29	PA 54	37°50'53.90"N 13°20'44.70"E	Marne di San Cipirello	Serravallian-low. Tortonian		XXXVIII	XLIV	
30	PA 56	37°50'43.90"N 13°21'48.80"E	Marne di San Cipirello	Serravallian-low. Tortonian		XXXVIII		
31	PA 57	37°50'50.10"N 13°21'2.60"E	Calcareniti di Corleone	Burdigalian-Langhian		XXXIX		
32	PA 25	37°57'25.60"N 13°19'2.90"E	Calcareniti di Corleone	Burdigalian-Langhian		XXXIX		
33	PA 14	37°51'8.02"N 13°25'47.39"E	Amerillo	Late Cretaceous-late Eocene		XXXIX		
34	PA 24	37°57'33.40"N 13°18'44.20"E	Amerillo	Late Cretaceous-late Eocene		XL		
35	PA 35	37°52'20.50"N 13°10'55.90"E	Amerillo	Late Cretaceous-late Eocene		XL		
36	PA 37	37°52'22.50"N 13°10'52.00"E	Amerillo	Late Cretaceous-late Eocene		XL		
38	PA 55	37°50'53.00"N 13°20'55.60"E	Amerillo	Late Cretaceous-late Eocene		XLI		
39	PA 20	37°56'42.20"N 13°27'35.69"E	Amerillo	Late Cretaceous-late Eocene		XLI		
40	PA 17	37°50'32.65"N 13°26'42.51"E	Hybla	up. Aptian-low. Albian		XLI	XLIV	
41	PA 16	37°50'31.78"N 13°26'20.20"E	Hybla	up. Aptian-low. Albian		XLII	XLIV	
42	PA 03	37°58'16.11"N 13°14'50.39"E	Hybla	up. Aptian-low. Albian	XX		XLIV	
43	PA 04	37°58'13.18"N 13°14'42.10"E	Hybla	up. Aptian-low. Albian		XLII		
44	PA 29	37°57'31.90"N 13°16'39.40"E	Buccheri	Toarcian-Tithonian		XLIII		
45	PA 19	37°56'48.96"N 13°27'19.17"E	Buccheri	Toarcian-Tithonian	XX	XLIII		
45	PA 19b	37°56'48.96"N 13°27'19.17"E	Inici	Hettangian-Sinemurian			XLIV	

Organic matter optical analysis- vitrinite reflectance

R_o% meas.
0.286
0.298
0.313
0.321
0.329
0.333
0.335
0.343
0.343
0.343
0.372
0.374
0.362

R_o% meas. (reworked)
0.403
0.404
0.405
0.417
0.439
0.443
0.468
0.468
0.474
0.476
0.480
0.480
0.483
0.483
0.486
0.491
0.504
0.531
0.577
0.59

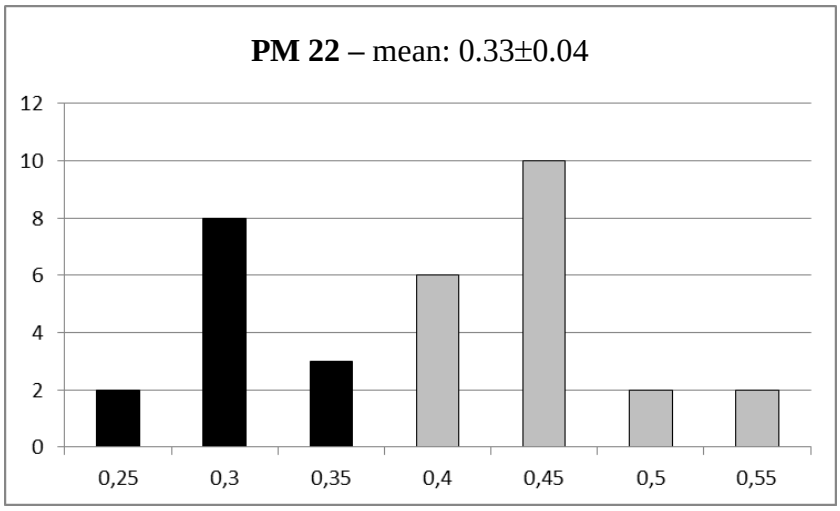

R_o% meas.
0.354
0.373
0.378
0.392
0.396
0.406
0.411
0.421
0.426
0.439
0.443
0.450
0.463
0.471
0.495

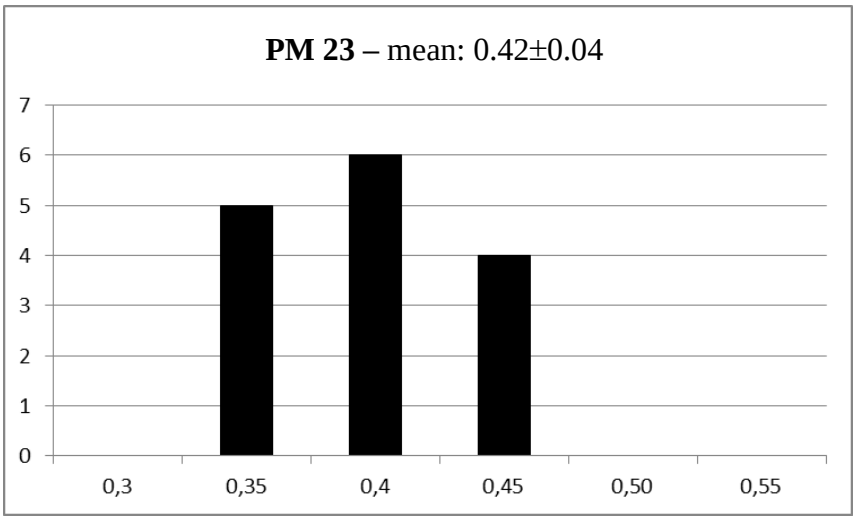

R_o% meas.
0.397
0.413
0.443
0.451
0.459
0.469
0.473
0.480
0.486
0.488
0.492
0.521

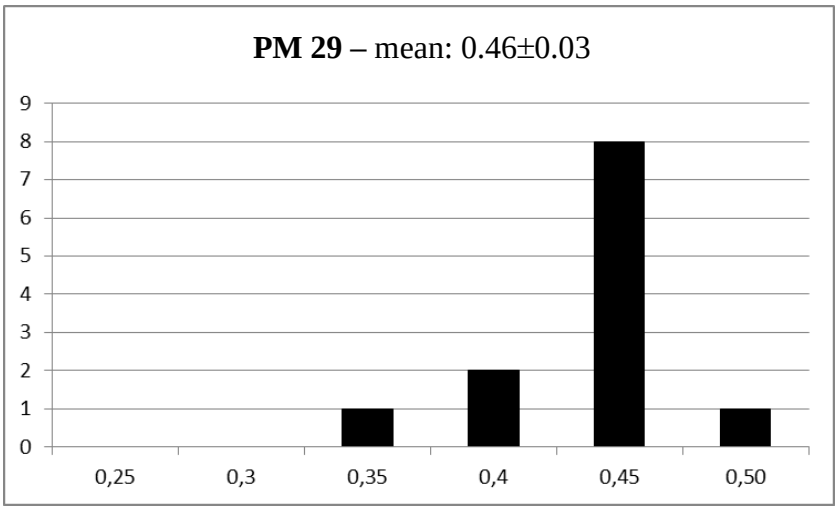

R_o% meas.
0.357
0.362
0.394
0.408
0.409
0.43
0.442
0.447
0.456
0.475
0.511
0.512
0.515
0.52
0.527
0.532
0.544
0.549

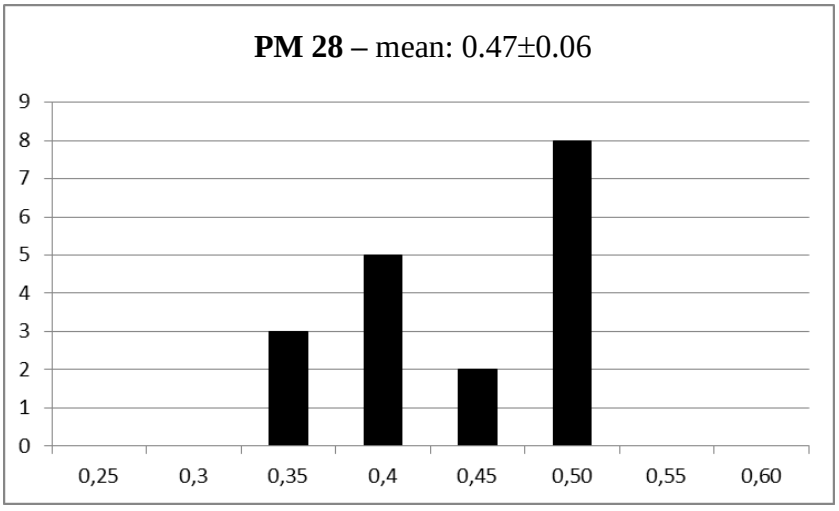

R_o% meas.
0.417
0.434
0.439
0.448
0.455
0.470

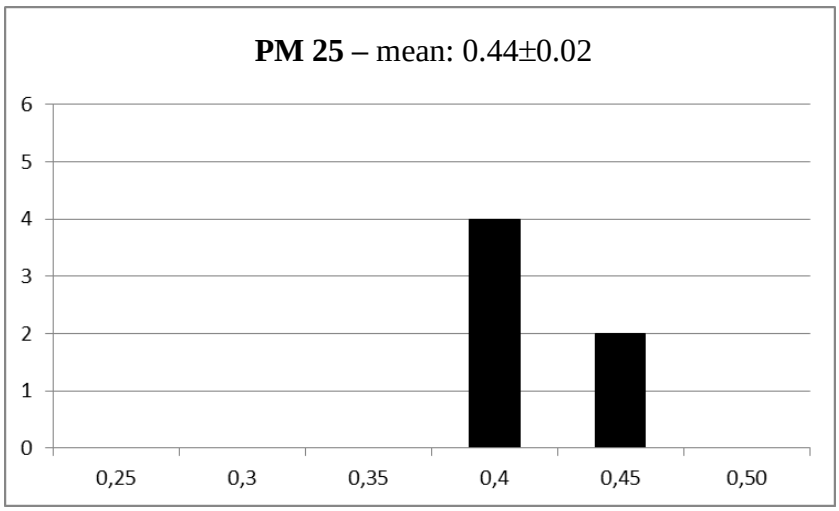

R_o% meas.
0.438
0.457
0.464
0.465
0.466
0.474
0.484
0.535
0.417

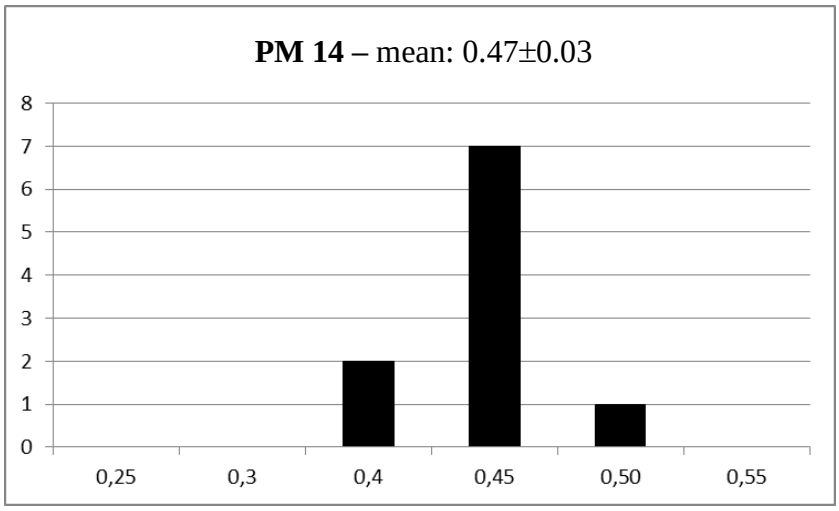

R_o% meas.
0.301
0.302
0.32
0.332
0.342
0.358
0.381
0.389
0.394
0.413
0.414
0.417
0.421
0.43
0.435
0.44

R_o% meas.
0.443
0.445
0.446
0.447
0.449
0.452
0.458
0.459
0.476
0.478
0.478
0.483
0.485
0.486
0.491
0.498

R_o% meas. (reworked)
0.511
0.513
0.529
0.529
0.53
0.55
0.552
0.553
0.553
0.555
0.556
0.556
0.575
0.58
0.595

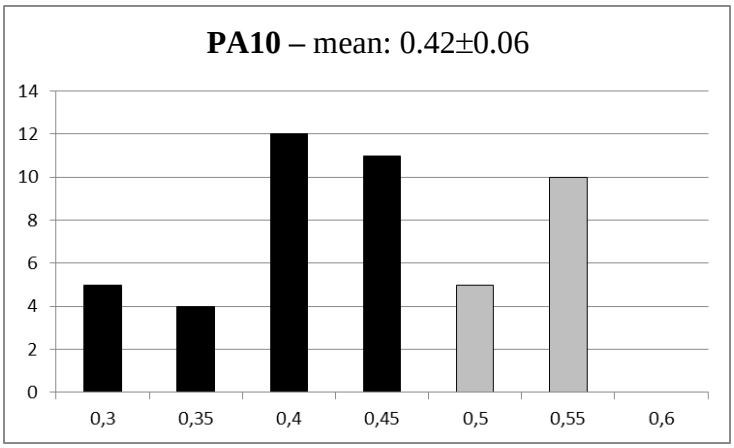

R_o% meas.
0.39
0.352
0.401
0.402
0.403
0.417
0.420
0.433
0.433
0.436
0.444
0.446
0.454
0.466
0.469

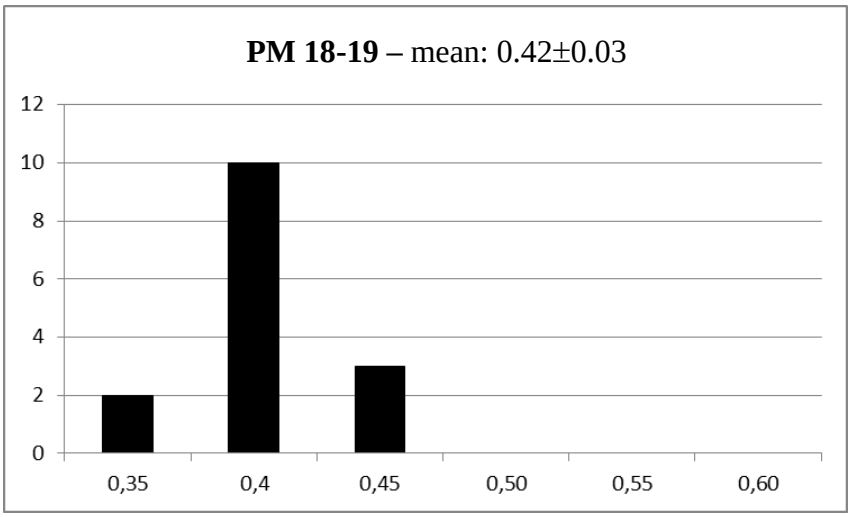

R_o% meas.
0.307
0.309
0.343
0.357
0.361
0.370
0.384
0.389
0.420
0.423
0.474
0.476

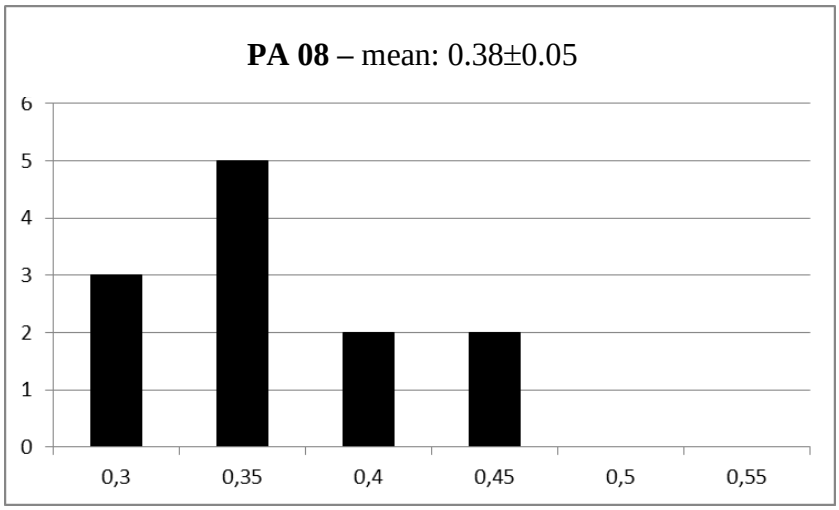

R_o% meas.
0.297
0.325
0.326
0.363
0.376
0.418
0.432
0.444
0.470
0.491

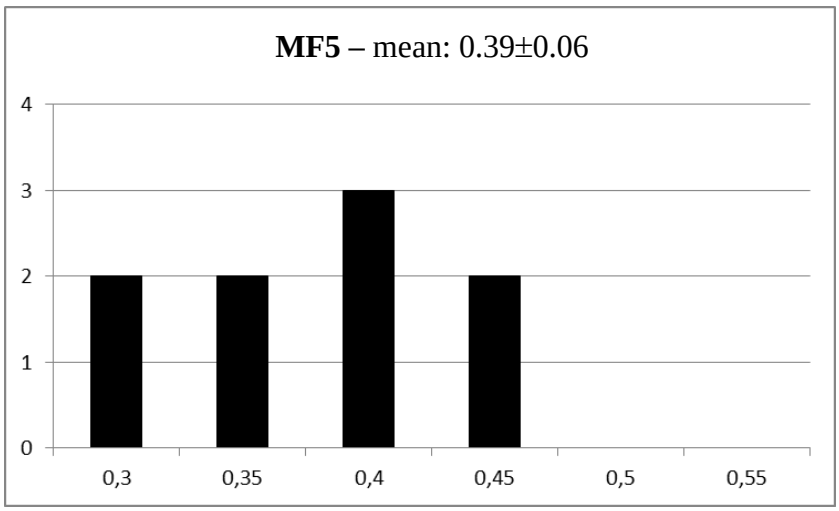

R_o% meas.
0.312
0.324
0.332
0.404
0.405
0.415
0.428
0.429
0.431
0.446
0.451
0.476
0.497
0.511

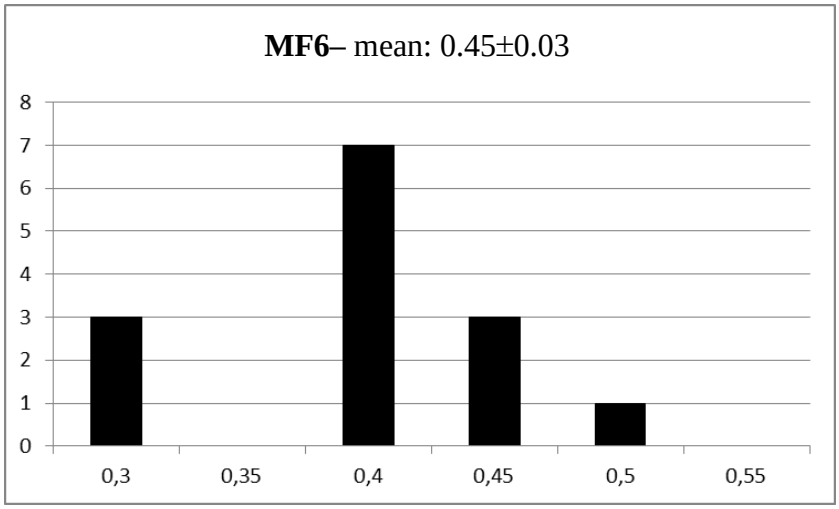

R_o% meas.
0.402
0.405
0.435
0.441
0.462
0.472
0.519
0.534
0.535

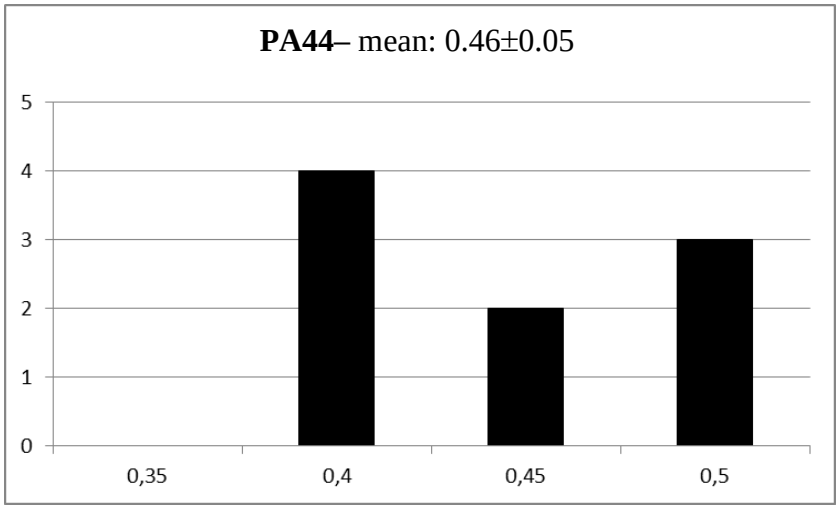

R_o% meas.
0.301
0.350
0.369
0.429
0.449
0.489

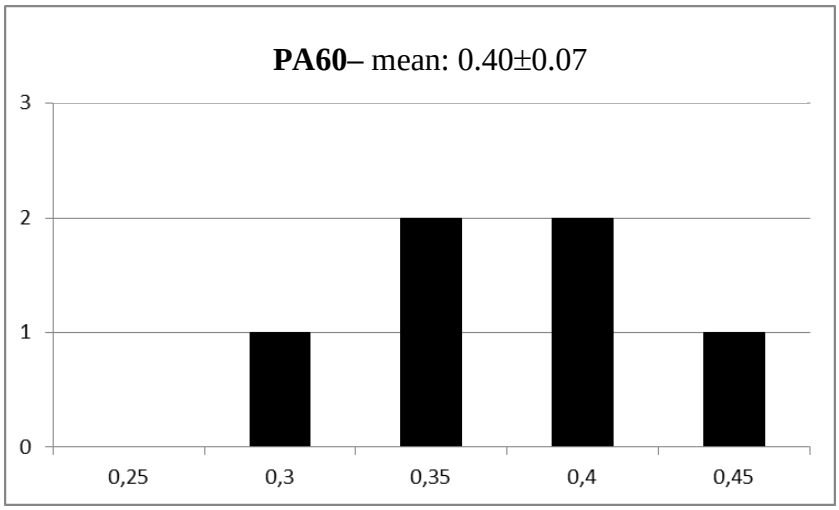

R_o% meas.	R_o% meas.
0.454	0.583
0.455	0.587
0.461	0.589
0.464	0.593
0.478	0.597
0.479	0.607
0.503	0.607
0.513	0.610
0.514	0.620
0.516	0.624
0.523	0.631
0.523	0.632
0.529	0.634
0.556	0.651
0.568	0.655
0.568	0.656
0.568	0.658
0.576	0.674
0.577	0.684

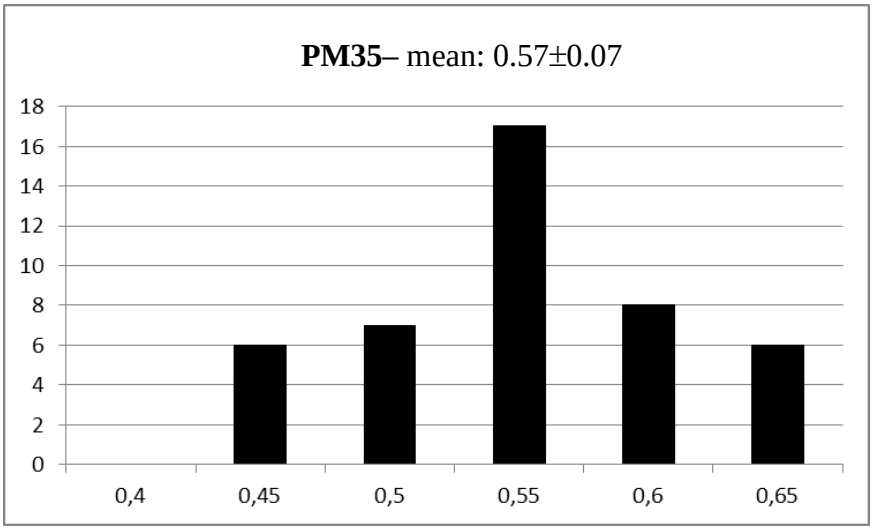

R_o% meas.
0.503
0.509
0.509
0.513
0.516
0.558
0.587
0.594

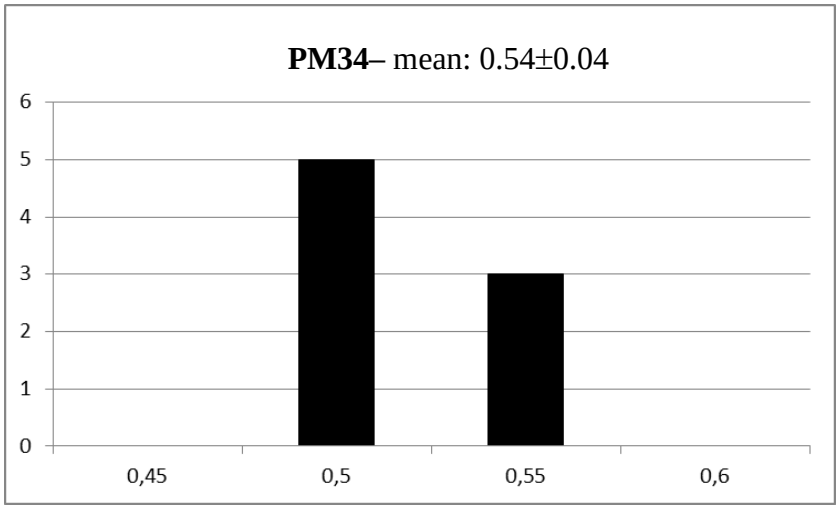

R_o% meas.
0.507
0.517
0.519
0.527
0.530
0.534
0.546
0.547
0.566
0.581
0.593
0.598
0.603
0.603
0.609
0.619
0.625
0.633

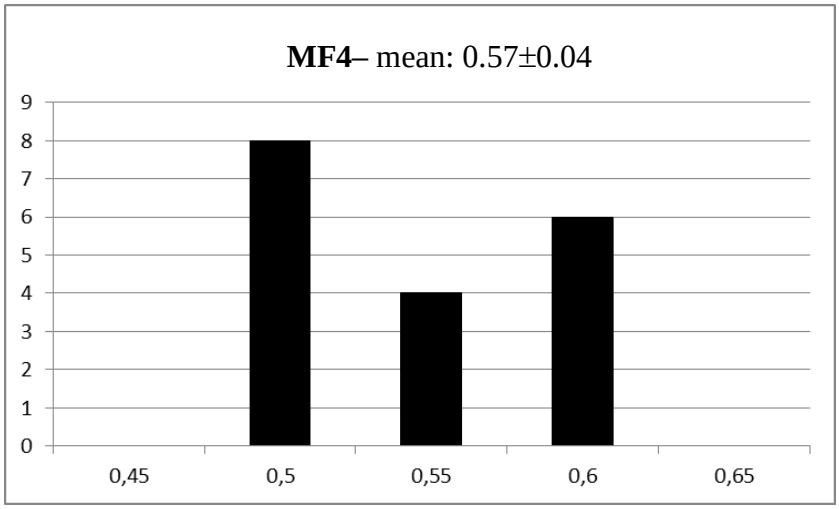

R_o% meas.
0.604
0.606
0.610
0.625
0.626
0.658
0.678
0.681
0.681
0.691
0.696
0.697
0.709
0.710
0.716
0.737

R_o% meas.
0.757
0.757
0.759
0.761
0.786
0.787
0.793
0.819
0.824
0.835
0.843
0.844
0.862
0.872
0.872

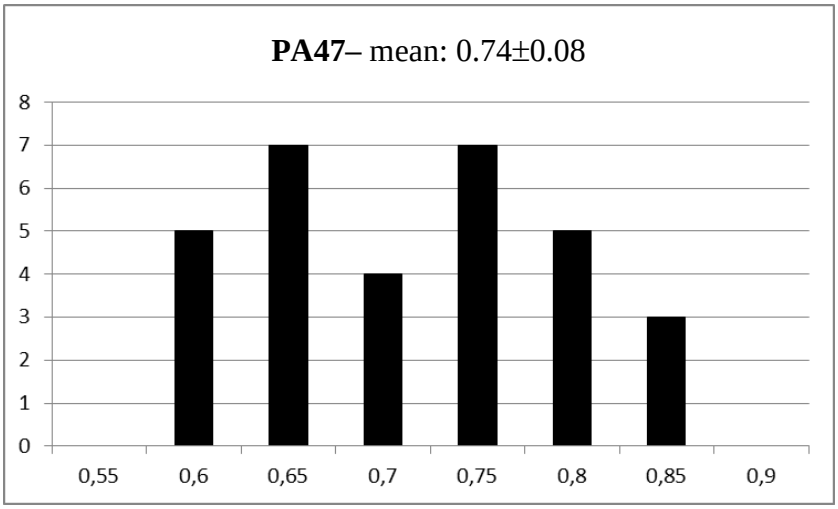

R_o% meas.
0.574
0.600
0.626
0.674
0.695
0.701
0.783
0.792

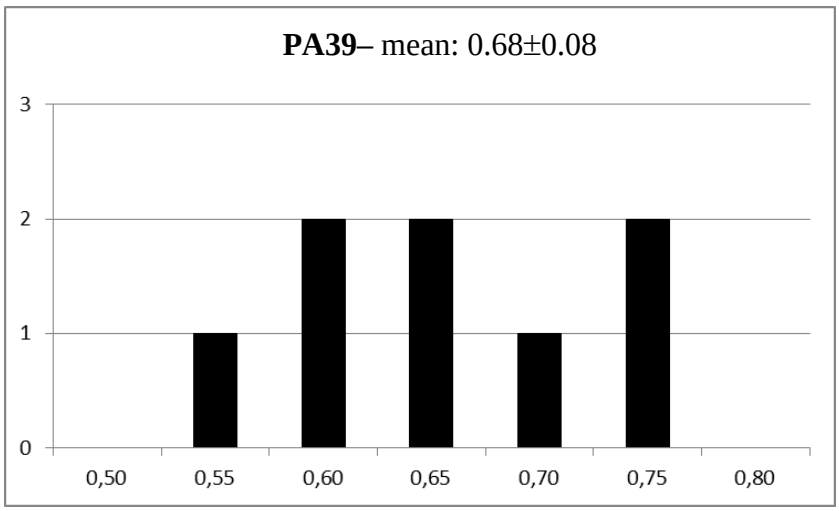

R_o% meas.
0.776
0.781
0.793
0.806
0.868
0.869
0.880
0.901

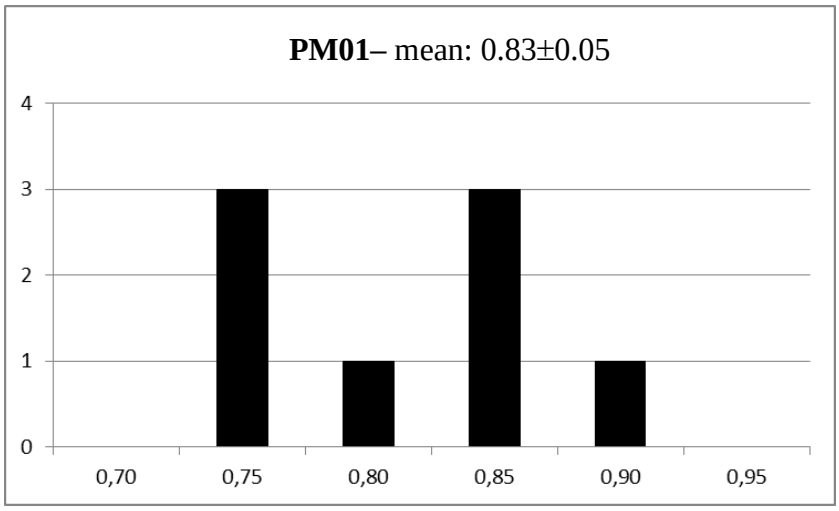

R_o% meas.
0.735
0.735
0.737
0.756
0.781
0.791
0.808
0.824
0.827
0.852
0.853
0.856
0.866
0.867
0.877
0.882

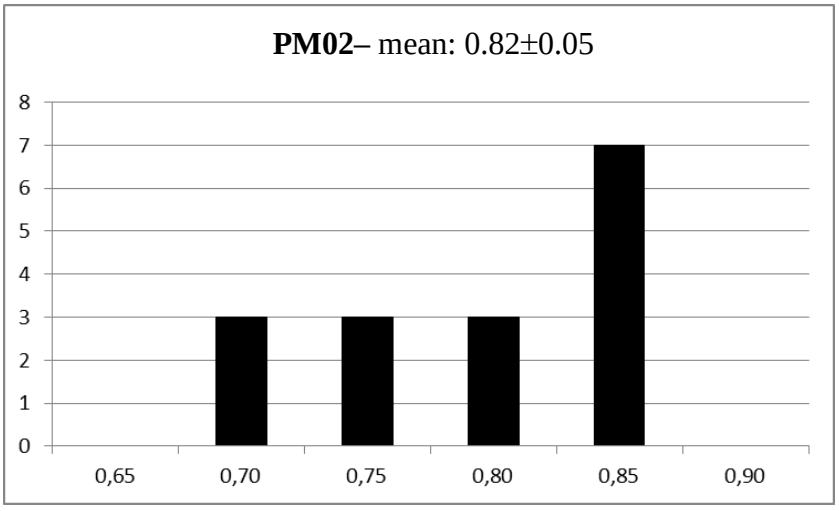

R_o% meas.	R_o% meas.
0.826	0.921
0.853	0.924
0.865	0.925
0.873	0.932
0.883	0.938
0.885	0.952
0.899	0.953
0.906	0.956
0.908	0.966
0.911	0.967
0.918	0.969
0.919	0.988
0.920	0.990

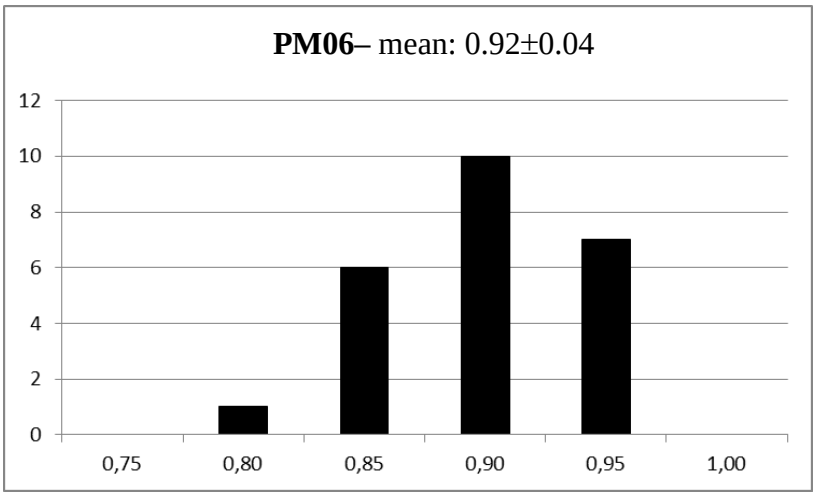

R_o% meas.
0.764
0.788
0.796
0.809
0.809
0.832
0.833
0.864
0.871
0.882

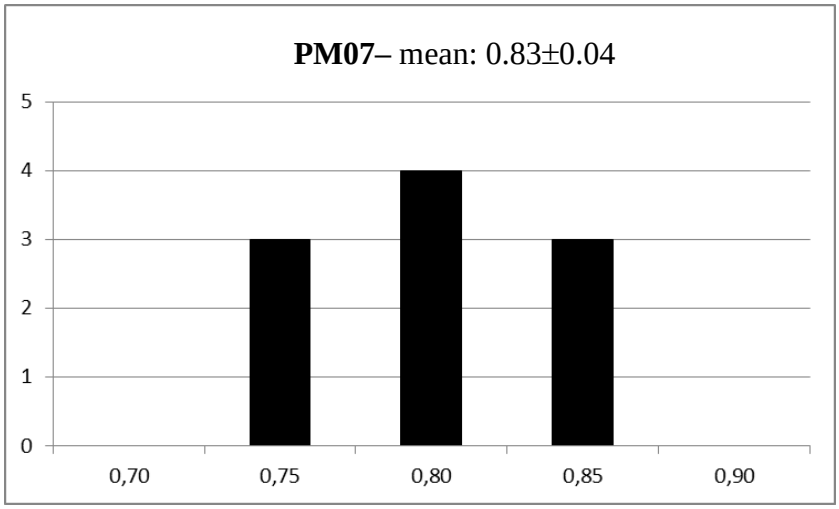

R_o% meas.
0.856
0.868
0.903
0.919
0.920
0.920
0.921
0.923
0.924
0.930
0.948
0.949
0.958
0.962
0.964
0.965
0.965
0.978

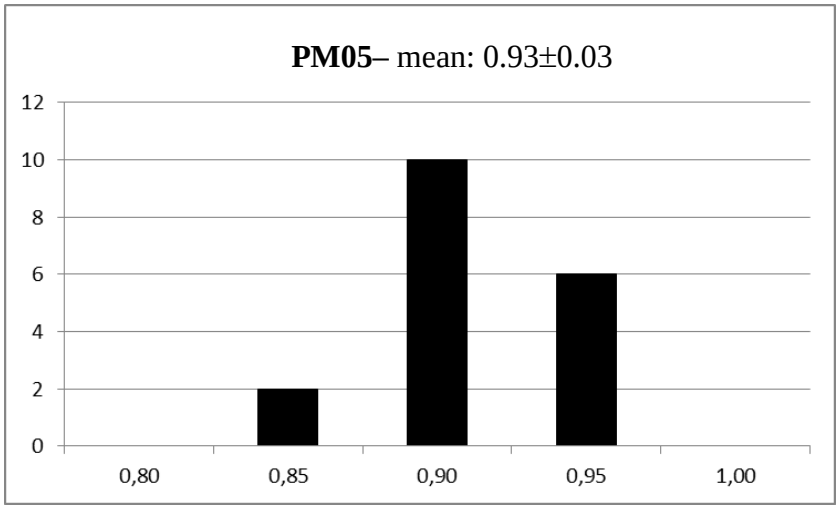

R_o% meas.
0.323
0.325
0.343
0.346
0.347
0.350
0.351
0.360
0.370
0.373
0.375
0.376
0.378
0.378
0.383
0.384
0.389
0.394
0.404
0.404
0.413
0.422
0.423

R_o% meas.
0.425
0.428
0.433
0.443
0.457
0.458
0.463
0.465
0.470
0.471
0.473
0.475
0.481
0.484
0.484
0.485
0.486
0.489
0.492
0.494
0.497
0.497

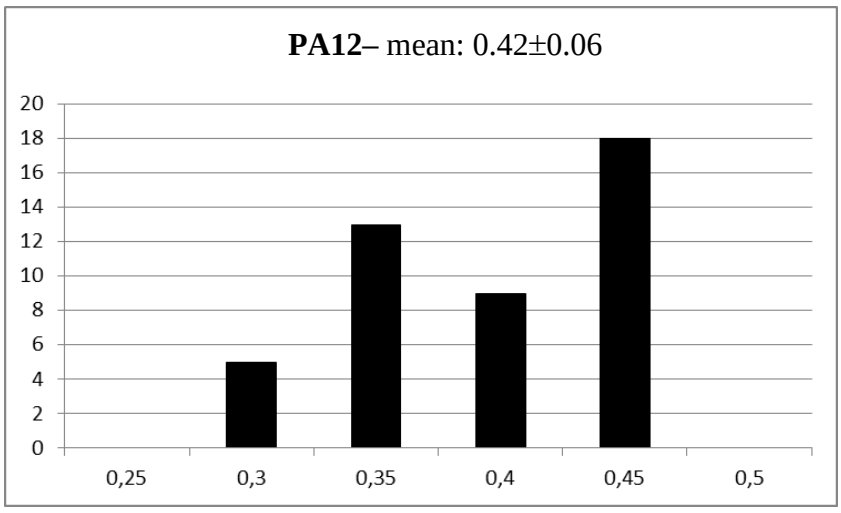

R_o% meas.
0.51
0.60
0.63
0.63
0.64

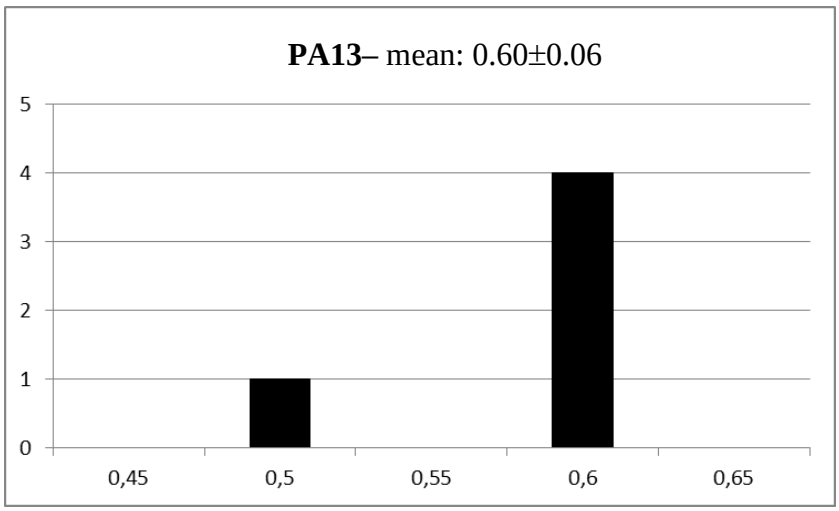

R_o% meas.
0.441
0.449
0.467
0.467
0.471
0.475
0.484
0.499
0.501
0.521
0.525
0.527
0.530
0.548
0.551

R_o% meas.
0.552
0.556
0.582
0.583
0.584
0.586
0.587
0.589
0.602
0.603
0.604
0.616
0.628
0.666
0.681
0.696

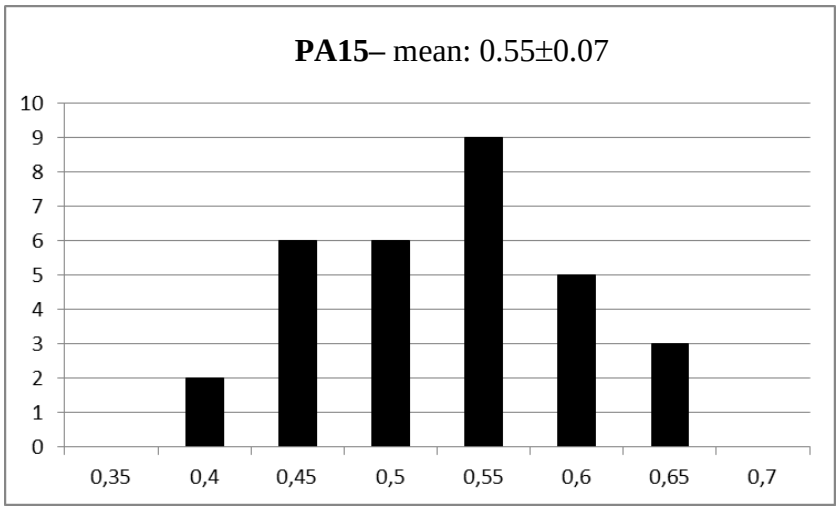

R_o% meas.
0.365
0.376
0.419
0.420
0.424
0.437
0.454
0.462
0.467
0.472

R_o% meas.
0.481
0.500
0.504
0.507
0.527
0.573
0.602
0.602
0.622

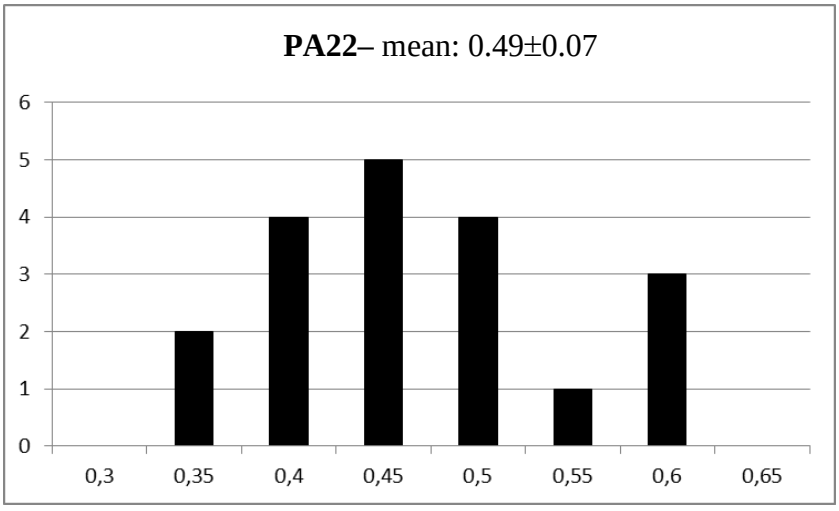

R_o% meas.
0.377
0.423
0.432
0.451
0.465
0.487
0.564
0.579
0.588

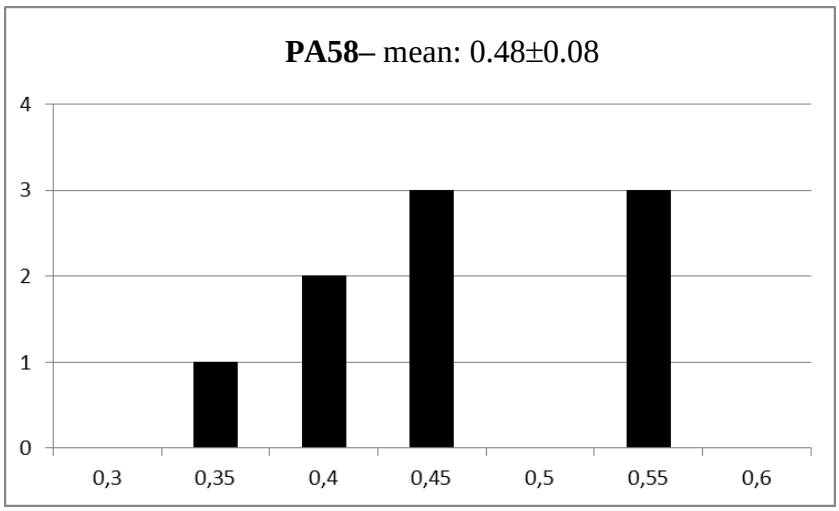

R_o% meas.	R_o% meas.
0.303	0.372
0.305	0.403
0.311	0.403
0.315	0.408
0.320	0.417
0.321	0.429
0.322	0.443
0.325	0.455
0.326	0.464
0.327	0.465
0.328	0.468
0.355	0.486
0.359	0.506
0.366	0.511
0.368	0.537
0.369	0.538

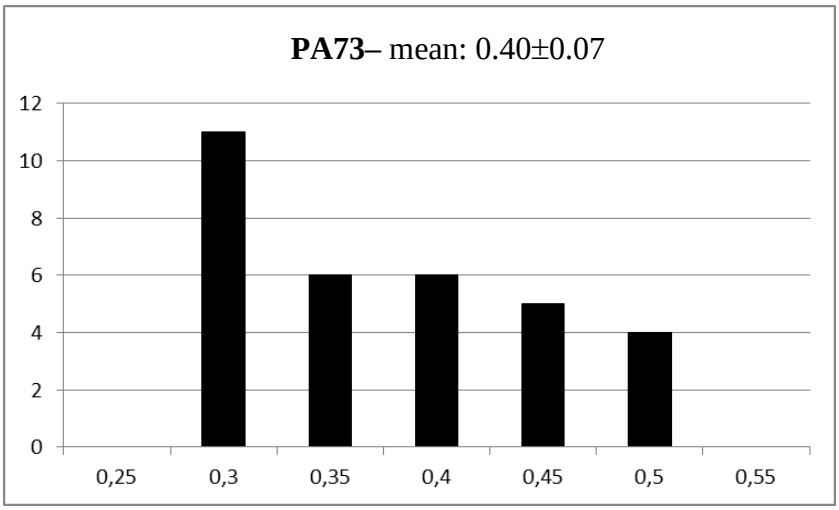

R_o% meas.
0.512
0.513
0.514
0.516
0.541
0.565
0.577
0.630
0.632
0.632
0.655
0.695

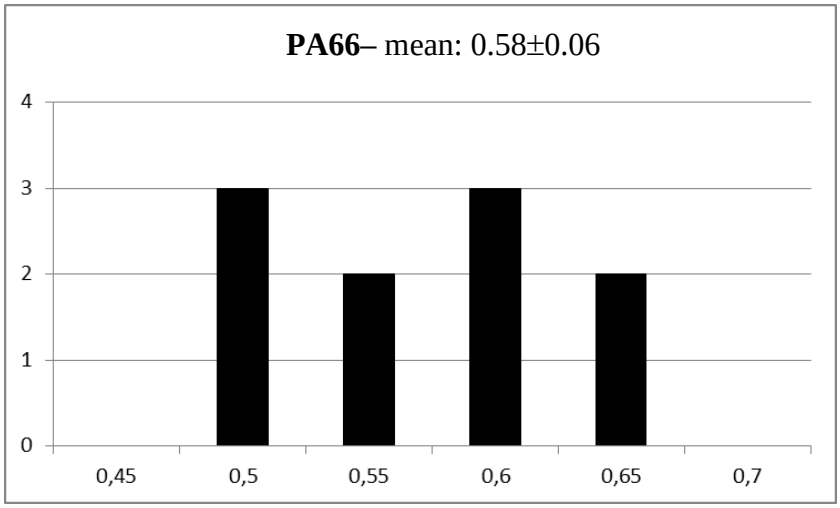

R_o% meas.	R_o% meas.
0.555	0.671
0.565	0.679
0.566	0.682
0.593	0.688
0.600	0.720
0.607	0.752
0.607	0.765
0.615	0.766
0.636	0.771
0.649	0.776
0.649	0.788
0.652	0.788
0.664	0.793
0.664	0.799

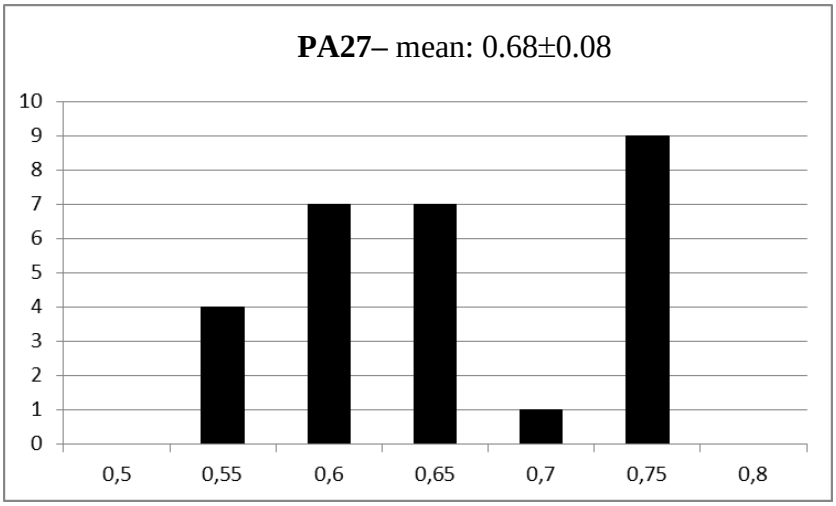

R_o% meas.	R_o% meas.
0.538	0.635
0.556	0.640
0.559	0.642
0.567	0.643
0.583	0.673
0.588	0.674
0.614	0.707
0.615	0.719
0.616	0.727
0.630	0.727
0.631	0.748

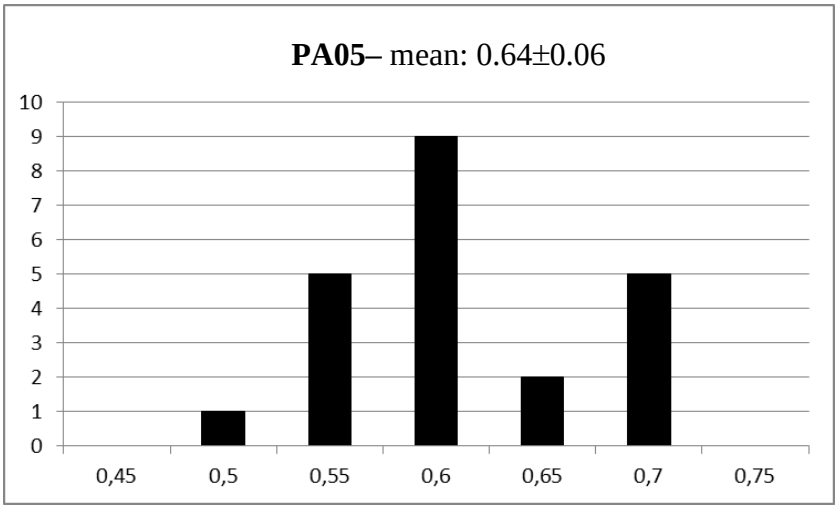

R_o% meas.	R_o% meas.
0.356	0.477
0.386	0.486
0.388	0.497
0.395	0.498
0.398	0.499
0.400	0.507
0.416	0.511
0.422	0.520
0.427	0.535
0.434	0.556
0.435	0.563
0.436	0.579
0.441	0.586
0.464	0.586
0.468	0.590

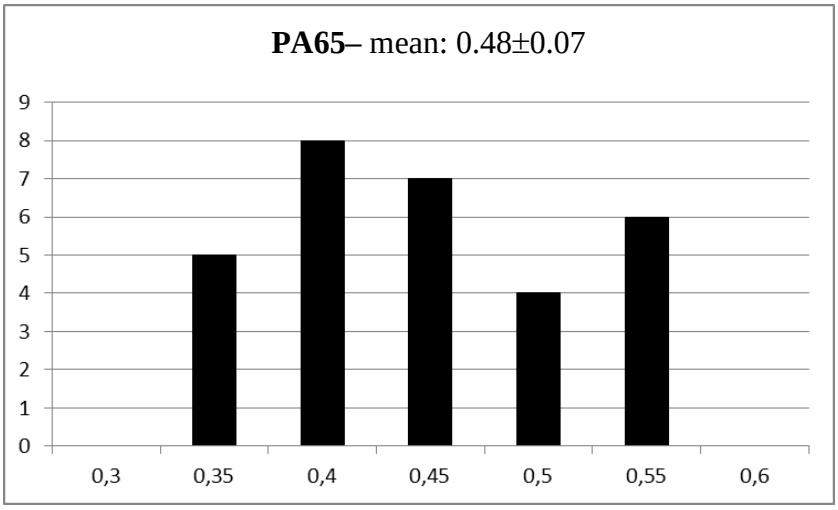

R_o% meas.
0.871
0.880
0.881
0.884
0.919
0.960
0.988
1.012
1.033
1.033

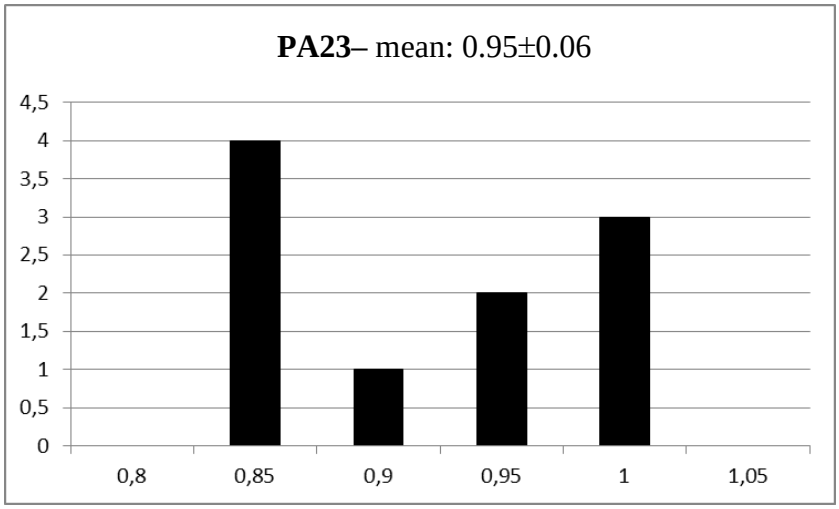

R_o% meas.
0.761
0.779
0.822
0.849
0.850
0.867
0.918
0.940
0.944
0.946
0.972
0.987

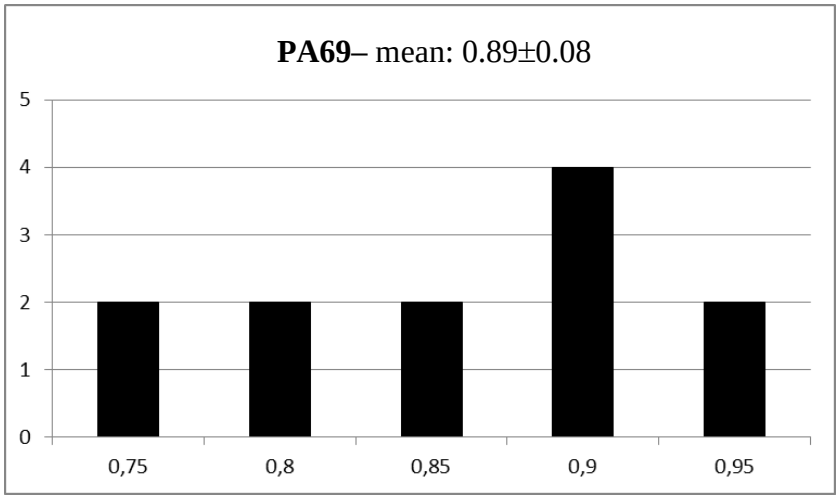

R_o% meas.
0.350
0.352
0.388
0.411
0.442
0.446
0.479
0.493
0.508
0.509
0.512
0.569
0.575
0.598

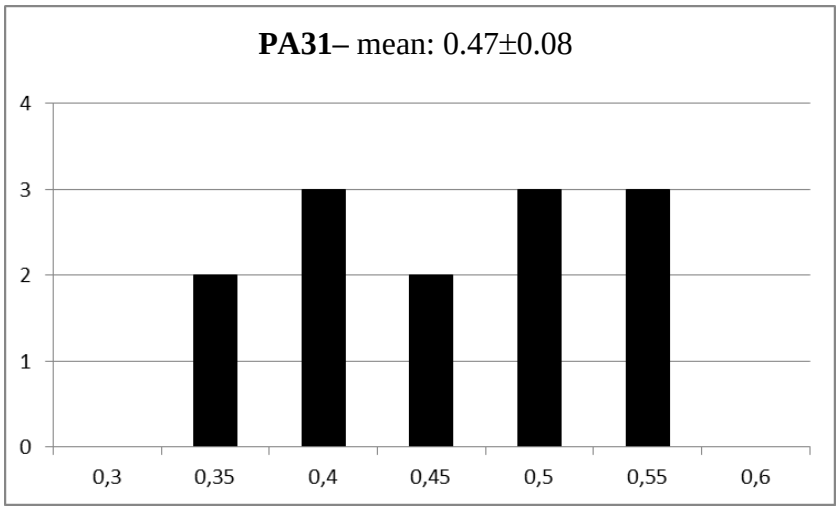

R_o% meas.
0.257
0.299
0.316
0.323
0.329
0.332
0.344
0.369
0.410
0.414
0.425
0.440
0.476
0.494

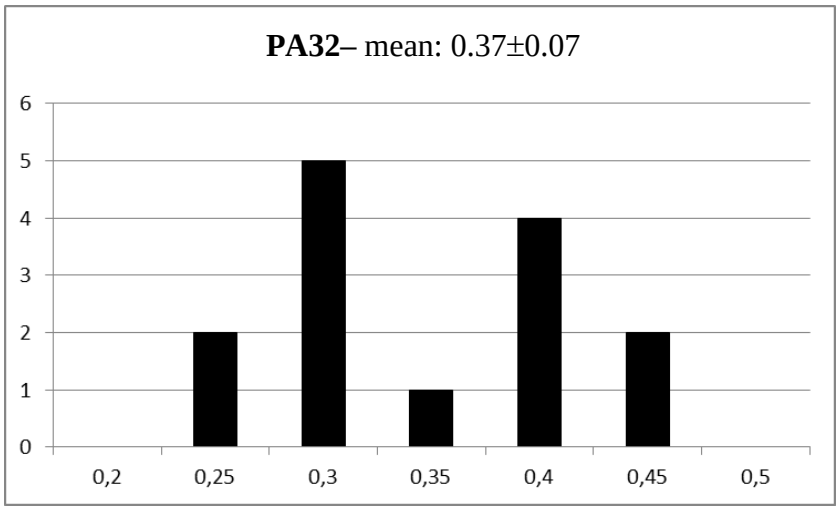

R_o% meas.
0.245
0.298
0.299
0.302
0.317
0.337
0.338
0.345
0.346
0.347
0.355
0.362
0.366
0.384
0.392
0.420
0.438
0.439

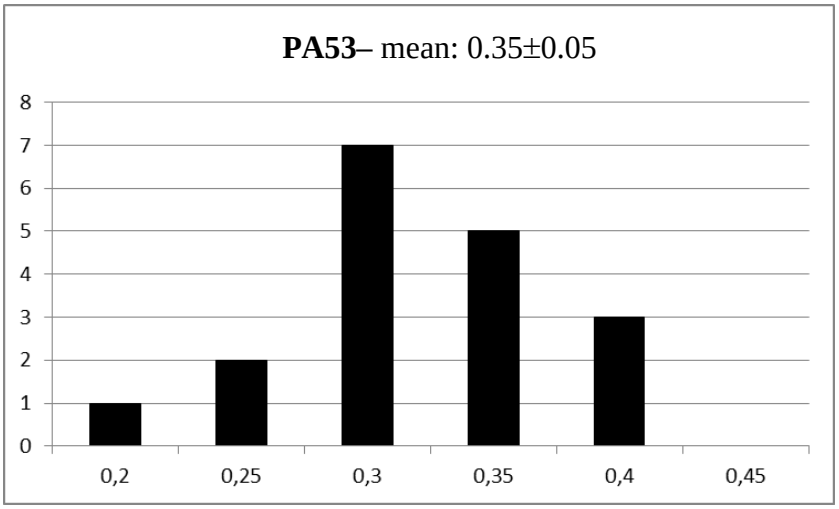

R_o% meas.
0.250
0.272
0.294
0.314
0.320
0.354
0.364
0.365
0.369
0.448

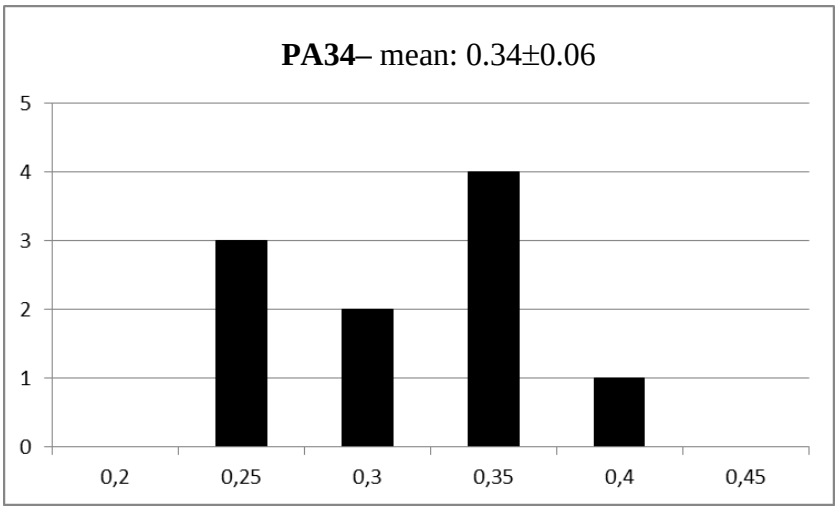

R_o% meas.
0.305
0.338
0.349
0.393
0.414
0.436

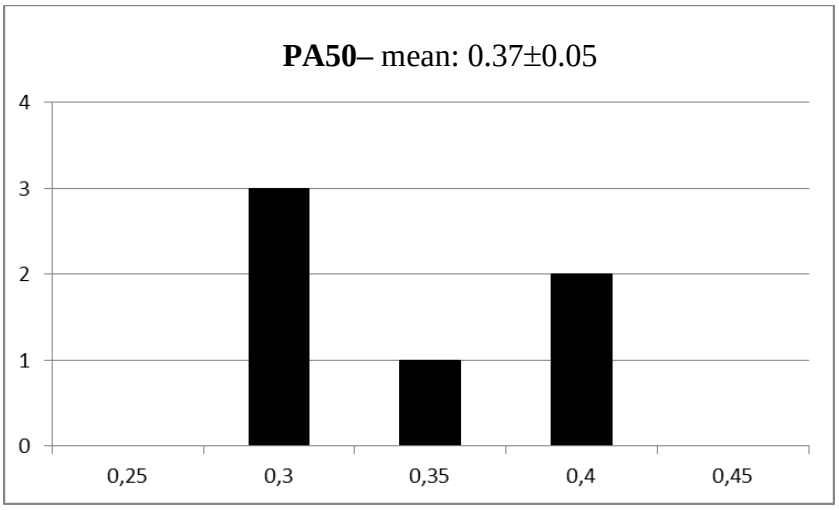

R_o% meas.
0.204
0.206
0.218
0.223
0.237
0.239
0.243
0.243
0.245
0.258
0.259
0.264
0.268
0.270
0.270
0.279
0.283
0.284
0.289
0.292
0.297
0.310

R_o% meas.
0.311
0.317
0.321
0.329
0.331
0.333
0.336
0.340
0.341
0.341
0.343
0.348
0.349
0.350
0.351
0.351
0.366
0.369
0.373
0.374
0.377
0.380
0.385

R_o% meas.
0.389
0.393
0.394
0.395
0.401
0.402
0.404
0.409
0.410
0.414
0.418
0.418
0.427
0.429
0.431
0.431
0.432
0.433
0.435
0.438
0.442
0.445
0.449

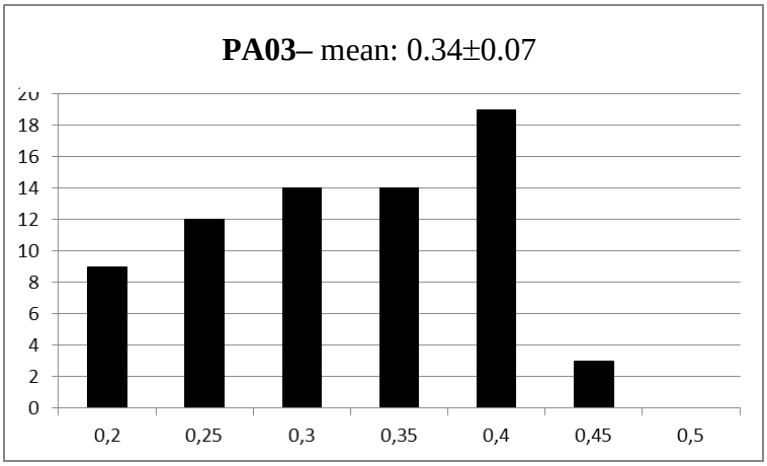

R_o% meas.
0.350
0.350
0.370
0.380
0.392
0.396
0.401
0.409
0.413
0.431
0.432
0.466
0.468

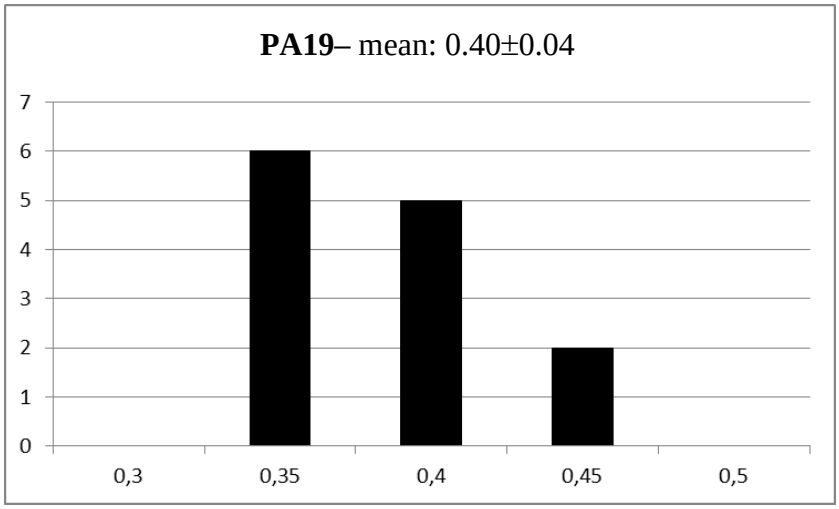

X-ray diffraction on (<2 μm) clay minerals

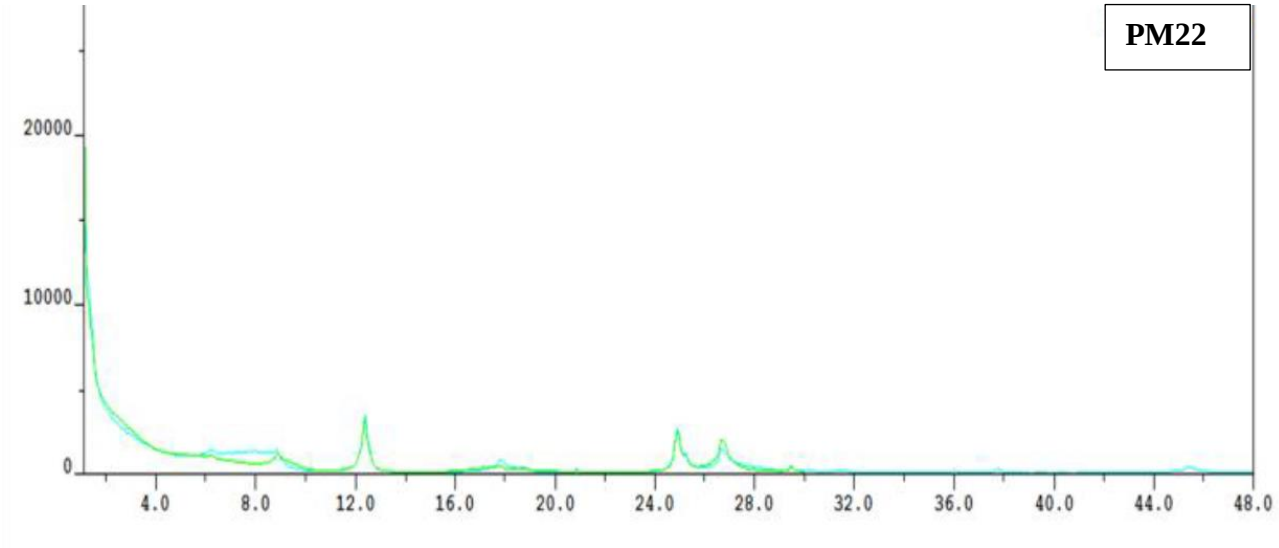

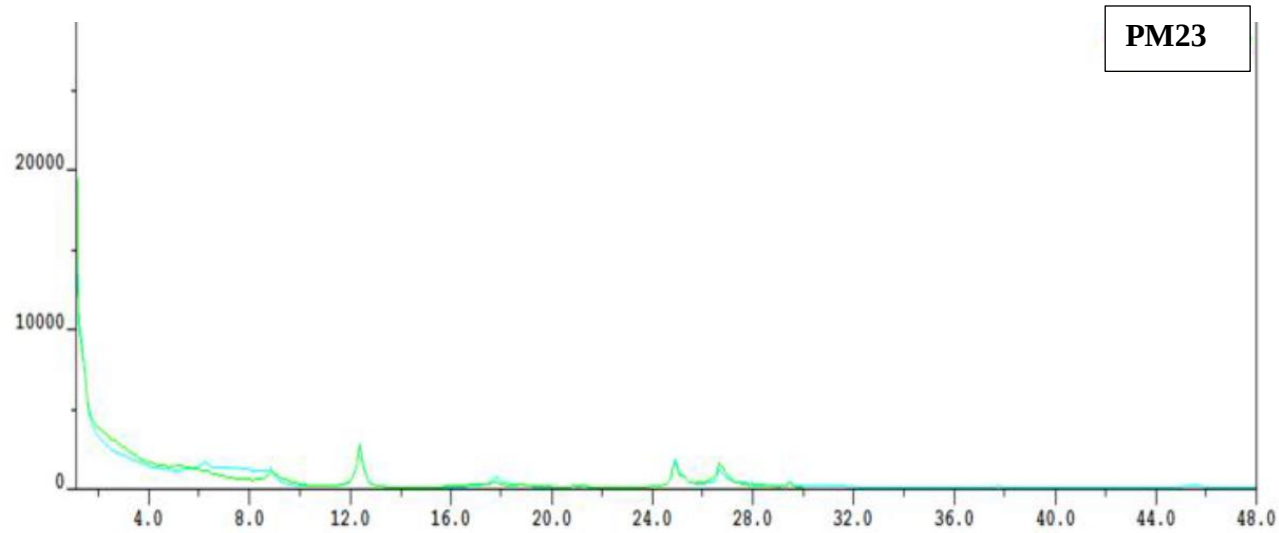

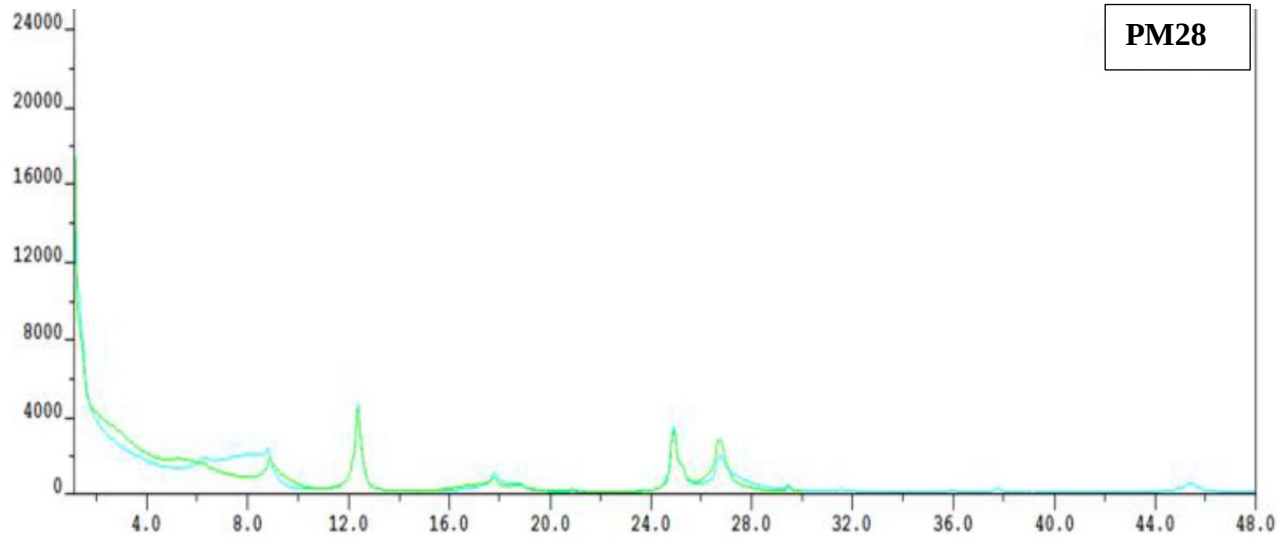

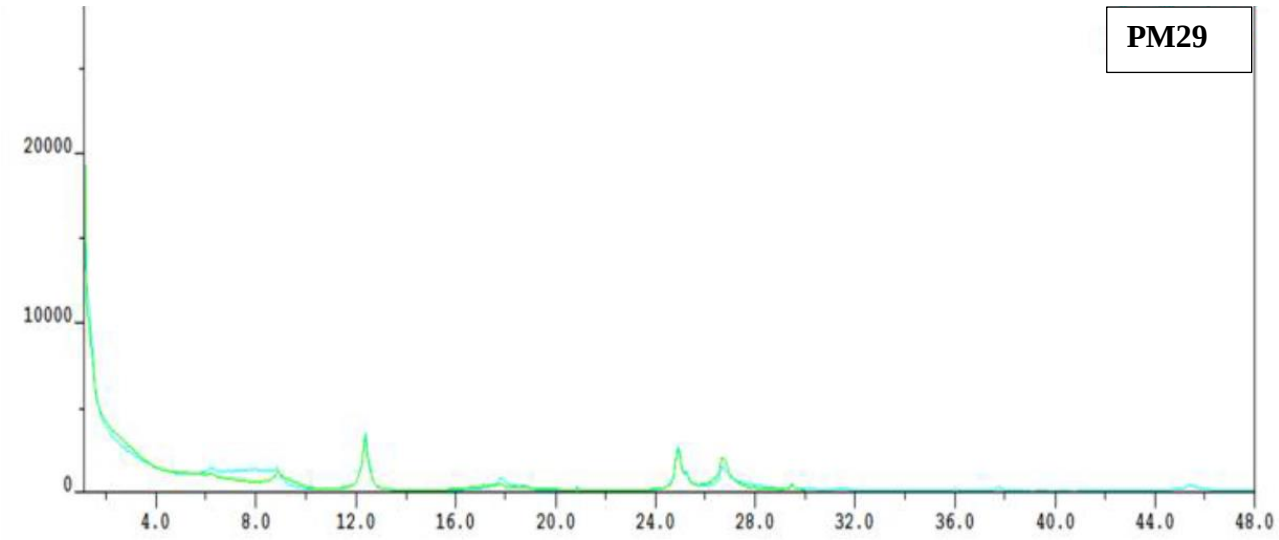
PM29
20000
10000
0
4.0
8.0
12.0
16.0
20.0
24.0
28.0
32.0
36.0
40.0
44.0
48.0

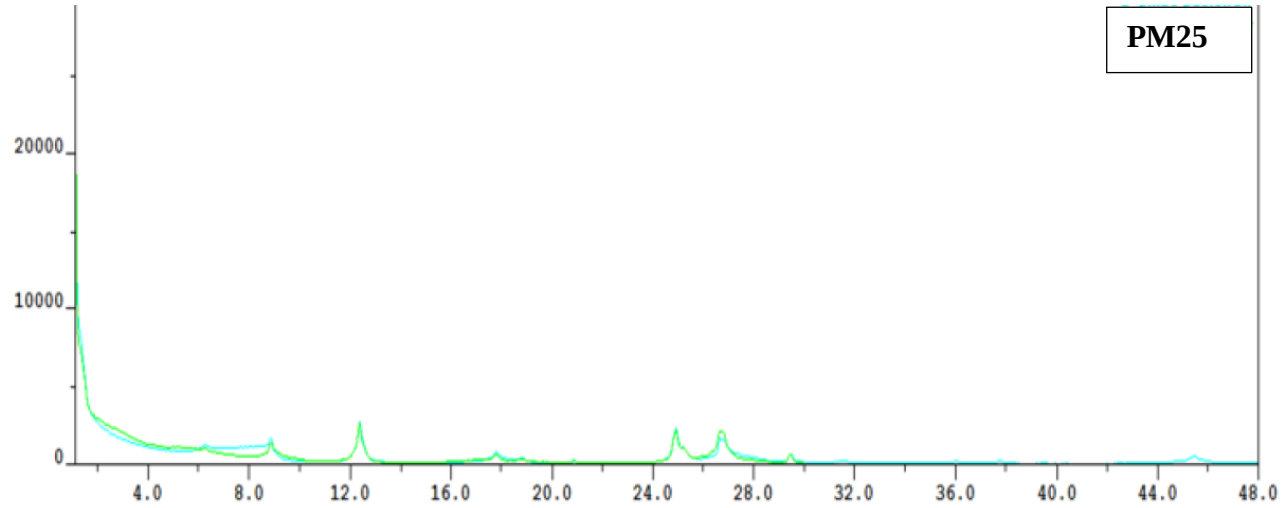
PM25
20000
10000
0
4.0
8.0
12.0
16.0
20.0
24.0
28.0
32.0
36.0
40.0
44.0
48.0

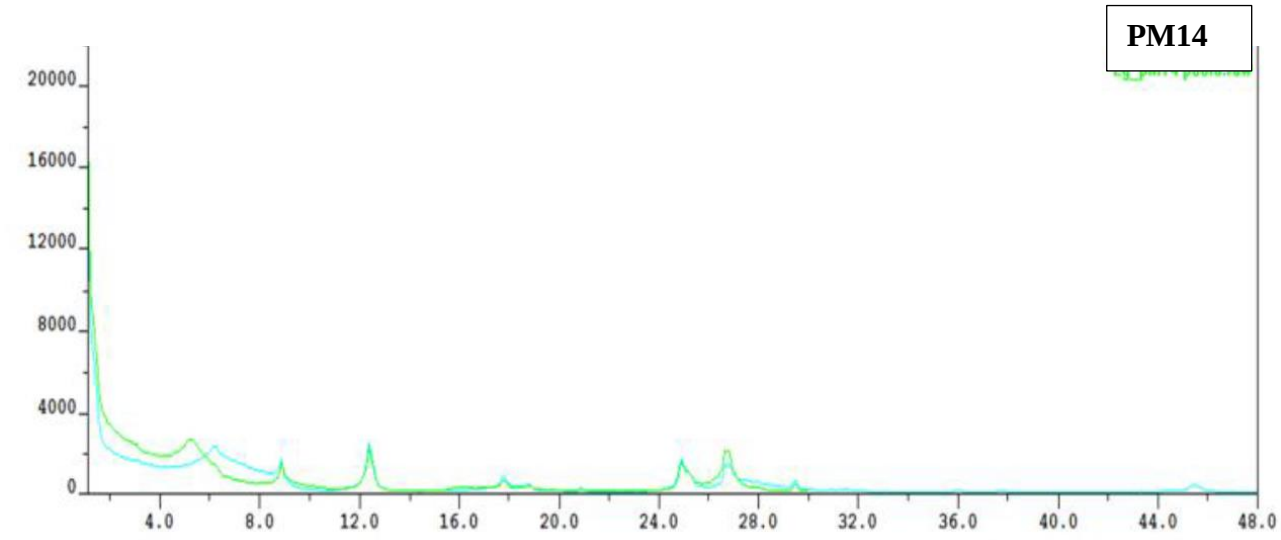
PM14
20000
16000
12000
8000
4000
0
4.0
8.0
12.0
16.0
20.0
24.0
28.0
32.0
36.0
40.0
44.0
48.0

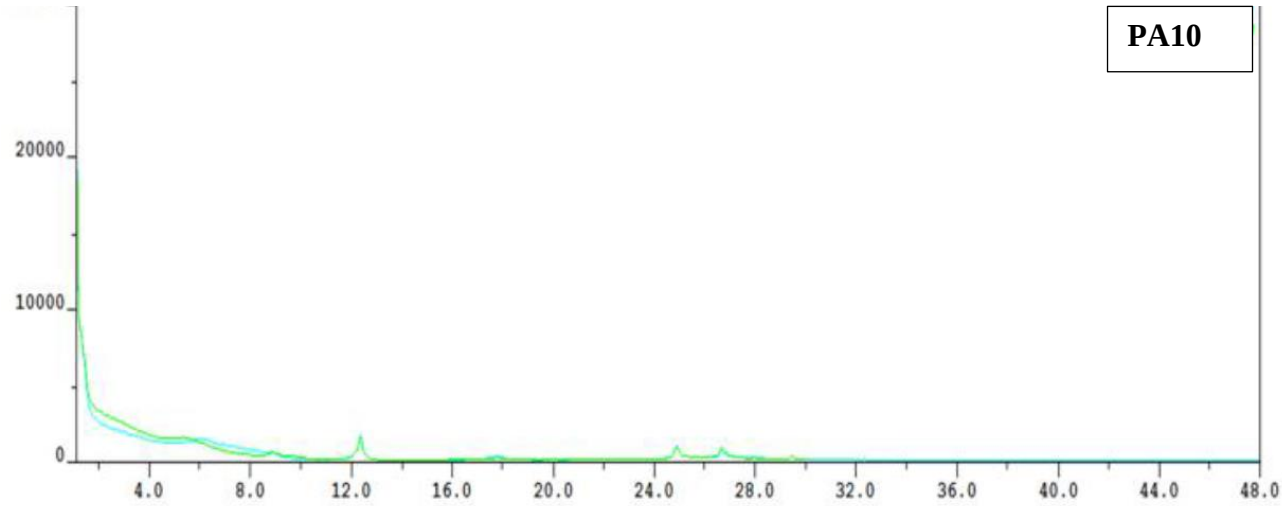
PA10
20000
10000
0
4.0
8.0
12.0
16.0
20.0
24.0
28.0
32.0
36.0
40.0
44.0
48.0

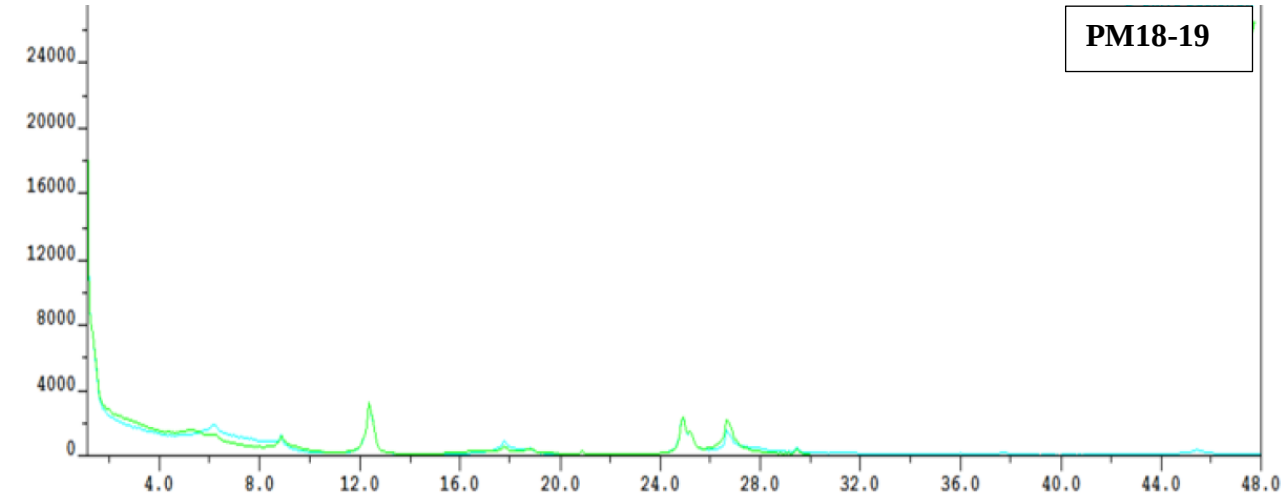
PM18-19
24000
20000
16000
12000
8000
4000
0
4.0
8.0
12.0
16.0
20.0
24.0
28.0
32.0
36.0
40.0
44.0
48.0

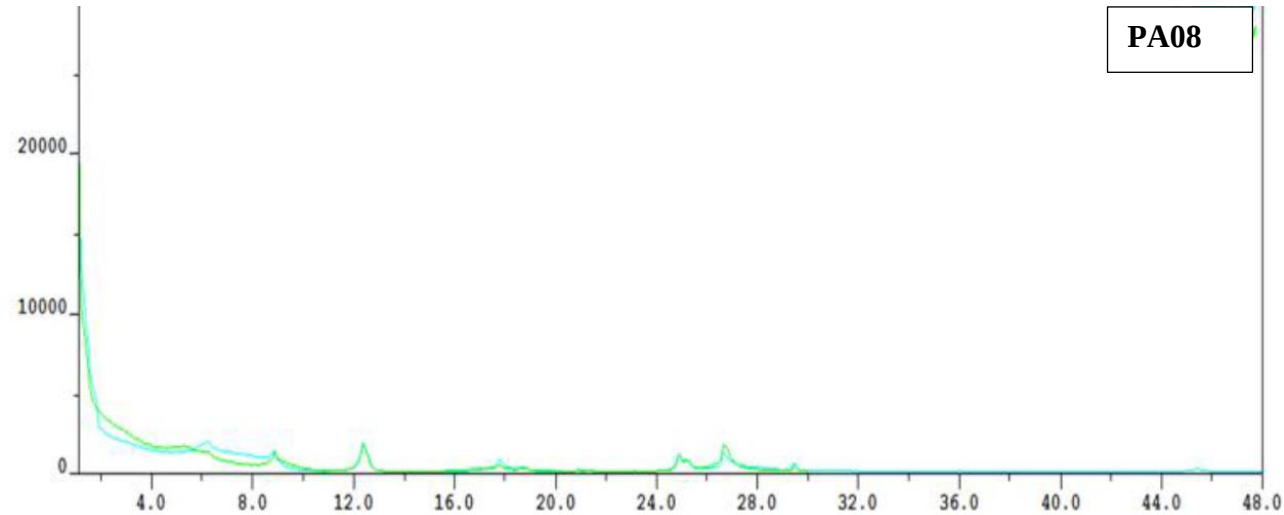
PA08
20000
10000
0
4.0
8.0
12.0
16.0
20.0
24.0
28.0
32.0
36.0
40.0
44.0
48.0

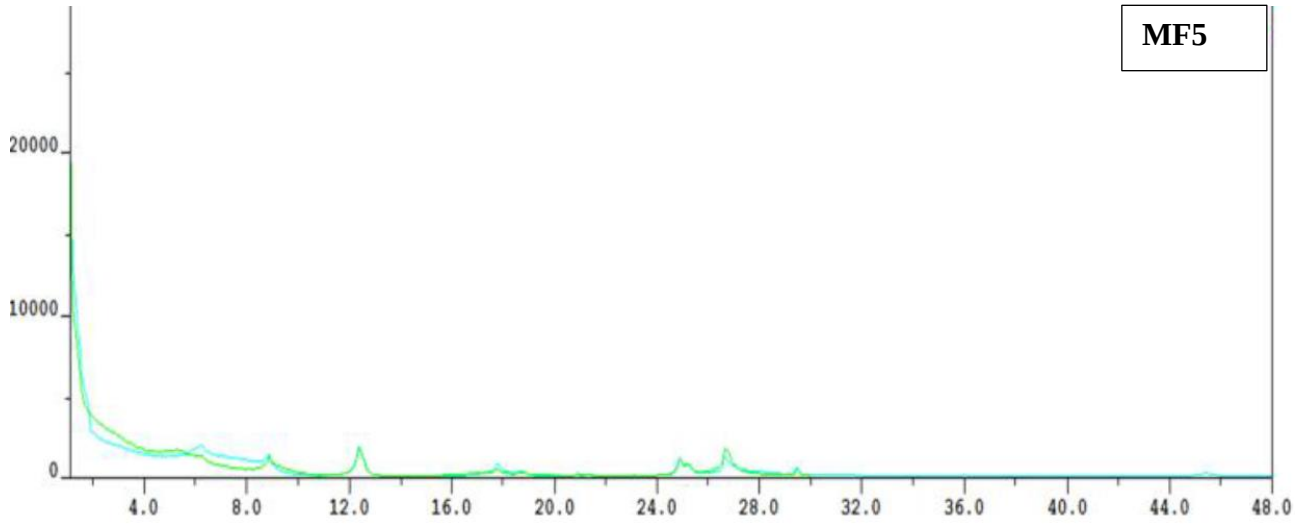
MF5
20000
10000
0
4.0
8.0
12.0
16.0
20.0
24.0
28.0
32.0
36.0
40.0
44.0
48.0

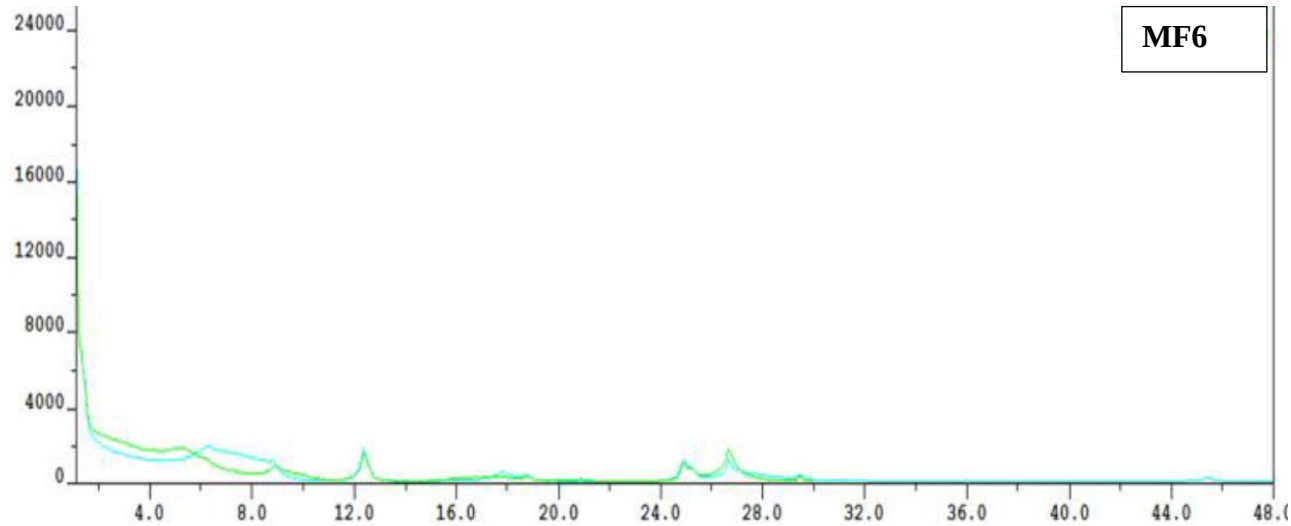
MF6
24000
20000
16000
12000
8000
4000
0
4.0
8.0
12.0
16.0
20.0
24.0
28.0
32.0
36.0
40.0
44.0

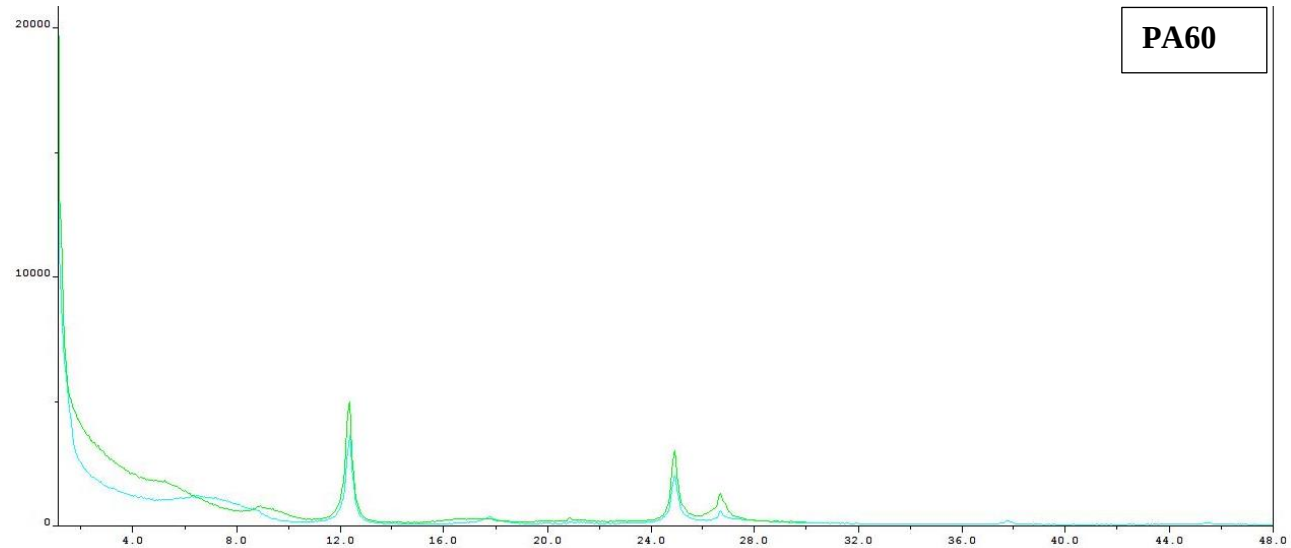
PA60
20000
10000
0
4.0
8.0
12.0
16.0
20.0
24.0
28.0
32.0
36.0
40.0
44.0
48.0

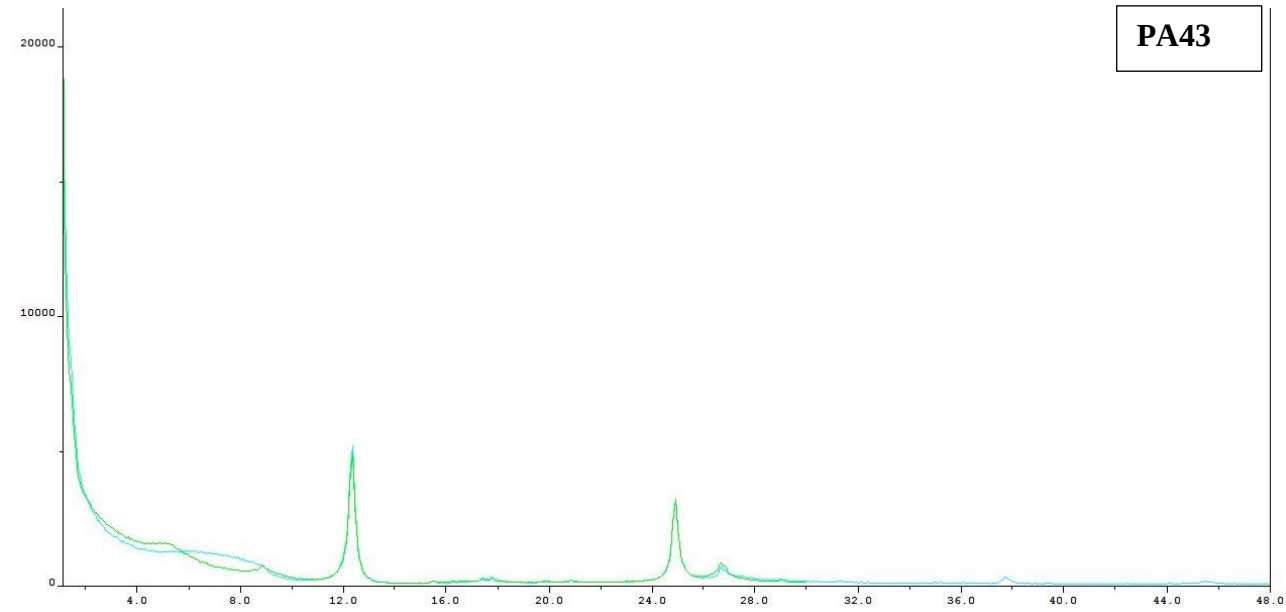
PA43
20000
10000
0
4.0
8.0
12.0
16.0
20.0
24.0
28.0
32.0
36.0
40.0
44.0
48.0

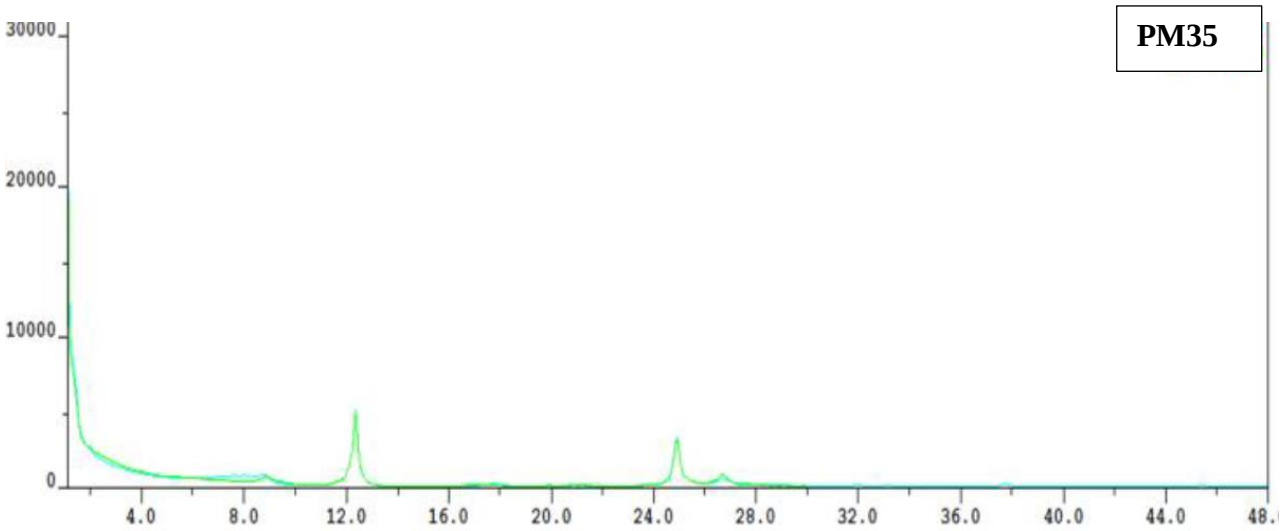
PM35
30000
20000
10000
0
4.0
8.0
12.0
16.0
20.0
24.0
28.0
32.0
36.0
40.0
44.0

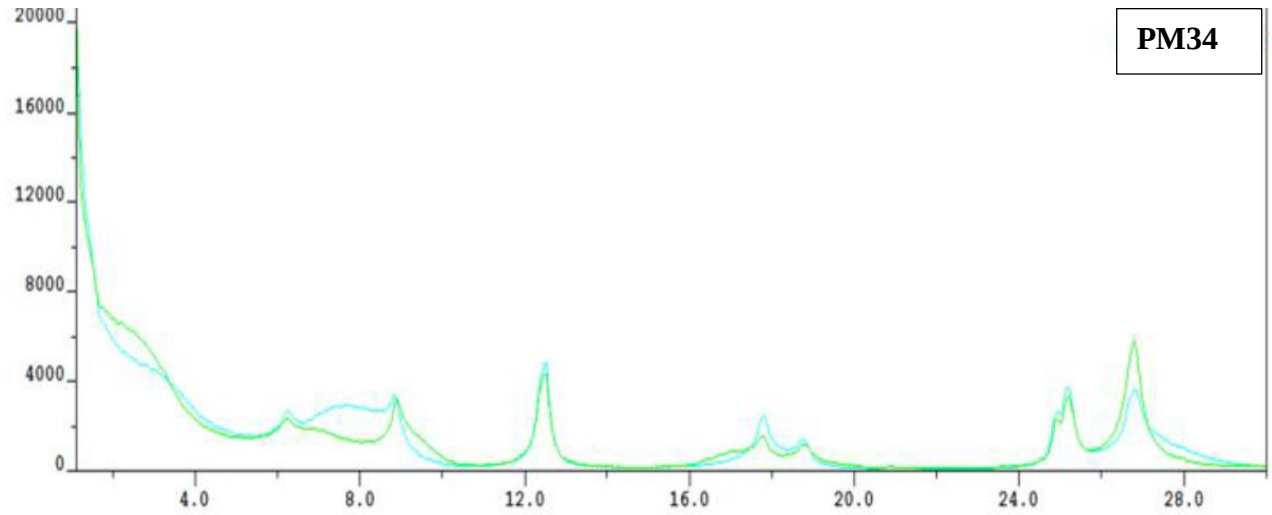
PM34
20000
16000
12000
8000
4000
0
4.0
8.0
12.0
16.0
20.0
24.0
28.0

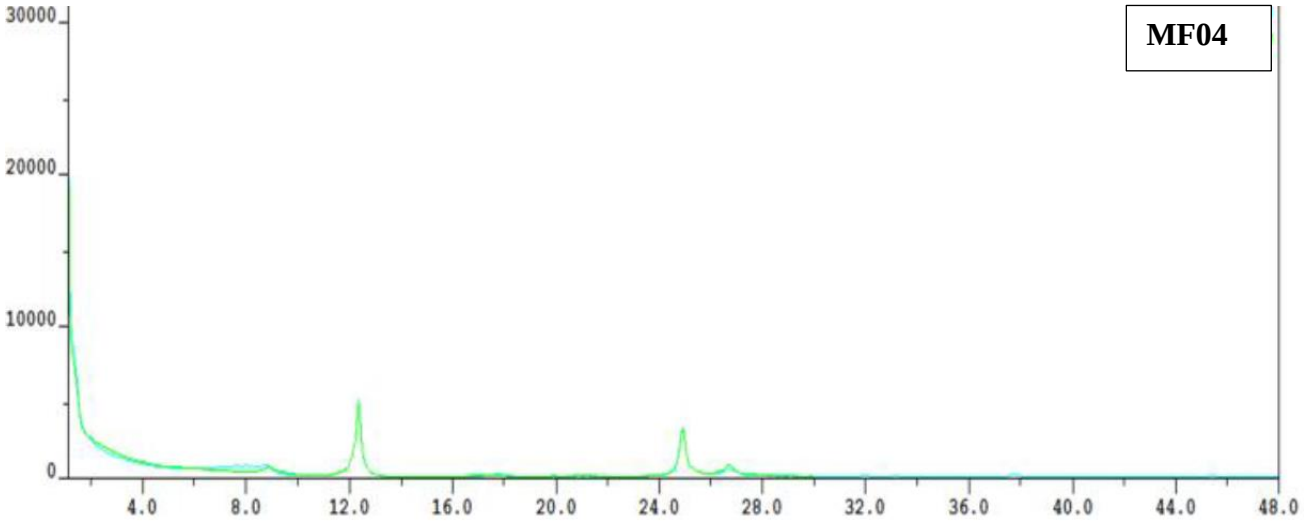
MF04
30000
20000
10000
0
4.0
8.0
12.0
16.0
20.0
24.0
28.0
32.0
36.0
40.0
44.0
48.0

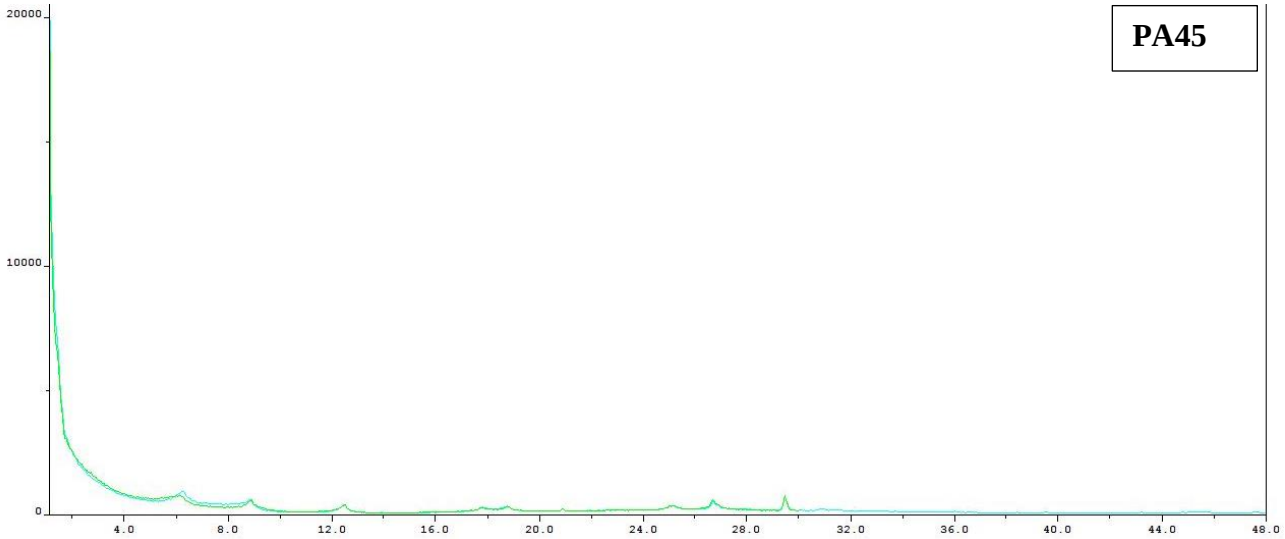
PA45
20000
10000
0
4.0
8.0
12.0
16.0
20.0
24.0
28.0
32.0
36.0
40.0
44.0
48.0

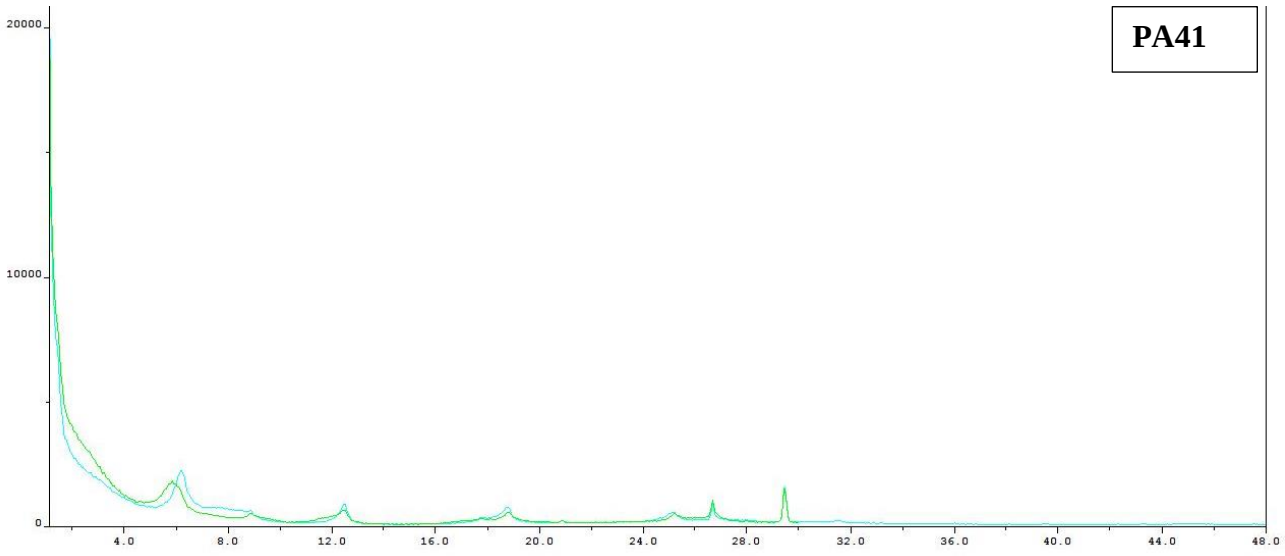
PA41
20000
10000
0
4.0
8.0
12.0
16.0
20.0
24.0
28.0
32.0
36.0
40.0
44.0
48.0

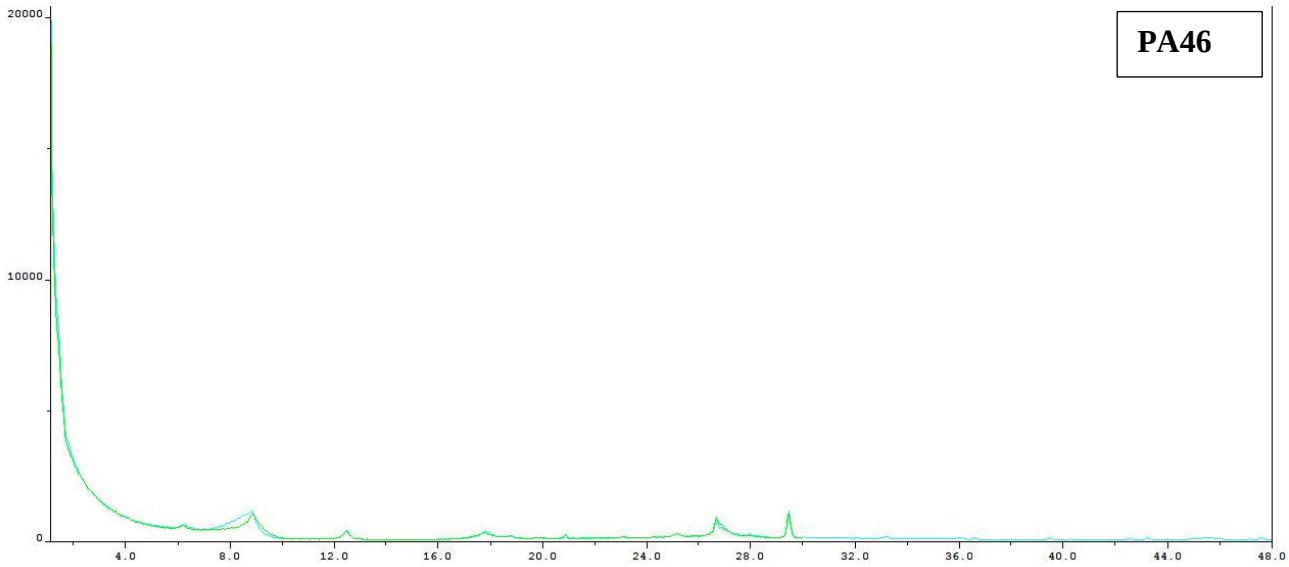
PA46
20000
10000
0
4.0
8.0
12.0
16.0
20.0
24.0
28.0
32.0
36.0
40.0
44.0
48.0

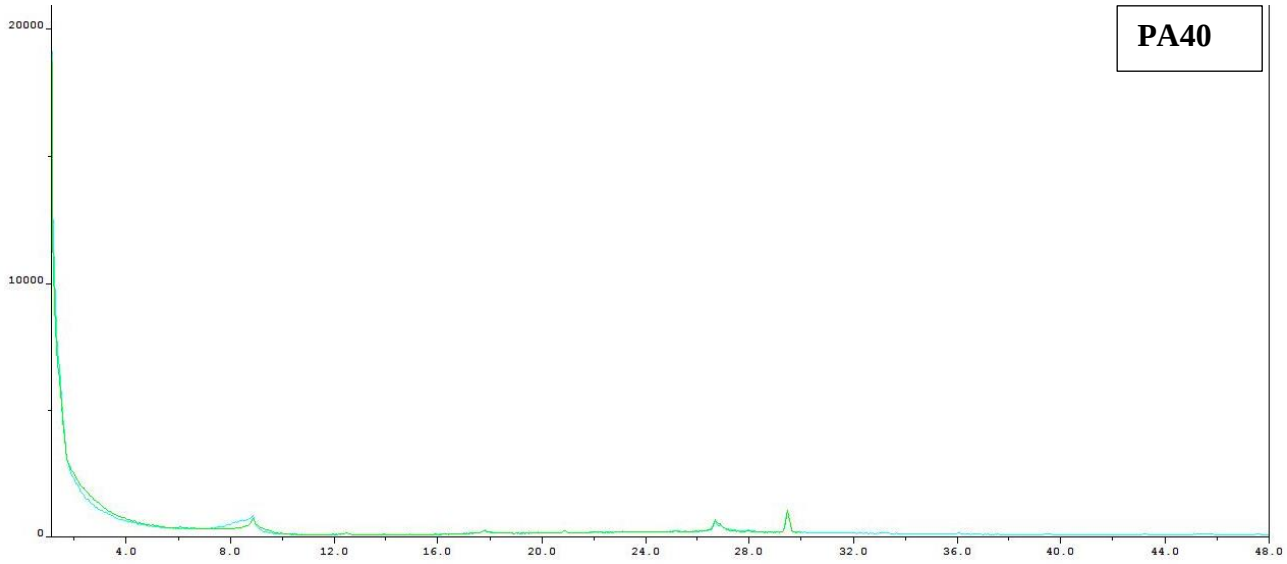
PA40
20000
10000
0
4.0
8.0
12.0
16.0
20.0
24.0
28.0
32.0
36.0
40.0
44.0
48.0

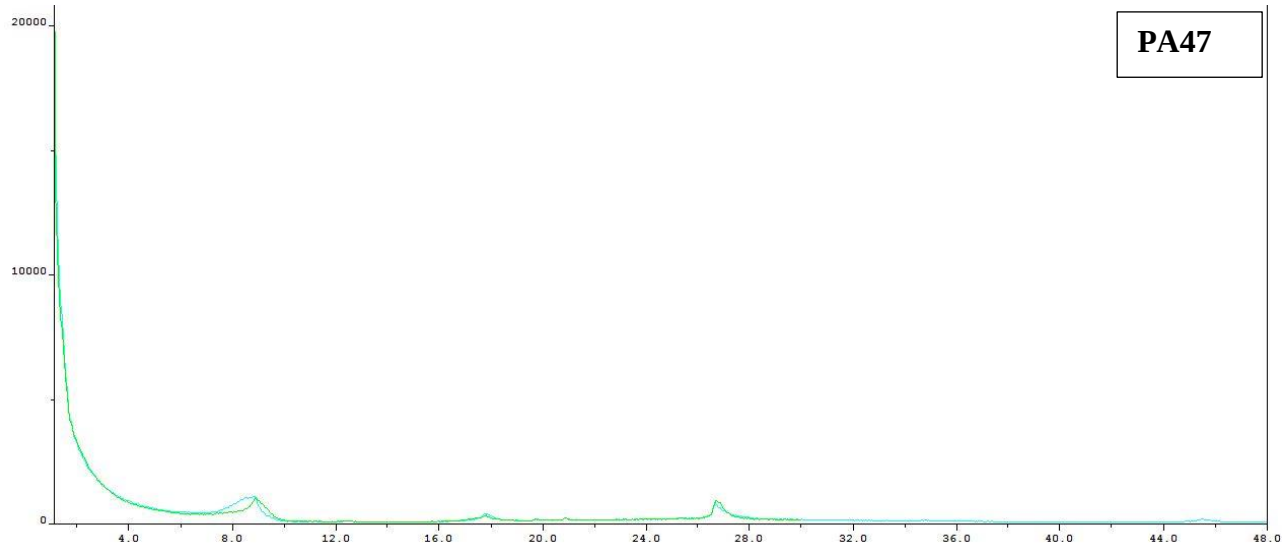
PA47
20000
10000
0
4.0
8.0
12.0
16.0
20.0
24.0
28.0
32.0
36.0
40.0
44.0
48.0

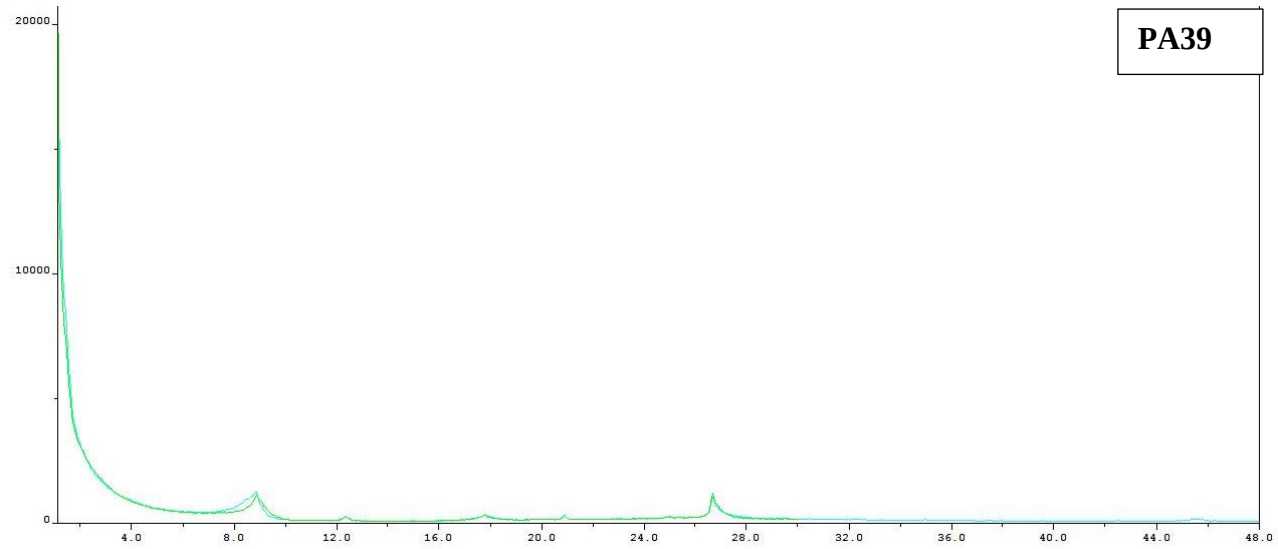
PA39
20000
10000
0
4.0
8.0
12.0
16.0
20.0
24.0
28.0
32.0
36.0
40.0
44.0
48.0

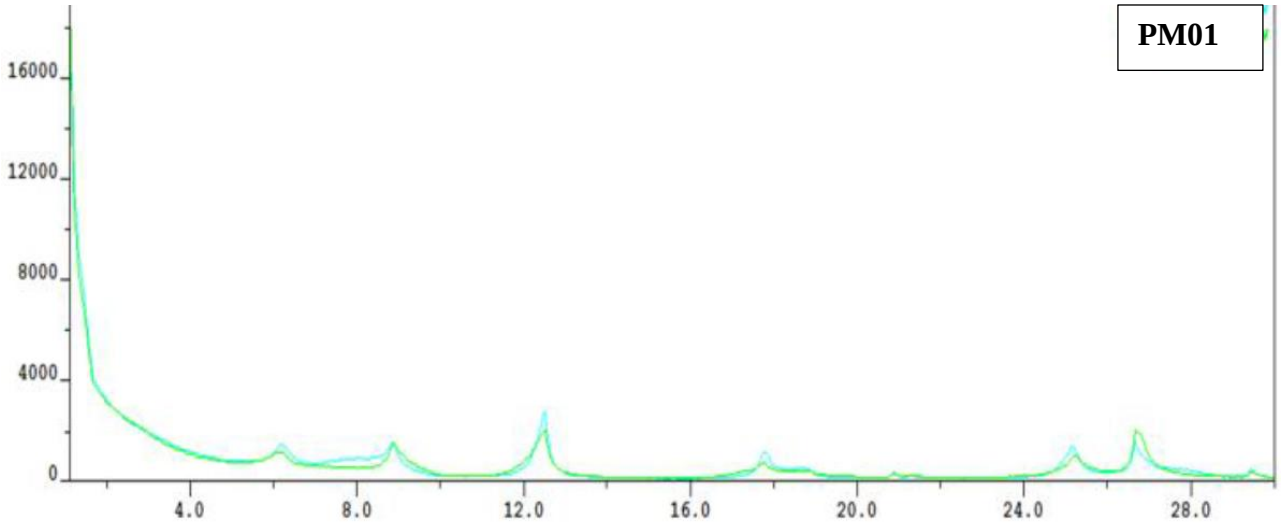
PM01
16000
12000
8000
4000
0
4.0
8.0
12.0
16.0
20.0
24.0
28.0

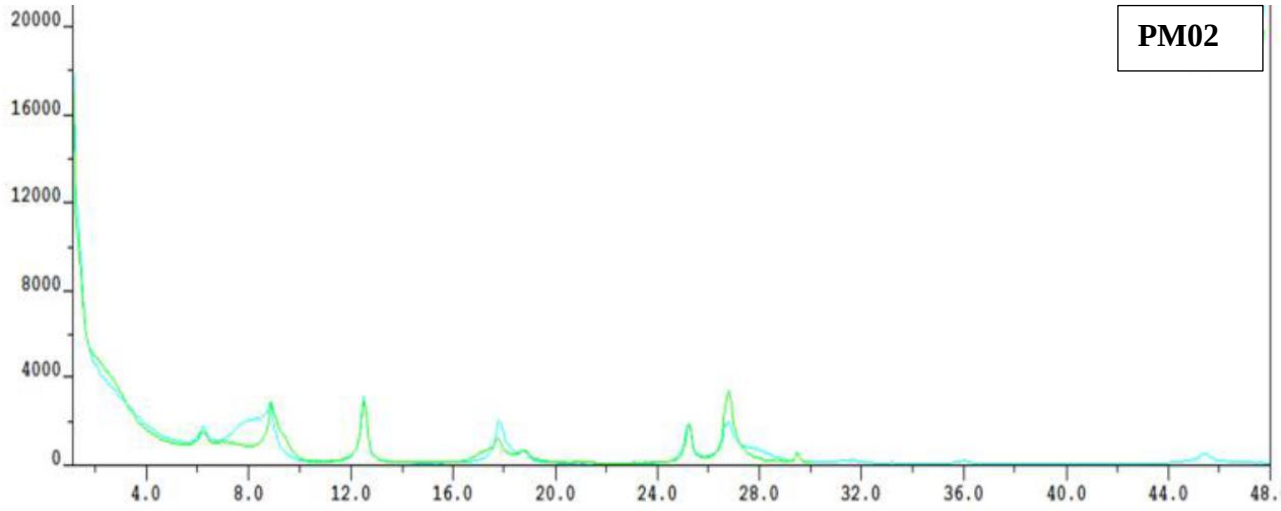
PM02
20000
16000
12000
8000
4000
0
4.0
8.0
12.0
16.0
20.0
24.0
28.0
32.0
36.0
40.0
44.0
48.

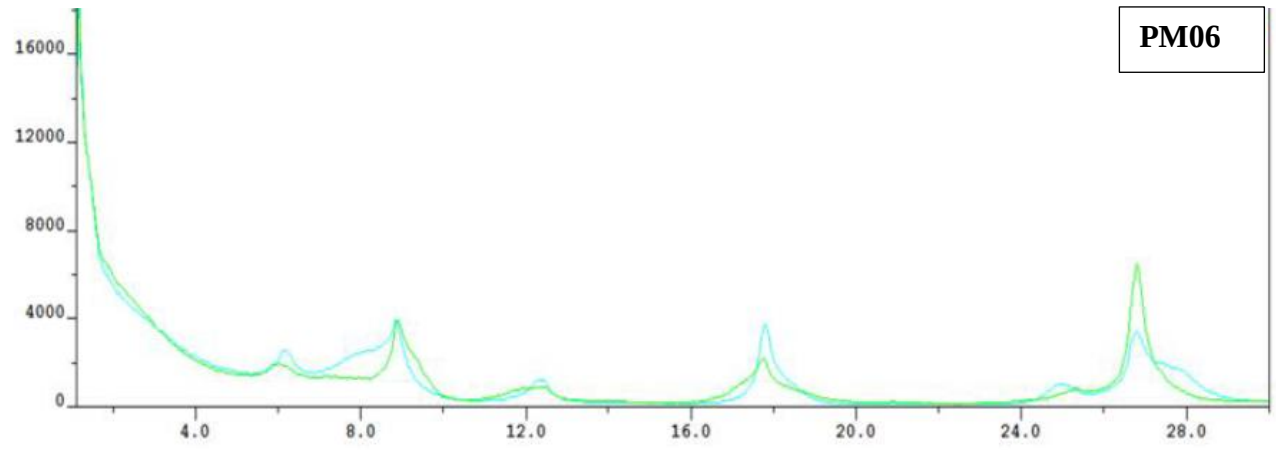
PM06
16000
12000
8000
4000
0
4.0
8.0
12.0
16.0
20.0
24.0
28.0

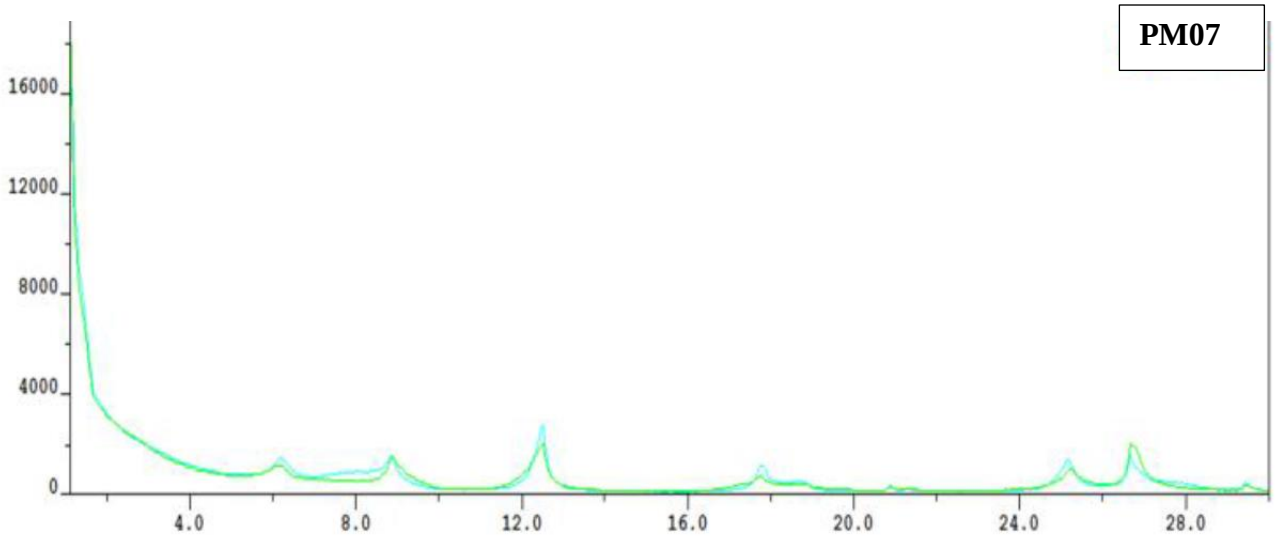
PM07
16000
12000
8000
4000
0
4.0
8.0
12.0
16.0
20.0
24.0
28.0

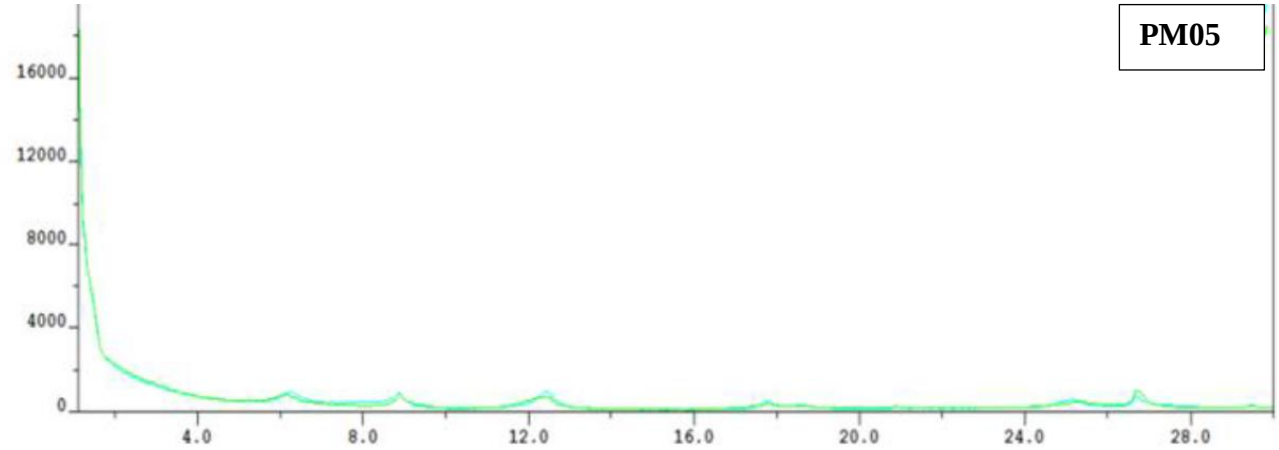
PM05
16000
12000
8000
4000
0
4.0
8.0
12.0
16.0
20.0
24.0
28.0

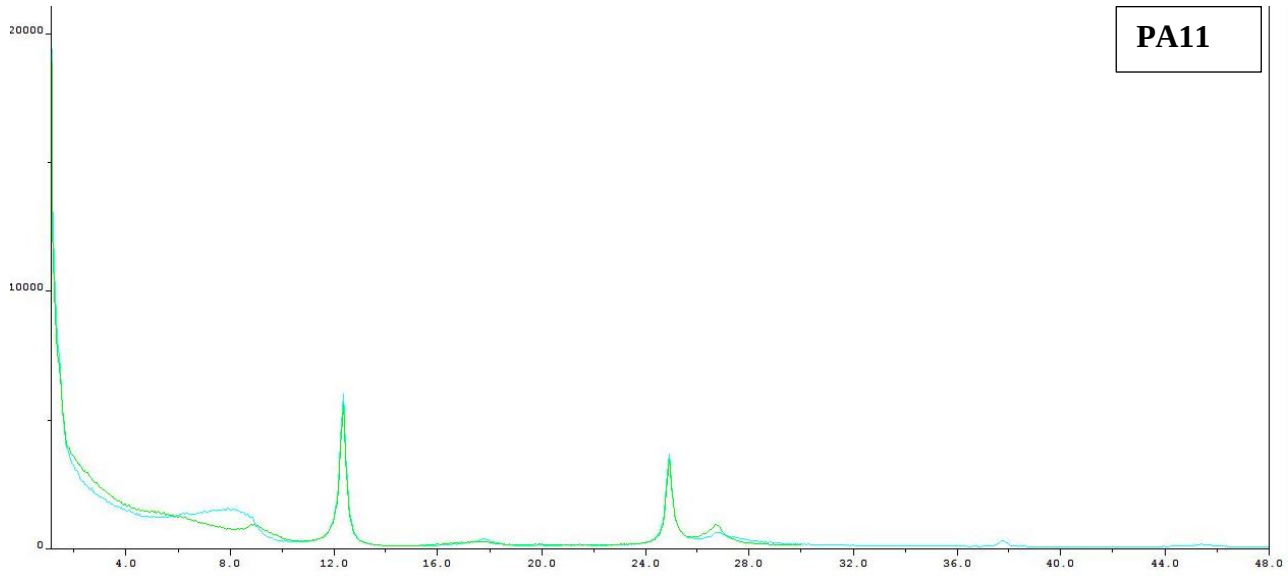
PA11
20000
10000
0
4.0
8.0
12.0
16.0
20.0
24.0
28.0
32.0
36.0
40.0
44.0
48.0

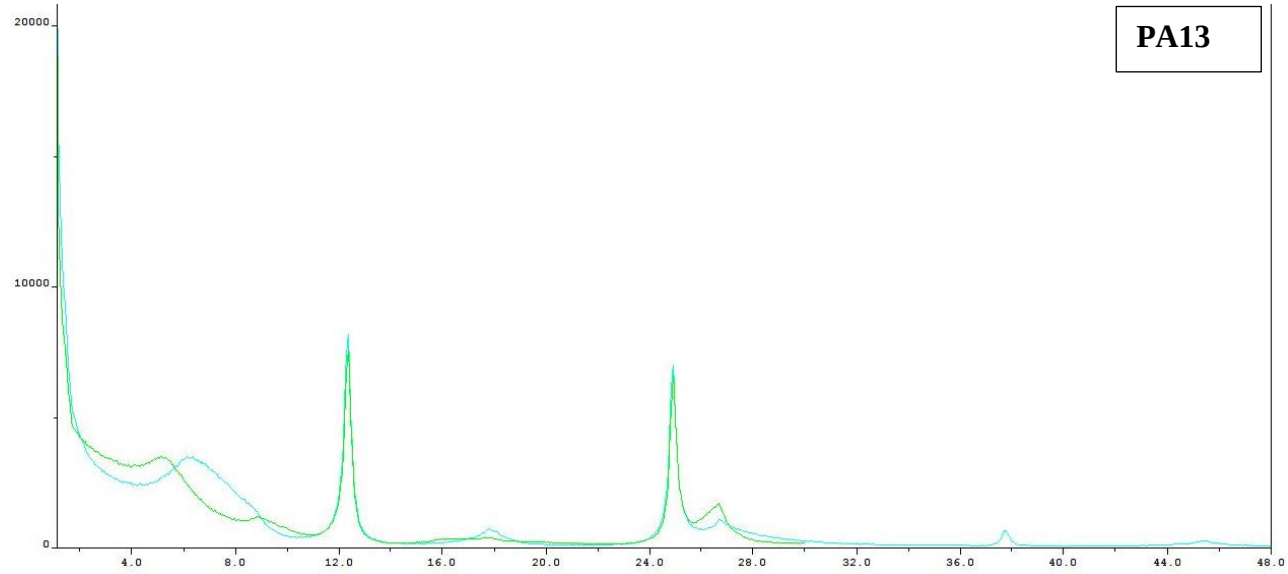
PA13
20000
10000
0
4.0
8.0
12.0
16.0
20.0
24.0
28.0
32.0
36.0
40.0
44.0
48.0

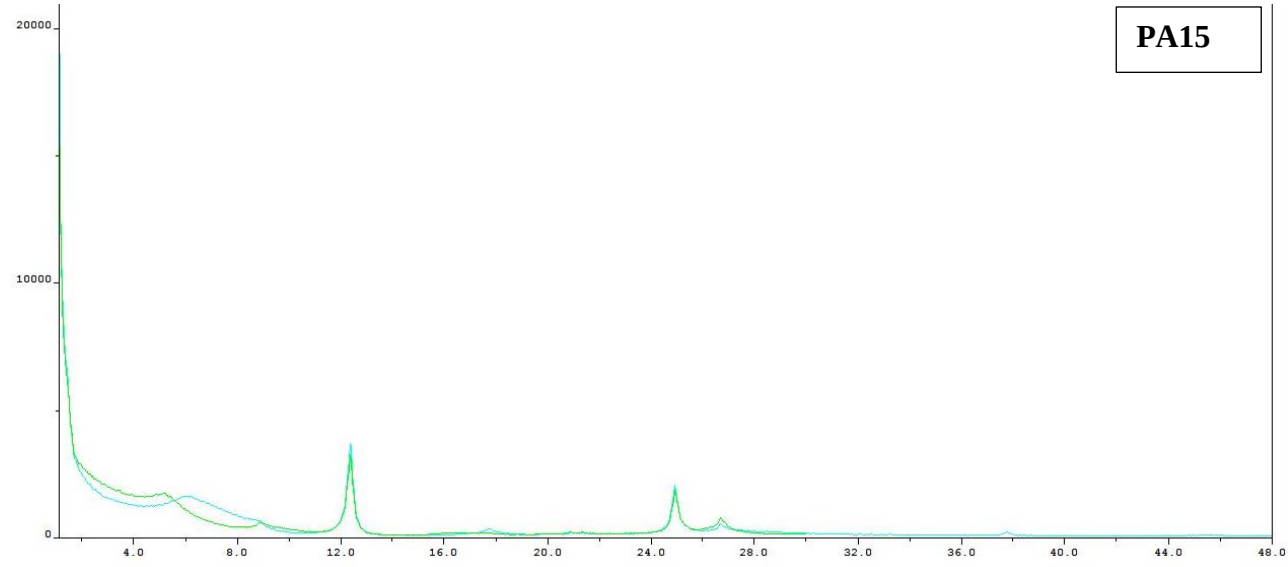
PA15
20000
10000
0
4.0
8.0
12.0
16.0
20.0
24.0
28.0
32.0
36.0
40.0
44.0
48.0

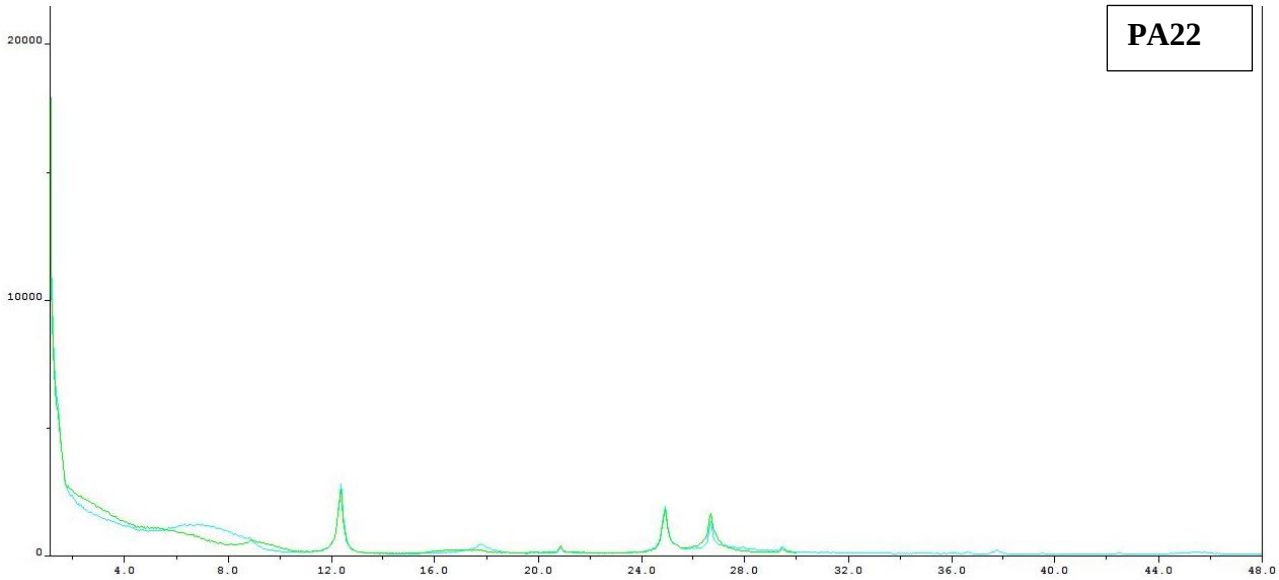
PA22
20000
10000
0
4.0
8.0
12.0
16.0
20.0
24.0
28.0
32.0
36.0
40.0
44.0
48.0

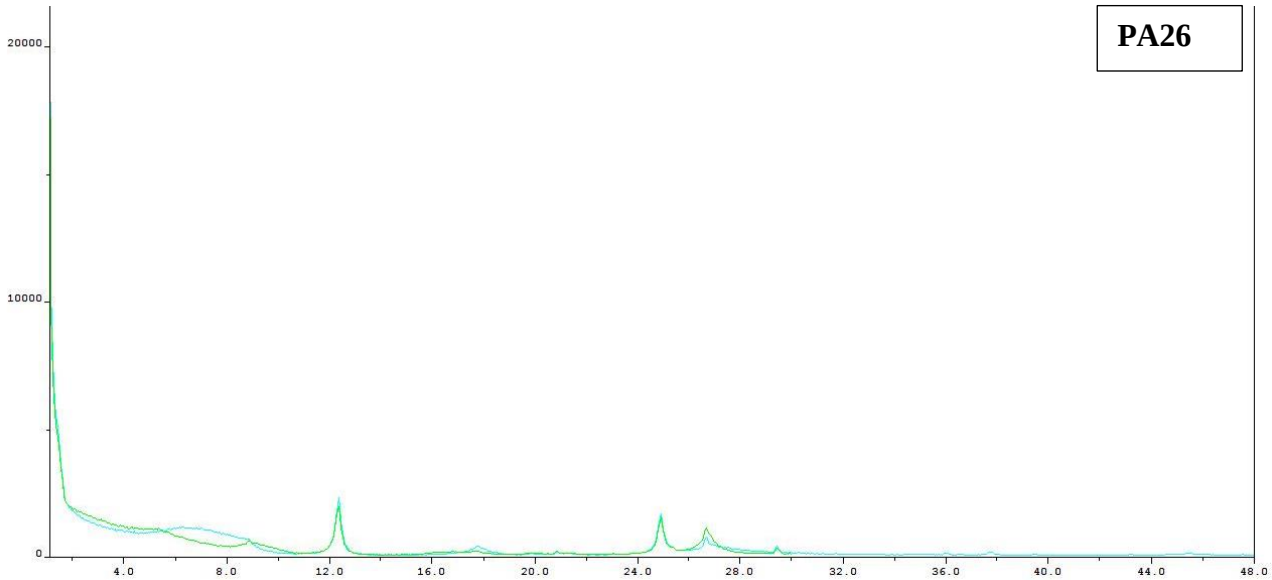
PA26
20000
10000
0
4.0
8.0
12.0
16.0
20.0
24.0
28.0
32.0
36.0
40.0
44.0
48.0

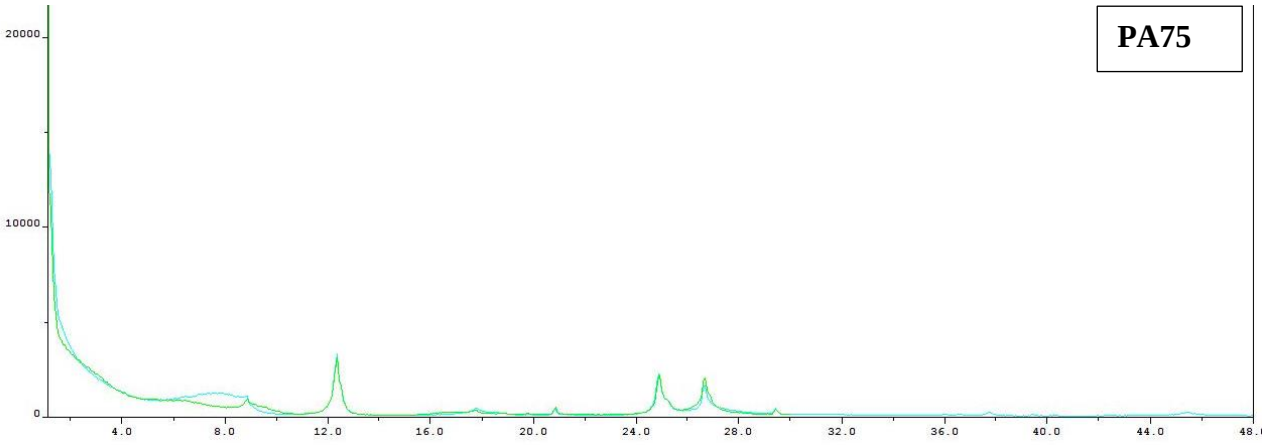
PA75
20000
10000
0
4.0
8.0
12.0
16.0
20.0
24.0
28.0
32.0
36.0
40.0
44.0

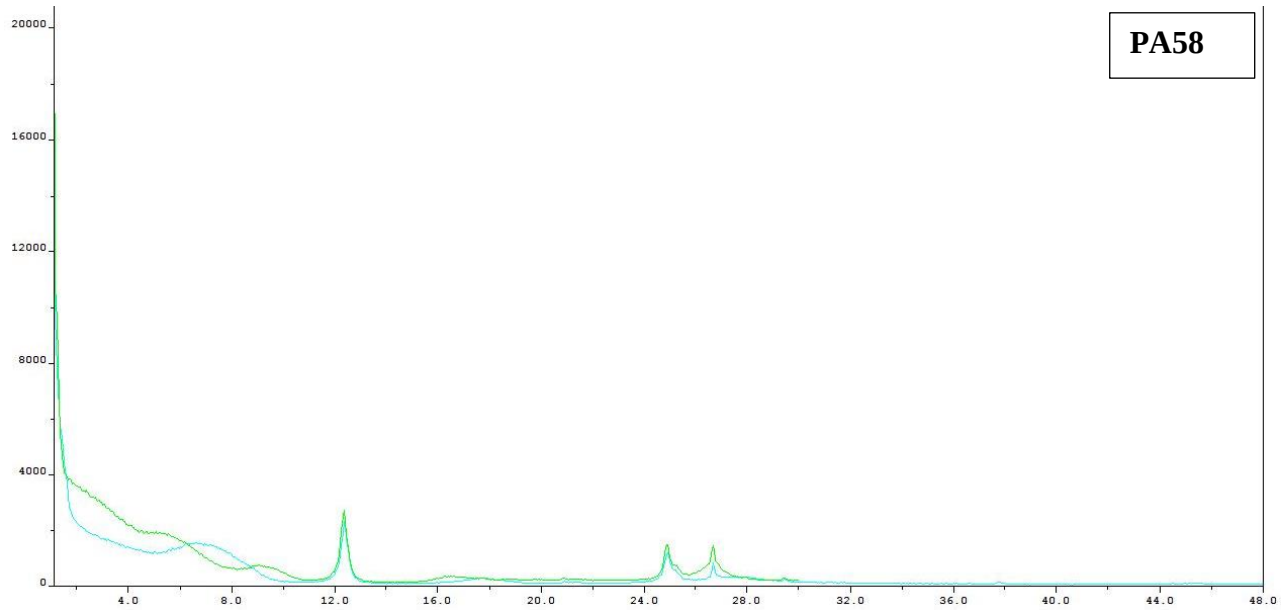
PA58
20000
16000
12000
8000
4000
0
4.0
8.0
12.0
16.0
20.0
24.0
28.0
32.0
36.0
40.0
44.0
48.0

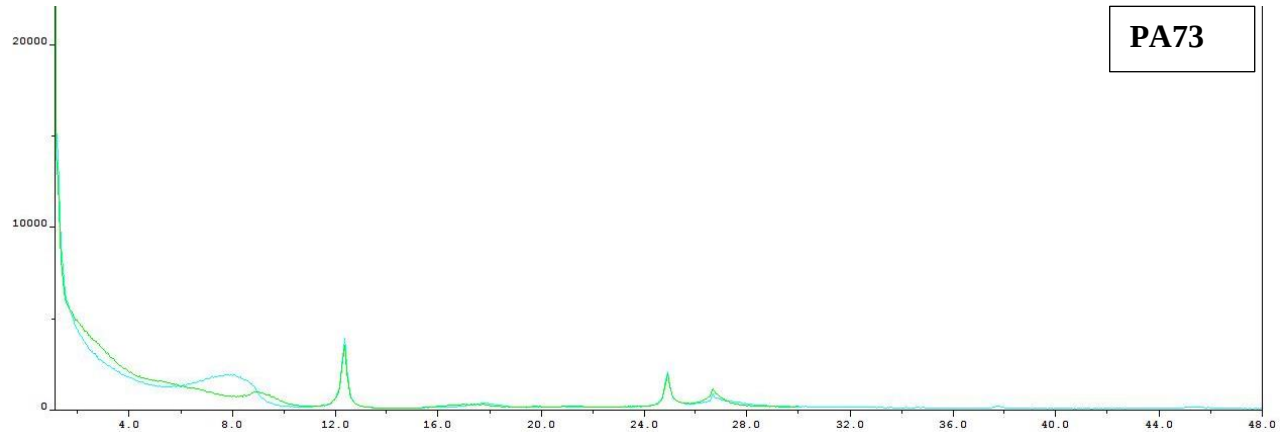
PA73
20000
10000
0
4.0
8.0
12.0
16.0
20.0
24.0
28.0
32.0
36.0
40.0
44.0
48.0

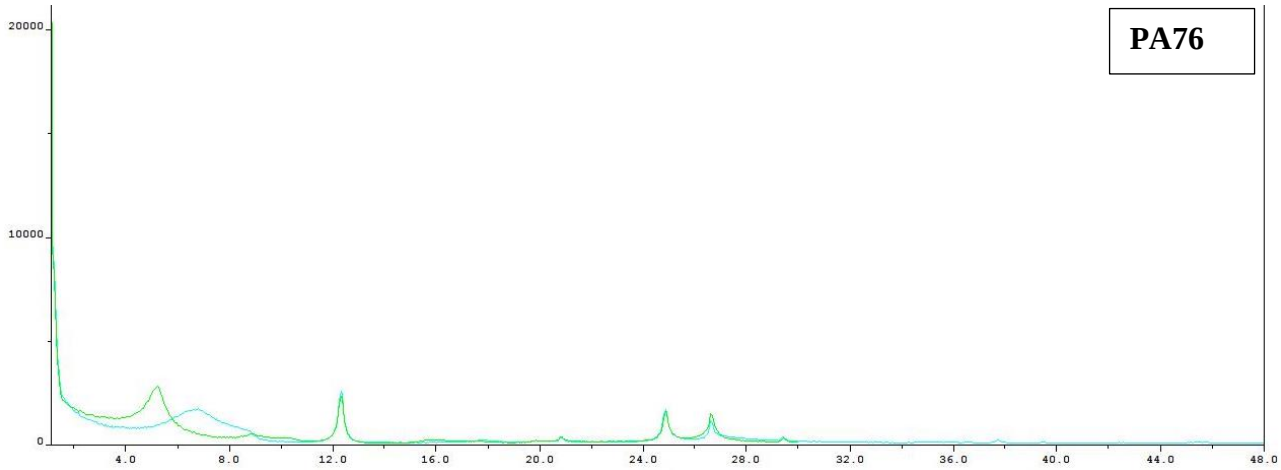
PA76
20000
10000
0
4.0
8.0
12.0
16.0
20.0
24.0
28.0
32.0
36.0
40.0
44.0
48.0

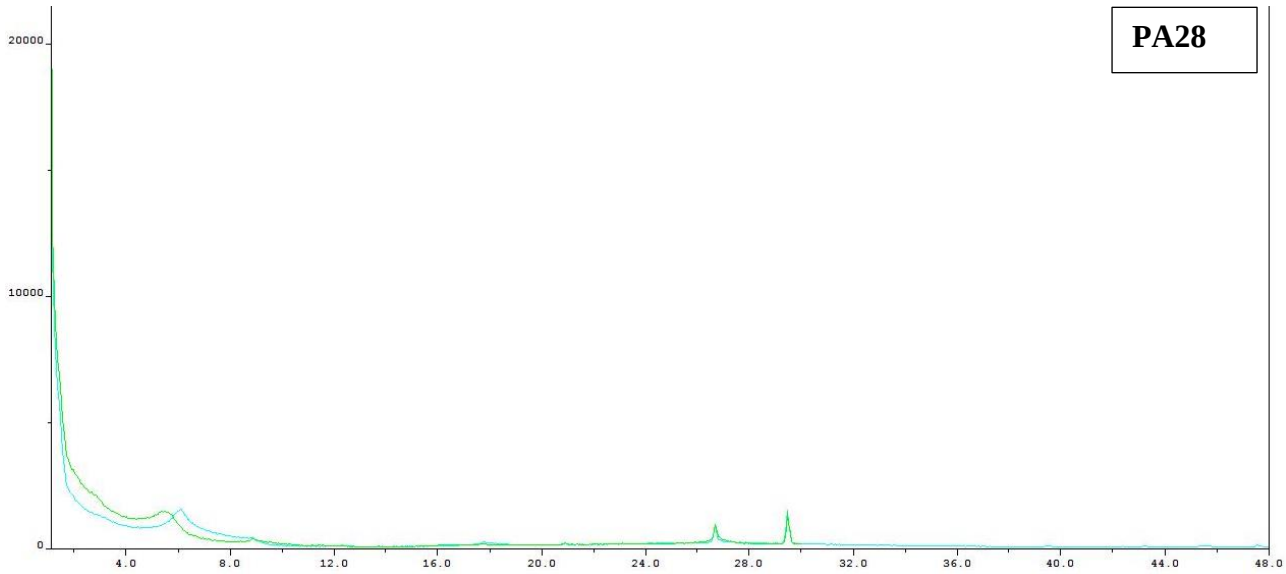
PA28
20000
10000
0
4.0
8.0
12.0
16.0
20.0
24.0
28.0
32.0
36.0
40.0
44.0
48.0

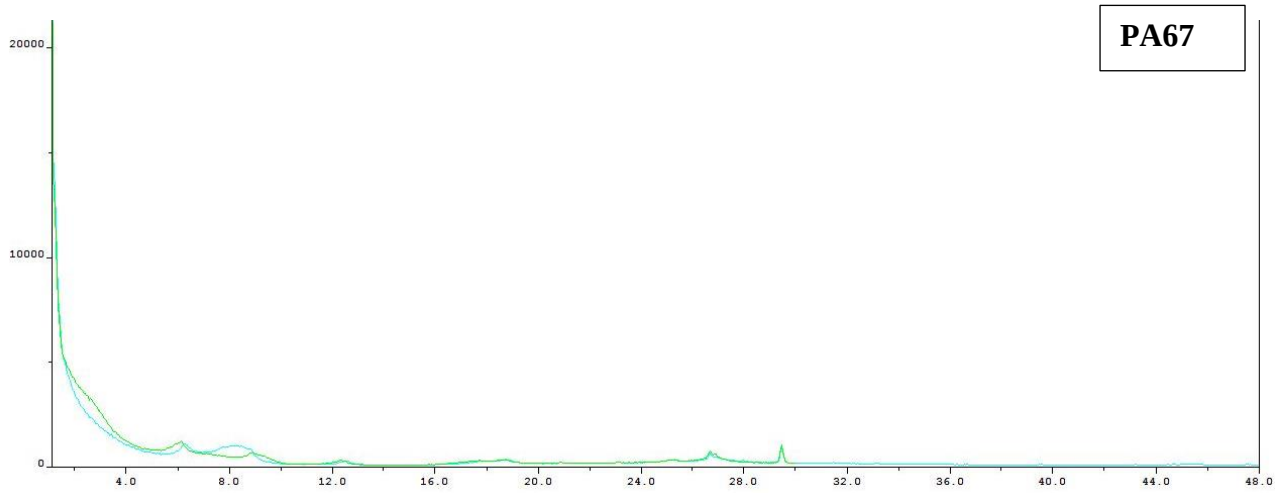
PA67
20000
10000
0
4.0
8.0
12.0
16.0
20.0
24.0
28.0
32.0
36.0
40.0
44.0
48.0

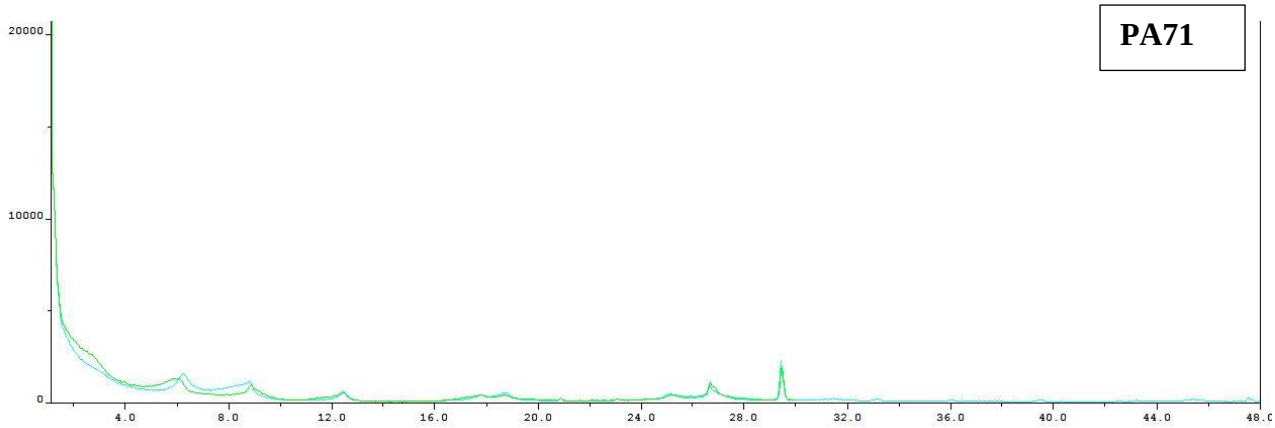
PA71
20000
10000
0
4.0
8.0
12.0
16.0
20.0
24.0
28.0
32.0
36.0
40.0
44.0

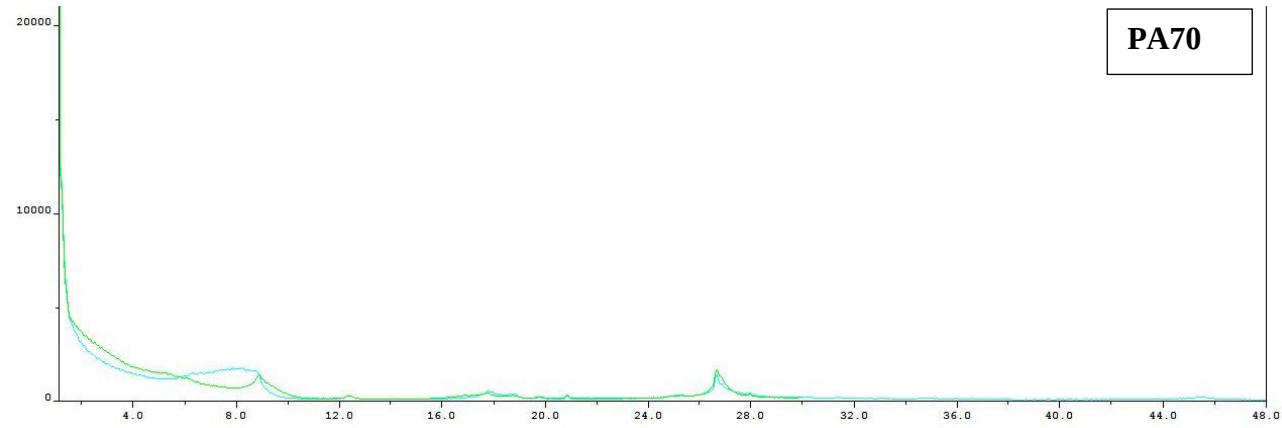
PA70
20000
10000
0
4.0
8.0
12.0
16.0
20.0
24.0
28.0
32.0
36.0
40.0
44.0
48.0

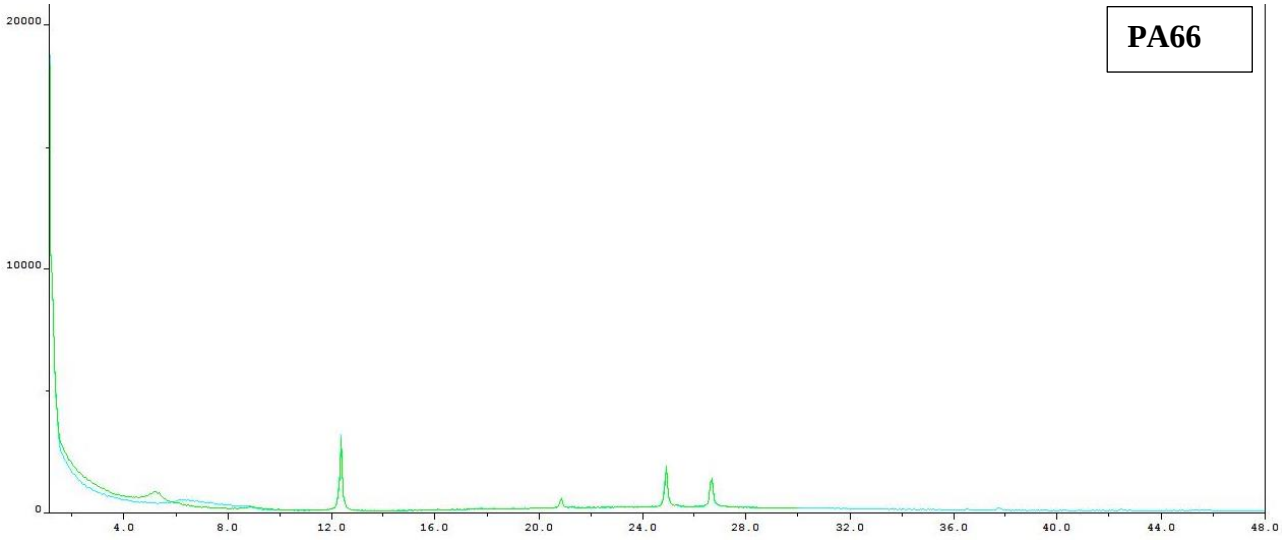
PA66
20000
10000
0
4.0
8.0
12.0
16.0
20.0
24.0
28.0
32.0
36.0
40.0
44.0
48.0

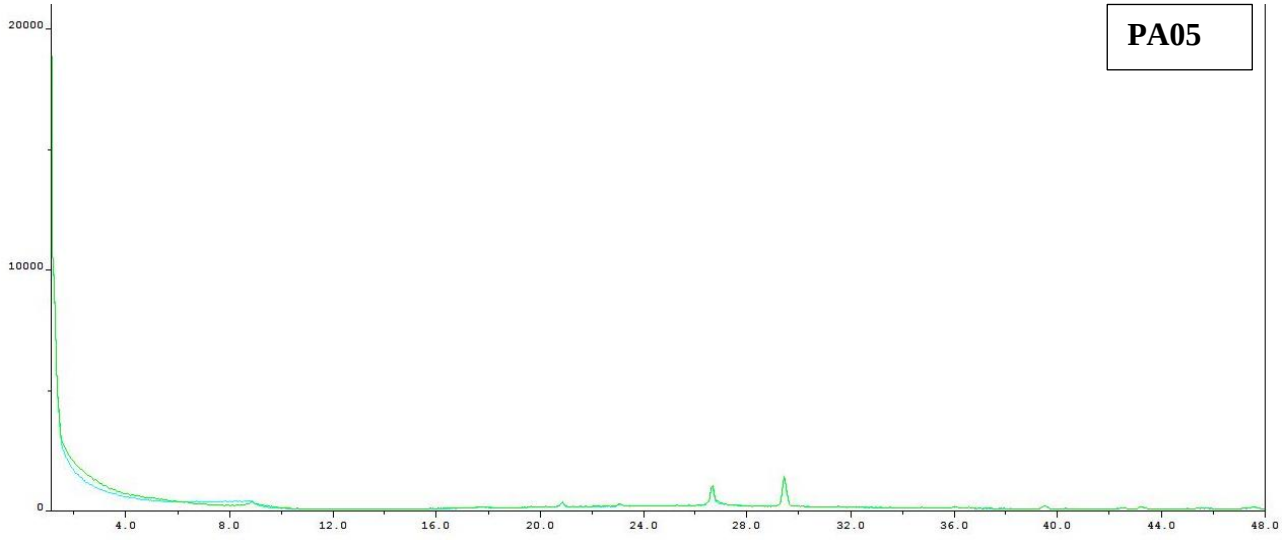
PA05
20000
10000
0
4.0
8.0
12.0
16.0
20.0
24.0
28.0
32.0
36.0
40.0
44.0
48.0

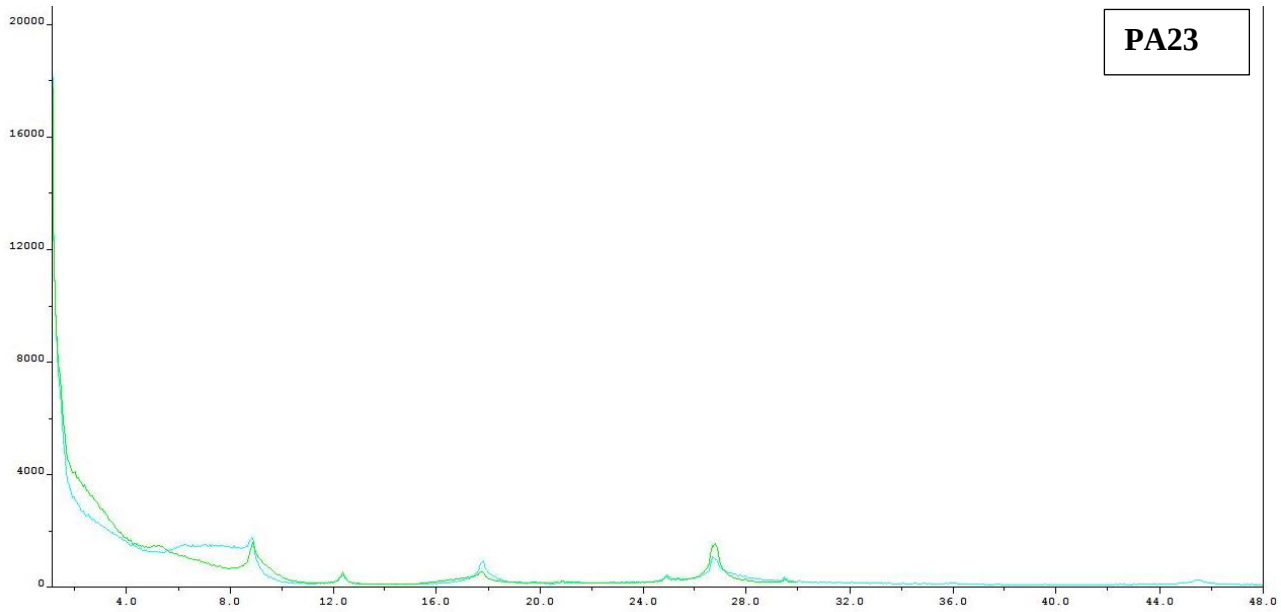
PA23
20000
16000
12000
8000
4000
0
4.0
8.0
12.0
16.0
20.0
24.0
28.0
32.0
36.0
40.0
44.0
48.0

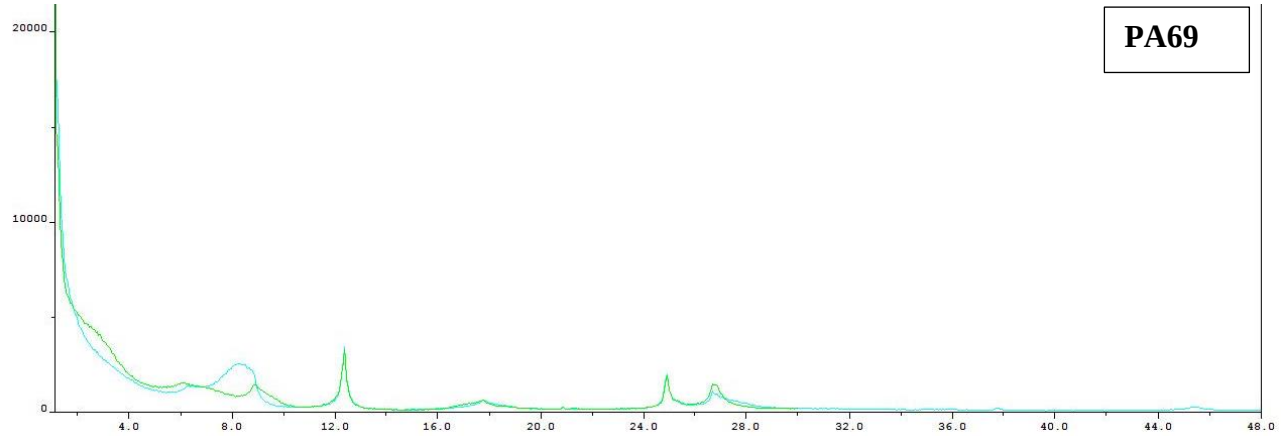
PA69
20000
10000
0
4.0
8.0
12.0
16.0
20.0
24.0
28.0
32.0
36.0
40.0
44.0
48.0

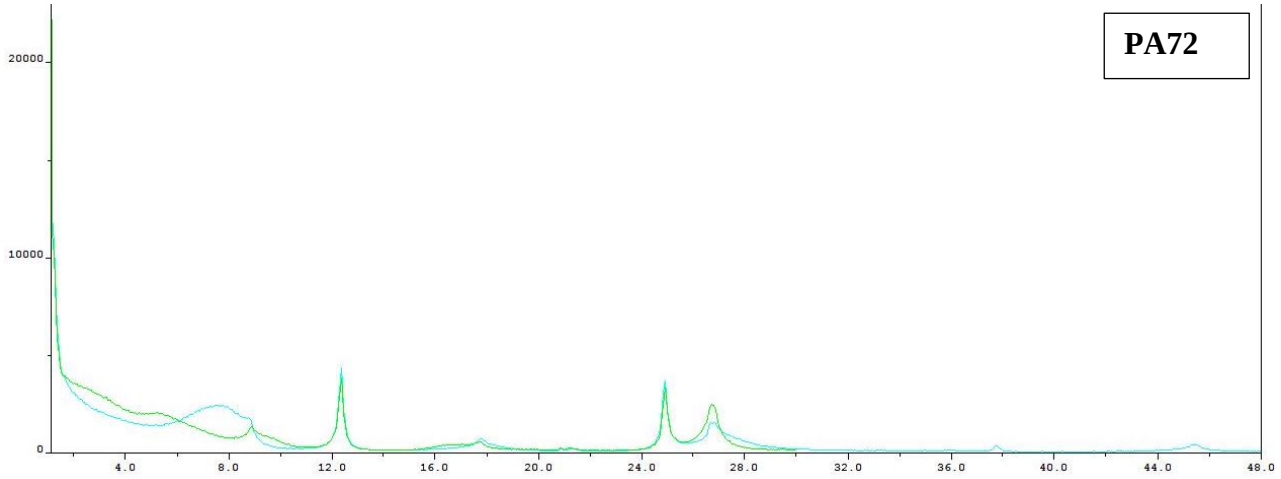
PA72
20000
10000
0
4.0
8.0
12.0
16.0
20.0
24.0
28.0
32.0
36.0
40.0
44.0
48.0

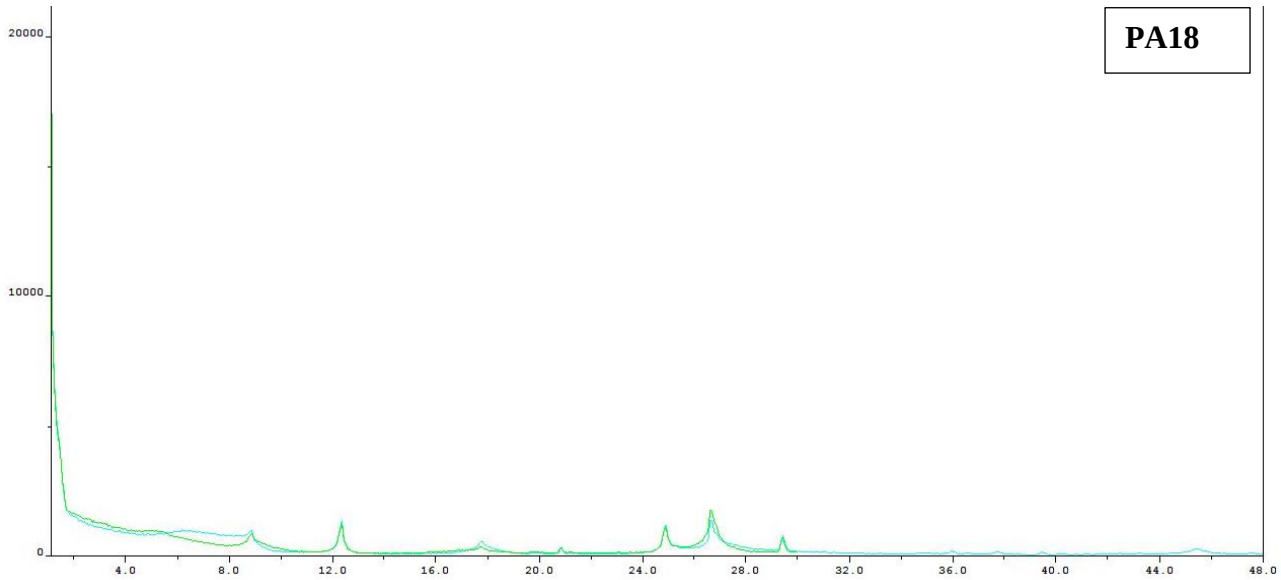
PA18
20000
10000
0
4.0
8.0
12.0
16.0
20.0
24.0
28.0
32.0
36.0
40.0
44.0
48.0

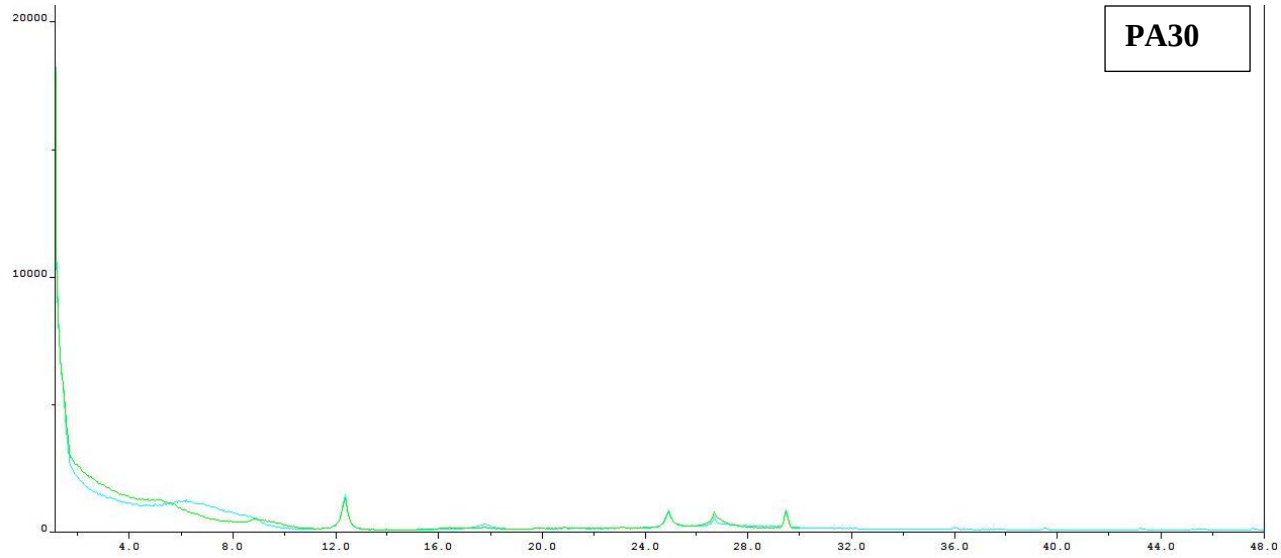
PA30
20000
10000
0
4.0
8.0
12.0
16.0
20.0
24.0
28.0
32.0
36.0
40.0
44.0
48.0

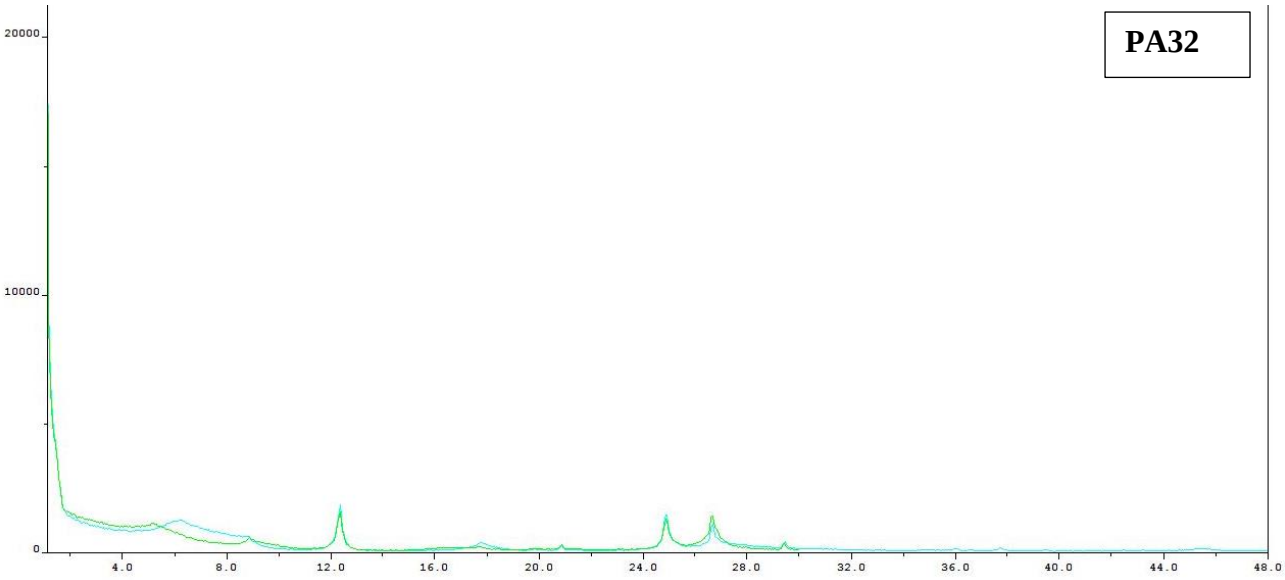
PA32
20000
10000
0
4.0
8.0
12.0
16.0
20.0
24.0
28.0
32.0
36.0
40.0
44.0
48.0

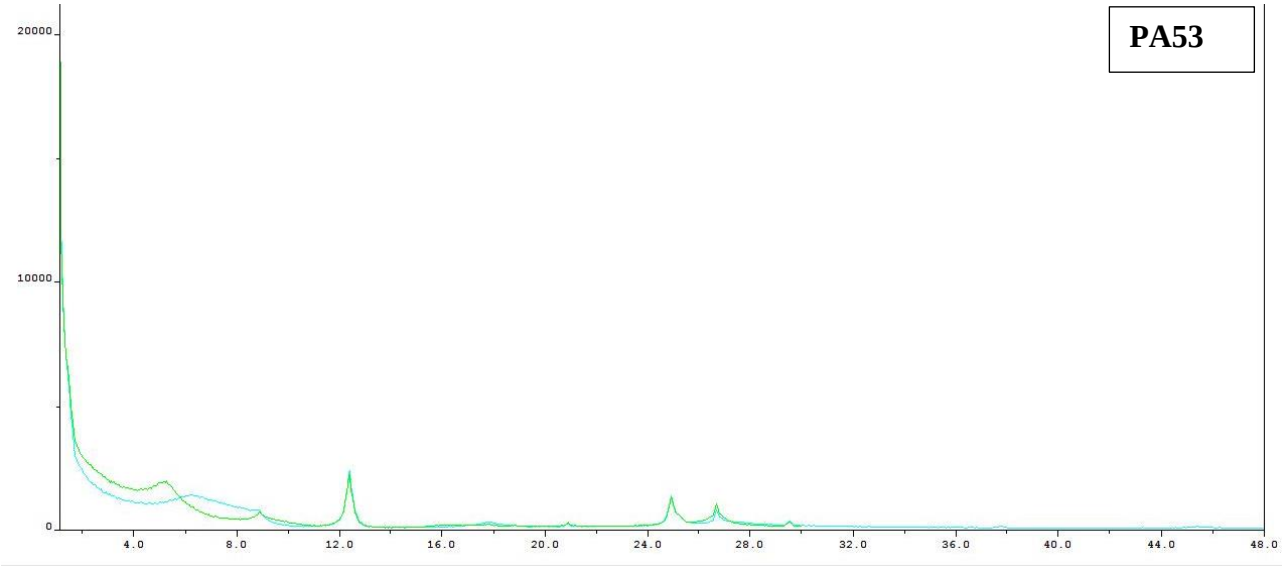
PA53
20000
10000
0
4.0
8.0
12.0
16.0
20.0
24.0
28.0
32.0
36.0
40.0
44.0
48.0

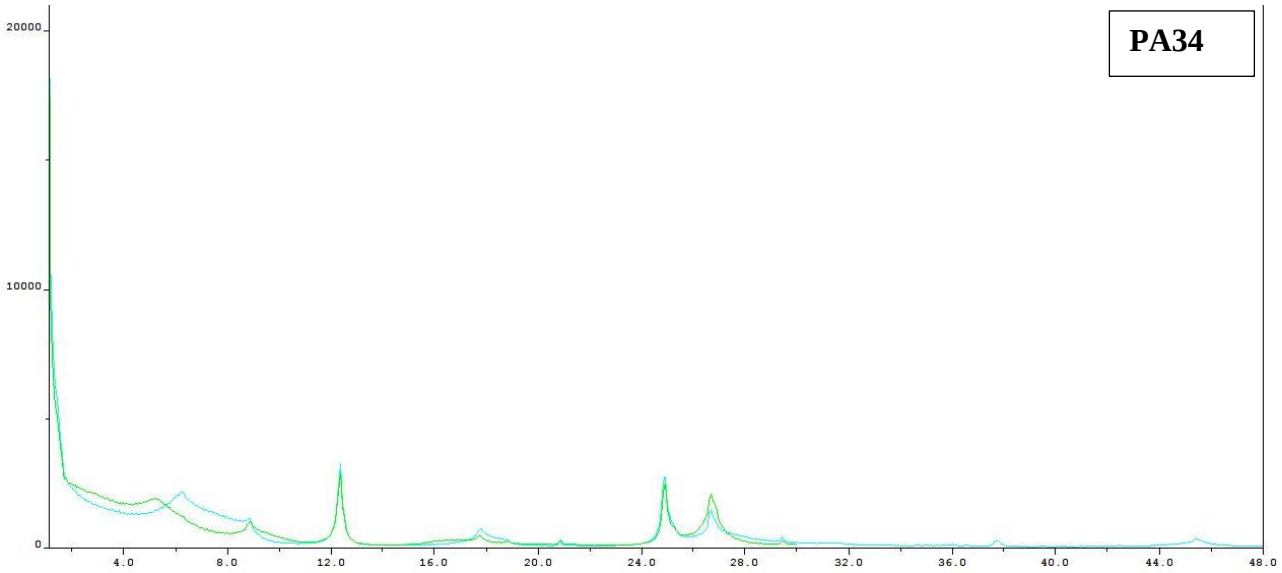
PA34
20000
10000
0
4.0
8.0
12.0
16.0
20.0
24.0
28.0
32.0
36.0
40.0
44.0
48.0

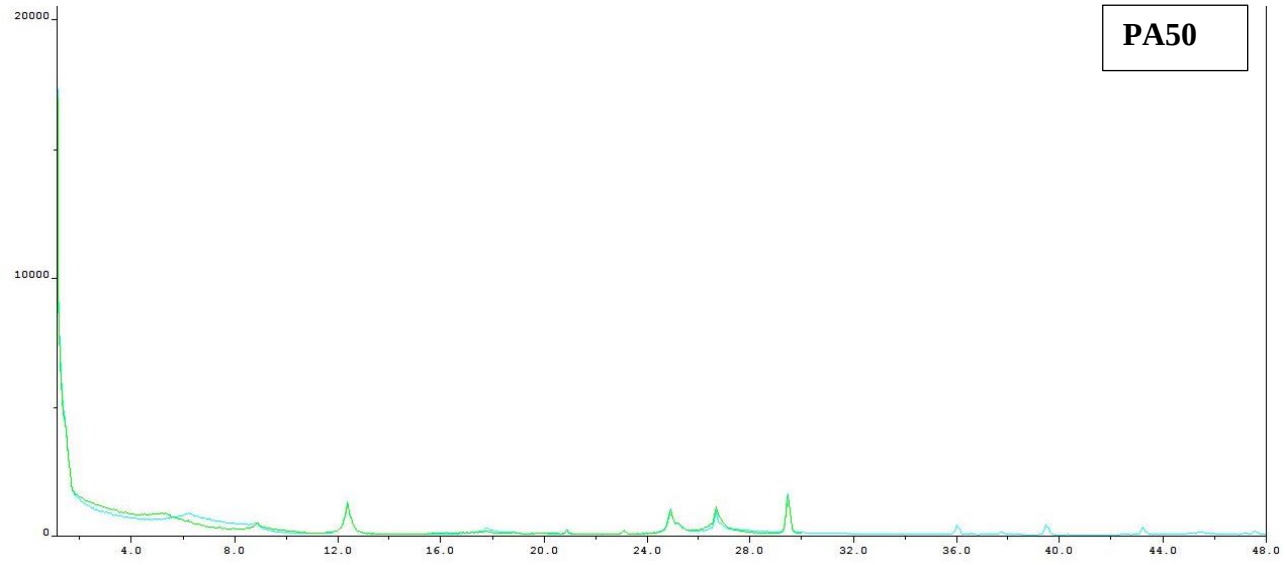
PA50
20000
10000
0
4.0
8.0
12.0
16.0
20.0
24.0
28.0
32.0
36.0
40.0
44.0
48.0

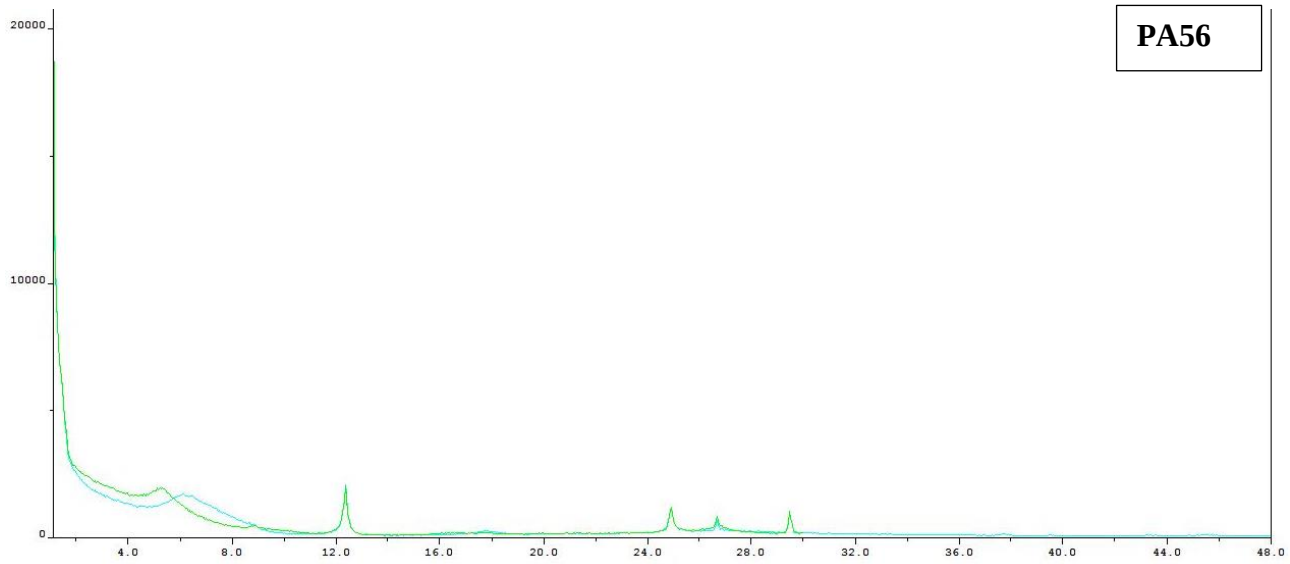
PA56
20000
10000
0
4.0
8.0
12.0
16.0
20.0
24.0
28.0
32.0
36.0
40.0
44.0
48.0

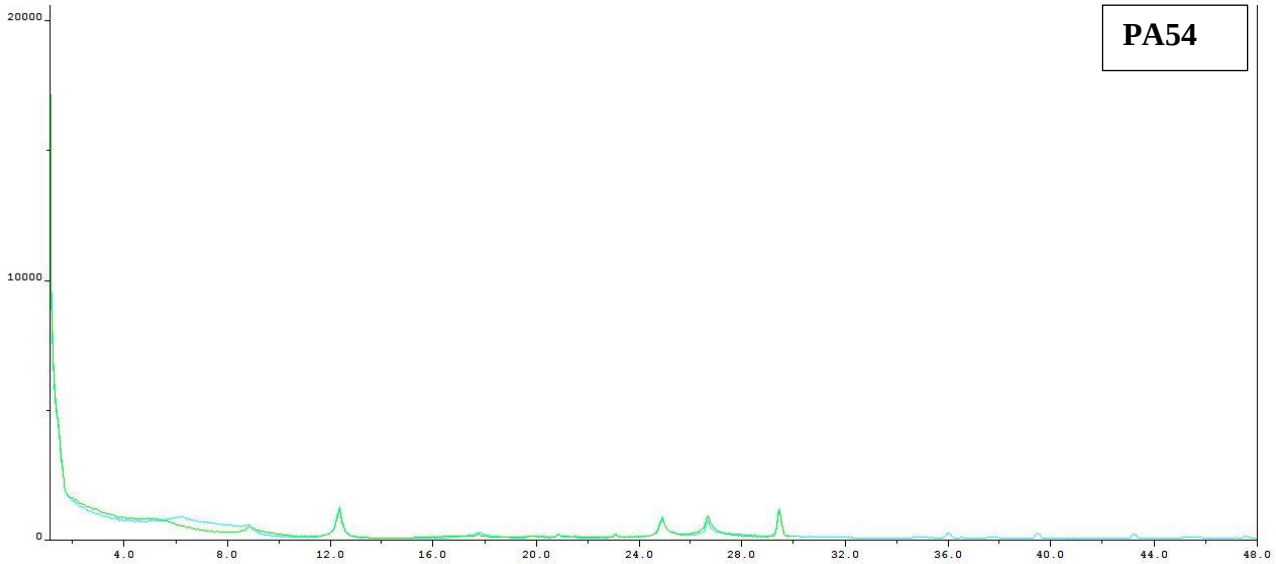
PA54
20000
10000
0
4.0
8.0
12.0
16.0
20.0
24.0
28.0
32.0
36.0
40.0
44.0
48.0

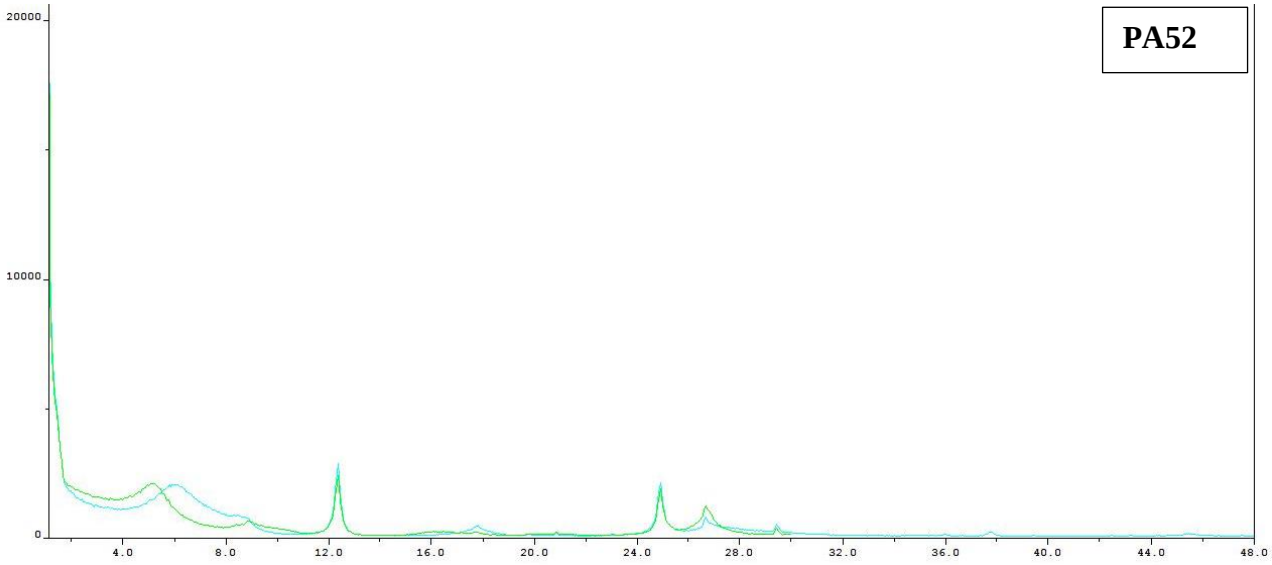
PA52
20000
10000
0
4.0
8.0
12.0
16.0
20.0
24.0
28.0
32.0
36.0
40.0
44.0
48.0

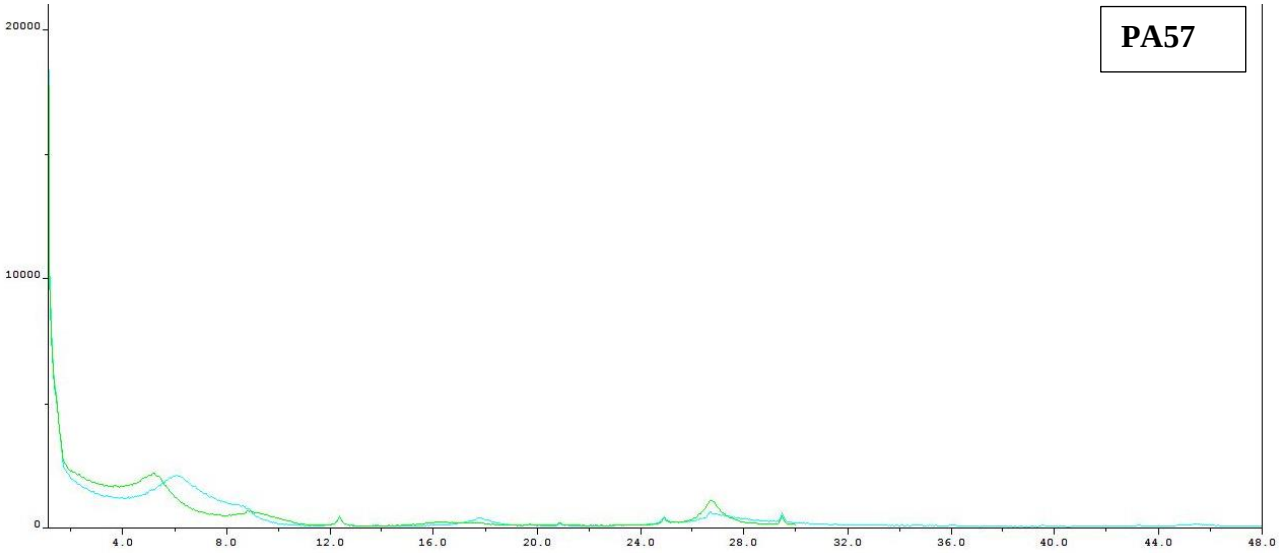
PA57
20000
10000
0
4.0
8.0
12.0
16.0
20.0
24.0
28.0
32.0
36.0
40.0
44.0
48.0

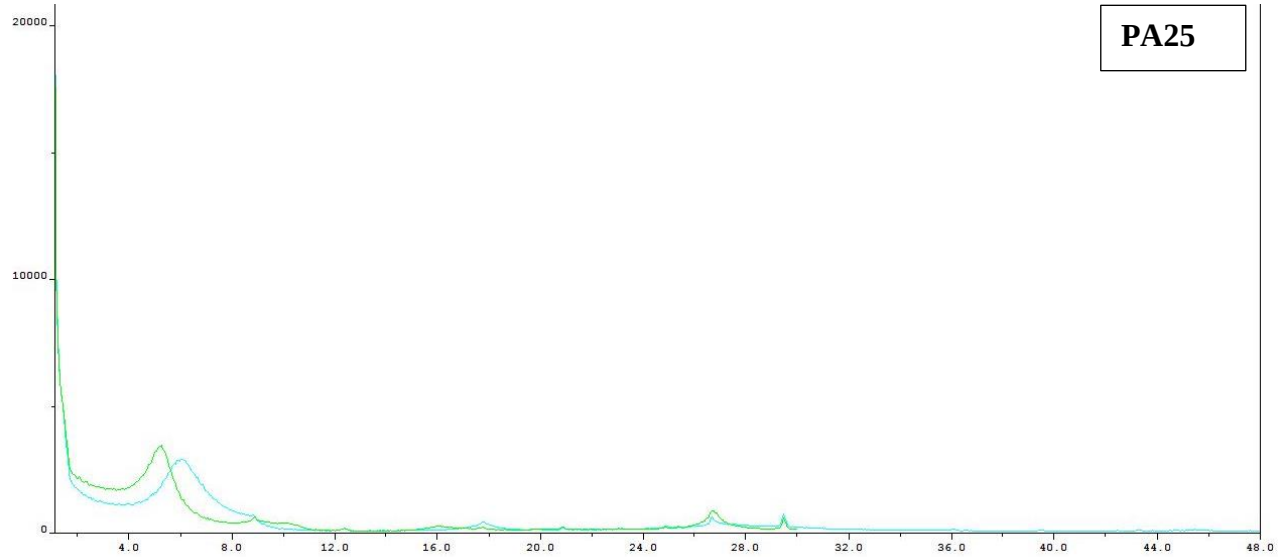
PA25
20000
10000
0
4.0
8.0
12.0
16.0
20.0
24.0
28.0
32.0
36.0
40.0
44.0
48.0

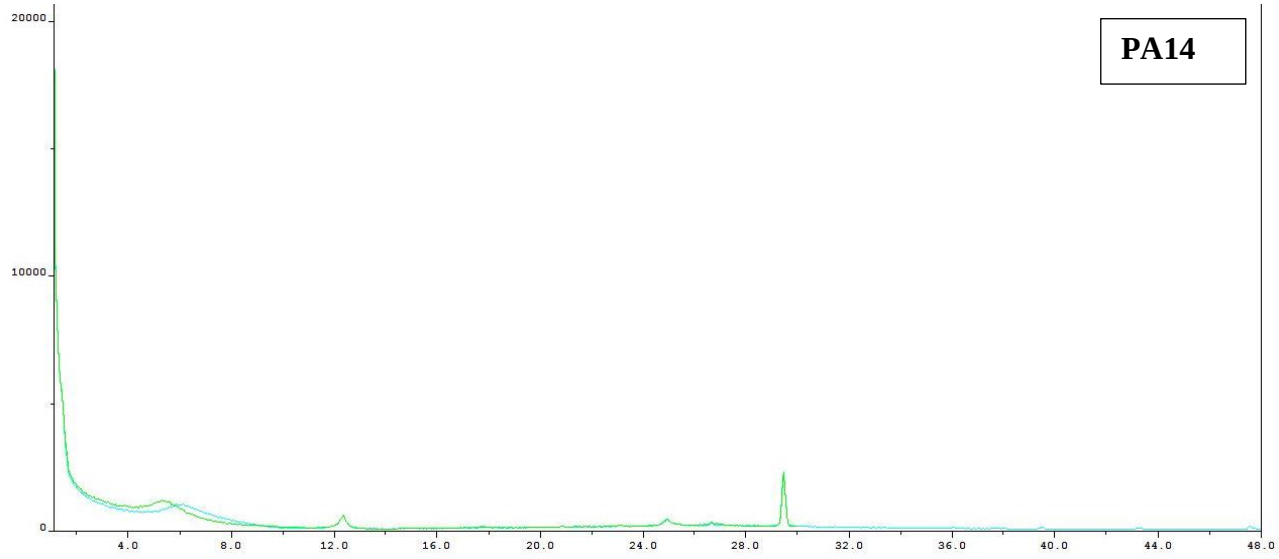
PA14
20000
10000
0
4.0
8.0
12.0
16.0
20.0
24.0
28.0
32.0
36.0
40.0
44.0
48.0

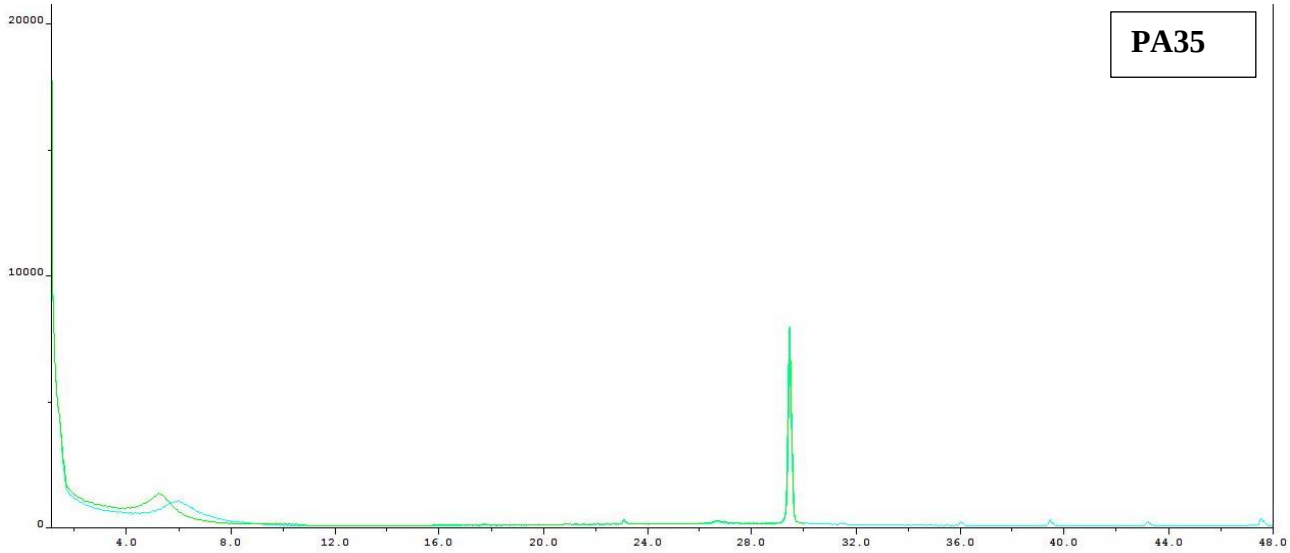
PA35
20000
10000
0
4.0
8.0
12.0
16.0
20.0
24.0
28.0
32.0
36.0
40.0
44.0
48.0

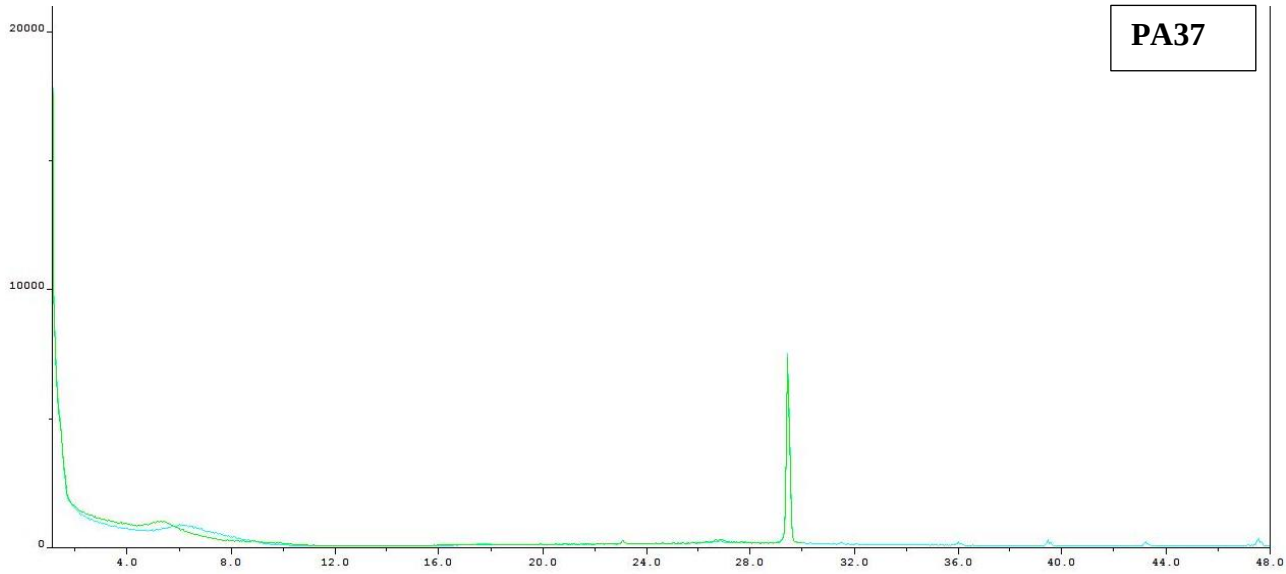
PA37
20000
10000
0
4.0
8.0
12.0
16.0
20.0
24.0
28.0
32.0
36.0
40.0
44.0
48.0

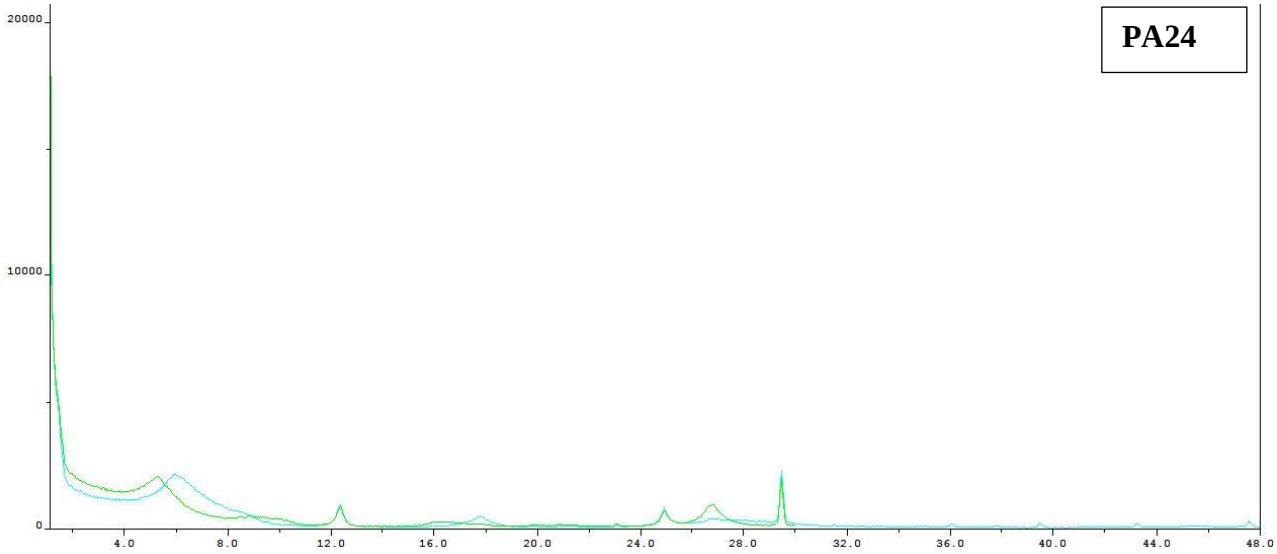
PA24
20000
10000
0
4.0
8.0
12.0
16.0
20.0
24.0
28.0
32.0
36.0
40.0
44.0
48.0

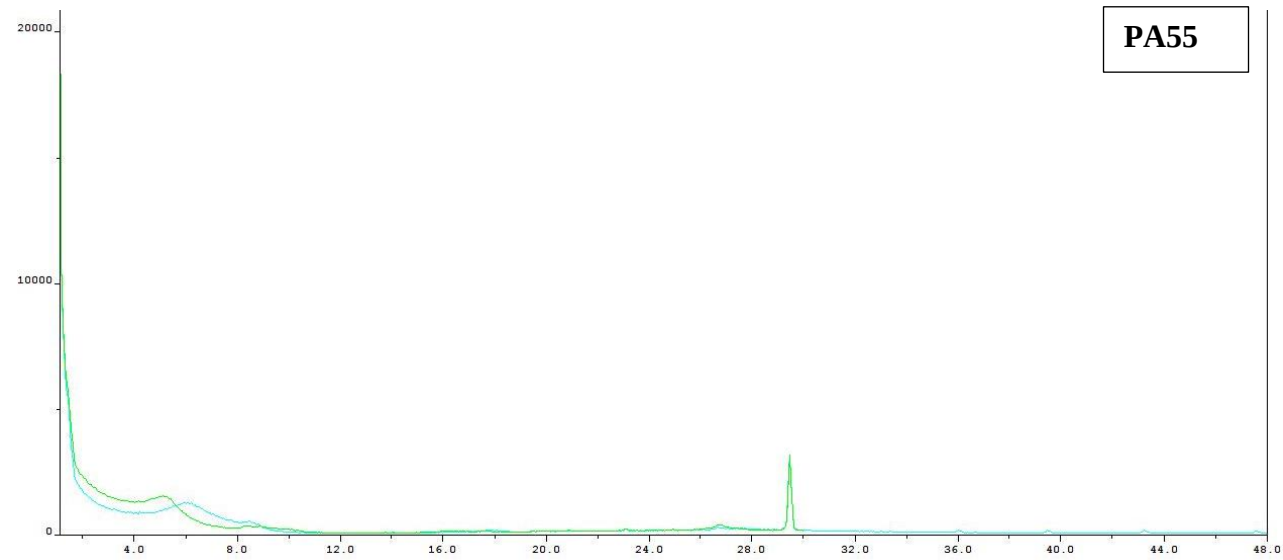
PA55
20000
10000
0
4.0
8.0
12.0
16.0
20.0
24.0
28.0
32.0
36.0
40.0
44.0
48.0

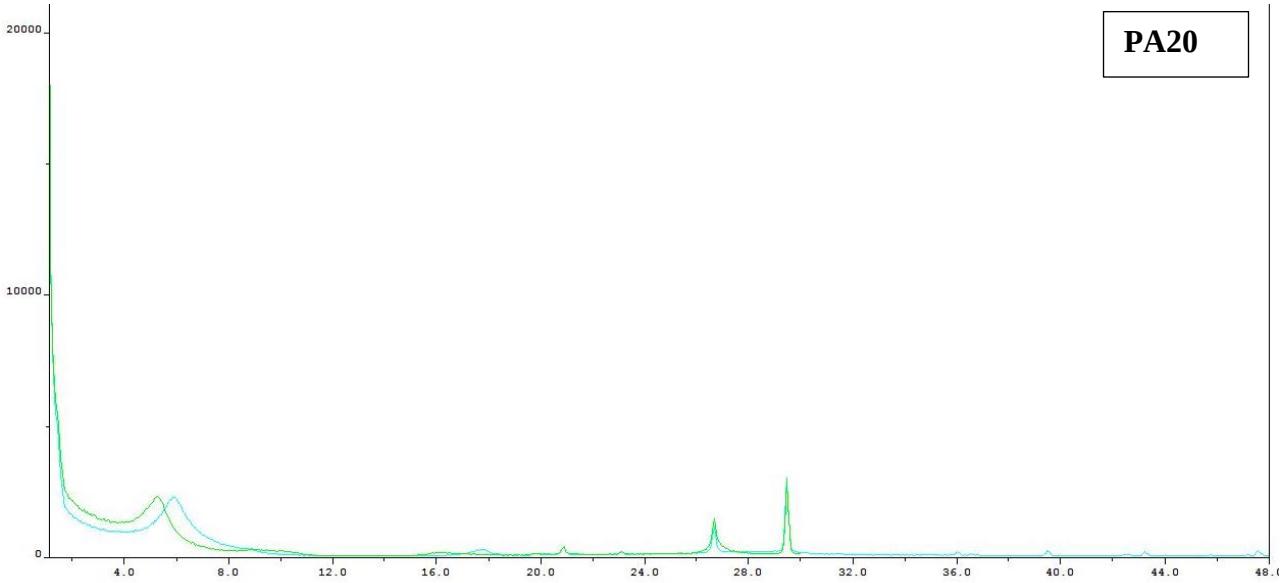
PA20
20000
10000
0
4.0
8.0
12.0
16.0
20.0
24.0
28.0
32.0
36.0
40.0
44.0

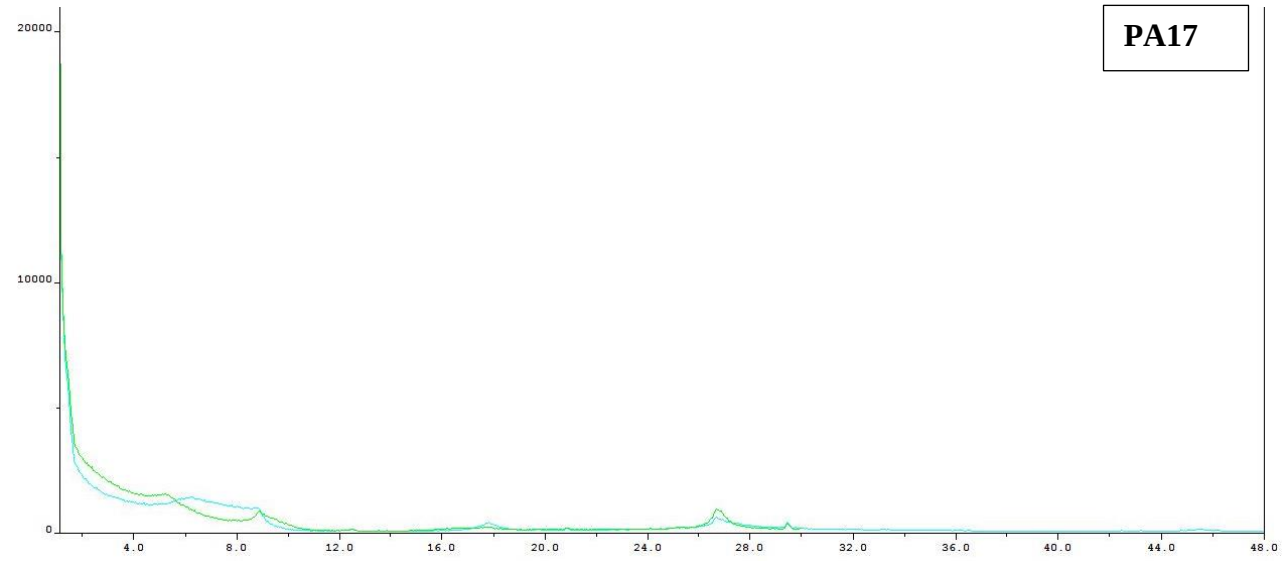
PA17
20000
10000
0
4.0
8.0
12.0
16.0
20.0
24.0
28.0
32.0
36.0
40.0
44.0
48.0

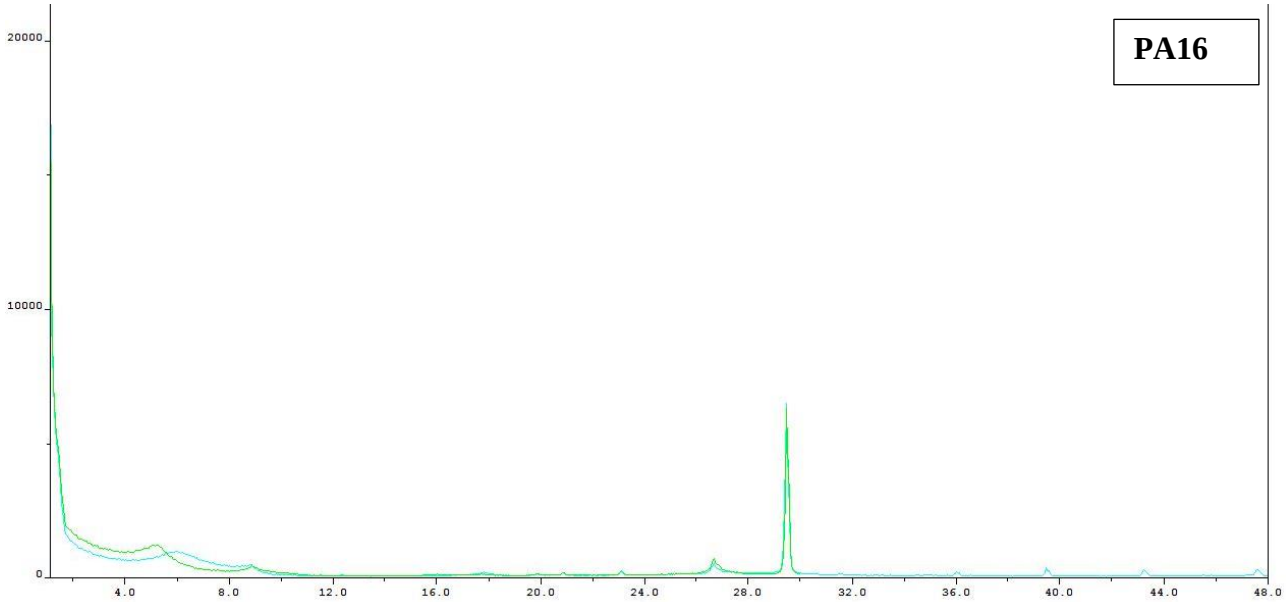
PA16
20000
10000
0
4.0
8.0
12.0
16.0
20.0
24.0
28.0
32.0
36.0
40.0
44.0
48.0

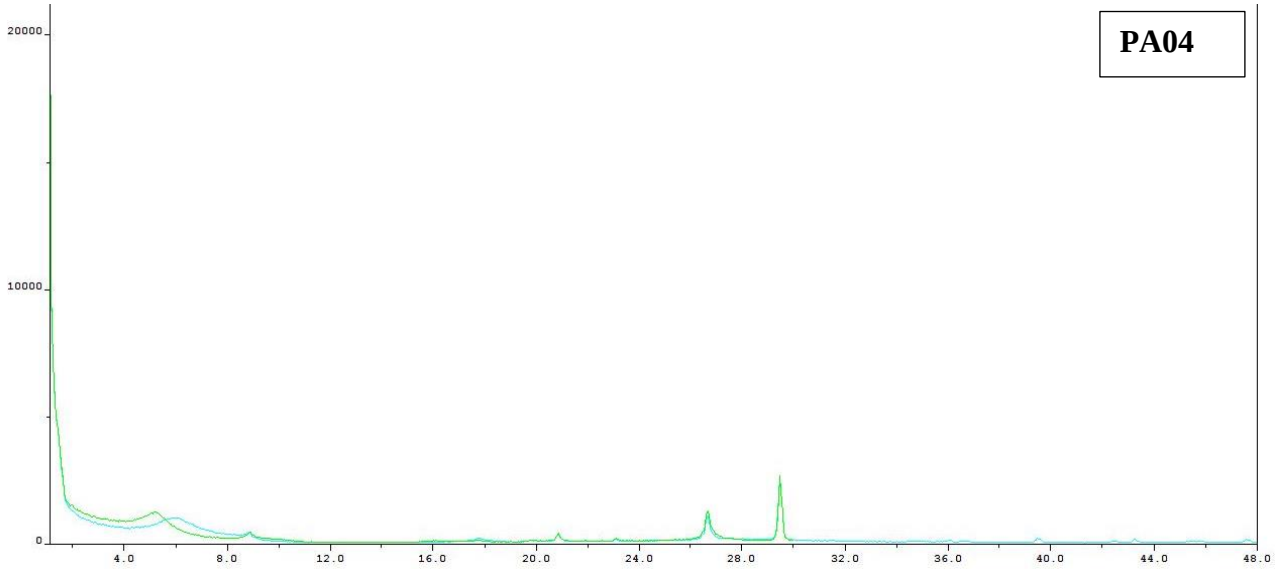
PA04
20000
10000
0
4.0
8.0
12.0
16.0
20.0
24.0
28.0
32.0
36.0
40.0
44.0
48.0

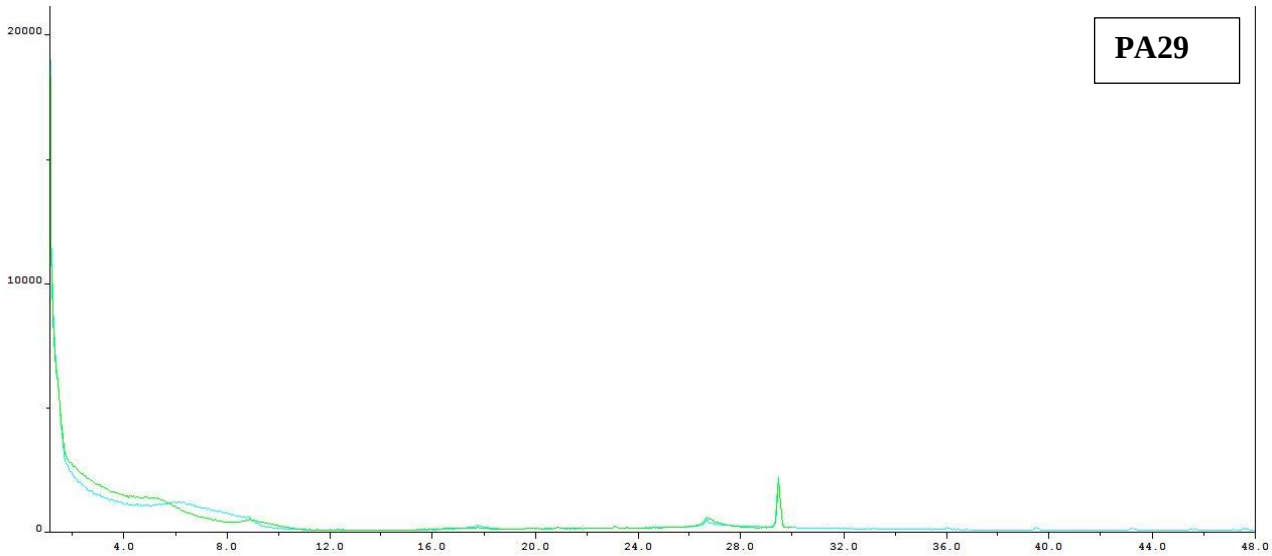
PA29
20000
10000
0
4.0
8.0
12.0
16.0
20.0
24.0
28.0
32.0
36.0
40.0
44.0
48.0

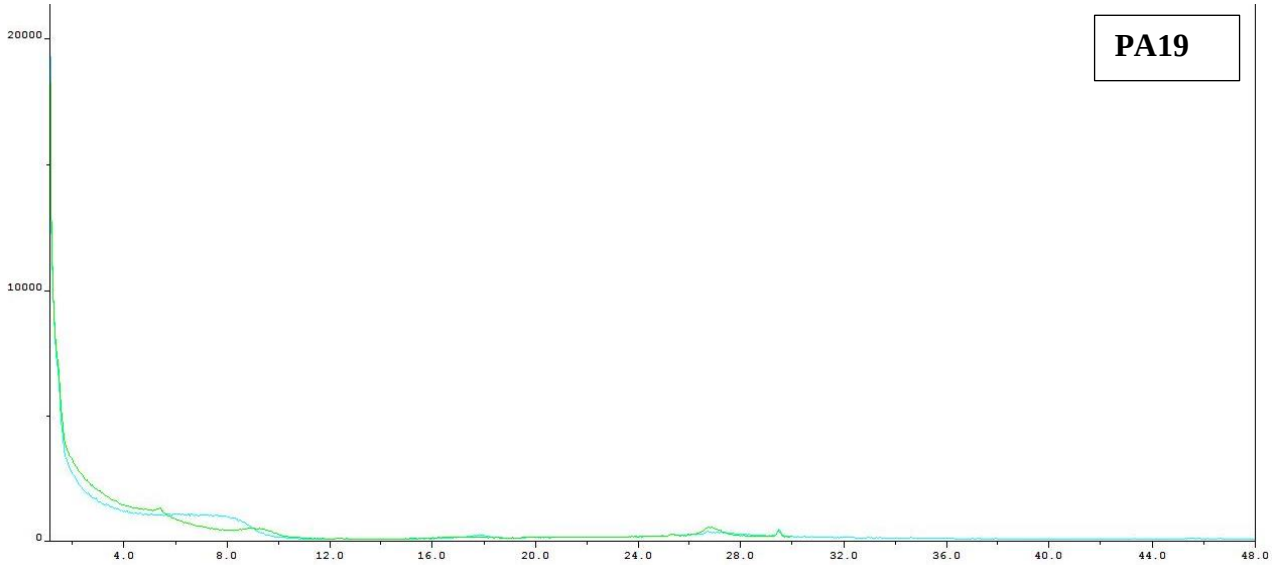
PA19
20000
10000
0
4.0
8.0
12.0
16.0
20.0
24.0
28.0
32.0
36.0
40.0
44.0
48.0

Rock-Eval analysis

Sample	PA05	PA44	PA47	PA64	PA17	PA19	PA65	PM35	PA39	PA78	PA23	PA54	PA72	PA80	PA66	PA34	PA3	PA22	PA16	PA70	PA27	PA69	PM6	PM2
Qty(mg)	49.09	53.77	49.21	53.39	50.54	53.74	53.01	50.99	49.65	52.93	51.75	51.3	52.95	52.91	53.71	52.29	52.21	51.1	53.55	53.08	50.62	52.58	51.24	50.46
S1(mg/g)	0	0.02	0	0	2.15	0	0	0.01	0	0	0	0.01	0	0	0	0	0.57	0	0.01	0	0	0	0	0
S2(mg/g)	0.05	0.22	0.02	0.01	94.73	0.06	0.12	0.27	0.01	0	0.03	0.67	0	0	0	0.11	8.47	0.03	0.17	0	0.01	0	0	0
S3(mg/g)	0.37	2.25	0.27	0.43	10.34	0.03	0.17	0.82	0.33	0.48	0.4	1.04	0.18	0.42	0.13	1.02	0.22	0.23	0.81	0.01	0.29	0.48	0.3	0.29
S3'(mg/g)	9.8	4.8	1.7	5.1	19.2	2.6	3.8	3.7	4.5	5.6	6.9	11.8	4	4.5	1.1	6.8	7.9	0.7	9.3	0.1	1.4	2	1.4	4.2
S3CO(mg/g)	0.06	0.18	0.02	0.02	4.84	0.01	0.02	0.02	0.03	0.01	0.03	0.14	0.02	0.02	0.02	0.15	0.05	0.01	0.06	0.02	0.05	0.01	0.01	0
S3'CO(mg/g)	0.1	0.2	0.1	0.1	1.1	0	0.1	0.1	0	0	0	0.3	0	0	0	0.1	0.2	0	0.1	0	0.1	0	0	0
S4CO2(mg/g)	19.04	9.21	10.73	2.14	429.2	0.8	1.95	11.44	6.33	0.21	0.08	15.97	0.12	3.93	4.58	7.88	12.6	1.51	3.58	0	5.46	1.54	7.44	1
S5(mg/g)	195.37	2.56	1.09	32.84	0.53	392.61	380.18	3.48	10.48	3.77	246.44	151.54	425.45	13.71	1.52	19.06	356.84	0	300.86	0.01	0.18	2.58	1.52	133.88
S4CO(mg/g)	2.42	0.54	1.14	0.33	40.68	0.08	0.22	1.14	0.78	0.15	0.11	1.11	0.04	0.34	0.7	0.51	2.12	0.08	0.29	0.02	0.45	0.14	0.79	0.19
Tmax(°C)	452	391	501	455	410	434	433	450	494	476	437	433	422	502	512	424	420	446	433	-41	507	-41	-41	-41
TpkS2(°C)	493	432	542	496	451	475	474	491	535	517	478	474	463	543	553	465	461	487	474	0	548	0	0	0
PC(%)	0.02	0.09	0.01	0.02	8.55	0.01	0.02	0.05	0.01	0.01	0.01	0.1	0.01	0.01	0	0.05	0.76	0.01	0.04	0	0.01	0.01	0.01	0.01
RC(%)	0.62	0.27	0.34	0.07	13.45	0.02	0.06	0.36	0.2	0.02	0	0.49	0	0.12	0.15	0.23	0.43	0.04	0.11	0	0.17	0.05	0.23	0.04
TOC(%)	0.64	0.36	0.35	0.09	22	0.03	0.08	0.41	0.21	0.03	0.01	0.59	0.01	0.13	0.15	0.28	1.19	0.05	0.15	0	0.18	0.06	0.24	0.05
pyroMINC(%)	0.27	0.14	0.05	0.14	0.55	0.07	0.11	0.1	0.12	0.15	0.19	0.33	0.11	0.12	0.03	0.19	0.22	0.02	0.26	0	0.04	0.05	0.04	0.11
oxiMINC(%)	5.33	0.07	0.03	0.9	0.01	10.71	10.37	0.09	0.29	0.1	6.72	4.13	11.6	0.37	0.04	0.52	9.73	0	8.21	0	0	0.07	0.04	3.65
MINC(%)	5.6	0.21	0.08	1.04	0.56	10.78	10.47	0.2	0.41	0.26	6.91	4.46	11.71	0.5	0.07	0.71	9.95	0.02	8.46	0	0.05	0.12	0.08	3.77
HI	8	61	6	11	431	200	150	66	5	0	300	114	0	0	0	39	712	60	113	0	6	0	0	0
OI	58	625	77	478	47	100	212	200	157	1600	4000	176	1800	323	87	364	18	460	540	0	161	800	125	580

Low-temperature thermochronology (U-Th)/He on apatite

Sample name	MB_PA11_01	MB_PA22_02	MB_PA23_01	MB_PA23_02	MB_PA23_03	MB_PA23_04	MB_PA23_05	MB_PM35_01	MB_PM35_02	MB_PM35_03
notes1	Close to blk	0	0	0	0	0	0	0	0	0
notes2	0	0	0	0	0	0	0	0	0	0
sample/run type	ap	ap	ap	ap	ap	ap	ap	ap	ap	ap
He date	23/05/2017	23/05/2017	23/05/2017	23/05/2017	23/05/2017	23/05/2017	23/05/2017	23/05/2017	23/05/2017	23/05/2017
pmol He	3.25122E-05	0.000783074	0.005661256	4.49283E-05	6.4151E-05	0.004952806	9.89732E-05	6.53222E-05	0.011381073	0.000436778
1s ± pmol He	8.80369E-06	2.48426E-05	0.000118658	9.76584E-06	9.0714E-06	0.000108477	1.01243E-05	9.89165E-06	0.000234147	1.76575E-05
% 1s ± He	27.07815671	3.172446959	2.095973637	21.73651867	14.1406941	2.190203382	10.22930557	15.14286238	2.057337759	4.04266629
U+Th date	05/06/2017	05/06/2017	05/06/2017	05/06/2017	05/06/2017	05/06/2017	05/06/2017	05/06/2017	05/06/2017	05/06/2017
(238/233)m	0.0038	0.2134	0.1024	0.0484	0.0045	0.1272	0.0058	0.0041	0.0598	0.0086
(238/233)m 1s ±	0.0003	0.0012	0.0007	0.0006	0.0003	0.001	0.0003	0.0001	0.0003	0.0002
(232/229)m	0.0045	0.3509	0.0414	0.0282	0.0043	0.0984	0.0049	0.0036	0.066	0.2881
(232/229)m 1s ±	0.0005	0.0017	0.0005	0.0006	0.0003	0.0009	0.0004	0.0002	0.0006	0.0013
(152/147)m	0.0043	0.2826	0.0594	0.045	0.0041	0.1076	0.0044	0.0043	0.0857	0.0938
(152/147)m 1s ±	0.0002	0.0009	0.0008	0.0006	0.0002	0.0007	0.0002	0.0001	0.0008	0.0009
(44/42)m	0.0143	0.1295	0.0567	0.0464	0.0151	0.096	0.0178	0.0142	0.0445	0.0526
(44/42)m 1s ±	0.0001	0.0008	0.0004	0.0004	0.0001	0.0015	0.0001	0.0001	0.0003	0.0007
ng U	-0.00146659	0.099612721	0.046083123	0.020041697	-0.00112902	0.058042889	-0.00050209	-0.00132192	0.025539332	0.000848202
1s ± ng U	8.17428E-05	0.001444944	0.000675958	0.000317058	8.0645E-05	0.000856743	7.93449E-05	5.36544E-05	0.000372761	6.37585E-05
% 1s ± ng U	-5.57365684	1.45056142	1.466824342	1.581990421	-7.14294561	1.476052002	-15.8028006	-4.05883052	1.459556726	7.516901035
ng Th	0.001817427	0.189362517	0.021795527	0.01464889	0.00170915	0.052656007	0.002033992	0.001330157	0.035114261	0.155361848
1s ± ng Th	0.00015261	0.002719787	0.000343908	0.00026885	0.00011761	0.0007834	0.000134838	0.000103294	0.000526626	0.002228668
% 1s ± ng Th	8.397018862	1.43628569	1.577885101	1.83529335	6.88138386	1.487768783	6.629247753	7.765524203	1.499748256	1.434501283
ng Sm	0.001258942	0.832061013	0.144465717	0.106163961	0.00075528	0.277456117	0.001510815	0.001258942	0.216095559	0.238605319
1s ± ng Sm	0.000228092	0.012090609	0.002295109	0.001687871	0.00022758	0.004101199	0.000228436	0.000118178	0.003271631	0.003621978
% 1s ± ng Sm	18.11774531	1.453091689	1.588687353	1.589872034	30.1312957	1.478143342	15.12007061	9.38711146	1.513974107	1.517978693
ng Ca	na	775.9411739	277.1699855	208.4474978	2.31844825	543.5406778	19.9409426	na	195.8191748	249.7609547
1s ± ng Ca	na	13.68152089	5.034094336	3.91471298	0.94899963	10.51087858	1.014706898	na	3.629452355	4.893992887
% 1s ± ng Ca	na	1.763216252	1.816248006	1.878033088	40.9325342	1.93377957	5.088560348	na	1.853471376	1.959470764
Th/U	-1.27128326	1.95017509	0.485198965	0.7498331	-1.55300438	0.930664803	-4.15583683	-1.03226942	1.410484732	187.9054991
raw date (Ma)	-5.84814432	0.998709483	20.40514744	0.352798743	-16.5377374	12.96214154	-3000571.85	-12.096178	61.61539662	2.131760106
1s ± date (Ma)	1.6565012	0.033385075	0.50140507	0.076829197	2.99951562	0.3235586	5272.149446	1.954057094	1.447888527	0.0912133
1s ± date %	-28.3252449	3.342821504	2.457247965	21.77706087	-18.1374003	2.496181658	-0.17570482	-16.1543348	2.349881047	4.278778844
morph comments	Abr, Round	incl	fract	fract		fract				Abr, coat
Ft 238U	0.593	0.687	0.558	0.590	0.737	0.622	0.642	0.542	0.551	0.473
Ft 235U	0.541	0.645	0.503	0.538	0.701	0.573	0.595	0.486	0.496	0.411
Ft 232Th	0.541	0.645	0.503	0.538	0.701	0.573	0.595	0.486	0.496	0.411
Ft 147Sm	0.865	0.898	0.852	0.864	0.915	0.876	0.883	0.847	0.850	0.820
Rs (um)	33.30	44.74	30.23	33.00	54.22	36.22	38.51	29.01	29.73	24.45
corr date (Ma)	na	1.48	36.96	0.61	na	21.14	na	na	113.94	5.13
1s ± date (Ma)	2.70	0.05	0.91	0.13	3.93	0.53	941.50	3.49	2.70	0.22
comments	no Ca				no Ca		no Ca	no Ca		
comments			high error bc small/low He							
1s ± date %	-28.21	3.35	2.47	21.78	-17.92	2.50	-1.33	-16.05	2.37	4.28
ppm eU (morph)	-1.10	87.77	91.72	39.21	-0.29	61.63	-0.01	-1.68	82.28	72.71
ppm eU w/ Sm (morph)	-1.10	90.03	92.89	40.02	-0.29	62.73	-0.01	-1.67	84.67	74.59
ppm U (morph)	-1.55	60.66	82.54	33.46	-0.45	50.80	-0.31	-2.19	62.19	1.65
d ppm U (morph)	0.09	0.88	1.21	0.53	0.03	0.75	0.05	0.09	0.91	0.12
ppm Th (morph)	1.92	115.32	39.04	24.46	0.69	46.09	1.26	2.21	85.51	302.36
d ppm Th (morph)	0.16	1.66	0.62	0.45	0.05	0.69	0.08	0.17	1.28	4.34
ppm Sm (morph)	1.33	506.73	258.76	177.25	0.30	242.84	0.93	2.09	526.21	464.37
d ppm Sm (morph)	0.24	7.36	4.11	2.82	0.09	3.59	0.14	0.20	7.97	7.05
nmol 4He/g (morph)	0.03	0.48	10.14	0.08	0.03	4.33	0.06	0.11	27.71	0.85
d nmol 4He/g (morph)	0.01	0.02	0.21	0.02	0.00	0.09	0.01	0.02	0.57	0.03
mol Ca	0.00E+00	1.94E-08	6.91E-09	5.20E-09	5.78E-11	1.36E-08	4.97E-10	0.00E+00	4.88E-09	6.23E-09
d mol Ca	2.36E-11	3.41E-10	1.26E-10	9.77E-11	2.37E-11	2.62E-10	2.53E-11	2.36E-11	9.05E-11	1.22E-10
mass ap (g)	0.00E+00	1.95E-06	6.97E-07	5.24E-07	5.83E-09	1.37E-06	5.02E-08	0.00E+00	4.93E-07	6.28E-07
d mass ap (g)	2.38E-09	3.44E-08	1.27E-08	9.85E-09	2.39E-09	2.64E-08	2.55E-09	2.39E-09	9.13E-09	1.23E-08
ppm U (Ca)	#DIV/0!	51.02	66.08	38.21	-193.54	42.44	-10.01	#DIV/0!	51.83	1.35
d ppm U (Ca)	#DIV/0!	1.16	1.54	0.94	80.42	1.03	1.66	#DIV/0!	1.22	0.10
ppm Th (Ca)	#DIV/0!	96.99	31.25	27.93	292.98	38.50	40.54	#DIV/0!	71.27	247.22
d ppm Th (Ca)	#DIV/0!	2.21	0.75	0.73	121.61	0.94	3.39	#DIV/0!	1.70	6.00
ppm Sm (Ca)	#DIV/0!	426.18	207.15	202.42	129.47	202.87	30.11	#DIV/0!	438.59	379.68
d ppm Sm (Ca)	#DIV/0!	9.74	5.00	4.98	65.81	4.94	4.80	#DIV/0!	10.50	9.41
nmol 4He/g (Ca)	#DIV/0!	0.40	8.12	0.09	11.00	3.62	1.97	#DIV/0!	23.10	0.70
d nmol 4He/g (Ca)	#DIV/0!	0.01	0.23	0.02	4.76	0.11	0.23	#DIV/0!	0.64	0.03
ppm eU (Ca)	#DIV/0!	73.81	73.42	44.78	-124.69	51.49	-0.48	#DIV/0!	68.58	59.45
ppm eU w/ Sm (Ca)	#DIV/0!	75.72	74.37	45.70	-124.37	52.40	-0.38	#DIV/0!	70.57	60.98
eU (morph)/eU (Ca)	#DIV/0!	1.19	1.25	0.88	0.00	1.20	0.03	#DIV/0!	1.20	1.22